Jak-stat pathway in the control of mycobacterial infections

Pean, Claire

Awarding institution:
King's College London

JAK-STAT PATHWAY IN THE CONTROL OF MYCOBACTERIAL INFECTIONS

Claire Péan

Thesis submitted to the University of London for the degree of Doctor of Philosophy

Centre for Molecular and Cellular Biology of Inflammation (CMCBI)
King's College London
School of Medicine

-September 2013-

Declaration

I, Claire Péan, confirm that the work presented in this thesis is my own. Where information has been derived from other sources, and where data have been generated in collaboration with other researchers, I confirm that this has been indicated in the thesis.

Acknowledgements

The work presented in this thesis was carried out between October 2009 and September 2013 at the CMCBI, within the division of Immunology, Infection and Inflammatory Disease (DIIID) at King's College London.

I would like to thank all members (actual and past) of Marc Dionne's group, Brian Stramer's group, of Frederic Geissmann's group, and of Pierre Guermonprez's group for their knowledge, advice and support. I am especially grateful to the fly team and in particular to Katie Woodcock, Martina Pilátová, Sharon Tan and Valérie Vivancos, who helped me considerably and who were very supportive. I would like to thank Sharon Tan for her help and for her kind and joyful personality; Will Jackson for his help and fruitful discussions; and lately Kevin Bronda who helped with experiments. I would also like to thank my thesis committee, Dr. Marc Dionne, Prof. Adrian Hayday and Dr. Deborah Dunn-Walters for monitoring my progression over these four years.

I would like to express my deepest gratitude to my supervisor Marc Dionne, who has supported and encouraged me throughout my thesis. His broad knowledge, his love for science, and his kindness, made me really enjoy this experience. I could not imagine a better and friendlier supervisor.

I would like to thank my friends and colleagues: Benoit and his lovely wife Céline for their wisdom and encouragements; Silva and Aurélien for their emotional support; Eric, Stéphanie and Chloé for moral support and interesting discussions. I would also like to thank my family and my close friends who always believed in me and encouraged me in pursuing my dreams.

Finally, I would like to thank my partner Raphaël Vigan for his support, for his patience, and for sharing this experience with me.

Abstract

Though mammalian JAKs and STATs have been extensively studied over the past 20 years, many aspects of their in vivo function remain unclear. In particular, their roles in control of infection with pathogens remain murky and confusing. One difficulty in understanding how these pathways regulate inflammation is the presence of complex compensatory mechanisms between the different JAK and STAT proteins. In the Dionne lab, we use the fruit-fly *Drosophila melanogaster* as a model to study the in vivo functions of the JAK/STAT pathway in mycobacterial infection. Flies contain only one JAK (hop), one STAT (STAT92E), and three identified interleukin-like signals to activate signalling (upd, upd2, upd3).

I show that, in Drosophila, the STAT-activating cytokine Upd3 is harmful to the host upon mycobacterial infection. Flies lacking *upd3*, or in which the JAk/STAT pathway is inhibited in phagocytes, show improved survival, decreased mycobacterial numbers, and delayed immune cell death. Strikingly, I find that JAK/STAT signalling acts in concert with other inflammatory signals to regulate expression of *Atg2* in *Drosophila* phagocytes. In isolation or upon infection, STAT activation inhibits *Atg2* expression and the ability of other, unknown signals to promote *Atg2* expression. Increased *Atg2* expression, as is seen in infected animals lacking either the cytokine Upd3 or STAT92E, promotes killing of intracellular bacteria and accumulation of large lipid droplets of unusual shape. I suggest an autophagy-independent mechanism by which Atg2 could reduce bacterial growth, involving the control of lipid body morphology.

In this thesis, I show a mechanism by which JAK/STAT controls bacterial growth through inhibition of autophagy gene expression and demonstrate that this inhibition is detrimental to the survival of the host. In addition, I demonstrate that *upd3* signalling is also required for glucose homeostasis suggesting a role for Upd3 in regulating gluconeogenesis and glycolysis.

Table Of Contents

Table of Figures

Table of Tables

Abbreviations

AA	Arachidonic Acid
Akt	also known as Protein Kinase B (PKB)
AMPs	Antimicrobial Peptides
ANK	ANKyrin
Atg	Autophagy protein
Atta	Attacin
BCG	Bacillus Calmette–Guérin
Bsk	Basket
CAMP	Cationic Antimicrobial Peptide
cDNA	Complementary Deoxyribonucleic Acid
CFUs	Colony Forming Units
crq	croquemort
COX	Cyclooxygenase
CZ	Cortical Zone
DAP	Diaminopimelic acid
DC	Dendritic Cells
Dome	Domeless
dpp	decapentaplegic
Dpt	Diptericin
Dro	Drosocin
Drs	Drosomycin
dsRed	Discosoma red fluorescent protein
EBF	Early B-cell Factor
E.coli	*Escherichia coli*
EDTA	Ethylenediamine-tetra-acetic acid
ERK	Extracellular signal-Regulated Kinases
FACS	Fluorescence Activated Cell Sorting
dFADD	*Drosophila* Fas-Associated protein with Death Domain
FOXO	Forkhead boX transcription factor O
FRET	Fluorescence Resonance Energy-Transfer

GFP	Green Fluorescent Protein
GNBP	Gram-Negative Bacteria-binding Proteins
Gp130	Glycoprotein 130
Hep	Hemipterous
Hml	Hemolectin
H_2O_2	Hydrogen Peroxide
Hop	Hopscotch
dIAP	*Drosophila* Inhibitor of Apoptosis Protein
ICL	Isocitrate Lyase
IFN-γ	Interferon γ
IL	Interleukins
ILIs	Intracytoplasmic Lipid Inclusions
IMD	Immune deficiency
InR	Insulin Receptor
IR	Inverted Repeats
JAK	Janus kinase
JNK	c-Jun N-terminal Kinase
LC3	Microtubule-associated protein 1A/1B-light chain 3
LDs	Lipid Droplets
Lys	Lysine
LXA4	Lipoxin A4
MAP	Mitogen-activated Protein
MFI	Mean Fluorescence Intensity
Mm	*Mycobacterium marinum*
MOI	Multiplicity Of Infection
Msn	Misshapen
Mtb	*Mycobacterium tuberculosis*
MyD88	Myeloid Differentiation primary response gene (88)
MZ	Medullary Zone
NADPH	Nicotinamide Adenine Dinucleotide Phosphate-Oxidase
NF-κB	Nuclear Factor kappa-light-chain-enhancer of activated B cells

NK	Natural Killers
NO	Nitric Oxide
NOD	Nucleotide Oligomerization Domain
iNOS	inducible Nitric Oxide Synthase
NOX2	NADPH Oxidase
NRAMP	Natural Resistance Associated Membrane Protein
OADC	Oleic Albumin Dextrose Catalase
ORO	Oil Red O
PBS	Phosphate Buffered Saline
PE	Phosphoethanolamine
PGE2	Prostaglandin E2
PGN	Peptidoglycan
PGRP	Peptidoglycan Recognition Protein
PGRS	Polymorphic CG-Repetitive Sequences
p.i.	post-injection
PI3K	Phosphoinositide-3-kinase
PI3P	Phosphatidylinositol 3-phosphate
ProPO	Prophenoloxidase
PRR	Pattern Recognition Receptor
PSC	Post Signalling Centre
RIP	Receptor Interacting Protein
mRNA	messenger Ribonucleic Acid
RNAi	RNA interferene
RNI	Reactive Nitrogen Intermediates
ROS	Reactive Oxygen Species
RpL1	Ribosome protein L4
RT-PCR	Reverse transcription polymerase chain reaction
S2R^{+}	Schneider 2 cells Receptor +
Socs36E	Suppressor of cytokine signalling 36E
SPE	Spätzle processing enzyme
spz	Spätzle

STAT	Signal Transducers and Activators of Transcription
TAB	TAK-1 binding protein
TACO	Tryptophan Aspartate containing COat protein
TAG	Triacylglycerol
TAK	TGF-β Activated Kinase
TARGET	Temporal And Regional Gene Expression Targeting system
TCA	Tricarboxylic Acid cycle
TB	Tuberculosis
Tep2	Thioester-containing protein 2
TGF	Transforming Growth Factor
TGS	Triacylglycerol Synthase
Th	T helper
TLR	Toll-Like Receptor
TNF	Tumor Necrosis Factor
TNF-R	Tumor Necrosis Factor receptor
dTOR	*Drosophila* Target Of Rapamycin
TotA	Turandot peptide A
TRASH	TRAnsposon-Site Hybridization
Wng	Wengen

Chapter 1 Introduction

1.1 A worldwide resurgence of tuberculosis

In this chapter, I will first present the epidemiology of the disease and the importance of understanding its biology. In a second section, I will describe the immunology of the infection, and will then concentrate on macrophage immunity. Finally, I will present the new drug and vaccine strategies to control the infection and to eradicate the pathogen.

1.1.1 Epidemiology

Tuberculosis (TB) is the second worst infectious disease in terms of mortality, just after HIV/AIDS (World Health Organization (WHO) 2011). It is estimated that one third of the world population is infected, with 1.4 million deaths per year (World Health Organization 2012; World Health Organization (WHO) 2011). These alarming numbers have been rising since the 90s despite the declaration of tuberculosis as a “Global health emergency” by the World Health Organization (WHO) in 1993 (World Health Organization (WHO) 1993). The main etiological agent, *Mycobacterium tuberculosis*, was identified in 1882 by Robert Koch who later received the Nobel Prize for his finding (Koch 1882).

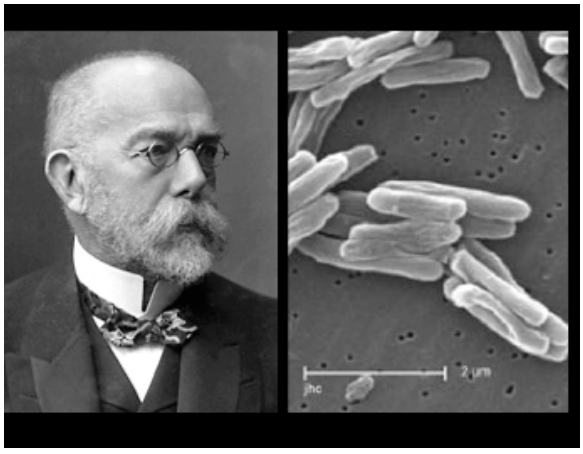

Figure 1-1: Robert Koch (1843-1910) and the main causative agent of tuberculosis, *Mycobacterium tuberculosis*

At the time of his discovery, tuberculosis was a major public concern, which accounted for up to 25% of death in Europe in the early 19th century (Lawn & Zumla 2011). Several improvements in public health and treatments resulted in decreases in incidence and deaths. In 1906, Albert Calmettes and Camille Guérin developed the first attenuated vaccine from the bovine strain *Mycobacterium bovis*, the bacillus Calmette-Guérin (BCG) (Bonah 2005). Today, it remains the only available vaccine. It is administered routinely to infants to protect them against severe forms of TB such as the meningeal form. However, its efficacy in adult pulmonary TB is poor (Ottenhoff & Kaufmann 2012). In terms of drug treatments, the administration of streptomycin alone gave promising results in the late 19th century, but it was rapidly hindered by the emergence of multi-resistant strains (Ottenhoff & Kaufmann 2012). The preferred treatment is now the first-line 6-month regimen of the antibiotics rifampicin and isoniazid in combination with two additional drugs (pyrazinamide, and either ethambutol or streptomycin) for the first two months of treatments (Koul et al. 2011). It is 95% effective against drug susceptible strains, but for multi-resistant strains, found in 8% of patients, the treatment length is considerably increased and the efficacy is reduced (Koul et al. 2011). Besides, this medication is toxic and the compliance is low, especially in countries with poor medical care. It is a major concern as the disease is prevalent in developing countries (World Health Organization (WHO) 2011). Typically, TB is considered as a disease of poverty tightly associated with malnutrition, overcrowding and poor medical care, but industrialized countries are not safe. In fact, they are also experiencing a resurgence of TB due to treatments with immunosuppressive drugs (anti-TNF and corticosteroids), to promiscuity in prison and to the resulting incubation of multi-drug resistant strains (Lawn & Zumla 2011).

The disease spreads through inhalation of infectious aerosol droplets from people with active TB and the infectious rate is especially high in populations living in close proximity (Lawn & Zumla 2011). Most individuals are immuno-competent and are able to eliminate the pathogen or maintain it in a latent state. However, in 10% of cases, a breach in the immune system happens and the disease can shortly develop or be reactivated from latent infections (World Health Organization (WHO) 2011). TB can affect several parts of the body and induces several symptoms in patients. The most common disease is the pulmonary TB where *M.tuberculosis* affects alveolar tissues. The classical symptoms are weight loss, loss of appetite, fever, night sweats and persistent cough sometimes with blood (World Health Organization 2012; Lawn &

Zumla 2011). The most important risk factor is HIV infection, which accounts for 13% of the world's TB cases (World Health Organization (WHO) 2011). Current measures aiming to control TB are insufficient because of the lack of robustness of diagnosis in low-income countries, the compliance with the constraining treatment, the emergence of multi-drug resistant strains and the insufficient protection given by BCG vaccine against pulmonary TB (Gengenbacher & Kaufmann 2012). In consequence, TB represents an economic burden for developing countries and financial needs for TB management are estimated at US$ 8 billion per year for low and middle-income countries. There are increasing funds allocated to research to improve diagnosis, prognosis, prophylaxis and treatments. But according to the World Health Organization, these funds remain insufficient (World Health Organization 2012).

1.1.2 Immunology of Tuberculosis

Since the discovery of *M.tuberculosis* in 1882, several other related species have been identified as causative agents. They are part of the *Mycobacterium tuberculosis* complex (MTBC) and they operate in similar ways to infect their human host. This section will present the outlines of our current knowledge of pulmonary *M.tuberculosis* infection, the most widely studied disease case.

***M.tuberculosis*, a tough pathogen**

M.tuberculosis is a slow growing, facultative intracellular pathogen that can infect several animal species. It is an acid-fast, aerobic, non-spore forming and non-motile rod-shaped bacillus. Upon inhalation of infectious aerosols, the bacteria reach the lung airways and the alveolar tissue, where they get phagocytosed by dendritic cells, alveolar macrophages, interstitial macrophages or epithelial cells (Ottenhoff & Kaufmann 2012).

A prominent feature: the delay in adaptive immunity

A characteristic of the immune response to *M.tuberculosis* is the delay in the onset of adaptive immunity compared to other bacterial infections (Wallgren 1948; Urdahl et al. 2011). Recent studies in mice and humans have highlighted mechanisms that contribute to it: the pathogen-mediated inhibition of apoptosis of infected cells, the delayed migration of dendritic cells from the lung to the local lymph node and the influence of regulatory T cells (Treg) (Urdahl et al. 2011). Apoptosis is a programmed cell death that results in nuclear fragmentation, cell shrinkage and blebbing. In contrast to necrosis, that is the result of cellular injury, apoptosis can be triggered by infected cells to eliminate pathogens. Apoptotic cells can then be engulfed by dendritic cells (DCs) and contribute to the presentation of pathogen antigens via cross-presentation (Urdahl et al. 2011). DCs then migrate to the local lymph node for T cell priming. However, *M.tuberculosis* inhibits such mechanism by manipulating the host eicosanoid metabolism, an important mediator of damage repair and thereby cell death (Chen et al. 2008; Divangahi et al. 2010; Herb et al. 2008). In consequence, pathogen antigen-presentation by DCs is diminished and T cell activation is left to infected macrophages, which are poor activators of T cells and wherein antigen presentation may be manipulated by the pathogen. In addition, cell migration to the local mediastinal lymph node is delayed, therefore prolonging the quiescent proliferation of *M.tuberculosis* (Wolf et al. 2007; Wolf et al. 2008). To bypass effector T cell priming, mycobacteria also induce Treg proliferation that dampen the expansion of effector T cells (Urdahl et al. 2011). The precise mechanism by which the pathogen activates Treg cells is unknown but it is hypothesized that it results from pathogen manipulation of antigen-presentation in infected cells or from eicosanoid-specific activation of the aryl hydrocarbon receptor (AhR) that may promote the Treg response (Urdahl et al. 2011). Benefiting from this delay in adaptive immunity activation, the bacteria proliferate freely inside alveolar macrophages until reaching a burden difficult to control by the host. The infection then becomes persistent (**Error! Reference source not found.**).

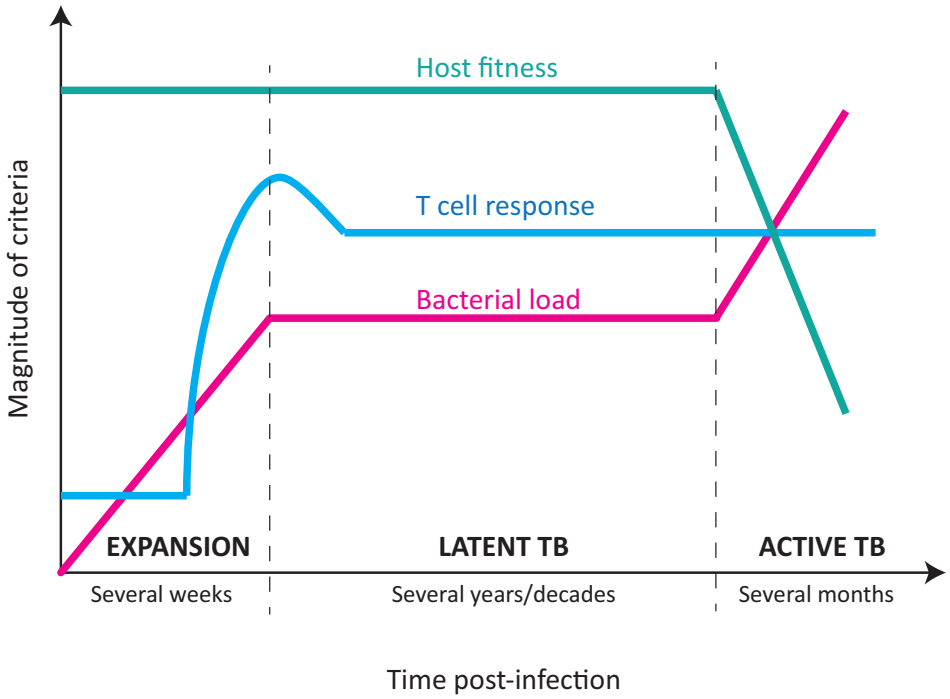

Figure 1-2 : Typical features of *M.tuberculosis* infection

Following infection of alveolar macrophages in the lung airways, *M.tuberculosis* proliferates freely before the onset of adaptive immunity. The granuloma starts to form to contain the infection. Upon T cell activation, bacterial growth is controlled and the pathogen goes into dormancy. Under some circumstances, the disease becomes active and pathology arises with patients experiencing typical TB symptoms. In immuno-compromised patients, the expansion phase can be directly followed by active disease. Figure adapted from (Urdahl et al. 2011).

The initiation of the granuloma, an attempt to contain bacterial growth

Following initial bacterial proliferation in the lung, mononuclear cells are recruited from neighbouring blood vessels to the emerging granuloma (**Figure 1-3**) (Saita et al. 2000; Alatas et al. 2004). Granulomas are organised inflammatory structures that gather various immune cells to contain the bacteria and protect surrounding tissue from further damage. But despite the granuloma's protective role, it does not eradicate the bacteria. Its formation is dependent on the production of Tumour Necrosis Factor (TNF) by infected macrophages (Roach et al. 2002; Kindler et al. 1989). In its early stage, the granuloma contains infected macrophages, foamy macrophages and other mononuclear phagocytes surrounded by lymphocytes. Some infected macrophages have also been shown to fuse to generate multinucleated giant cells, called the Langhans giant cells (Russell et al. 2009). The lymphocyte population is formed of a small portion of $CD8^+$ T cells and a larger population of $CD4^+$ T cells that will settle the fate of the granuloma. They have two major roles. First, they recognize infected macrophages and activate

them by secreting the type II interferon, IFN-γ (Russell et al. 2009). Second, they secrete various cytokines and chemokines to recruit and activate more immune cells to the granuloma (Cooper 2009). Activated macrophages are efficient at killing bacteria. In consequence, *M.tuberculosis* proliferation is hindered and its fitness is altered inside the granuloma (Wong et al. 2011; Decker et al. 2002). Once the bacillary growth is stabilized and contained within the granuloma, recruited $CD8^+$ T cells can exert their cytotoxic activity thereby enhancing mycobacterial clearance. T cells also work in collaboration with B cells that not only generate antibodies against the pathogen, but also modulate the inflammatory response through cytokine production (Maglione & J. Chan 2009). Such a potent system would logically eradicate the pathogen, but this is without considering the survival strategies of *M.tuberculosis*.

The maturation and stabilization of the solid granuloma: eradication or latency?

As the granuloma matures, it becomes larger, well-organized and it develops an extensive fibrous capsule that concentrates macrophage in the centre and maintains lymphocytes at the periphery (**Figure 1-3**) (Dheda et al. 2005; Cáceres et al. 2009; Russell 2007). The formation of the stratified, fibrous layer is thought to be driven by the bacteria to minimize its exposure to a strong antimicrobial response (Russell et al. 2009). It results in a decrease in blood vessels penetrating the granuloma and a concomitant hypoxic environment (Via et al. 2008). In response, *M.tuberculosis* activates hypoxic responsive genes that stimulate energy storage and transition into a dormant phase (Sherman et al. 2001; Park et al. 2003; Daniel et al. 2004). While in dormancy, mycobacteria are still able to replicate but at lower rates; they become resistant to anti-tuberculous drugs that mostly target highly replicative bacteria (Gill et al. 2009; Gengenbacher & Kaufmann 2012). At this stage, granulomas do not necessarily develop into an active site and can ultimately resolve.

The actively necrotic granuloma, the last step towards Tuberculosis

When the bacterial toxicity overcomes host immune responses, the granuloma becomes necrotic. Central foamy macrophages then liberate lipid droplets, which are thought to participate in the progression to active disease. As a result, the centre of the granuloma harbour

an accumulation of necrotic and lipidic debris forming a cheese-like structure, the caseum (**Figure 1-3**) (Gengenbacher & Kaufmann 2012; Russell et al. 2009; Kim et al. 2010). Caseation of the granulomas is thought to be a consequence of pathogen-mediated deregulation of host lipid metabolism possibly to promote its release and proliferation in the extracellular space (Kim et al. 2010). The structure then liquefies and cavitates, spilling infectious *M.tuberculosis*. At this point, bacteria can disseminate from adjacent blood vessels to other tissues or be released to the airways to be cough out in the form of highly infectious sputum (**Figure 1-3**) (Gengenbacher & Kaufmann 2012).

Histological samples revealed that in active disease, granulomas are present at all stages of development (Russell et al. 2009). Thus, pathogenesis in *M.tuberculosis* infection is the result of a complex interplay between the activation states of the bacteria and the host immune response. In one hand, the granuloma protects the host by containing the infection, and in another hand favours the expansion and dissemination of the disease (Ottenhoff & Kaufmann 2012; Davis & Ramakrishnan 2009).

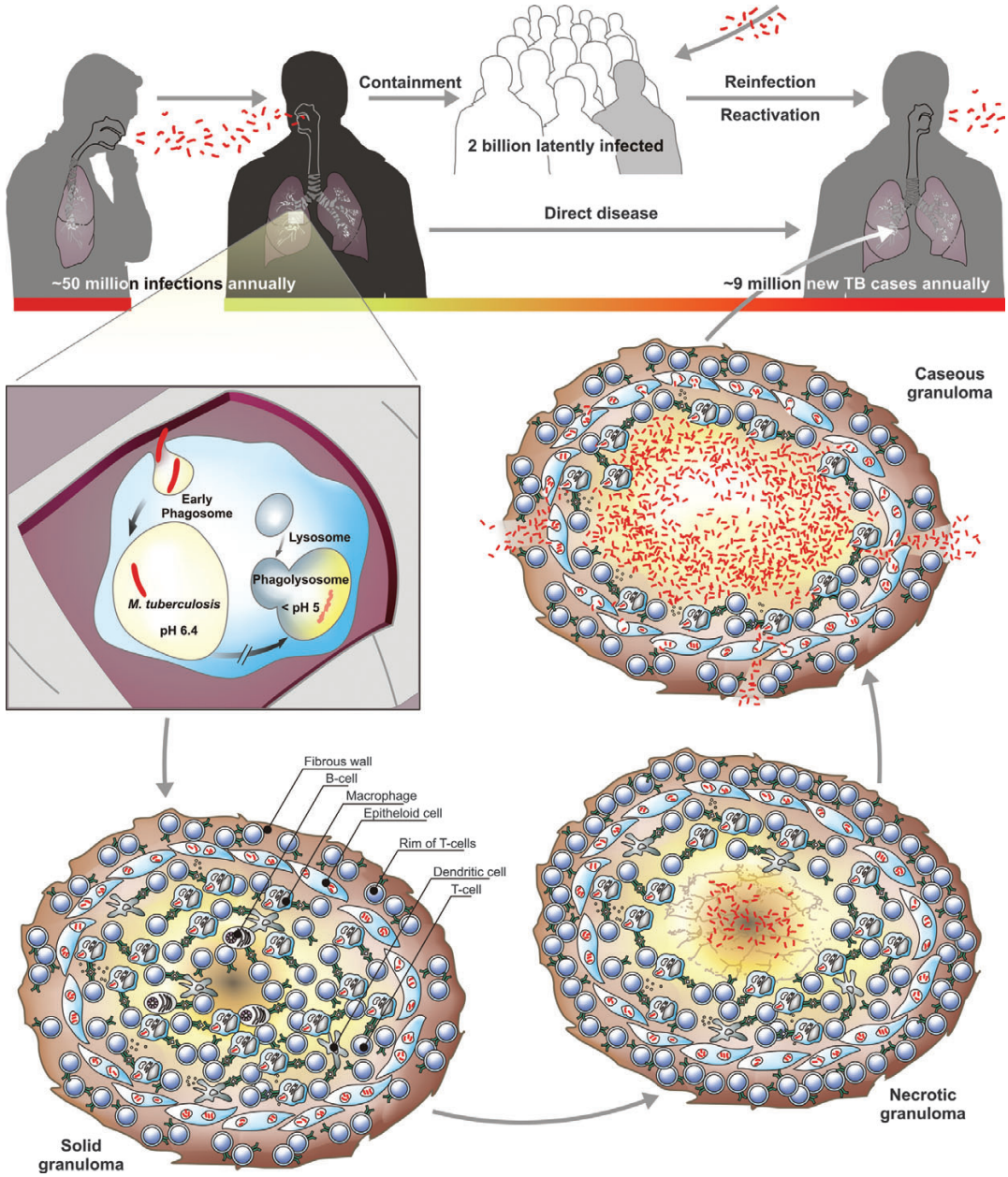

Figure 1-3: Transmission and pathology in tuberculosis

M.tuberculosis is transmitted via aerosol droplets from a person infected with TB. The bacteria reach the lung airways and proliferate within alveolar macrophages prior to the onset of adaptive immunity. The infected host cells induce a local inflammation with recruitment of leukocytes from the local blood vessels. Recruited cells start to form an organized structure, the early granuloma. Upon activation of effector T cells, more cells are recruited and the granuloma, which becomes stratified with T cells in the outer edge of the structure. In healthy individuals, the bacteria likely come to dormancy after T cell recruitment and the granuloma stays solid. In people at risk or upon reactivation, the centre of the granuloma becomes necrotic. The central cells lose their lipids and form the caseum where *M.tuberculosis* grow in high number. The bacteria are then released to the airways or disseminate through local blood vessels to create secondary sites of infection. Picture adapted from (Gengenbacher & Kaufmann 2012).

Cytokines, a complex sequence of activation and inhibition

The immune responses against pathogens are dependent on cytokines, which regulate immune cell activation and bactericidal functions. However, if subverted by pathogens and used inappropriately, they can contribute to pathologies and chronic infections.

IFN-γ is a key cytokine for protective immunity. It is secreted by T cells, Natural Killer (NK) cells and also alveolar macrophages stimulated by IL-12 (Flynn & J. Chan 2001). It also activates macrophages to enhance their bactericidal potential. In contrast, the Th2 cytokines IL-4 and IL-13, can inhibit the bactericidal mechanisms induced by IFN-γ (Harris et al. 2007). However, the relevance of Th2 cytokines in the pathology of *M.tuberculosis* in vivo remains to be demonstrated (Flynn & Chan 2001; Roy et al. 2008; Lin et al. 1996).

IFN-γ can work in synergy with TNF-α to produce nitric oxides and related nitrogen intermediates (RNI) via the inducible form of nitric oxide synthase (iNOS) (Flynn & Chan 2001). RNI are potent antimicrobial molecules that target the bacteria inside the phagosome. Besides intra-macrophage bactericidal effects, TNF-α has two other major roles that are intimately linked: It activates granuloma formation through the regulation of chemokines which recruit immune cells, and it modulates inflammation (Zuñiga et al. 2012; Roach et al. 2002). These functions were unfortunately discovered when a patient treated with anti-TNF died following acute dissemination of *M.tuberculosis* (Zuñiga et al. 2012; Flynn & Chan 2001; Maini et al. 1999). Therefore, rheumatoid patients that take anti-TNF and/or corticosteroid treatments have higher risk of contracting TB (Wallis 2008).

Another cytokine is important in promoting resistance to mycobacterial infection: the Th1 cytokine IL-12. IL-12 is induced following phagocytosis by macrophages and DCs. It mediates activation of dendritic cells and is required for an optimal T cell response (Cooper 2009). IL-12 activity is reduced by the anti-inflammatory cytokine IL-10, which dampens macrophage activation (Flynn & Chan 2001). Finally, other cytokines such as IL-6, TGF-β, IL-17 and IL-23 modulate immune responses against *M.tuberculosis*. IL-6 and TGF-β are important for the regulation of immune cell differentiation and responses, while IL-23 and IL-17 were shown to be essential for protective and regulatory immune responses (Cooper 2009; Zuñiga et al. 2012). Mycobacteria are able to modulate the kinetics and induction of cytokines to control the nature of the induced-inflammatory response. Different strains and mutants affect

these molecules differently rendering interpretations difficult (Cooper 2009). Therefore, more investigations are required to precisely understand how the bacteria manipulate host cytokine secretion to favour an anti-inflammatory state. One hypothesis is that, upon dormancy, mycobacteria hide from detection by releasing fewer antigens to the cytosol and subvert the host immune response to limit inflammation.

1.1.3 Macrophage immunity

M.tuberculosis persists in macrophages and can infect various innate immune cells as the lesion develops (Cooper 2009). Macrophages are thought to be a niche for the bacterial maintenance and proliferation since depletion of alveolar macrophages exerts protective effects in mice (Leemans et al. 2001). Therefore, precise analysis of macrophage effector functions together with mycobacterial evasion mechanisms is a prerequisite towards vaccine development. In particular, there is an urge to identify bactericidal functions that are attenuated or not induced during natural infection. Once re-activated these functions could restore the killing of mycobacteria, preventing development of the infection.

Recognition by Pattern Recognition Receptors (PRR)

Pattern Recognition receptors are important first lines of defence that can induce phagocytosis and activate immune responses.

M.tuberculosis uptake is dependent on various phagocytic receptors such as complement-receptors, mannose receptors, C-type lectin receptors and likely Fc-receptors (Schlesinger 1993; Brennan & Nikaido 1995). Upon binding of mycobacterial ligands, a signalling cascade is activated and provokes the invagination and budding of the plasma membrane to form a phagosome (Aderem & Underhill 1999). Phagosomes are dynamic organelles that sequentially and transiently fusion with vesicles from the endocytic pathway while undergoing fission events for recycling. These series of vesicle trafficking events have several functions. They render the phagosome more toxic to pathogens by acquisition of oxidative, acidifying, and hydrolytic functions and therefore allow the delivery of bacterial products to the antigen processing and presentation pathway (Fairn & Grinstein 2012). Full

bactericidal potential requires a last fusion event with the lysosome, an acidic organelle containing hydrolase enzymes and other degradative enzymes and in which acidification results from proton influx via the vacuolar proton pump, the H^+V-ATPase.

To enhance bactericidal mechanisms other PRRs have shown to be essential: the Toll-like Receptors (TLR) and the nucleotide oligomerization domain (NOD)-like receptors. TLRs have various functions such as stimulation of antigen presentation, activation of cytokine secretion and modulation of immune cell death. Indeed, TLRs have an important role in the initial phase of the infection since they stimulate antigen presentation of endogenous bacterial antigens via the major histocompatibility complex (MHC) class II (Blander & Medzhitov 2006). After initiation of the granuloma in *M.tuberculosis infection*, TLRs also participate in the formation of foamy macrophages (through TLR2 activation) (D'Avila et al. 2006). TLRs have also more direct action on bactericidal mechanisms via NF-kB activation and the subsequent cytokine production, and via vitamin D pathway activation for antimicrobial peptide synthesis. In particular, NF-kB activation was demonstrated after the specific binding of triacylated lipoprotein derived from *M.tuberculosis* to the TLR-2/TLR-1 heterodimeric receptor (Liu & Modlin 2008).

Other types of PRR, the NOD receptors, such as NOD2, also enhance innate immune responses via recognition of *M.tuberculosis* muramyl dipeptide (MDP) (Juárez et al. 2012).

Phagosomal maturation arrest is restored by IFN-γ

During *M.tuberculosis* infection, phagosome fusion with the lysosome is inhibited and the acidification is arrested at pH 6.4 instead of pH 4.5-5.0, thus preventing normal bactericidal functions (Sturgill-Koszycki et al. 1994; Vergne et al. 2004; MacMicking et al. 2003). In consequence, the pathogen can proliferate freely inside infected cells prior to the onset of an adaptive immune response. *M.tuberculosis* has several encoded mechanisms that target phagosomal maturation arrest.

First, it inhibits phago-lysosome fusion through secretion of a lipid phosphatase, SapM. SapM hydrolyses phosphatidylinositol 3-phosphate (PI3P), a membrane trafficking regulatory lipid that is essential for the acquisition of lysosomal constituents (Vergne et al. 2005). Second, *M.tuberculosis* secretes PtpA,a protein tyrosine phosphatase, that excludes host vacuolar H^+V-

ATPase to inhibit proton influx (Wong et al. 2011). Finally, the mycobacterial tryptophan aspartate containing coat protein (TACO), alias coronin 1, prevents lysosomal fusion by regulation of calcium-dependent processes. Indeed, Coronin 1 induces cytosolic influx of Ca^{2+} from infected phagosomes, which results in activation of the phosphatase calcineurin and a subsequent inhibition of lysosomal fusion (Jayachandran et al. 2007; Pieters 2008). The precise activity of calcineurin to prevent lysosomal delivery is however still unknown.

Upon macrophage activation by IFN-γ, phago-lysosomal fusion is rescued, possibly through the activation of LRG-47, a member of the guanoside triphosphate family that restore the trafficking of H^+V-ATPase to the phagosome (MacMicking et al. 2003). The phagolysosome becomes acidic, oxidative stress and lysosomal hydrolases are activated, and in consequence, the environment becomes extremely hostile for the pathogen (Via et al. 1998; Schaible et al. 1998). Surprisingly, *M.tuberculosis* is able to survive under such conditions and to proliferate, but at lower rate. An explanation to this was already suggested a hundred years ago, when Metchnikoff postulated that *M.tuberculosis* lipid-rich envelope could act as a barrier against proton entry (Metchnikoff 1905). Indeed, it was further demonstrated that acidification of the phagosome induce changes in the maintenance of cell wall and storage lipids through the bacterial master regulator PhoPR (Abramovitch et al. 2011). Recently, Vandal et al. also identified a bacterial membrane protein encoded by the Rv3671c gene, which preserves intrabacterial pH and allows bacterial survival under acidic conditions (Vandal et al. 2008; Vandal et al. 2009).

Ion influx/efflux change intraphagosomal homeostasis and toxicity

Proton influx towards the intraphagosomal lumen is considered to be the major mechanism of phagosome acidification. To maintain intraphagosomal homeostasis, compensatory cation efflux and anion influx are required. Ion influx/efflux is part of a complex osmotic process that is interconnected with the oxidative burst and which can considerably change the toxicity of the phagosome (Soldati & Neyrolles 2012). Macrophages can manipulate ion influx/efflux to limit bacterial growth and induce killing. For example, they can induce Fe^{2+} efflux to reduce accessibility of this crucial ion to *M.tuberculosis* to limit its replication. This is called the NRAMP model, NRAMP being the host iron/manganese transporter Natural

Resistance Associated Membrane Protein (Soldati & Neyrolles 2012). In addition, the host can translocate the transition metals Cu^{2+} and Zn^{2+} into the phagosome to poison microbes.

M.tuberculosis possesses diverse strategies to withstand increasing phagosomal toxicity and ensure its survival and growth. Indeed, mycobacterial cell wall controls nutrients and ionic permeability thanks to porin-like molecules that ensure transport of molecules inside and outside the cell. As an example, the channels of the porin OmpATb close upon acidification of the phagosome and represent a mechanism to adapt to toxic and acidic conditions (Soldati & Neyrolles 2012; Molle et al. 2006).

Nitro-oxidative stress is a major intraphagosomal killing process

Activated macrophages express two enzymes that generate Reactive Oxygen Species (ROS) and RNI: the phagocyte oxidase NOX2/gp91phox and the inducible nitric oxide synthase (iNOS) respectively. ROS are generated by electron transfer from cytosolic NADPH to molecular oxygen. It produces superoxide anions (O_2^-) that dismutate into hydrogen peroxide (H_2O_2) and generate toxic hydroxyl radicals. iNOS catalyses the oxidation of a guanidino nitrogen of L-arginine (L-Arg) to form nitric oxide (NO), which is then oxidized to form nitrogen dioxide (NO_2) and other toxic intermediates. NO and superoxide can synergize to produce peroxynitrite (OONO), a highly toxic chemical (Nathan & Shiloh 2000; Ehrt & Schnappinger 2009). IFN-γ increases oxidative stress via several mechanisms such as activation of the nitric oxide synthase 2 (NOS2) (Ehrt et al. 2001; Chan et al. 1992).

In response, *M.tuberculosis* is able to detoxify such molecules via several detoxification mechanisms:

(1) Via the catalase peroxidase KatG which is involved in hydrogen peroxide detoxification;

(2) Via mycothiol synthesis, an actinobacteria antioxidant;

(3) Via the envelop-bound superoxide dismutases (SodA & SodC) that contributes to ROS detoxification;

(4) Via F-420, a deazaflavin derivative that converts back NO_2 to NO;

(5) Via reduction of iNOS association to the phagosome;

(6) Via NADPH-dependent peroxidase and peroxynitrite reductases (AhpC, AhpD, DlaT, Lpd) that detoxify both ROS and RNI (Davis et al. 2007; Purwantini & Mukhopadhyay 2009; Newton et al. 2008; Wu et al. 1998; Ng et al. 2004; Ehrt & Schnappinger 2009).

If, despite these mechanisms, proteins are altered, *M.tuberculosis* has protein repair and degradation mechanisms. For example, ROI and ROS can generate sulfoxides using the sulfur of cysteine and methionine residues, and this process interferes with protein functions (Weissbach et al. 2002). To counteract this effect, the pathogen uses methionine sulfoxide reductases, MsrA & MsrB, which convert back methionine sulfoxide to methionine residues in proteins (Lee et al. 2009). Surprisingly, some proteasome-associated proteins have also shown to be protective: the mycobacterium proteasome ATPase (Mpa) and the proteasome-accessory factor (PafA) (Darwin 2003).

Besides protein alterations, nitro-oxidative stress generates DNA damage within the mycobacterial genome. From a transposon mutant screen for RNI susceptibility, Darwin et al. identified the excision repair gene uvrB, a DNA repair gene. In addition to this, DnaE2, a replicative DNA polymerase, and Lsr2, a histone-like protein that promote resistance to DNA damage, have been shown to have a protective role against nitro-oxidative stress suggesting a role for bacterial DNA repair mechanisms in resisting attacks from the host immune system (Colangeli et al. 2007; Boshoff et al. 2003). Interestingly, DnaE2 has also a crucial role in *M.tuberculosis* survival by inducing mutagenesis, a function linked to bacterial adaptation and to the emergence of drug resistance (Boshoff et al. 2003; Ford et al. 2011).

Intraphagosomal antimicrobial peptides to eradicate negatively charged cell walls

Inside the mature phagosomal compartment, *M.tuberculosis* also experiences the permeabilizing properties of cationic antimicrobial peptides (CAMPs) such as cathelicidin, hepcidin and ubiquitin-related proteins (Koul et al. 2011; Sow et al. 2007; Alonso et al. 2007; Fabri et al. 2011). CAMPs disrupt the negatively charged bacterial cell wall. To escape such aggression, *M.tuberculosis* uses the lysine transferase LysX to form lysinylated phosphatidylglycerol to positively charge its cell wall (Maloney et al. 2009). All bactericidal mechanisms and bacterial evasion strategies are recapitulated in **Figure 1-4**.

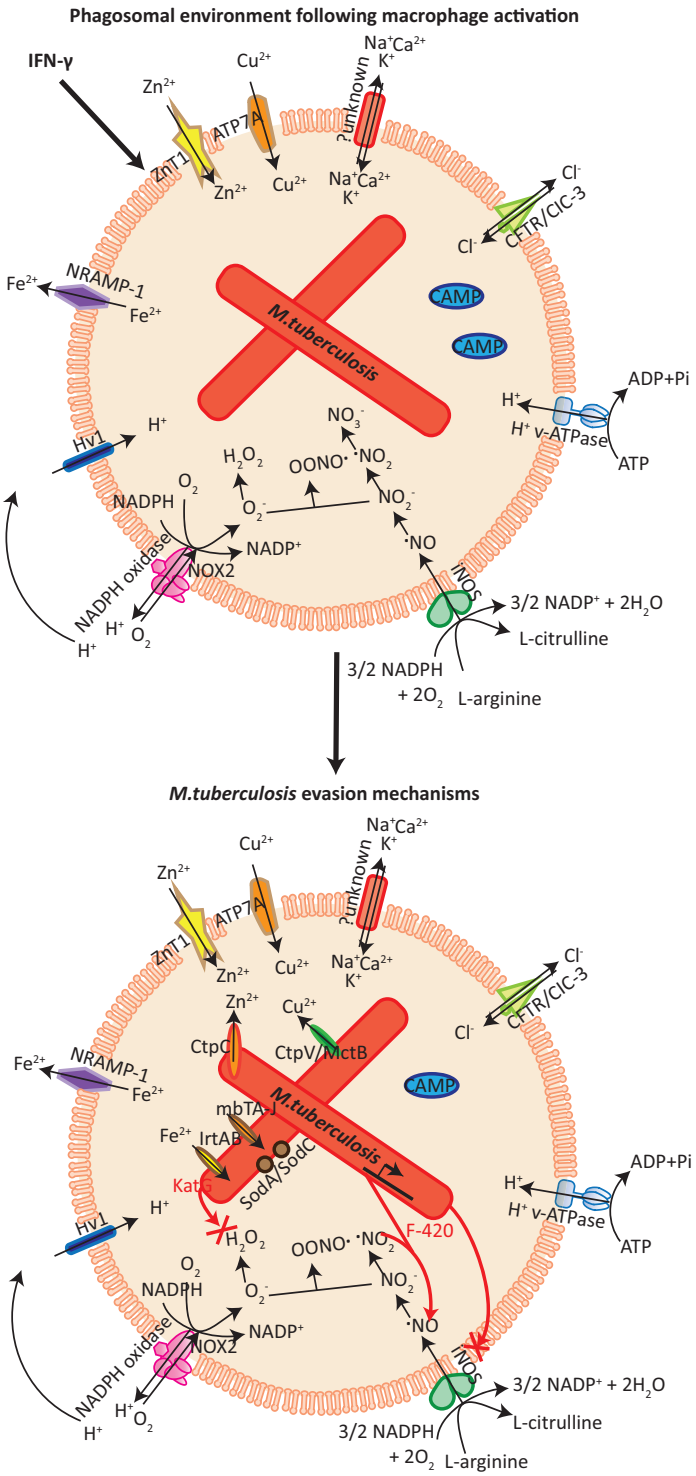

Figure 1-4: Macrophage bactericidal strategies and *M.tuberculosis* evasion mechanisms

Upon activation, macrophages activate several bactericidal mechanisms that render the phagosome toxic for the invader. The bacteria-containing vacuole becomes acidic, accumulates reactive oxygen species and reactive nitrogen intermediate through the respective activity of the H^{+}-vATPase, NOX2 and iNOS. To compensate for the influx of H^{+}, efflux of K^{+}, Ca^{2+} and Na^{+} are observed together with chloride influx. To prevent bacterial growth, the host deprives the phagosome of Fe^{2+}, an essential metal for enzymatic activity, and incorporates toxic transition metals such as Zn^{2+} and Cu^{2+}. In addition, phagosomes contain cationic antimicrobial peptides to directly kill the pathogen. To counterbalance the phagosomal toxicity, *M.tuberculosis* has developed various evasion strategies. The bacteria can detoxify ROS and RNI, prevent entry of toxic transition metals and attract Fe^{2+}. ADP: Adenosine diphosphate; ATP: Adenosine

triphosphate; CFTR: Cystic Fibrosis Transmembrane conductance Regulator; CtpC and CtpV: heavy metal efflux P-type ATPases; Hv1: proton channel; iNOS: inducible Nitric Oxide Synthase; mbTA-J: mycobactin biogenesis protein; MctB: mycobacterial copper transport proteins B;NADPH: Nicotinamide Adenine Dinucleotide Phosphate-oxidase; NRAMP: natural resistance-associated macrophage protein; SodA/C: Superoxide dismutases A&C; ZnT1: Zinc Transporter 1.

Can *M.tuberculosis* escape the phagosome?

This simple question is still a matter of debate. Such controversy arose from the idea that it would be simpler for *M.tuberculosis* to escape the phagosome than to develop various energy-consuming strategies to survive in acidic and toxic conditions. The cytosol is appealing in the sense that host defences are much more diffuses and the bacteria can easily escape from them. However, though this clearly happens for some mycobacteria such as *M.marinum*, it is still controversial for *M.tuberculosis* (Stamm et al. 2003). Recently, *M.tuberculosis* and *M.leprae* were observed in the cytosol of DCs in a mechanism dependent of the secreted bacterial proteins CFP-10 and ESAT-6 (van der Wel et al. 2007). Once in the cytosol, bacteria appear to replicate and rapidly induce cell death. One hypothesis is that cytosolic localisation of *M.tuberculosis* is a transient phenomenon tightly associated with necrosis. As a consequence, the bacteria may not use this mechanism to survive and proliferate but to spread to adjacent cells. Rapid necrosis and subsequent clearance of cell debris may explain why cytoplasmic bacilli have not been found in alveolar macrophages from TB patients (Welin & Lerm 2012). In agreement with this, it was recently shown that phagosomal rupture by *M.tuberculosis* results in toxicity and subsequent host cell death (Simeone et al. 2012). Authors used a single-cell fluorescence resonance energy-transfer (FRET)-based method in which THP-1 macrophages were loaded with a cytosolic FRET reporter (CCF4) that emits at 405nm and were infected with *M tuberculosis* that have a beta-lactamase activity on its cell surface. When bacteria escape the phagosome, beta-lactamase will cleave the cytosolic probe, which results in loss of FRET signal and an emission at 450 nm. Until then, the model of phagosomal escape was controversial due to the extensive use of electron microscopy where ultrastructure observations are somewhat difficult to interpret; but these results clearly confirm the presence of *M.tuberculosis* in the cytosol.

In addition, since other bacteria like *Listeria monocytogenes* acquire actin-based motility to spread between cells, this process was tested for *M.tuberculosis* (Cossart & Kocks 1994).

Using the social amoeba *Dictyostelium*, Hagedorn et al. showed that cytosolic *M.tuberculosis* and *M.marinum* can spread from cell to cell through an actin-based structure situated at the plasma membrane, the ejectosome (Hagedorn et al. 2009). However, mycobacteria seem to acquire actin tails only at the vicinity of the ejectosome.

Finally, the divergent results obtained by several group concerning phagosomal escape may be explained by differences in cell types, in Transmission Electron Microscopy (TEM) preparation techniques, in the multiplicity of infection, in the duration of cell activation, in the infection time and other factors (Welin & Lerm 2012). In any case, more investigation is needed to understand the precise function and context of phagosomal escape.

The importance of Autophagy in overcoming bacteria-induced phago-lysosomal arrest

Autophagy is a conserved process among eukaryotes in which a cytoplasmic cargo is captured within a double-membrane vesicle and delivered into the lysosome for degradation. Autophagosomes can sequester protein aggregates, large organelles and also micro-organisms (Levine et al. 2011). The interest in this process increased significantly since macrophage activation by IFN-γ was shown to induce autophagy in an LRG-47 dependent manner, and since autophagosome could fuse with lysosomes and overcome the phagosomal maturation arrest (Harris et al. 2007; Singh et al. 2006). Indeed, macrophage activation enhances the phagosomal localisation of the autophagosomal protein Beclin-1, thereby stimulating autophagy (Gutierrez et al. 2004). Interestingly Beclin-1 is a subunit of the phosphatidylinositol 3-kinase (PI3K) that is also a target for phagosomal arrest indicating that phagosomal maturation and autophagosome formation are closely linked.

Recently, IFN-γ-mediated autophagy was shown be dependent on the conversion of 25-hydroxyvitamin D to the bioactive 1,25-dihydroxyvitamin D, which induces the production and likely the phagosomal delivery of CAMPs such as cathelicidin (Yuk et al. 2009; Fabri et al. 2011).

Autophagy can be downregulated by the Th2 cytokines IL-4 and IL-13. However, their relevance in *M.tuberculosis* infection in vivo has not been assessed yet (Harris et al. 2007).

How does *M.tuberculosis* find its nutrient sources?

In the phagosomal environment, *M.tuberculosis* is subjected to constant attacks that limit its replication and elicit survival mechanism. These survival strategies are energy consuming and may require storage of nutrient sources for long-term survival. The first hint of such mechanism came from the genome of the best characterized strain of *M.tuberculosis*, H37Rv. Complete sequencing revealed that a large portion of its coding region is dedicated to the production of proteins and enzymes involved in lipogenesis and lipolysis, a feature that differs radically from other bacteria (Cole et al. 1998). The second cue came from the observation that the environmental challenges found in the phagosome trigger massive changes in mycobacterial gene expression including not only genes involved in adaptation to toxic environment but also genes involved in accumulation of nutrient resources (Daniel et al. 2011; McKinney et al. 2000; Pandey & Sassetti 2008; Rohde et al. 2007; Schnappinger et al. 2003). In consequence, while activated macrophages restrict the growth of intracellular pathogens by depriving them of essential nutrients, *M.tuberculosis* counteracts by using several host lipids as sources of carbon and energy (**Figure 1-5**) (Appelberg 2006). Such sources include host cholesterol, fatty acids and tryacylglerol (TGA) that are found in lipid droplets (**Figure 1-5**). For cholesterol import, *M.tuberculosis* encodes a gene cluster, *mce4*, required for the import of this important constituent of membranes. Interestingly, It seems to be a unique feature of mycobacteria as no other bacteria were shown to catabolise cholesterol. In consequence, bacteria reside predominantly in cholesterol-rich regions (Pandey & Sassetti 2008). To use fatty acids as a source of carbon, mycobacteria synthesize the isocitrate lyase (ICL), a glyoxylate shunt enzyme (McKinney et al. 2000). The glyoxylate shunt is a short-cut of the tricarboxylic acid cycle (TCA) that bypass the CO_2 generating step and allows the bacteria to synthesize carbohydrates from fatty acids (Bishai 2000). Finally, *M.tuberculosis* uses TGA from host cells after a complex sequence of events that first require the accumulation of lipid droplets.

The accumulation of lipid droplets in foamy macrophages is thought to be induced by the bacteria and to be dependent on bacterial oxygenated mycolic acids (MA) (Peyron et al. 2008). Lipid droplets are cytoplasmic lipid-rich organelles whose structure is composed of a neutral core and a phospholipid monolayer with a unique fatty acid composition (Tauchi-Sato et al. 2002). The neutral core contains triacylglycerol, cholesterol esters and diacylglycerol (D'Avila

et al. 2008). In foamy macrophages, the mycobacteria-containing phagosome and lipid droplets migrates towards each other. It was suggested that the host mediates this phenomenon as a defence mechanism. Indeed, it was hypothesized that accumulation of lipid droplets close to phagosomes is mediated in part by gp91phox, and that AA contained in lipid droplets can locally activate the NADPH oxidase.(van Manen et al. 2005). However, it was shown that, in the context of tuberculosis infection, lipid droplets constitute a nutrient-rich reservoir for *M.tuberculosis* persistence and not a threat. Mycobacteria were seen engulfed in lipid droplets accumulating intracytoplasmic lipid inclusions (ILIs) in a mechanism dependent on fatty acid import from lipid droplets TAG (Peyron et al. 2008; Daniel et al. 2011). Once fatty acids are incorporated, the mycobacterial triacylglycerol synthase (TGS) integrates them into triacylglycerols within ILIs for storage (Garton et al. 2002; Daniel et al. 2004). In consequence, mycobacterial TAG is thought to be a storage form of lipids for the long-term dormancy.

To find out which host signals triggered host lipid droplets formation, D'Avila et al. used a murine model of tuberculosis that revealed a TLR2-dependent mechanism in pleural macrophages (D'Avila et al. 2006). Interestingly, their study also pointed out an important link between eicosanoid metabolism, lipid droplets formation and bacterial pathogenicity (**Figure 1-5**). They demonstrated that lipid droplets compartmentalize substrates and key enzymes involved in eicosanoid synthesis such as the cyclooxygenase 2 (COX2). They suggested that lipid droplets, in activated macrophage, could constitute the predominant site for the synthesis of PGE2, a prostanoid that promotes protection against mitochondrial inner membrane perturbation and necrosis (Chen et al. 2008). However, *M.tuberculosis* activates the 5-lipooxygenase pathway to produce LXA4, an inhibitor of PGE2 synthesis, therefore enhancing necrosis and preventing apoptosis. Such feature then alter antigen cross-presentation by dendritic cells and subsequent activation of adaptive immunity (Divangahi et al. 2010).

Manipulation of host cell necrosis and apoptosis for mycobacterial spread

In the context of innate immunity, apoptosis is a mechanism that confines the cytoplasmic content of dying cells within membrane bound vesicles (apoptotic bodies) that are recognised by professional phagocytes. When apoptotic cells are infected with pathogens, clearance of apoptotic bodies leads to macrophages activation, inflammation and adaptive immunity. In that case, TLR and other PRR can sense the infection and trigger an immune response. In the contrary, necrosis is a traumatic cell death and *M.tuberculosis* exploits this mechanism of cell death to exit from macrophages and spread (Behar et al. 2011). Upon infection by *M.tuberculosis,* infected alveolar macrophages trigger apoptosis but the bacteria inhibits this mechanism thereby preventing antigen presentation by DCs and delaying the onset of adaptive immunity (Keane et al. 1997; Hinchey et al. 2007). Three mechanisms have been reported for the inhibition of apoptosis by the pathogen. First, as previously mentioned *M.tuberculosis* subverts the host eicosanoid biosynthetic pathway to favour necrosis over apoptosis (Chen et al. 2008; Divangahi et al. 2010). Second, *M.tuberculosis* uses a subunit of the bacillus type I NADPH-dehydrogenase, nuoG, to inhibit apoptosis and to increase virulence (Velmurugan et al. 2007). Third, *M.tuberculosis* prevents completion of the apoptotic envelope through proteolysis of annexin-1 which results in necrosis and subsequent dissemination of the infection in the lung (Gan et al. 2008).

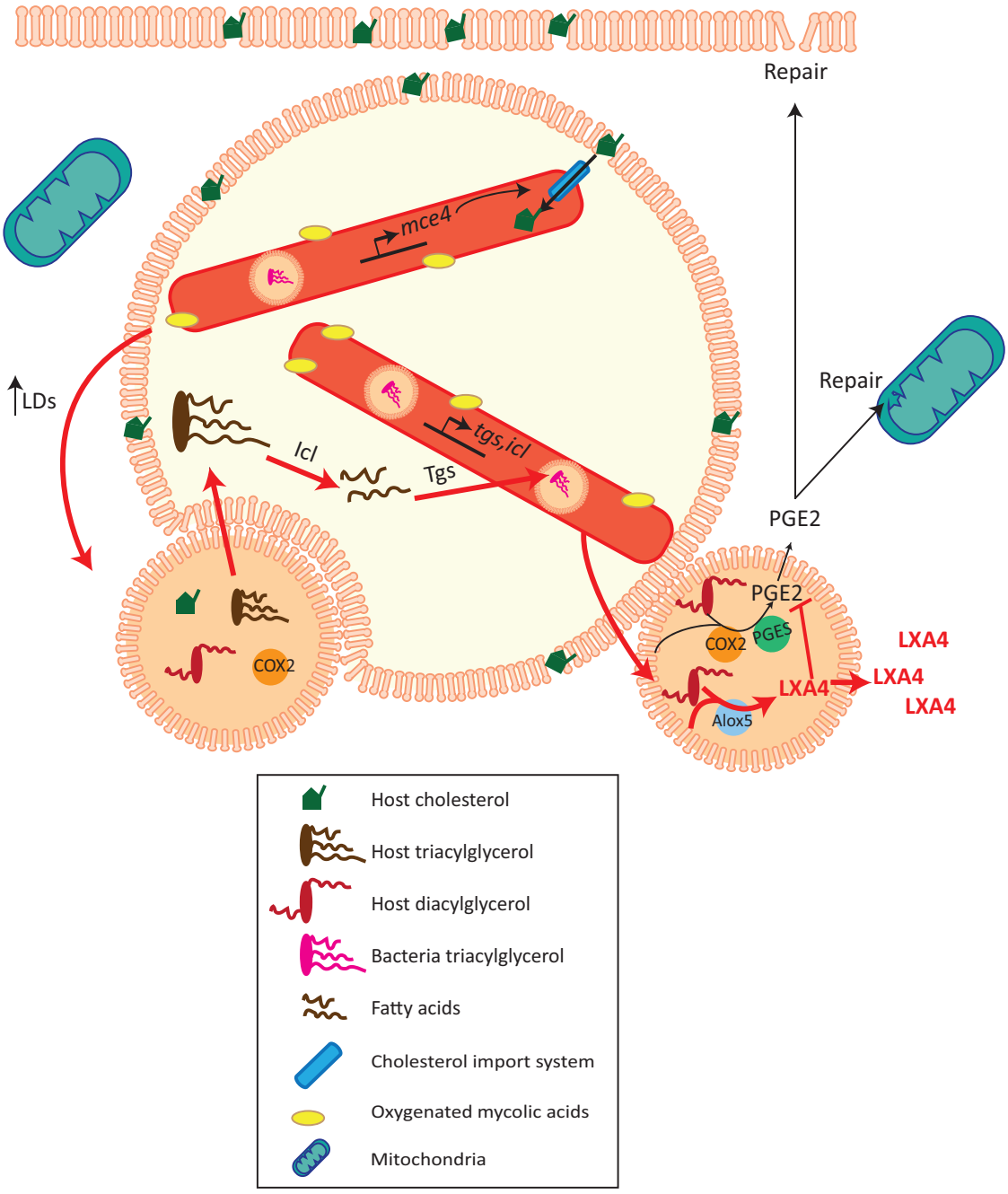

Figure 1-5: Intra-macrophage nutrient sources for *M.tuberculosis*

Upon macrophage activation, some macrophages at the centre of the granuloma accumulate lipid droplets and become foamy. It was shown that the bacteria trigger this accumulation to use host triacylglycerol contained in the lipid droplets as a source of fatty acids. Free fatty acids are then incorporated into the cytoplasm of the bacteria into intracytoplamic lipid bodies. These mechanisms are dependent on the action of several enzymes including the triacylglycerol synthase (TGS). Bacteria also synthesize carbohydrates from host fatty acids through the action of the isocitrate lyase (ICL). Lipid droplets are not only used as a source of nutrients but also as signalling molecules. Indeed, lipid droplets contain specific enzymes involved in eicosanoid synthesis that *M.tuberculosis* is able to divert to mainly produce LXA4. LXA4 antagonises the effect of PGE2 in repair of mitochondrial and plasma membrane micro disruptions, which is likely to favour necrosis. Finally, *M.tuberculosis* has also the ability to integrate and catabolize host cholesterol with the use of mce4, a cholesterol transporter. Alox5: Arachidonate 5-lipoxygenase; COX2: Cyclooxygenase 2; LDs: Lipid Droplets; mce4: mammalian cell entry gene 4; LXA4: lipoxin A4 ; PGE2: Prostaglandin E2.

1.1.4 Towards the discovery of new preventive and therapeutic treatments

TB treatments are still relying on a century old vaccine that has proven to be inefficient in preventing pulmonary TB, and on a toxic combination of drugs targeting mainly the highly replicative phase of *M.tuberculosis*. Such treatments have been inefficient in eradicating the bacteria and nowadays there are still 9 million new cases per year with a reservoir of 2 billion latently infected people (World Health Organization (WHO) 2011). The high economic burden associated with medical care and morbidity, urges the development of new preventive and therapeutic drugs. Such medications should aim to:

(1) Shorten treatment duration;

(2) Simplify treatment;

(3) Limit toxicity;

(4) Achieve complete eradication;

(5) Target efficiently multi-drug resistant strains;

(6) Being co-administered with immunoregulatory drugs.

So far, there are only few drugs that have entered the clinical pipeline and amongst these, only a tiny percentage can reach the last phases of clinical trials prior to commercialization. Currently, there are 10 drugs in the TB development pipeline: 6 in phase II and 4 in phase III trials (**Table**) (Zumla et al. 2013). Many new antibiotic candidates are molecules reengineered from previously discovered drug classes to improve their antimicrobial functions, their safety, their tolerability and their pharmacodynamics and pharmacokinetics properties. They belong to the class of the fluoroquinolones, the nitroimidazoles, the oxazolidinones and the 1,2-ethylene diamines (Koul et al. 2011). Other candidates were identified from phenotypic screen on the whole bacteria: diarylquinolines (TMC207), which target ATP synthesis, and benzothiazines (BTZ043) that are in pre-clinical development, and which target essential bacterial cell-wall arabinan synthesis (Koul et al. 2011; Andries et al. 2005). Both of these drugs target membrane-associated proteins. Phenotypic screens gave promising results and could be used to identify inhibitors or enhancers of validated metabolic or signalling pathways implicated in TB resistance. A particular interest would be to target mycobacterial nutrient resources and intra-mycobacterial homeostasis, especially in the

dormant phase of the infection. Indeed, there is an important need into developing more drugs from different classes to establish successful drug regimens and to increase the TB development pipelines (Koul et al. 2011).

Progresses have also being made in the development of new vaccine candidates. From an empty pipeline in the early 1990s, there are now 12 novel candidates that were improved from existing vaccines or that were newly discovered (Ottenhoff & Kaufmann 2012). Eight vaccines are actively in phase I/IIa trials and two of them are in phase IIb (**Table 1-1**). There are two main goals in the development of new TB vaccines: to replace the actual BCG vaccine by a recombinant BCG or a genetically attenuated *M.tuberculosis* strain, and to develop subunit vaccines in which recombinant *M.tuberculosis* proteins are mixed with proper adjuvants or with attenuated viral vectors.

For the attenuated vaccines, several strategies can be employed.

First, improvement of BCG can be made by introducing an immuno-dominant *M.tuberculosis* antigen that is absent from BCG such as the RD1 locus encoding ESAT-6 and CFP-10. Second, BCG vaccine can be engineered to improve targeting of essential immune pathways by facilitating antigen-presentation by DCs or by inhibiting phagosomal maturation arrest. Third, new vaccines can be generated from non-pathogenic mycobacteria such as *M.smegmatis* and by introducing virulent *M.tuberculosis* locus in their genome. Implement of *M.tuberculosis esx-3* locus in the *esx-3* mutant *M.smegmatis* was reported to be protective in a mouse model (Sweeney et al. 2011).

The challenge in designing new TB vaccine is to induce a strong response that target actively replicating bacteria and bacteria in dormant phase (therapeutic vaccines), and to induce protection to different bacterial strains in different ethnic and geographical groups (Ottenhoff & Kaufmann 2012).

Despite these improvements, more drugs and vaccines need to move from discovery to the development pipeline in order to increase diversity of treatments and to overcome the high drug rejection rate in clinical trials. The ultimate goal is the complete eradication of the pathogen from patient harbouring latent infection or active disease. However, there is also a need to identify specific biomarkers for protection and eradication to accelerate this process.

Candidate	Class	Type	Mode of action	Clinical Trial Phase
Drugs (from Zumla et al., 2013)				
Sutezolid/PNU100480	Oxazolidinone	Protein synthesis inhibitor	Inhibition of the formation of the translation iniation complex	II
AZD 5847	Oxazolidinone	Protein synthesis inhibitor	Inhibition of the formation of the translation iniation complex	II
SQ109	1,2-ethylene diamine	Cell wall and multi-target inhibitor	Inhibition of cell wall biosynthesis	II
Delamanid/OPC67683	Nitroimidazole	Cell wall and multi-target inhibitor	Produce microbicidal molecules such as NO and other RNI	III
PA 824	Nitroimidazole	Cell wall and multi-target inhibitor	Inhibition of cell wall biosynthesis	II
Moxifloxacin	Fluoroquinolone	DNA girase inhibitor	Inhibition of the topoisomerase ligase domain leading to DNA fragmentation	III
Gatifloxacin	Fluoroquinolone	DNA girase inhibitor	Inhibition of the topoisomerase ligase domain leading to DNA fragmentation	III
Bedaquiline/TMC 207	Diarylquinoline	ATP synthesis inhibitor	Depletion of the proton pump ATP synthase leading to imbalanced pH homeostasis	II
Rifapentine	Rifamycin	Transcription inhibitor	Inhibition of the beta subunit of RNA polymerase	III
Linezolid	Oxazolidinone	Protein synthesis inhibitor	Inhibition of the formation of the translation iniation complex	II
Vaccines (from Ottenhoff and Kaufmann, 2012)				
VPM 1002	Preventive	Recombinant BCG	Expression on listeriolysin and urease deletion	II
rBCG30	Preventive	Recombinant BCG	Expression of Ag85B	I
Oxford MVA85A/Aeras-485	Preventive	Viral-vector	Modified vaccina Ankara-expressing Ag85A	II
Crucell Ad35/Aeras-402	Preventive	Viral-vector	Replication deficient adenovirus 35-expressing Ag85A, Ag85B, TB10.4	II
AdAg85A	Preventive	Viral-vector	Replication deficient adenovirus 5-expressing Ag85A	I
Hybrid 1+IC31	Preventive	Fusion protein in adjuvant	Fusion of Ag85B and ESAT-6 in adjuvant IC31	I
Hybrid 56+IC31	Preventive	Fusion protein in adjuvant	Fusion of Ag85B, ESAT-6 & Rv2660c in adjuvant IC31	I
Hybrid 1+CAF01	Preventive	Fusion protein in adjuvant	Fusion of Ag85B and ESAT-6 in adjuvant CAF01	I
M72+AS01 or AS02	Preventive	Fusion protein in adjuvant	Fusion of Rv1196 and Rv0125 in adjuvant AS01 or AS02	II
Aeras-404: HyVac4+IC31	Preventive	Fusion protein in adjuvant	Fusion of Ag85B and TB10.4 in adjuvant IC31	I
RUTI	Therapeutic	Attenuated bacterial vaccine	Detoxified *M.tuberculosis* in liposomes	II
M.vaccae	Therapeutic	Attenuated bacterial vaccine	Inactivated *M.vaccae*	III

Table 1-1: *M.tuberculosis* drug and vaccine pipelines

1.2 New models for the study of *Mycobacterium*-host interaction

In this chapter, I will first present the limitations encountered with the traditional research models, and I will then describe the new host-pathogen models that led to recent major discoveries in the immunology of TB (**Table 1-2**).

1.2.1 Limitations of the traditional research models

Tuberculosis is a disease resulting from complex interactions between host immune responses and bacterial virulence. While our knowledge on the pathology has considerably increased over the past century, there are still many gaps that need to be filled in order to generate more efficient vaccines and drug treatments. Research on human patients is limited to the use of peripheral blood cells, patient biopsies and imaging techniques in conjunction with the study of genetic determinants. More invasive techniques are restricted for obvious ethical reasons and justify the need for experimental animal models. Early in tuberculosis research, animal models were instrumental for the discovery of the causative agent of tuberculosis. Indeed, Robert Koch used guinea pigs, rabbits, cows and apes that had developed spontaneous tuberculosis or tuberculosis from inoculated tubercles, to identify the infectious agent (Koch 1982). Several years later, he introduced a cure for tuberculosis, the mycobacterial-derived tuberculin, which was directly given to patients without prior official clinical trials. Regulations for testing medicines were inexistent at that time. While it was a remedy successful and safe in guinea pigs, humans were much more sensitive to it and subsequent deaths were reported. Koch himself experienced it and suffered from fever, shivering, nausea and intense pain (Gradmann 2001). Tuberculin was the centre of a huge scandal that tarnished Koch reputation and showed that despite the interest of animal models, researchers should be cautious in interpreting results from them. But even though the prospects for tuberculin treatment were bad, it is successfully used nowadays as a diagnostic test, the tuberculin skin test.

Originally, guinea pigs and non-human primates were used as experimental models and they are still frequently used for pre-clinical studies. Tuberculosis in guinea pigs and non-human primates have similar features to the human infection with complex innate and adaptive immune responses and similar granulomatous lesions (Kaufmann 2003). As an example, these models were successfully used to determine the oxygen tensions within the granuloma and to support the hypothesis that the hypoxic environment is an important feature of granulomatous lesions (Via et al. 2008). Cattle have also been established as a model for vaccine development against human tuberculosis (Hewinson et al. 2003). If the use of these animals has proven to be useful in drug testing, it is limiting in more fundamental research due to the cost and the lack of availability of genetic and immunological tools. In consequence, researchers have looked for animals that would allow studying patho-physiology and cellular immunity by using cutting-edge imaging techniques and by performing forward and reverse genetic screens to identify host determinants and bacterial virulence factors.

The most popular model, the inbred mouse, has led to the identification of several conserved immune mechanisms that helped understanding the pathology of TB in humans. The availability of genetic techniques such as conditional and constitutive gene knock-out and knock-in, together with availability of the full genomic sequence allowed the discovery of host determinants in pathology that were later verified in humans. For example, susceptibility in IFN-γ, IL-12, TNF-α and $CD4^+$ T cells mutants in mice were verified in humans with hereditary deficiency in IFN-γ, IL-12, with anti-TNF treatments or with HIV infection, which dramatically reduces the availability of $CD4^+$ T cells (Kaufmann 2003). BCG-infected mice also revealed the importance of IFN-γ and LRG-47 in stimulating autophagy, a process that could explain the restoration of mycobacterial killing in activated macrophages (MacMicking et al. 2003; Gutierrez et al. 2004). Later, the importance of LRG-47 was corroborated in human macrophages (Singh et al. 2006). However, there are major differences in the mouse model compared to humans. For example, mice develop disorganised, multi-bacillary, non-necrotic and non-caseating lesions rather than the organised, paucibacillary, caseous granulomas observed in human TB (Pozos et al. 2004). There are also differences in antigen presentation and in the importance of NO-mediated killing (Liu & Modlin 2008; Orme 2003). Despite the broad repertoire of immunologic reagents and assays and the facility of generating germ-line mutations, the mouse model is limited by the difficulty of forward genetic and phenotypic screens and by the lack of

crucial hallmarks of human tuberculosis. Moreover, various studies in mice used BCG as a model of tuberculosis, while it was shown to lack one of the main *M.tuberculosis* virulence locus, RD1, that could also explain major differences in the course of infection (Volkman et al. 2004).

In addition to the mouse model, there is extensive use of human cell lines to decipher cell immune mechanisms important in TB. They have been very important in identifying key molecules involved in resistance mechanisms and in host evasion strategies. Most of them are presented in the previous sub-section. Researchers have tried to culture the cell in an environment close to the one encountered in vivo such as hypoxic stress; they also developed artificial granuloma models to understand key molecular events (Daniel et al. 2011; Schnappinger et al. 2003; Puissegur et al. 2004). However, cell culture models do not fully recapitulate what is happening in vivo in the human host such as timing of infection, constraints of the environment and multiple stimulations.

Although mouse model and human cell cultures remain commonly used, there is an increasing interest in alternative models for selected aspects of the host-pathogen interactions that are difficult to assess in traditional models.

1.2.2 New host-pathogen models

Recently, *Dictyostelium discoidum*, *Drosophila melanogaster* and zebrafish were used as model hosts in infection with *Mycobacterium marinum*, a close relative of *M.tuberculosis* that is a natural pathogen of ectothermic vertebrates (Pozos et al. 2004; Tønjum et al. 1998). These hosts have shown to be very valuable for forward and reverse genetic screens, for in vivo analysis through intravital imaging and for the ability to generate RNAi. They have led to major discoveries such as the role of coronin-1 in preventing phago-lysosomal fusion, the role of the RD1 locus in macrophage recruitment and spreading, the role of macrophages in early dissemination and in granuloma formation prior to the development of adaptive immunity, and the role of the mycobacteria-induced changes in insulin signalling and wasting (Solomon et al. 2003; Davis et al. 2002; Davis & Ramakrishnan 2009; Dionne et al. 2006).

***M.marinum,* a new model pathogen**

M.marinum is a pathogen of fish and frogs causing a chronic and progressive disease that mainly affects the liver, kidney and spleen. The transmission route is poorly understood, however, infections trigger the formation of granulomas that can present central caseous necrosis similarly to *M.tuberculosis* in humans. *M.marinum* can cause a disease in humans: “the fish tank granuloma” or the “swimming pool granuloma”, which results in a skin granuloma in extremities where *M.marinum* is at its optimal temperature for growth, 25-35˚C (Stamm & Brown 2004). The disease rarely spreads, and dissemination was only observed in immunocompromised patients (Parent et al. 1995). *M.marinum* is then considered safe for use in healthy individuals under biosafety level 2.

The recent sequencing and assembly of *M.marinum* genome revealed orthology for 80% of coding regions in *M.tuberculosis* and an average amino acid identity of 85% (Stinear et al. 2008). This analysis combined with a previous report on mycobacterial species relationship based on 16S rRNA, DNA-DNA hybridization and fatty acid profile, suggested that *M.marinum* is the closest genetic relative to the *M.tuberculosis* complex and derived from a common ancestor (Tønjum et al. 1998). The size of *M.marinum* genome is about 1.5 times the size of *M.tuberculosis* genome probably reflecting genome loss due to lower range of hosts and environments. In addition, 14% of the *M.tuberculosis* genome is not shared with *M.marinum* indicating that some genes were most likely integrated by horizontal transfer (Tobin & Ramakrishnan 2008; Stinear et al. 2008).

Some key features of *M.tuberculosis* are conserved in *M.marinum* infections:

(1) Inhibition of phagosome-lysosome fusion;

(2) Requirement of PE-PGRS domain proteins for full virulence;

(3) Synthesis of a complex cell-wall conferring pathogenicity;

(4) Importance of the RD1 chromosomal region that encodes a secretion system necessary for ESAT-6 and CFP-10 pathogenic functions in cytolysis, dissemination and control of inflammation (Stamm & Brown 2004).

Two mutant screens have been performed for the identification of *M.marinum* virulence genes involved in macrophage infection, survival and proliferation in vitro, and in vivo survival using goldfish as a model. They revealed that 70-85% virulence determinants in *M.marinum* had homology with *M.tuberculosis* (Ruley et al. 2004; Mehta et al. 2006). Also, using a transposon-site hybridization (TRASH), Rubin et al. identified 126 genes required for intra-macrophage survival and 194 genes required for in vivo growth of *M.tuberculosis.* Only 3% were in *M.tuberculosis*-specific regions absent from *M.marinum* (Rengarajan et al. 2005; Sassetti & Rubin 2003; Tobin & Ramakrishnan 2008). Therefore, the genomic sequence and the virulence screens strongly suggest that *M.marinum* is an interesting model for deciphering *M.tuberculosis* pathogenic mechanisms.

M.marinum also has additional functions related to its broader range of hosts and environments. First, it is photo-chromogenic and appears yellow under light. The expression of pigmented molecules like carotenoids is associated with UV resistance and may be required for adaptation to an aquatic environments and for stress resistance during infection (Stamm & Brown 2004; Ramakrishnan et al. 1997). Second, it was found that *M.marinum* can escape from the phagosome and acquire actin-based motility for direct cell-to-cell spread, a trait that is dependent on haemolytic activity, and on ESAT-6 secretion (Stamm et al. 2003; Gao et al. 2004). Recent findings suggested that it could happen in *M.tuberculosis* infection following phagosomal rupture (Hagedorn et al. 2009; Simeone et al. 2012). However, despite the broad acceptance that *M.marinum* escape from the phagosome is part of its pathogenicity, such feature remains controversial for *M.tuberculosis*, especially because it was never observed in vivo. In addition, despite the formation of the ejectosome, *M.tuberculosis* does not seem to acquire actin tails for propagation (Stamm & Brown 2004).

Dictyostelium discoideum, a macrophage surrogate

Many non-pathogenic mycobacteria live in the soil together with the phagocytic and motile amoeba. Their close proximity let researchers imagined that pathogenicity may have emerged from adaptation to an intracellular lifestyle within free-living protozoa in the environment. An interesting model to study intra-macrophage immune mechanisms is the amoeba *dictyostelium discoideum.* In this organism, genetic studies are facilitated by the fact

that they have a haploid genome. Consequently, major discoveries have been initiated from studies in this organism such as the role of coronin-1 in inhibition of phagosome-lysosome fusion, and novel dissemination strategies for *M.tuberculosis* (Ferrari et al. 1999; Hagedorn et al. 2009).

Zebrafish, natural hosts for *M.marinum*

Zebrafish is a natural host for *M.marinum*. In addition to innate immunity Zebrafish have a complex adaptive immune system similar to mammals. For the first 3 weeks of their development, zebrafishs are optically transparent and possess fully competent macrophages. After that, adaptive immune cells can migrate from their development site, the thymus, to the infection sites. This feature allows the separate study of innate immunity from adaptive immunity.

Several major mechanisms for granuloma formation were discovered in the zebrafish. First, after *M.marinum* injection in the caudal vein, bacteria are phagocytised by macrophages which therefore expressed iNOS , TNF-α and IL-1β (Clay et al. 2007). As a result, macrophages extravasate into tissues and aggregate to form an ESX-1 dependent granuloma-like structures prior to the onset of an adaptive immune response (Lesley & Ramakrishnan 2008; Tobin & Ramakrishnan 2008). Second, imaging techniques have revealed that non-infected macrophages are attracted to the granuloma-like structure, get infected and and disseminate from the primary site to form other infection site (Davis et al. 2002; J. M. Davis & Ramakrishnan 2009). The finding that a virulent factor, ESX-1, can drive granuloma formation suggested that even if protective, the granuloma is subverted by mycobacteria for their dissemination. Third, following lymphocyte recruitment, the granuloma matures and becomes caseated (Lesley & Ramakrishnan 2008; Pozos et al. 2004). Strikingly, upon reinfection, newly injected bacteria can migrate into caseated granulomas, proposing that this structure may not be as impermeable as previously thought (Cosma et al. 2004).

These recent studies in zebrafish have pointed out the importance of innate immunity in protection against TB and the necessity to understand macrophage immunity prior to T lymphocyte priming.

Drosophila melanogaster, a genetically tractable animal host

Drosophila melanogaster is an established model for innate immune responses since the discovery of the drosophila gene Toll and later identification of mammalian Toll-like receptors (TLRs) (Lemaitre et al. 1996; Lemaitre 2004). *Drosophila* does not possess adaptive immunity, which then allows the examination of innate immune functions in isolation. *Drosophila* offers a unique advantage for forward and reverse genetic studies, RNA interference and in vivo screens; it has been used as a model for various infections (Dionne & Schneider 2008). Upon infection with *M.marinum*, the bacteria is rapidly phagocytosed into Drosophila phagocytes and arrests phagosomal maturation similarly to *M.tuberculosis* in mammals (Dionne et al. 2003). *M.marinum* does not activate NF-kB pathways and antimicrobial peptide responses (AMPs) suggesting that intracellular microbicidal mechanisms may be more relevant for controlling the initial proliferation of bacteria (Dionne et al. 2003; Lemaitre & Hoffmann 2007). In addition, this model led to the identification of host factors deregulated upon infection, AKT and FOXO, which contribute to the infection-induced wasting (Dionne et al. 2006).

Model host	Model bacteria	Advantages	Limitations	Recent Major discoveries	Authors
Human cells	*Mtb, BCG, Mm, M.avium*	Assessment of intracellular defence mechanisms and environment; Development of an in vitro granuloma model.	Relevance in vivo;	Requirement of the proteasome for oxydative stress resistance Role of autophagy in immune defenses against Mtb Toll-dependant selection of microbial antigens for presentation by DCs Foamy macrophages are nutrient-rich reservoirs for Mtb Eicosanoids regulate adaptative immunity in Mtb	Darwin et al., 2003 Gutierrez et al., 2004 Bander et al., 2006 Peyron et al., 2008 Divangahi et al., 2010
Mice	*Mtb, BCG*	Innate immunity and adaptive immunity similar to humans; Reverse genetics available; Pool of transgenic mice accessible; Availability of immunologic reagents.	Forward genetic screen is difficult; Contrary to humans, progressive multi-bacillari non-caseating granuloma; No latency; Lacks RD1 locus; Relevance to human Mtb infection.	Persistence requires the glyoxylate shunt enzyme ICL IFN-γ induces LRG-47 Transcriptional adaptation of Mtb within macrophages DnaE2 polymerase mediate survival through inducible mutagenesis BCG induces TLR2-mediated formation of lipid droplets Initiation of adaptive immunity depend on antigen production in local lymph node, not the lung	McKinney et al., 2000 McMicking et al., 2003 Schnappinger et al., 2003 Boshoff et al., 2003 D'Avila et al., 2006 Wolf et al., 2008
Guinea Pigs, non-human primates, Cattle, Rabbits	*Mtb*	Test for human vaccination and drug treatments; Major features are conserved: organised, pauci-bacillary and caseating granuloma.	Different to human Mtb infection; Differences in drug toxicity, efficacy.	Tuberculous granuloma are hypoxic Mtb mutation rate is maintained during latency	Via et al., 2008 Ford et al., 2011
Dictyostelium	*Mm*	Assessment of intracellular defence mechanisms and environment; Haploid genome.	Relevance in vivo; Relevance to humans.	Coronin-1 retention on phagosomes prevent lysosomal delivery Mycobacteria can spread by non-lytic injection, using the ejectosome	Ferrari et al., 1999 Hagedorn et al., 2009
Zebrafish	*Mm*	Study of innate immunity separately from adaptive immunity; Imaging techniques through transparent zebrafish early in development; Similar granuloma as humans; Reverse and forward genetic screens; Pool of transgenic zebrafish accessible.	Relevance to human Mtb infection.	Superinfecting mycobacteria home to established tuberculous granuloma Mtb use macrophages to disseminate despite their control of bacterial growth Role of granuloma in expansion and dissemination in early infection	Cosma et al., 2004 Clay et al., 2007 Davis et al., 2008
Flies *(Drosophila)*	*Mm*	Study of innate immunity in isolation; Reverse and forward genetic screens; Extensive mutant, RNAi library; In vivo screens.	No adaptive immunity; No granulomas; Relevance to human Mtb infection.	Mycobacteria-induced wasting is dependant on Akt and foxo dysregulation	Dionne et al., 2006

Table 1-2: Model hosts for *M.tuberculosis* infection in humans

1.3 *Drosophila melanogaster*, a model to study innate immunity

In this chapter, I will first describe the emergence of *Drosophila* as a genetic tool and as a model for several fields of research. I will then present the different organs and pathways involved in the immune response to infection.

1.3.1 *Drosophila,* the golden genetic tool

The notion of genetics was initiated in the mid 19th century by the work of Gregor Mendel, who observed that inheritance of specific traits follows a specific mathematical pattern. He presented his results in 1865, but he was only acknowledged for his discovery in the 20th century when other scientists working on similar issues re-discovered his work. The Mendel's law on inheritance and the additional work on heredity from William Batson, Hugo de Vries, Carl Correns and Thomas Hunt Morgan contributed to the core of classical genetics before the advent of molecular biology. Thomas Hunt Morgan received the Nobel Prize in Physiology and Medicine in 1933 for his discoveries relative to the role of chromosomes in heredity. He was one of the first scientists to use *Drosophila melanogaster* as a model organism. In his famous fly room at Columbia University, he generated mutants through physical and chemical means and identified the recessive white-eyed mutation. Together with the study of other mutants, he established a hypothesis on sex-linked traits and on the phenomenon of crossing over. Because of his success with *Drosophila*, many laboratories around the world started to use this organism as a model. For the past 100 years, the *Drosophila* community progressively expanded concomitantly with the number of publications (**Figure 1-6**). Transcending its first use in genetics, *Drosophila* has been widely exploited for developmental biology and neurology and is now a model to study innate immunity (**Figure 1-6**).

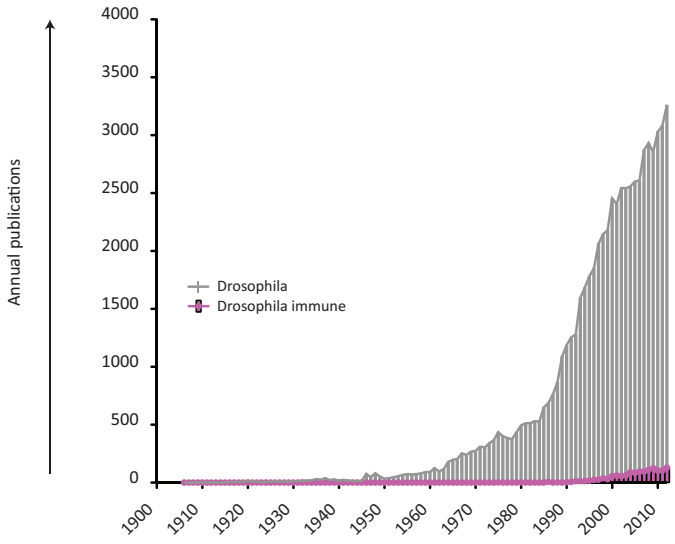

Figure 1-6: Annual publications on *Drosophila*

Annual publications listed on PubMed that include "*Drosophila*" in the title or abstract (grey). Publications on *Drosophila* immune responses, that include "*Drosophila*" and "immune" in their title or abstract, are relatively recent and represent less than 200 papers in 2012 (pink) (Figure made from the annual PubMed publication data).

Drosophila researchers benefit from a vast number of resources (sequencing project, gene disruption projects, RNA-sequencing) and comprehensive databases for developmental features, gene expression pattern and genetic or protein-protein interactions (**Table 1-3**). Together with a policy of free exchange of material and information among the community, it is a great stimulus for *Drosophila* research that is responsible for many important contributions.

Resource	Purpose	Providers
Flybase	First repository for of genetic and molecular data on Drosophilidae	Harvard University; University of Cambridge; Indiana University; University of New Mexico
Bloomington stock center	Collection, maintenance and distribution of *Drosophila* strains	Indiana University
BDGP	Sequencing the euchromatic genome of *Drosophila*, gene disruption, gene expression	University of california, Berkeley; Lawrence Berkeley National Laboratory, Carnegie Institution of Washington, Baylor College of Medicine
DGRC	Collection and distribution of DNA clones, cell lines, microarray support, assistance, developping and testing emerging genomics technologies	Indiana University
VDRC	Vienna Drosophila RNAi Center	Campus Vienna Biocenter.
The interactive fly	Cyberspace guide to *Drosophila* development and metazoan evolution	Thomas B. Brody
DroID	Gene and protein interaction database for *Drosophila*	Finley laboratory
FlyAtlas	Gene expression profile	Venkat Chintapalli, Jing Wang, Julian Dow at the University of Glasgow

Table 1-3: Example of available *Drosophila* resources

Representative, but non-exhaustive, view of available tools to *Drosophila* researchers.

The sequencing of the *Drosophila* genome is now complete and revealed a genome encoding around 13600 genes in four different chromosomes with 5536 genes duplicated and 8065 distinct gene families (Rubin et al. 2000; Adams et al. 2000; Smith et al. 2007).

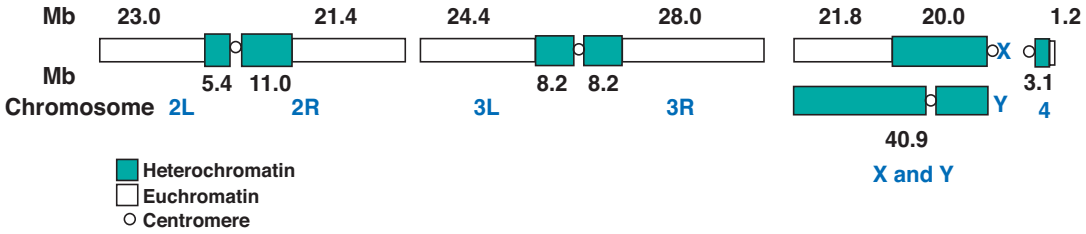

Figure 1-7: The four *Drosophila* chromosomes

Schematic representation of mitotic chromosomes of *D.melanogaster*. The arms of the autosomes are designated by a chromosome number and their position relatively to the centromere: 2R, 2L, 3R, 3L, and 4. The euchromatic length is derived from the sequence analysis, while the heterochromatic length was deduced from the total chromosome length. The X and Y chromosome are peculiar. The Y chromosome is almost entirely heterochromatic while the X chromosome heterochromatin block is highly variable. Figure adapted from (Adams et al. 2000).

Interestingly, 60% of human disease-associated genes have an ortholog in the fly. Among these orthologs, genes involved in intracellular metabolic pathways are highly represented (Rubin et al. 2000). When these genes are disrupted in *Drosophila,* they often cause human-like diseases such as neurological disorders, cardiovascular disorders, developmental disorders, metabolic dysfunctions, cancer and immune diseases. Some of the human disease genes that are absent in the fly are linked to differences in physiology between the two organisms. For example, the fly is an invertebrate organism with an open circulatory system and with only an innate immune system; so disease-associated genes implicated in adaptive immunity will not have equivalents in the fly. When using *Drosophila* as a model, researchers do not expect to recreate similar disease as in humans; the important point is to recapitulate specific aspects of the disease that could help deciphering uncharacterized mechanisms.

Usually, the tools in use are:

(1) Mutant line screens with second site modifiers screens that enhance or suppress the starting point phenotype;

(2) Inducible tissue-specific RNAi through the Gal-4/UAS system from the yeast;

(3) Use of immunofluorescent lines for dissected organs or live-imaging.

What makes *Drosophila* different from other organisms is not only the ease to generate transgenic animals, the low maintenance cost and quick generation time, but also the availability of balancer chromosomes. H.J Muller invented balancers in 1918, when he identified the chromosome C1B as a suppressor of exchange on the X chromosome. It allowed him to isolate new X-linked lethal mutations (Greenspan 2004). Balancer chromosomes are modified chromosomes that prevent crossing-over during meiosis, thereby allowing the conservation of invisible recessive mutations without constant screening. This is of particular interest when one considers the rate of crossing-over among animals, especially *Drosophila*. Balancer chromosomes are the product of multiple nested chromosomal inversions and exist on the X, second and third chromosome but not on the fourth chromosome. Balancers are usually recessive lethal and were engineered to carry a marker mutation. Of particular interest, they allow the construction of breeding stocks from homozygous lethal mutations.

A rapid life cycle convenient for research

Flies are yellow-brown with red eyes. Their life cycle varies depending on the temperature. They are usually raised at 25˚C and their development into adulthood takes up to 10 days. Female are generally courted by multiple males that play a courtship song through vibration of their wings. After mating, they start to lay their eggs into rotting fruits of decaying material. The embryos soon hatch and become larvae that progressively grow until being encapsulated into the puparium for metamorphosis (**Figure 1-8**). After emergence, the adult flies can live up to 2 ½ months at 25˚C. Males and females exhibit sexual dimorphism and interestingly, males do not show meiotic recombination. This specificity is largely used to generate new mutant lines. In terms of anatomy, flies have an open circulatory system in which organs are in contact with the hemolymph, a fluid that contain water, inorganic salts, and organic compounds. They possess a heart-like organ, the dorsal vessel made of pericardial

cells; a respiratory system, the trachea; a liver-like organ, the fat body; a compartmentalized digestive system, the gut; and a brain widely used to study neurological development and functions.

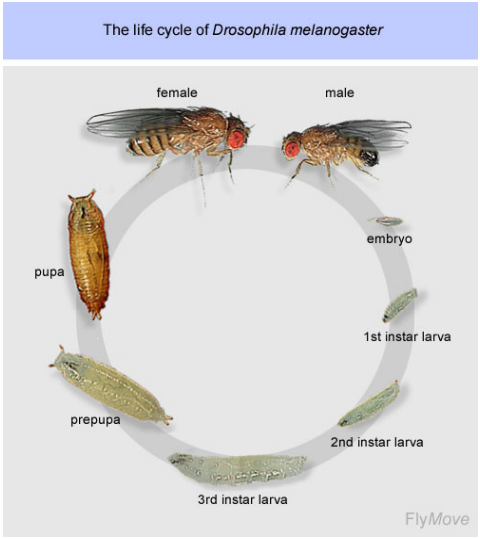

Figure 1-8: Life cycle of *Drosophila melanogaster*

After mating, females lay their eggs in decaying material. The embryos develop and hatch, giving rise to first instar larvae. The larvae grow progressively until reaching a pupariation stage in which they undergo massive tissue remodelling. Upon completion, the adults emerge and males and females exhibit a sexual dimorphism. Figure taken from Flymove (http://flymove.uni-muenster.de).

A model for innate immunity

Insects have a sophisticated immune system involving cellular immunity and humoral immunity with secretion of antimicrobial peptides and presence of serine proteolytic cascade in the hemolymph. *Drosophila* is not a vector of human or plant diseases; in consequence natural pathogens have not been intensively studied. Instead, most of the infectious models are not natural pathogens and are injected in the abdomen or ingested from contaminated food. The wide range of pathogens used for study in immunity include extracellular bacteria such as *Escherichia coli* and *Micrococcus luteus*, intracellular bacteria such as *Listeria.monocytogens* and mycobacteria, fungi, parasites, and viruses.

The next subsections will present the different organs implicated in innate immunity and the major innate immune pathways.

1.3.2 The immune organs

The fat body is one of the major immune tissues in the fly. It was described as an analogue to the mammalian liver due to the presence of specific markers: the alcohol dehydrogenase and the yolk proteins that have homology to the lipases found in mammalian liver and pancreas (Søndergaard 1993). The fat body is flanked by adipocytes which origin lies in the mesoderm. They are distributed throughout the flies to allow the rapid release of secreted peptides into the hemolymph (Lemaitre & Hoffmann 2007; Lawrence & Johnston 1986). Upon injection of bacteria in the body cavity, the fat body responds by secreting various molecules among which the antimicrobial peptides (AMPs) are the best characterized. About 20 inducible AMPs have been identified. They are small cationic peptides that are very effective against $Gram^-$ bacteria (Diptericin, Drosocin, Attacin), or against $Gram^+$ bacteria and fungi (Defensin, Drosomycin, Metchnikowin). AMPs have been intensively studied in *Drosophila* and they constitute one of the major and more powerful lines of defence against various pathogens. However, recent studies have highlighted the complexity of the immune responses in insects. Indeed, upon infection, the fat body not only releases AMPs but also immune effectors that participate in various processes. An example is Turandot A, a stress peptide upregulated by the JAK-STAT pathway downstream of the ligand Upd3, a cytokine secreted by the fly blood cells (Agaisse et al. 2003). Recently, the works of several laboratories suggest that the fat body modulates the secretion of proteins involved in a complement-like system. The opsonin-like molecule TEP1, a thioester-containing protein with similarities to the complement C3/α2-macroglobulin superfamilies, is released upon JAK-STAT and Toll activation (Lagueux et al. 2000; Agaisse et al. 2003). It may function together with an immunoglobulin (Ig)-superfamily receptor, the Down syndrome cell adhesion molecule (Dscam). Immune-competent cells are also able to release more than 18 000 isoforms of Dscam and their function in phagocytosis was confirmed using *E.coli* (Watson et al. 2005). Little is known about the precise function of the different isoforms but they suggest an unsuspected molecular complexity of the innate immune system in insects.

To evaluate the extend of immune peptides in the hemolymph, researchers have performed extensive large-scale analysis at the transcriptome and proteome levels to identify peptides upregulated upon challenge in larval and adult flies (De Gregorio et al. 2001; Irving et al. 2001; Boutros et al. 2002; Vierstraete et al. 2003; Vierstraete et al. 2004; Levy et al. 2004).

At steady state, the hemolymph contained proteases and proteases inhibitors, serpins, prophenoloxydase-activating enzymes and molecules with potential immune functions such as odorant-binding proteins and peptidoglycan. Upon immune challenge, several immune-induced effectors are increasingly found in the hemolymph. They include catalases and transferrin that are implicated in ROS formation/detoxification and iron sequestration respectively (Levy et al. 2004).

The fat body contributes largely to the pool of toxic peptides present in the hemolymph and constitutes a major line of defence against invaders (**Figure 1-9**). However, the trachea and the gut, two natural routes of infection, are constantly challenged by pathogens and may have acquired mechanisms to contain the infection and prevent the systemic release of microorganisms in the circulation (**Figure 1-9**). Indeed, it was shown that they secrete various toxic molecules such as ROS, AMPs and lysozymes to kill invaders (Lemaitre & Hoffmann 2007). Strikingly, AMPs are produced constitutively in the epidermis, the respiratory tract and the reproductive and digestive systems, which are constantly prone to infection. Another interesting point is that, *Drosomycin,* which is normally regulated by the Toll pathway during the systemic response, is regulated by the Imd pathway in the respiratory tract indicating that they are distinct regulatory mechanisms for local and systemic immunity (Tzou et al. 2000; Ferrandon 2009). Natural infections in the gut also induce a strong ROS response that is under the control of the *Drosophila* dual oxidase (dDuox), a NADPH oxidase enzyme (Ha et al. 2005). Silencing of Duox resulted in blocked ROS expression and mortality upon *Erwinia carotovora carotovora-15 (Ecc15)* infection, indicating that this enzyme may be the unique source of epithelial ROS. Interestingly, NF-kB mutants were resistant to such infection suggesting that ROS may represent the most critical immune strategy in the gut.

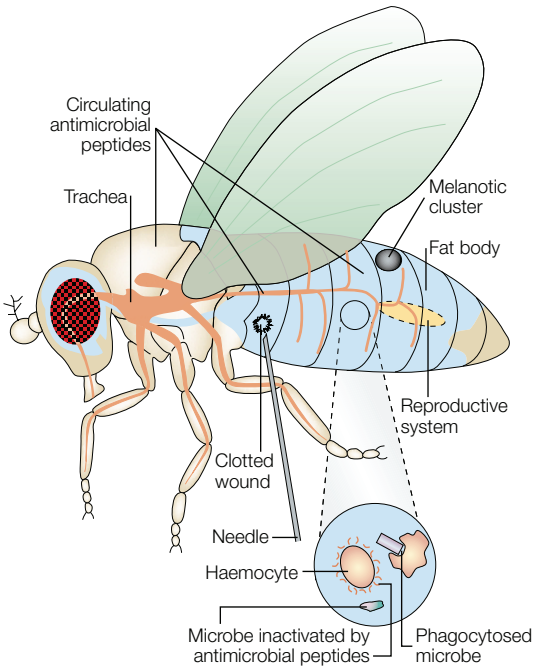

Figure 1-9: Innate immune tissues in *Drosophila*

The hallmark of *Drosophila* innate immunity is the secretion of antimicrobial peptides from the fat body (in blue), analogueous to the mammalian liver. Some tissues, such as the trachea (orange), the reproductive system and the gut, respond to local aggressions by secreting AMPs and/or ROS. The cellular immune response in adult fly is limited to sessile plasmatocytes that are attached to tissues. Adult plasmatocytes derive from embryonic and larval hemocytes and are most likely composed of different subsets with differential AMP and cytokine expression. Melanotic clusters form locally at wounding sites and more generally in response to infection. Figure adapted from (Kimbrell & Beutler 2001).

The epithelium can also have a role in immune defences through the processes of coagulation and melanisation. Upon injury, clotting is critical to prevent hemolymph loss and is initially formed of fibres that trap blood cells. Progressively, melanisation and epithelial movements close the wound trapping and thus immobilizing bacteria (Scherfer et al. 2004). Specific proteins participate in clotting such as hemolectin, a phagocyte-specific factor, and fondue, an abundant hemolymph protein regulated by Toll (Scherfer et al. 2006; Goto et al. 2001). In the last step, the wound closure requires a specific blackening reaction called melanisation that results in melanin deposit at the site of injury (**Figure 1-9**). In embryos and larvae, this process is partly mediated by specific blood cells, the crystal cells, that express proPO, an enzyme involved in melanin synthesis (Lemaitre & Hoffmann 2007).

Melanisation plays a role not only in wound healing but also in encapsulation and sequestration of microorganisms. Upon Gram$^-$ infection, bacteria induce the proteolytic cleavage of PGRP-LC, a PRR binding DAP-type peptidoglycan, which regulates melanisation (Schmidt et al. 2008). Its role in innate immunity was further demonstrated by Ayres et al. who showed that a mutation in CG3066, a gene encoding a protease active in the melanisation cascade, induced changes in tolerance and resistance after challenge with a wide range of pathogens (Ayres et al. 2008).

Finally, the hemolymph of larvae and adult flies contains a vast number of blood cells that constitute a powerful cellular immune defence mechanism for the eradication of intracellular and extracellular pathogens. Their development and functions are presented below.

1.3.3 The myeloid cells

Drosophila has three blood cell types characterized by their structure and function: the plasmatocytes, the lamellocytes and the crystal cells. The plasmatocytes represent 90-95% of the whole population and participate in the removal of microbes and dead cells; the lamellocytes are large and flat cells that encapsulate invaders that are too big to be phagocytosed; crystal cells are non-phagocytic cells that contribute to the melanisation process by storing large amount of proPO. Although these three cell types are motile and functional in larvae, adult flies carry only sessile plasmatocytes that are attached to tissues, and that are simply named hemocytes.

Hematopoiesis, a two-wave process giving rise to several blood cell types

Hematopoiesis occurs in two waves, one at the embryonic stage and another one at the larval stage (**Figure 1-10**). Embryonic hemocytes derive from the cardiogenic mesoderm and give rise to a fixed number of hemocytes. Among them, are plasmatocytes that have migrated from the head throughout the embryo and a small number of crystal cells that remain around the proventriculus, an anterior structure of the midgut (Tepass et al. 1994; Lebestky et al. 2000). A portion of mesodermal cells from the head migrates dorsally alongside vascular progenitors to form a dedicated organ, the lymph gland. The lymph glands develop progressively during larval

stages and were thought to be the major source of larval hemocytes. However, this idea has been recently challenged and it was demonstrated that lymph glands do not release hemocytes before metamorphosis. Instead, lineage analysis of transplanted cells, confirmed that embryonic hemocytes are maintained in the hemolymph of larvae and proliferate, constituting the pool of circulating blood cells (Holz et al. 2003).

The fully mature lymph gland is organised in primary and secondary lobes flanked mostly with immature hemocytes (**Figure 1-10**). The primary lobe is compartmentalised into a medullary zone with hemocyte precursors, a cortical zone with proliferating and maturing hemocytes, and a post-signalling centre (PSC) that controls cell differentiation (Jung et al. 2005). The PSC controls the balance between multipotent pro-hemocytes and differentiating hemocytes by maintaining JAK-STAT signalling activity in pro-hemocytes. Upon immune challenge, such as wasp parasitisation, JAK-STAT signalling is interrupted by a non-signalling JAK-STAT receptor, Latran, and pro-hemocytes transform into lamellocytes to encapsulate the large wasp eggs (Makki et al. 2010; Krzemień et al. 2007). In addition to JAK-STAT signalling, the Toll pathway has also been implicated in hemocyte proliferation and differentiation (Qiu et al. 1998).

At the onset of pupariation, most pro-hemocytes differentiate into mature hemocytes and the lymph gland disintegrates liberating the blood cells into the circulatory system. Interestingly, mature hemocytes participate in metamorphosis by ingesting and digesting doomed larval tissues (Lanot et al. 2001). After emerging, the adult possesses only sessile plasmatocytes that derived from larval and embryonic hemocytes suggesting that there might be different subsets (**Figure 1-10**) (Holz et al. 2003; Crozatier & Meister 2007). Indeed, this idea was further proposed by Clark et al. , who showed that adult plasmatocytes exhibit differential expression of TGF-β proteins in response to infection (Clark et al. 2011).

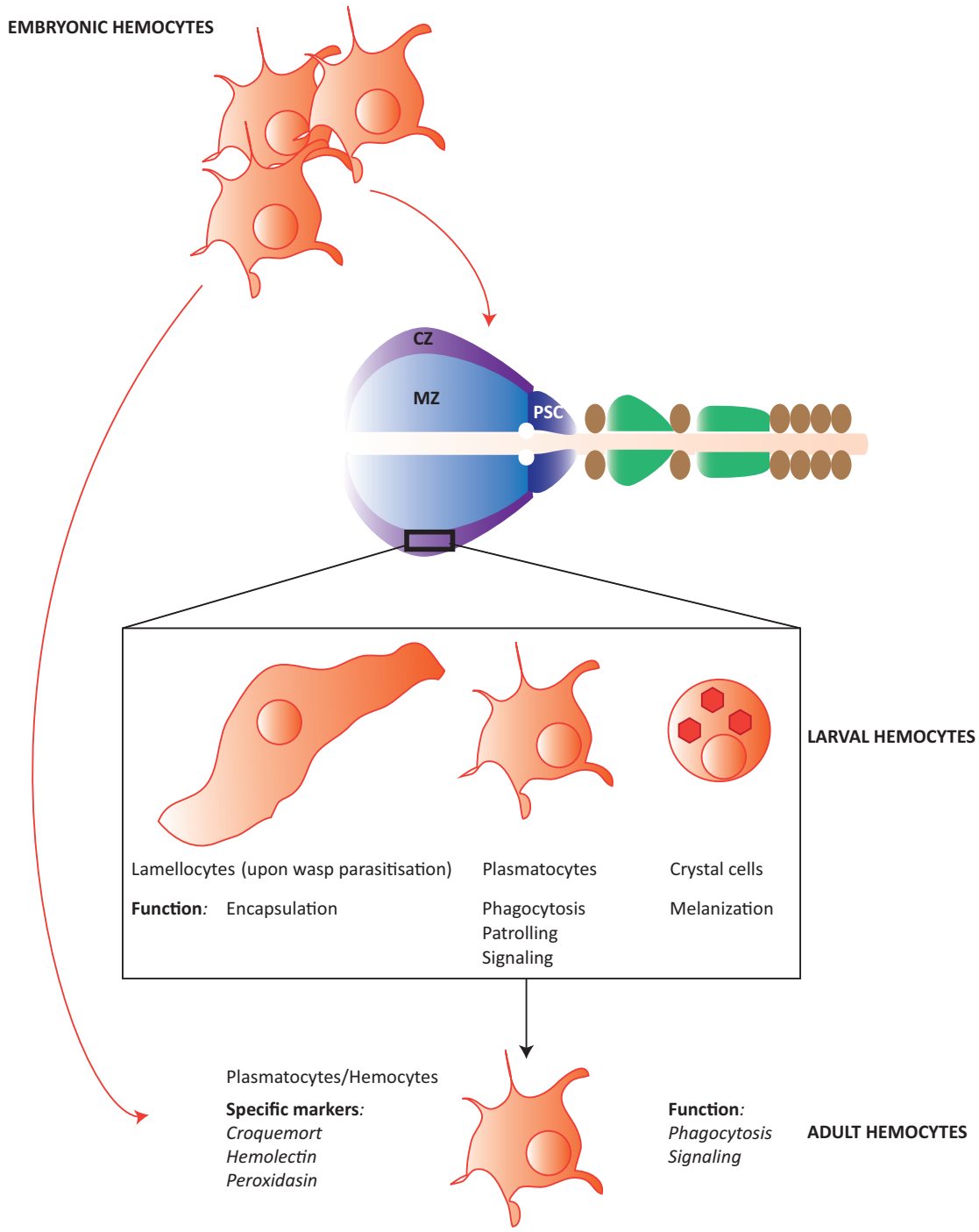

Figure 1-10: Myeloid lineage in *Drosophila*

During embryogenesis, hemocyte precursors migrate dorsally and are grouped into the lymph gland, a hematopoietic organ that is part of the newly formed dorsal vessel. There, the hemocytes differentiate and proliferate. The primary lobe is formed of the medullary zone (MZ), where pro-hemocytes are found; of the cortical zone (CZ), which is a maturation site; and the post-signalling centre (PSC), which has a unique population of hemocytes that signal to pro-hemocytes for their differentiation and proliferation. Secondary lobes (green) contain immature hemocytes except in random site of maturation. Pericardial cells are found surrounding the secondary lobes (brown). In the cortical zone, 2 types of hemocytes are found; the plasmatocytes and a low percentage of crystal cells. Upon was parasitisation, pro-hemocytes can differentiate into lamellocytes to encapsulate the wasp eggs. Larvae also contain circulating hemocytes that are most likely originated from the embryonic hemocytes. After metamorphosis, hemocytes from embryonic and larval origins form subsets of plasmatocytes. No crystal cell and lamellocyte markers were found in adults. The fate of these cells is unknown.

Hemocytes have various immune functions

Hemocytes functions range from phagocytosis and intracellular killing to encapsulation, melanisation and more generally signalling.

Phagocytosis has been studied in several genomic and proteomic screens that have identified key molecules involved in pathogen recognition and initiation of the phagosome (Rämet, Manfruelli, et al. 2002b; Agaisse et al. 2005; Stuart et al. 2007). Stuart et al. organised these proteins into a protein-protein interaction network in *Drosophila* S2 cells revealing the multifunctionnality of the organelle. Some of the functional groups are listed below:

(1) V-ATPase;
(2) Calcium regulated calcineurin/calmodulin;
(3) Thioredoxin peroxidases;
(4) TCA cycle and pentose-phosphate shunt;
(5) Oligosaccharide transport;
(6) Amino-acid transport and fatty acid metabolism;
(7) Protein-nuclear transport;
(8) RNA splicing;
(9) Actin-myosin regulation;
(10) Spliceosome;
(11) Rabs.

From that, they predicted the architecture of the phagosome and putative biomodules that led them to the identification of the exocyst, a macromolecular complex previously reported in exocytosis. Mammalian proteins identified in proteomic studies had 70% of orthology with proteins of *Drosophila* phagosome indicating conserved mechanisms.

Second, hemocytes have a role in intracellular killing and encapsulation. A precise description of phagocytic receptors and intra-phagocytes bactericidal mechanisms will be given in the next section “Intracellular infections in *Drosophila melanogaster*”. Encapsulation is an immune reaction that is restricted to invertebrates and in which large invading pathogens are immobilised by specialised immune cells, the lamellocytes. To study this defence mechanism, researchers have used parasiting wasps that lay their eggs into the hemocoel of larvae.

Circulating plasmatocytes attach to the egg chorion and stimulate the massive differentiation of pro-hemocytes into lamellocytes (Krzemień et al. 2007; Meister 2004b). The released lamellocytes then form a layer surrounding the invader that blackens due to melanisation (Russo et al. 1996). The invader is probably killed by asphyxiation or by local production of free oxygen radicals and nitric oxides (Nappi et al. 2000; Nappi et al. 1995). It is not known how circulating plasmatocytes sense the intrusion and stimulate differentiation of pro-hemocytes into lamellocytes. Early studies demonstrated that implantation of fat body tissue from the same species induces encapsulation of the foreign body only when the basal membrane was damaged (R. M. Rizki & T. M. Rizki 1980). Interestingly, implantation of intact fat body tissues from non sibling species also stimulated encapsulation by lamellocytes suggesting that the destruction of the basement membrane or direct non-self recognition may trigger lamellocyte differentiation. Since the post-signalling centre is responsible for lamellocyte proliferation, it is hypothesized that circulating plasmatocytes send a signal to the PSC, possibly through a cytokine, and that Collier, an orthologue of mammalian early B-cell factor (EBF) may enable the PSC to respond (Crozatier et al. 2004).

As previously mentioned, melanisation is the production of black pigments of melanin that participate in wound healing and bacterial killing through the toxicity of melanin synthesis intermediates. The melanisation cascade involves humoral and cellular components such as crystal cells. The crystal cells express two genes encoding phenoloxydases in larvae that catalyse the oxidation of tyrosine-derived phenols into quinones which polymerize to form melanin (Meister 2004b). They are fragile cells that store large amount of phenoloxydases in a crystallized form (Urdahl et al. 2011; Meister 2004a; T. M. Rizki & R. M. Rizki 1959). Upon challenge with bacteria, fungi or parasites, the crystal cells release their content in the hemolymph, possibly after cytokine secretion by plasmatocytes (Bidla et al. 2007).

Finally, hemocytes also possess a signalling role by secreting various cytokines, a role in blood clotting through secretion of hemolectin, a role in formation of the basement membrane through expression of collagen IV and peroxidasin and a role in the secretion of antimicrobial peptides (Irving et al. 2005; Fessler et al. 1994; Agaisse et al. 2003; Goto et al. 2001).

1.3.4 The Toll/Imd pathway

The discovery of the Toll pathway in *Drosophila* and later of the Toll-like receptors in mammals revealed a common ancestry and overturned a dogma wherein recognition of pathogens was aspecific (Lemaitre et al. 1997; Lemaitre et al. 1996; Medzhitov et al. 1997). The *Drosophila* genome encodes nine Toll proteins, with only one clearly implicated in innate immunity, Toll1 or Toll (Tauszig et al. 2000; Ooi et al. 2002). Unlike in mammals, Toll is not a pattern recognition receptor. It recognizes Spätzle, a cytokine that is activated after recognition of pathogens by PRR and after the subsequent cleavage of the zymogen by the Spätzle processing enzyme (SPE) (Jang et al. 2006). Components of the Toll pathway include: the activating cytokine Spätzle, the transmembrane receptor Toll, the adaptors Tube and MyD88, the Pelle kinase, the IkB-homologue Cactus, and the NF-kB-like transactivators Dorsal and Dif (**Figure 1-11**) (Lemaitre & Hoffmann 2007). Deletion of any component of the pathway, with the exception of Dorsal, causes a decrease in several antimicrobial peptides and a susceptibility to $Gram^+$ bacteria and fungi (Lemaitre et al. 1997; Lemaitre et al. 1996; Rutschmann et al. 2002). Upon challenge, many Toll pathway members are upregulated in a Toll-dependent manner (De Gregorio et al. 2002).

The Imd pathway was inferred by the identification of the *immune deficiency (Imd)* mutation that impairs the expression of several antimicrobial peptides (Lemaitre et al. 1995; Corbo & M. Levine 1996; Levashina et al. 1998). *Imd* encodes a protein with a death domain similar to that of mammalian Receptor Interacting Protein (RIP) that plays a role in NF-kB activation and apoptosis (Georgel et al. 2001). Components of the Imd pathway include: the DAP-type-specific PRR PGRP-LC and PGRP-LE, the Mitogen-activated Protein 3 kinase (MAP3K) TAK1, TAK-1 binding protein2 (TAB2), the inhibitor of apoptosis protein DIAP2, the IKK signalosome proteins IKKβ/ird5 and IKKγ/Kenny, the dFADD adaptor, the Dredd caspase, and the NF-kB-like transcription factor Relish (Lemaitre & Hoffmann 2007). Mutation in these factors affects the production of several antimicrobial peptides and generates a susceptibility to $Gram^-$ bacteria and Bacillus species, all carrying DAP-type peptidoglycans. The Imd pathway shares similarities with the mammalian TNF receptor pathway (Falschlehner & Boutros 2012).

The Toll and Imd pathways are the major immune pathways in fly and they regulate almost 80% of the genes induced upon bacterial infection (De Gregorio et al. 2002). The Toll

pathway responds to infection with bacteria carrying Lys-type PGN and the Imd pathway to DAP-type peptidoglycans. Upon infection with various types of bacteria, the Imd or Toll pathways are differentially activated. Although some antimicrobial peptides are dependent mainly on one pathway (Diptericin for Imd, IM1 for Toll), the Toll and Imd pathways are not mutually exclusive and can synergize to induce some antimicrobial peptides possibly through the formation of Dif/Relish heterodimers (Tanji et al. 2010). In addition, the sequential activation of Imd and Toll differs suggesting a temporal coordination of both pathways. Indeed, genes regulated by the Imd pathway show an acute phase profile, whereas Toll induced genes have a late and sustainable expression pattern (Boutros et al. 2002; Lemaitre et al. 1997).

1.3.5 The JAK-STAT pathway

Activation of the JAK-STAT pathway leads to various responses during development and adult stages in *Drosophila*. JAK-STAT signalling coordinates stem cell proliferation and multilineage differentiation on the *Drosophila* intestinal stem cell lineage, regulates regional specification, in which uniform populations of cells acquire differences and ultimately give rise to distinct organs. This signalling pathway is also required for the initial choice of sexual identity and is important in intestinal stem cell activity (Ekas et al. 2006; Beebe et al. 2010; Jinks et al. 2000; Buchon, Broderick, Chakrabarti, et al. 2009a). However, the role of the JAK-STAT pathway in innate immunity is poorly documented in *Drosophila*. It is associated with blood cell homeostasis, hemocyte proliferation and differentiation, and with the control of viral load upon Drosophila C virus infection in adults (Agaisse & Perrimon 2004; Dostert et al. 2005). The JAK-STAT pathway has three ligands: upd, upd2 and upd3 that act in an autocrine and paracrine manner. They have different activation potentials and exhibit different interactions with the extracellular matrix (Hombría et al. 2005; Wright et al. 2011). Upon septic injury, *upd3* is expressed by hemocytes, is secreted, and activates the JAK-STAT pathway in the fat body through binding to its receptor, Domeless (Dome) (Agaisse et al. 2003). It results in receptor dimerisation and activation of the unique Janus kinase, Hopscotch (Hop), which phosphorylate the cytoplasmic domain of Dome. This tyrosine phosphorylation creates docking sites for the SH2 domain of STAT, which will then be recruited to Dome to be phosphorylated by Hop. STAT then dimerises and translocates to the nucleus to activate the transcription of its target genes

(**Figure 1-11**). In a recent study, Bina et al. identified genes up and down-regulated after 2h, 4h, or 10h of stimulation with Upd (Bina et al. 2010). Among the upregulated genes, several have been previously described as JAK-STAT targets such as *TotA*, a stress induced gene, *Tep1*, coding a complement C3/α2-macroglobulin-like protein, and *Soc36E*, an inhibitor of JAK-STAT. However, most of these studies did not approach JAK-STAT signalling in the context of infection. To date, the requirement of the JAK-STAT pathway during infection has been documented for the *Drosophila* C virus infection, in which JAK-STAT was involved in the control of viral load; and for lamellocyte differentiation upon wasp parasitisation (Makki et al. 2010; Dionne & Schneider 2008). In this later study, a shorter form of Domeless, Latran, was shown to switch off JAK-STAT signalling to allow differentiation of pro-hemocytes to lamellocytes. More work need to be done to understand the precise contribution of JAK-STAT in controlling pathogenesis, especially against bacteria, a question that still remains unanswered in mammals due to the complex compensatory mechanisms between the different JAK-STAT proteins.

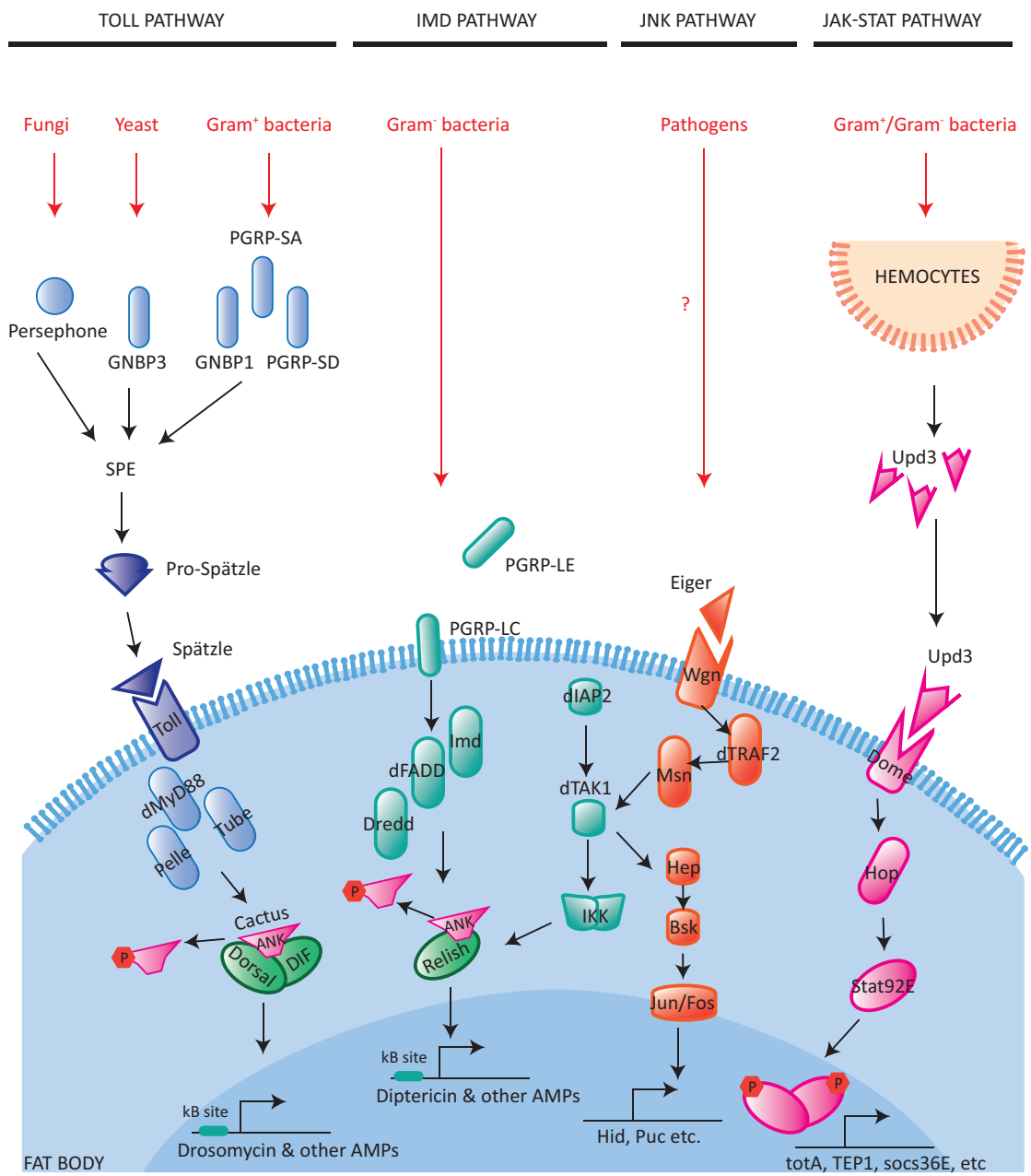

Figure 1-11 Innate Immune pathways

Four major immune pathways have been described in *Drosophila* innate immunity. The Toll pathway is activated in response to Lys-type peptidoglycan that is found at the surface of Gram$^+$ bacteria, fungi and yeast. These pathogens are recognised by distinct PRR that activate the Spätzle processing enzyme (SPE), an enzyme that cleaves Spätzle. Mature Spätzle binds as dimer to Toll. Toll dimerises and then recruits and activate a cascade of proteins: dMyD88, Tube and Pelle. Cactus is then phosphorylated and degraded by the proteasome, while Dif and Dordal are released and activate the transcription of specific target genes such as *Drosomycin*. Dordal and Dif possibly form homodimers and heterodimers with Relish, another NF-kB like molecule. The Imd pathway is activated in response to DAP-type peptidoglycans that are found at the surface of Gram$^-$ bacteria and Bacillus species. The Imd cascade includes dFADD, Imd, and Dredd. Dredd associates to Relish and probably cleaves it after IKK-induced phosphorylation of Relish. Relish then forms homodimers that activate the transcription of specific target genes such as *Diptericin*. The IKK complex is activated by dTAK1, a component of the JNK pathway. These two pathways have been suggested to interact at the level of dTAK1 and at the level of Basket that has been implicated directly in the transcription of some antimicrobial peptide genes. The JNK pathway and its activating cytokine, Eiger, are important for resistance and tolerance to infection. However, the precise context of JNK activation upon infection is unknown. The JAK-STAT pathway is activated in response to Upd3 binding to its

receptor Domeless. Receptor dimerisation attracts Hop, a Janus kinase (Jak) that phosphorylates a cytoplasmic domain of the receptor thereby creating SH2-docking sites for STAT92E. STAT is recruited to the SH2 site and is then phosphorylated by hop. When activated STAT form dimers, which migrate to the nucleus to activate the transcription of stress responsive genes. Upd3 is secreted by hemocytes upon bacterial challenge. ANK (AnKyrin repeats), Bsk (Basket), GNBP (Gram Negative Binding Protein), Hep (Hemipterous), Hop (Hopscotch), IKK (IkB kinase), Imd (Immune deficiency), Msn (Misshapen), MyD88 (Myeloid differentiation Primary Response Gene (88)), PGRP (PeptidoGlycan Recognition Protein), SPE (Spätzle Processing Enzyme), dTRAF (TNF-Receptor Associated Factor), Wng (Wengen).

1.3.6 Other pathways involved in innate immunity

Apart from the Toll, Imd and JAK-STAT cascades, other pathways are involved in immune responses, such as the JNK pathway, the p38 pathway and TGF-β signalling.

The JNK pathway participates in several processes from wound healing to hemocyte activation and AMP production (Boutros et al. 2002; Kallio et al. 2005; Delaney et al. 2006; Rämet, Lanot, et al. 2002a). Such various functions imply that it may collaborate with other immune signalling pathways. Indeed, a crosstalk between Imd and JNK was demonstrated first via the shared component TAK1 and second, via JNK–dependent expression of antimicrobial peptides in the fat body (**Figure 1-11**) (Delaney et al. 2006; Boutros et al. 2002). The JNK pathway is activated upon binding of its ligand Eiger, a TNF-α homolog, to its receptor Wengen (**Figure 1-11**). Eiger is a type II transmembrane protein with a C-terminal TNF homology domain that can induce apoptosis by activation of the JNK pathway (Igaki et al. 2002). Eiger is mostly localised at the plasma membrane but can also be cleaved at residue 145 and be released from the surface as a soluble factor (Kauppila et al. 2003). *eiger* mutants were challenged with a broad range of intracellular and extracellular pathogens and were immunocompromised with respect to extracellular pathogens but had no change or reduced sensitivity to intracellular pathogens (D. S. Schneider et al. 2007). Upon infection with extracellular bacteria, *eiger* mutants die faster and have more bacteria. These results indicate that Eiger may play a dual role upon infection: it increases resistance to extracellular pathogens and increases tolerance to intracellular pathogens such as *Salmonella typhimurium* (Brandt et al. 2004). In addition, *eiger* mutants have a decreased feeding rate, an altered melanisation, a decreased phagocytosis of *Staphylococcus aureus*, and an enhanced transcription of *Diptericin* (Mabery & Schneider 2010; Bidla et al. 2007; Schneider et al. 2007). The p38 pathway was recently shown to play a role in innate immunity by mediating phagocytic encapsulation of bacteria to limit bacterial burden in

the hemolymph of adult flies (Shinzawa et al. 2009). Indeed, authors showed that tolerance to infection can be increased by enhancing containment of bacteria inside immune cells and this, even if the pathogen still proliferates inside phagocytes. Finally, multiple TGF-β superfamily signals modulate the adult *Drosophila* immune response: Decapentaplegic (Dpp) is an important inhibitor of inflammation following sterile injury and Dawdle limits melanisation (Clark et al. 2011).

1.4 Intracellular infections in *Drosophila melanogaster*: host defence and mechanisms of pathogenesis

In *Drosophila*, the Toll/Imd pathways and the tissue repair mechanisms have been widely studied over the past 20 years. In contrast, cellular immunity is relatively less characterized. We know that crystal cells play an important role in melanisation, that lamellocytes encapsulate large pathogens and that plasmatocytes are able to patrol the hemolymph and phagocytose invaders and damaged cells. However, what happens to microorganisms after phagocytic uptake? It is assumed that once phagocytosed, pathogens are killed through phagosome-lysosome fusion, and that bacterial debris can modulate inflammation and activation of surrounding cells. If this is true for extracellular pathogens, it is not quite right for intracellular pathogens that have learned to survive and expand into this hostile environment. Besides, intracellular pathogens represent a large group of life-threatening infectious agents in humans that is worth investigating. The following review presents the basis of our understanding of pathogen recognition and phagocytosis, of intracellular killing mechanisms, and of pathogenesis in the fly relatively to mammals. It focuses on intracellular pathogens in immune cells and mention only quickly endosymbionts that reside in non-immune cells. Of note, although viruses are intracellular pathogens, they are not described in this review.

1.5 Thesis outline

The initial proliferation of *M.tuberculosis* in macrophages is a determinant for long-term infection in humans; it is then crucial to assess why phagocytes and immune signalling fail at controlling bacterial proliferation. In addition, once the granuloma is established, macrophages undergo strong metabolic changes and accumulate lipids that are thought to lead to pathogenesis. What drives such changes in host metabolism?

This thesis aims at answering these questions using *Drosophila melanogaster* as a model host for the simplicity to undergo reverse genetic approaches and in vivo analysis. In flies, the Toll and Imd pathways do not seem to be activated in response to mycobacterial infection, that is why studying the JAK-STAT pathway and the JNK pathway appeared more relevant (Dionne et al. 2003). In my hand, the JNK pathway gave only weak phenotypes. In consequence, this thesis focuses on the JAK-STAT pathway and its cytokine Upd3, an IL-6 analogue.

The JAK-STAT pathway has been extensively studied in mammals for the past twenty years and we know that it controls blood cell development and the acute phase response during infection. However, we still do not understand the precise function of JAK-STAT in innate immunity and pathogenesis specifically upon *M.tuberculosis* infections. Recently, cytokine signalling was linked to intracellular immune responses. IFN-γ stimulates intra-macrophage killing mechanisms through STAT1 signalling by restoring phago-lysosomal functions and stimulating autophagy, while inhibitory signals such as IL-4 and IL-13 possibly signal through STAT6 to inhibit autophagy (Murray 2007; Harris et al. 2007). How does JAK-STAT signalling control these functions? We still do not know and modern genetic techniques have been unsuccessful in giving a clear answer (O'Shea & Plenge 2012). This thesis attempts at deciphering the mechanisms by which the JAK/STAT pathway controls infection using reverse genetic approaches by the mean of inducible tissue-specific RNAi, epistasis analysis and intravital imaging techniques. Since *M.marinum* is a facultative intracellular pathogen, both humoral and cellular immune responses have been examined together with the changes in metabolism.

Chapter 2 recapitulate the material and methods used for this study.

Chapter 3 present the striking observation that Upd3 signalling is detrimental for the host upon *M.marinum* infection. For this, I used a previously reported mutant line, os^s, a spontaneous mutation in the *upd3* locus, and also an inducible hemocyte-specific *upd3* RNAi line (Agaisse et al. 2003). These flies have an enhanced resistance to mycobacteria infection, as assessed by fly survival, bacterial load and immune cell death.

Chapter 4 demonstrates that Upd3 signals from and to hemocytes, and that changes in resistance to mycobacteria is partly controlled by Atg2-dependent mechanisms. As suggested by a recently published forward genetic screen to discover new factors involved in blood cell proliferation, JAK-STAT downregulates some autophagy genes upon Upd stimulation in Kc167 cell lines (Bina et al. 2010). In this thesis, I show that JAK-STAT specifically controls *Atg2* expression in vivo and in vitro, and that it favours bacterial proliferation. As STAT is an activator of transcription, it suggests that such regulation is indirect and may require an intermediate transcriptional repressor. I then identified a novel transcriptional repressor, *net*, that, when mutated, strongly upregulates *Atg2* expression.

Chapter 5 attempts at describing how Atg2 controls bacterial growth in phagocytes. From the literature, Atg2 was suggested to associate with autophagy and lipid droplets (Velikkakath et al. 2012). Since the autophagy phenotype is unclear, I decided to investigate the role of Atg2 in lipid droplet formation and morphology. Interestingly, dead and active *M.marinum* trigger an accumulation of lipid droplets in *Drosophila* cell lines recapitulating the foamy phenotype in macrophages at the centre of the granuloma. Changes in lipid droplet morphology are prevented upon *Atg2* overexpression suggesting a role for Atg2 in lipid droplet fusion. As lipid droplets may constitute a nutrient-rich reservoir for bacterial persistence, such modifications could explain lower bacterial burden due to lack of accessibility to nutrients (Peyron et al. 2008).

Chapter 6 presents another potential function of JAK-STAT in regulating glucose metabolism. Interestingly, while fly fitness is improved upon *upd3* mutation, the lifespan at steady state is reduced indicating a two-edge sword mechanism. In one hand JAK-STAT signalling is harmful upon mycobacterial infection while it is beneficial during ageing. It may be a direct consequence of changes in lipid metabolism in the whole organism, not only in

hemocytes. However, I failed to observe such phenotype in the whole fly. Instead os^{s} mutants harbour a strong increase in glucose and insulin signalling at steady state and upon infection. The importance of insulin signalling in pathogenesis have been previously assessed (Dionne et al. 2006). Here, I show that it is controlled partly by Upd3 signalling.

Chapter 7 aims at discussing the results of the previous chapters while putting them in the context of *M.tuberculosis* infection in human.

Chapter 2 Material and Methods

2.1 To start with

2.1.1 Fly genetics

Flies have 4 pairs of chromosomes. In the conventional nomenclature, a semi-colon separates each chromosome, a coma separates insertions or mutations in the same chromosome, and a slash distinguishes between the two chromosome pairs. Fly genotypes are always italicized and some gene names start with a capital letter: *Stat92E, TotA, Hml, Diptericin* etc.

Balancer chromosomes

Recessive alleles in flies are maintained using balancer chromosomes. These are multiply inverted chromosomes unlikely to undergo exchange with their homolog in female flies (males do not have recombination). These chromosomes also carry dominant marker mutations that are often recessive lethal themselves; SM6a or CyO which carries the dominant marker Curly (curly wings), TM6c which carries Sb1 (bristles short and thick), FM7h which carries the dominant allele Bar (Eye restricted to narrow vertical bar), and TM6b, Tb^1 whose larvae, pupae and adults are shorter and thicker than wild-type.

Mutant lines

The mutant lines used in this thesis (os^s, net^1, net^x, w^{1118}) arose from spontaneous mutations. The os^s and net^x mutations are so far, uncharacterised.

RNAi lines

The RNAi line strategy uses the Gal4-UAS system developed by Brand and Perrimon (Brand & Perrimon 1993). It is a binary system using a transcriptional activator from Saccharomyces cerevisiae, *Gal4*, and a *Gal4* responsive promoter, the upstream activation sequence (UAS), upstream of a reporter gene. The system is used to visualise the expression pattern of an enhancer and involve a tissue-specific promoter driving a reporter gene such as GFP or LacZ. To silence a gene of interest, the Gal4/UAS system is used to drive the

expression of a hairpin RNA from inverted repeat sequence of the target mRNA. Hairpin RNA are double stranded RNA processed by Dicer into 25 basepair fragments of single stranded RNA, which direct sequence-specific degradation of the target mRNA (Ryder & Russell 2003). To allow a temporal control of expression, the Temporal And Regional Gene Expression Targeting system (TARGET) has been developed by McGuire et al., and is based on a temperature-sensitive Gal80 protein (McGuire et al. 2003). The $Gal80^{ts}$ molecule was under the control of a tubulin promoter to repress the transcription activity of Gal4 in a temperature dependent fashion at all stage of development in the fly. $Gal80^{ts}$ optimal expression is at 19˚C and is inhibited at 29˚C (McGuire et al. 2004). The Gal4/UAS/$GAL80^{ts}$ system was extensively used in this thesis to allow hemocyte specific knock down of *upd3* and *Stat92E*.

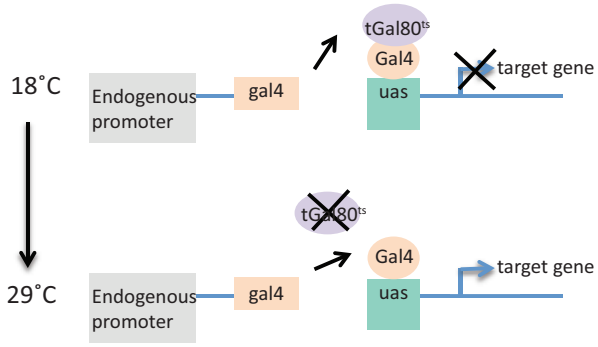

Figure 2-1: The TARGET system

The transcriptional activator Gal4 is under the control of an endogenous promoter, which activates the transcription of a target gene in a tissue-specific manner. The tubulin-Gal80ts ($tGal80^{ts}$) molecule represses the activity of Gal4 at 18˚C and prevents the transcription of the target gene. However, at 29˚C, $tGal80^{ts}$ is inactive allowing the transcription of the target gene.

2.1.2 Fly breeding

Fly culture and crosses were carried out at 25°C using standard fly medium (2% polenta, 10% w/v Brewer's yeast, 0.8% agar, 8% fructose and water), except for experiments in Chapter 6 using sugar-free food, where the 8% fructose was removed from the recipe. For experiments using temperature sensitive genomic insertions, flies were raised at 18˚C and then put at 29˚C after emerging.

2.1.3 Fly stocks

Flies were kept in 18˚C, 25˚C or 29˚C incubators. The incubators create a 60% humidity environment and run a 12-hour light/dark cycles to maintain the fly circadian rhythm, which is essential in fly immunity (Stone et al. 2012). Phenotypic traits of fly stocks were regularly checked for conservation of the correct genotypes. Additionally, fly stocks were checked for culture contaminants, such as mites and fungi, which may compromise experimental observations. Since flies can be only maintained as live cultures, stocks were kept in duplicates, usually, at 18˚C and transferred at 25˚C for expansion prior to virgin and male collection for crosses.

The fly stocks used in this thesis are listed in the next page.

Identification	1 chr	2 chr	3 chr	4 chr	Characteristics
os^{s}	*os^{s}*				Hypomorphic mutation of *upd3*, small eyes, in isogenic *Drosdel* background
w,os^{s}	*w,os^{s}/FM7h*				Hypomorphic mutation of *upd3* with *white^{1118}* allele, small eyes, in isogenic *Drosdel* background
upd3-IR	*w*	*upd3-IR/SM6a*			Line with *upd3* inverted repeats for RNAi strategy
upd3-gal4, UAS-GFP	*w*	*upd3-gal4,* *UAS-* *GFP/CyO*			Line driving GFP expression in *upd3* expressing tissues
domeΔcyt.3-1	*w*		*UAS-domeΔcyt.3-1*		Line carrying a gene encoding a dominant-negative form of Domeless
Stat-IR (I)	*w, UAS-Stat92E-IR*				Line with *Stat92E* inverted repeats for RNAi strategy, 1st chromosome
Stat-IR (II)	*w*	*UAS-Stat92E-IR/SM6a*			Line with *Stat92E* inverted repeats for RNAi strategy, 2nd chromosome
Stat-IR (I,II)	*w, UAS-Stat92E-IR*	*UAS-Stat92E-IR/SM6a*			Line with *Stat92E* inverted repeats for RNAi strategy, 1st & 2nd chromosome
10x-stat-GFP (II,III)	*w*	*10xStat92E-GFP/SM6a*	*10xStat92E-GFP/TM6c, Sb^{1}*		Five copies of a 441 bp genomic fragment from the *Socs36E* intron 1, which contains at least two *Stat92E*-binding sites, were placed upstream of an *hsp* minimal promoter driving *GFP*. To observe STAT activation.
crq-gal4	*w*		*crq-gal4/TM6c, Sb^{1}*		Hemocyte-specific driver
crq-gal4, UAS 2xeGFP	*w*		*crq-gal4, UAS 2xeGFP/ TM6b, Tb*		Hemocyte-specific driver that drives *GFP* expression in hemocytes
HmlΔ-gal4, UAS-2xeGFP	*w*	*HmlΔ-gal4, UAS-2xeGFP*			Hemocyte-specific driver that drives *GFP* expression in hemocytes
HmlΔ-gal4, tgal80^{ts}, UAS-2xeGFP	*w*	*HmlΔ-gal4, UAS-2xeGFP*	*tubulin-gal80ts/ TM6c, Sb1*		Hemocyte-specific driver that drives *GFP* expression in hemocytes in a temperature-inducible manner
HmlΔdsRed.nuc	*w*	***HmlΔdsRed.nls/SM6a***			Hemocyte-specific expression of nuclear deRed
crq-gal4, tgal80^{ts}	*w*	*tubulin-gal80ts/ SM6a*	*crq-gal4/TM6c, Sb1*		Temperature-inducible, hemocyte specific driver
net^{1}	*w*	*net^{1}*			Loss of function allele of *net*, from spontaneous mutation
net^{x}	*w*	*net^{x}*			Loss of function allele of *net*, uncharacterised

w	*w*	w^{1118} control, in isogenic *Drosdel* background
+	*+;+;+*	w^{+} control, in isogenic *Drosdel* background

Table 2-1: Fly stocks used in this thesis

2.1.4 Collecting virgins and males for crosses

Flies were anesthetised with CO_2 on porous gas pads and observed under a light microscope. To avoid neuronal activity impairment from anesthetization, flies were kept for a maximum of 15 minutes on the pad; a time sufficient for selection of the required genotypes using a soft bristled paint brush. Males and females are distinguished through several phenotypic differences: genital, different patterning, presence of sex combs structures on the first pair of legs of male flies. Virgin females are identified by their white and transparent body, by their abnormal body shape and by a dark spot in the translucent abdomen that is a fly version of the meconium. Virgin females will not mate during the first 8 hours of emergence; therefore they are collected twice a day, especially in the morning when the majority of flies emerge from the pupae stage (Greenspan 2004). To further confirm that collected females were virgin, flies were kept for 2-3 days and checked for the presence of larvae. Males were collected at anytime; ideally, they must be 3 to 10 days old for optimal mating efficiency (Sullivan et al. 2000).

Crosses were realised to generate essential fly stocks such as:

(1) crq-gal4, tgal80^{ts};

(2) Stat-IR (I,II);

but also to collect experimental flies carrying the Gal4/UAS/tGal80^{ts} system.

2.1.5 Experimental flies

Crosses between drivers (promoter-Gal4) and responder genes (UAS-gene) were realised by crossing 3 to 4 virgin females from one genotype with 2-3 males from the other genotype. After mating, a female lays around a 100 eggs per day on the surface of the culture medium. *Drosophila* is a typical holometabolous insect with four developmental stages: embryo, larva, pupa and adult, whose generation time is around 10 days at 25˚C and 20 days at 18˚C

(Sullivan et al. 2000). Soon after eclosion, flies with the correct genotype were selected based on phenotypic markers (characteristic trait, absence of balancers, and eye colour) and were put on fresh food. For reproducibility and to avoid changes in fitness or in immune responses due to fertilisation, only adult males were used (McGraw et al. 2004). Five to eight days after eclosion, flies were used for experimentation. An example cross is presented in **Figure 2-2**.

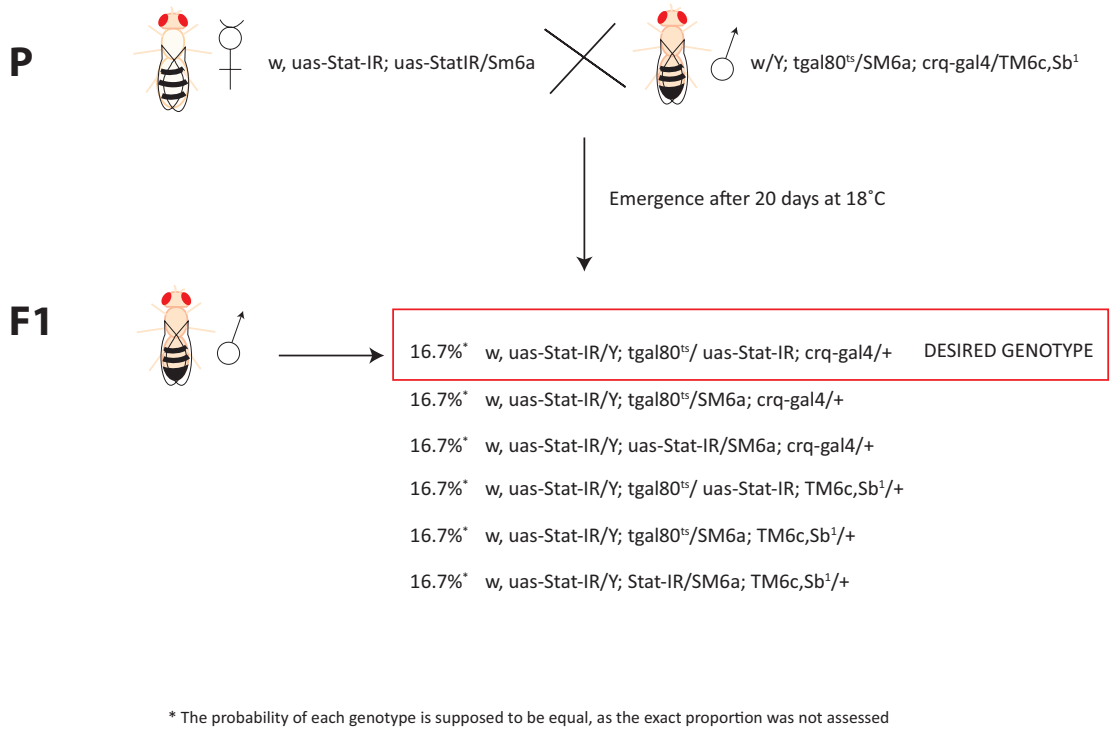

Figure 2-2: *Stat92E* knock down in adult hemocytes

Virgin females carrying two copies of *Stat92* inverted repeats (*Stat-IR*) were crossed to males carrying the temperature-inducible hemocyte-specific driver *w/Y; tgal80^{ts}/SM6a; crq-Gal4/TM6c, Sb^{1}* to generate *Stat92E* knock down in adult hemocytes. The lines used for the cross are called the parents (P). The first generation of progeny (F1) contains males of 6 different genotypes. By making the assumption that all genotypes were obtained with the same probability (no detrimental or beneficial combination), the probability of obtaining the desired genotype is 16.7%. The selected flies (*w/Y, UAS-stat-IR; tgal80^{ts}/ UAS-Stat-IR; crq-gal4/+)* were then put at 29˚C to activate the transcription of *Stat92E* inverted repeats.

2.1.6 Bacterial culture

M.marinum cultures were grown at 29°C in T25 flasks for 7 to 10 days before experimentation. The culture medium is made of Middlebrook 7H9 broth supplemented with 10% Middlebrook oleic acid-albumin-dextrose-catalase (OADC) enrichment, 0.2% glycerol, 0.2% tween-80, and with ampicilin (100 µg/mL) and nalidixic acid (10 µg/mL) antibiotics. The dsRed *M.marinum* was engineered to contain a kanamycin resistance gene, therefore cultures were grown in the same medium supplemented with kanamycin (30 µg/mL).

2.1.7 Cell culture

The commonly used *Drosophila* cell line for RNAi studies is the S2 cell line that is derived from late embryonic stages and is commonly referred as hemocyte-like cell line (Schneider 1972). Three hemocyte-like cell lines were tested for their capacity of phagocytosis of *M.marinum:* S2 cells, $S2R^+$ cells that also derived from embryonic animals but from another source, and mbn2 cells that derived from larval hemocytes of the mutant lethal(2) malignant blood neoplam (l(2)mbn) (Schneider 1972; Yanagawa et al. 1998; Samakovlis et al. 1992). Only $S2R^+$ cells had taken up *M.marinum* after 24 hours of infection, therefore all experiments were performed in $S2R^+$ cells.

$S2R^+$ cells were cultured in M3 medium (Sigma Aldrich) supplemented with 10% Fetal Bovine Serum (FBS, Sigma Aldrich) and 1% of Penicillin-Streptomycin (PAA). Cells were kept at 25˚C in T75 flasks (Sigma Aldrich). Once a week, floating cells were removed, a 10mL fresh medium was added, adherent cells were detached with a cells scaper (Starstedt) and pipetted up and down several times to remove clumps. Cells were split into new T75 flask in fresh medium (1:10 dilution)

2.1.8 Imaging

To allow color-blind people to analyse the images, images acquired in the red channel were converted to magenta.

2.2 In vivo experiments

2.2.1 Genomic DNA extraction and diagnostic PCR for *os*^{s}

A single fly was mashed with a pipette tip containing 50 µL of squishing buffer (10mM Tris HCl, 25mM NaCl, 1mM EDTA, SDS 1%, 200µL/mL proteinase K). The fly was mashed for 5-10 s with the pipette without expelling the solution. The liquid was then expelled, and the samples were then incubated 30 minutes at 37˚C , and then 10 minutes at 85˚C. Samples were spun for 1 min and then kept on ice. 1 to 2µL were used per PCR.

The PCR mix for amplification of genomic fragments was as follow:

(1) 1x polymerase buffer (NEB)

(2) 1 mM of each primer

(3) 0.2 mM of dNTPs

(4) 1.5 mM MgCl2

(5) 1-2 unit of Taq Polymerase (NEB)

(6) genomic DNA 1.25µL

(7) ddH2O

The PCR reaction was performed into three phases characterised by different thermal cycling conditions. The initial denaturation step was performed at 94˚C for 3 minutes and then the samples were subjected to 25 cycles. Each cycles was composed of a denaturation step (95˚C, 30s), where DNA is separated into two single strands, of an annealing step (53˚C, 30s), where primers anneal to their complementary sequences, and of an elongation step (72˚C, 1'30 min). The reaction was terminated with a final extension (72˚C, 5min).

The primers used for the *os*^{s} diagnostic PCR are mentioned below.

Exon 1, FWD	5'-ACACACATAACCACTGCACG-3'
Exon 1, REV	5'-AAAATGCTATGATTCACATGTGG-3'
Exon 2-3, FWD	5'-CTGTTGCTAGACTTTTCTCATG-3'
Exon 2-3, REV	5'-CAACAACTCTCGCGGCTG-3'
Exon 4, FWD	5'-AAGTTTACAAGTTCATGGACAG-3'
Exon 4, REV	5'-GAGATACCCAGTTTTCTCGATA-3'

Table 2-2: PCR primers for *os*^{s} diagnostic PCR

2.2.2 *Mycobacterium marinum* injections

Single cell suspensions were prepared to accurately quantify the bacterial concentration. For that, seven to ten days *M.marinum* cultures (in exponential growth) were spun at 3000g for 5 minutes at room temperature to pellet bacteria and to remove the culture medium. Bacteria were resuspended in a solution of phosphate buffered saline (PBS) containing 0.2% tween-80 and the solution was spun at 200g to pellet *M.marinum* clumps. The suspension (containing single bacteria and some doublets) was collected, and after measuring the OD_{600}, was diluted to obtain the desired bacterial concentration. Bacteria were injected at an OD_{600} of 0.050 (approximatively 500 Colony Forming Unit – CFU per 50 nL injected) unless otherwise stated. Injections were carried out with a pulled glass capillary needle attached to a microinjection dispense system (Picospritzer) that was calibrated to dispense 50 nL of bacterial solution per fly (Dionne et al. 2003). Anaesthetized flies were injected in the abdomen, close to the junction with the thorax. Flies were never kept on the CO_2 pad for more than 10 minutes, and, after injection, were immediately transferred onto a new vial. Injected flies were usually kept at 25˚C, and at 29˚C when carrying the tGal80^{ts} construct or when imaging upd3-GFP expression in hemocytes by intravital imaging. In the 25˚C incubator, vials were changes every 4 days, while they were changed every 2 to 3 days at 29˚C.

2.2.3 pHrodo-labelled *E.coli* injections

Flies were injected with pHrodo-conjugated E.coli, a rhodamine sensor of pH (pHrodo E. coli BioParticlesH, Invitrogen) according to the protocol described in Pilátová et al. (Pilátová & Dionne 2012). After one hour, flies were immobilised on coverslips and imaged using a fluorescent (Leica) or confocal microscope (Leica TCS SP5) and the image capture software (Leica LAS-AF). The images were then processed using Imaris (Bitplane), a scientific software used for data visualisation, analysis and segmentation.

2.2.4 Beads injections

Beads were injected to block phagocytosis as previously described (Schneider & Shahabuddin 2000; Elrod-Erickson et al. 2000). Dark 4% w/v 0.2 µm polystyrene beads (C37278-Life Technologies) were spun for 10 minutes at maximal speed for resuspension in PBS 1X. Beads were washed twice for 10 minutes at maximal speed and then resuspended in twice their original volume to have a final 2% concentration. Beads were injected in the abdomen similarly to *M.marinum* injections.

2.2.5 Survival curves

For survival analysis, 5 to 8 days old males were injected with 500 CFUs of *M.marinum* or with sterile-filtered PBS containing 0.2% tween-80. Around 20 flies were used per genotype and per condition (*M.marinum* or PBS) and were monitored twice a day for death. Survival curves were plotted according to the Kaplan-Meier method (see the Statistics section).

2.2.6 Quantitative RT-PCR

RNA extraction was carried out in TRIzol (Invitrogen and Ambion) following the manufacturer's instructions. For each genotype and for each condition, 3 to 6 samples were processed for real-time RT-PCR. Each samples contained 2 to 3 flies that were homogenised in 100 µl of TRIzol, in a 1.5mL microfuge tube, using a small pestle. Samples were left to sit for at

least 5 minutes at room temperature before adding 20µl of chloroform to separate RNA from DNA and proteins. Samples were shaken thoroughly, left for 3 minutes and then span at 4˚C for 15 minutes at 12000g. The upper aqueous phase containing RNAs was decanted into a new tube containing 50µl of isopropanol. Samples were vortexed thouroughly, left 10 minutes at room temperature and then span at 4˚C for 15 minutes at 12000g. The supernatant was discarded and the RNA pellet was washed once with 75% ethanol for 5 minutes at 5000g. Once RNA was extracted, it was further processed for reverse transcription. The ethanol was discarded, and the RNA pellet was resuspended in 40µl of RNAse free DNAse I solution (34µl of RNAse free water, 4µl of 10xDNAse I buffer, 2µl of DNAse I at 1U/µl from Thermoscientific). RNA was treated for 30 minutes at 37˚C to remove residual genomic DNA. The reaction was arrested by adding 12.5% of 25 mM EDTA and by putting the samples at 68˚C for 10 minutes. Reverse transcription was performed using the First-Strand cDNA synthesis kit containing a M-MULV-derived reverse transcriptase (Thermoscientific). Samples were first primed with random hexamers for 5 minutes at 70˚C and then treated with M-MulV reverse transcriptase (Thermoscientific), Ribolock RNAse inhibitor (Thermoscientific) and 10mM of desoxyribonucleotides (dNTPs) for 1 hour at 37˚C. The enzymatic reaction was arrested by switching samples to 70˚C for 10 minutes. The resulting 20µl samples were stored at -20˚C before being processed for real-time RT-PCR using a Corbett Rotor-Gene 6000.

Fly samples were diluted by 100 before being analysed. A relative standard was generated by serial dilution (1:5) of a mixture of all samples, resulting in a set of 7 standards. A no-template control was also added. The real-time RT-PCR was performed using SYBR green Sensimix (Bioline) in a total 10µl reaction volume (4.8µl of Sensimix, 0.2µl of primers, 5µl of water). The cycling conditions were as follow: Hold 95˚C for 10 minutes, then 40 cycles of 95˚C for 15s, 57˚C for 30s, 72˚C for 30s. Values were normalised to *RpL1*, a housekeeping gene whose expression is stable under *M.marinum* infection.

Below is the list of primers used for real-time RT-PCR:

Gene name	Forward primer	Reverse primer
Attacin	CACAATGTGGTGGGTCAGG	GGCACCATGACCAGCATT
Atg1	GTCAGCCTGGTCATGGAGTAT	CGTCCCCTTGACACTGAGAT
Atg2	CAAAAGACCTGTACGCAGAGC	TACTGAGCAACAGGTTTCGTC
Atg4	TGGGTCCTGGGAAAGAAGTA	AATGTCCCGTCGGATGAG
Atg18	CGTCAACTTCAACCAGAACAT	TTGTCCAGGGTCGAGTCC
Diptericin	ACCGCAGTACCCACTCAATC	CCCAAGTGCTGTCCATATCC
Drosocin	CCATCGAGGATCACCTGACT	CTTTAGGCGGGCAGAATG
Drosomycin	GTACTTGTTCGCCCTCTTCG	CTTGCACACACGACGACAG
Hemolectin	CGATGATGACGACGAGGATA	GGCTTTGAGGATGTTGAAGC
Ilp2	ATCCCGTGATTCCACCACAAG	GCGGTTCCGATATCGAGTTA
InR	GCACCATTATAACCGGAAACC	TTAATTCATCCATGACGTGAGC
net	GGACCCGTGTACACACCAT	GCATAGGCTGGAACAGCTTG
rpl1	TCCACCTTGAAGAAGGGCTA	TTGCGGATCTCCTCAGACTT
Turandot A	CCAAAATGAATTCTTCAACTGC	GAATAGCCCATGCATAGAGGAC
Socs36E	AAAAAGCCAGCAAACCAAAA	AGGTGATGACCCATTGGAAG
Stat92E	ACTAGTGGAACACCGCATCA	AGTCCGCCATTCCAAAGTC
upd	GCACACTGATTTCGATACGG	CTGCCGTGGTGCTGTTTT
upd2	CGGAACATCACGATGAGCGAAT	TCGGCAGGAACTTGTACTCG
upd3	ACTGGGAGAACACCTGCAAT	GCCCGTTTGGTTCTGTAGAT

Table 2-3: qPCR primers used in this thesis

2.2.7 Bacterial count

To measure the number of bacteria per fly at specific timepoints after infection, a real-time RT-PCR method was used as previously described (Dionne et al. 2006). Twelve flies were injected per condition and per timepoint, and kept in individual vials until collection. Three flies were first homogenised per sample in a 3:1 mixture of chloroform and methanol and then in a proportional volume of TRIzol to extract fly and *M.marinum* RNA. After DNAse I treatment (30 minutes), samples were processed for reverse transcription. Products were detected by SYBR green fluorescence and quantities were related to an absolute standard with known concentration of *M.marinum*. For *M.marinum* detection, the *PyrG* primers were used. *M.marinum PyrG* encodes a CTP synthase that is expressed strongly and uniformly in broth, macrophages, and frog granulomas, rendering it suitable for quantification of bacteria (Chan et al. 2002).

pyrG, FWD	5'-ACCGCTACGAGGTCAACAAT-3'
pyrG, REV	5'-ATTCGACGAACTCCAC CAAG-3'

Table 2-4: Primer sequences of the *M.marinum*-specific gene *PyrG*

2.2.8 Intravital imaging

Intravital imaging was used to observe bacterial fluorescence, to count hemocytes upon infection and to quantify upd3-GFP fluorescence in hemocytes. For these experiments flies were injected with different doses of bacteria and images taken at different timepoints. The details of the experiments are presented below.

Experiment	Injection	T˚C	Fluorescence	Timepoints
Bacterial fluorescence	500 CFUs	25˚C	dsRed *M.marinum*	From day 5 post-injection until death
Hemocyte count	500 CFUs	25˚C	HmlΔgal4,UAS-2xeGFP and crq-gal4, UAS-2xeGFP with and without tgal80^{ts}	Each day post-injection until death
***upd3* transcription in hemocytes**	5000 CFUs	29˚C	HmlΔdsred.nuc and upd3-gal4, UAS-GFP	48 hours post-injection

Table 2-5: The different imaging experiments

Just prior to imaging, flies were anaesthetised, and their back was glued onto a cover slip using a drop of superglue. This method was useful to image the dorsal side of the fly, in which hemocytes and bacteria can be easily imaged and quantified in a reproducible manner. Also this technique allowed positioning the fly wings on the side to prevent obstruction of the imaging area. After being glued, flies were imaged within 15 minutes using a confocal microscope (SP5, Leica) equipped with an environmental controlled chamber and a gas anesthesia apparatus. Flies that died during the procedure were excluded from the analysis.

Images were acquired via the Leica LAS-AF software using either the 10X, NA (numerical aperture) 0.4 objective or the 40X Oil NA 1.25 objective. GFP was excited at 488nm with an argon laser and dsRed with the 561nm laser. Sequential excitation between frames was used when both fluorescent proteins were analysed. The images resolution was 1024x1024 at a scan speed of 400Hz. To image whole flies with the 10x objective, tile scanning was used and the merged images were automatically generated by the Leica software. The confocal microscope also contained a CO_2 chamber to anaesthetize flies while imaging. Images were acquired for 10 to 25 minutes depending on the experiment. Images were then processed using Imaris (Bitplane).

2.2.9 Western Blotting

Three male flies were smashed in 0.075 ml of 2X Laemmli loading buffer (1M Tris 6.8, 8% SDS, 40% glycerol, 0.02% bromophenol blue, 0.1% β-mercaptoethanol). Samples were kept at -80˚C until being processed. Immediately prior to loading, samples were heated for 5 minutes at 95-100˚C and then span quickly. Ten µL of this lysate was loaded per lane and 5µL of ladder (P7710S_NEB) was loaded onto the first lane. Proteins were transferred to nitrocellulose membranes using a transfer buffer (25mM Tris-base, 0.2M Glycine, 20% methanol, water). Antibodies used were as follows: from rabbit, anti-Akt (Cell Signalling Technologies #9272, used 1:1,000), anti- S505-phosphorylated *Drosophila* Akt (CST #4054, 1:1,000). The phospho-Akt antibody and the total-Akt antibodies likely detect different epitopes, because the phospho-Akt antibody is *Drosophila* specific and the total Akt antibody was made against residues from human Akt. . Secondary antibodies were HRP anti-rabbit IgG (CST #7074). HRP signal was

detected with Supersignal West Pico (Pierce). The images were processed using the Image Lab™ software from Bio-Rad.

2.2.10 Triglyceride, Glycogen, and Glucose Assays

Flies were transferred into fasting media (PBS+1% agar) around noon for 1 hour and then homogenised in 75 µL of TE + 0.1% Triton X-100. The combination of fasting and collection of samples at the same time during the day increased the reproducibility of measurements. Three flies were used per sample and usually a minimum of 3 repeats was done per genotype, per condition and per timepoint. For all assays, 10 µL of lysate was used and samples were processed immediately as described in Dionne et al. (Dionne et al. 2006). Samples were heated at 90˚C for 5 minutes to resuspend the fat and the solution was homogenised by piptetting up and down several times.

The triglyceride measurement technique was developed by McGowan et al. and aims at liberating glycerol from triglycerides, phosphorylating it using glycerol kinase, and then dephosphorylating the glycerol phosphate with glycerol oxidase to liberate peroxides (McGowan et al. 1983). The liberated peroxide is then measured by absorbance at 490-500nm using a standard chromogenic substrate. Samples are measured twice, with and without lipase (Sigma Aldrich) to deduce the quantity of free glycerol in the samples.

The glycogen reaction uses a similar principle. The glycogen is first degraded into glucose using amyloglycosidase and then phosphorylated and dephosphorylated. Glucose was measured with liquid glucose oxidase reagent (Pointe) and amyloglucosidase (Sigma Aldrich) was added at the concentration of 1U/mL (Sigma Aldrich).

For both assays, absorbance was measured at 490nm on a plate reader (Viktor, PerkinElmer) and was related to measurements of standards made by serial dilutions of glycerol or glucose for the triglyceride and glucose assay respectively.

2.2.11 Lifespan assay

Males were collected soon after emerging for 3 consecutive days; 20 flies per genotype were then put onto vials containing fresh food and kept at 25˚C for the duration of the experiment. Vials were changed every 3 to 4 days by direct transfer (no CO_2) to prevent flies from being stuck to the food. Fly death was recorded daily.

2.3 In vitro experiments

In vitro experiments were performed with the help of Sharon Tan, a previous student and research Assistant in Marc Dionne's laboratory.

2.3.1 Cloning

Cloning strategies for *pPAC-GFP-LC3*, *pPAC-GFP-Atg2* and *pPAC-upd3*

GFP-LC3

A *pEGFP-C1* plasmid containing a GFP-tagged LC3 from the Yoshimori lab was used for subcloning into pPAC-*HA*, a plasmid containing a *Drosophila* actin promoter strongly expressed in $S2R^+$ cells. In the pEGFP-C1 plasmid, LC3 originated from rat brain total cDNA using the following LC3 primers: forward-5'-CCGGAATTCATGCCGTCCGAGAAGACCTT-3', and reverse 5'-TTCGAATTCGCACCATAGTTATAAACCAG-3' (Kabeya et al. 2000). GFP-LC3 was obtained by insertion of the rat LC3 gene onto the BglII and EcoRI sites of *pEGFP-C1*, a fusion expression vector from Clontech Laboratories (Kabeya et al. 2000).

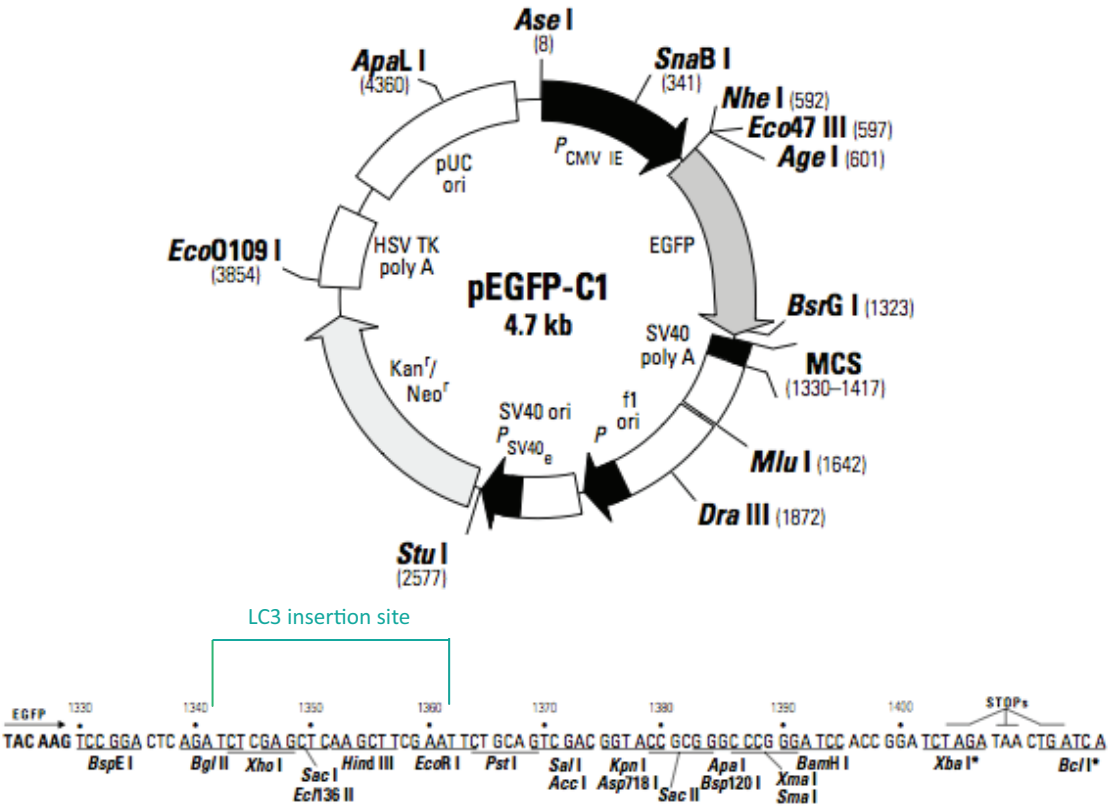

Figure 2-3: *pEGFP-C1* plasmid with LC3 insertion

To subclone into ppPAC-HA, the digestion strategy implied cutting with AfeI and SalI (GFP_LC3 fragment) for insertion into the EcoRV and XhoI restriction sites on the pPAC-HA plasmid.

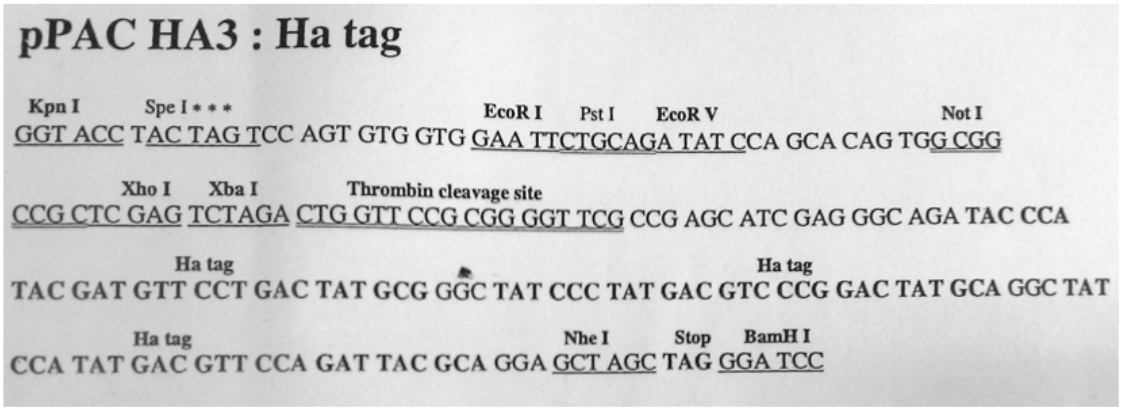

Figure 2-4: *pPAC-HA*, multiple cloning site

GFP-ATG2

A *p415-GPD-GFP-KIAA0404* (KIAAA0404 = human atg2a) plasmid from the Mizushima laboratory was used for subcloning into *pEGFP-C1* for GFP fusion on the N-terminus of *Atg2a.* For that *p415-GPD-GFP-KIAA0404* was digested with XbaI (blunted) and SalI and inserted into pEGFP-C1 between BglII (blunted) and SalI.

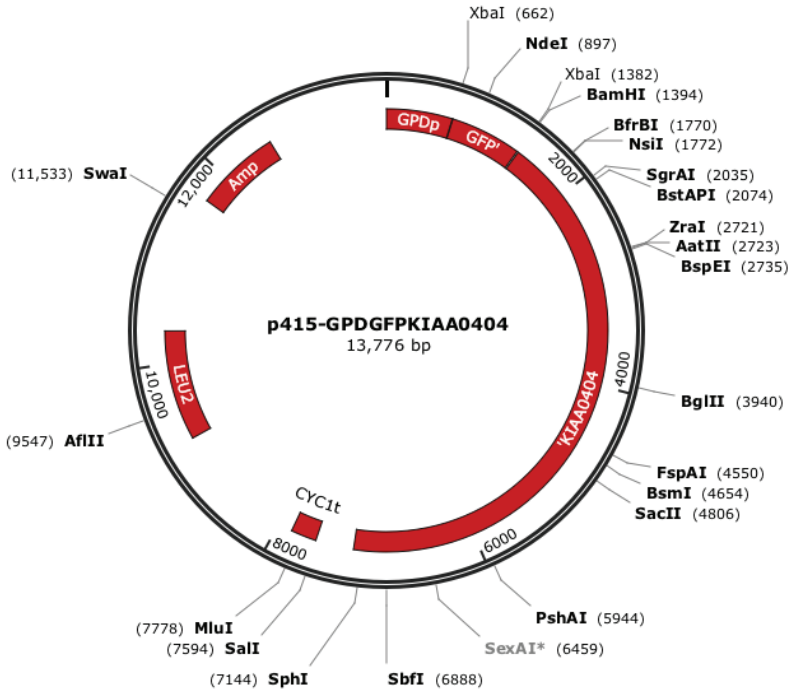

Figure 2-5: p415-GPD-GFP-KIAA0404 plasmid

pEGFP-Atg2a was then cut out with NheI and SalI (blunted) and inserted into *pPAC-HA* between XbaI and NheI (blunted).

UPD3

The *upd3* sequence was amplified from the genomic DNA of *UAS-upd3* flies, which were generated in the Bruce Edgar's laboratory. The primer sequence used for amplification is the following: forward 5'-ATATGAATTCTAAATGACGACAGCTGACCGC-3', and reverse 5'-TCT CGTCTAGAGTTTCTTCTGGATCGCCTTTG-3'. This fragment was cut with EcoRI and XbaI and was ligated into pPAC-HA between EcoRI and XbaI.

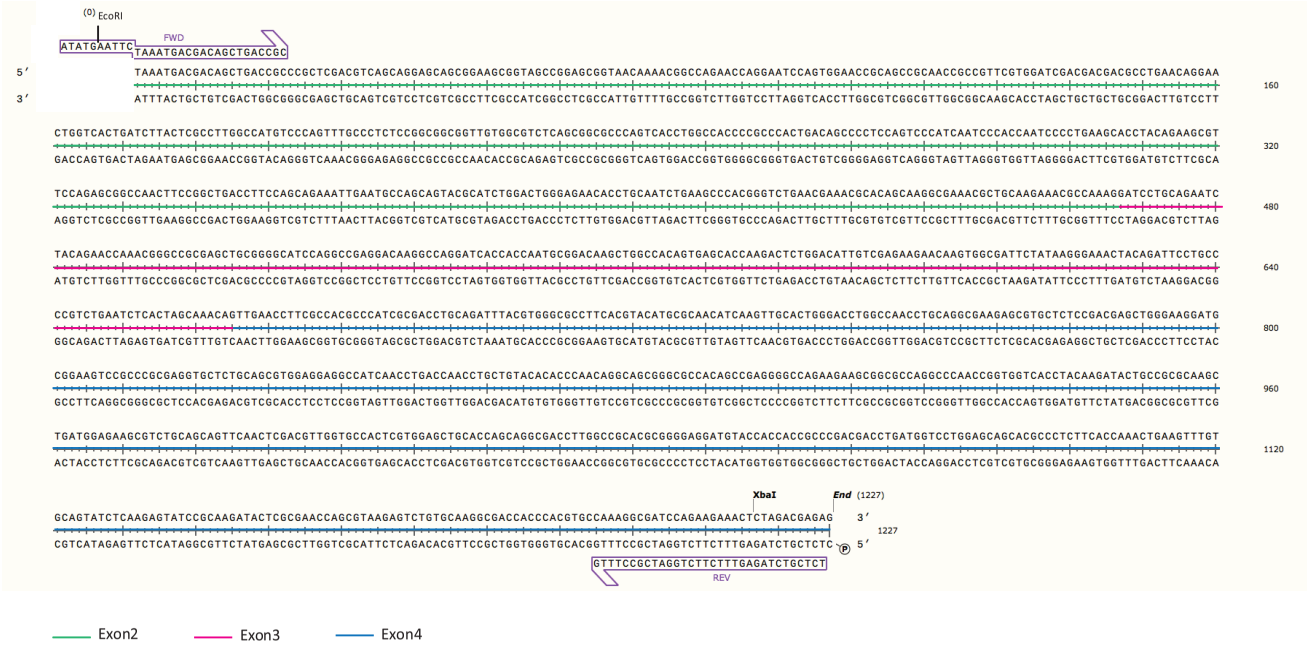

Figure 2-6: upd3 amplicon

Digestion and gel electrophoresis

Plasmids were digested with the above-mentioned restriction enzymes from NEB for 1 to 2 hours at 37˚C. The restriction digests were separated based on their size via gel electrophoresis using 1% TAE as running buffer. Gels were made with 1% agarose and were labelled with ethidium bromide (1/10000). The bands were revealed using a Bio-Rad Gel Doc EZ Imager and the correct fragment size was determined by comparison to a 1kB molecular weight maker ladder (NEB). The correct band was excised with a scalpel and extracted from the gel via the Qiaquick Gel Extraction kit according to manufacturer's instruction.

Ligation and transformation

The ligation was done overnight at 4˚C by mixing the purified DNA fragment with the digested pPAC-HA plasmid and with a T4 DNA ligase (NEB). After ligation, the reaction was kept on ice.

An aliquot of frozen competent *E.coli* was thawed on ice and then resuspended with the plasmid DNA. After 30 minutes on ice, a 30s heat-shock treatment at 42˚C was given to allow the incorporation of the plasmid DNA into the competent bacteria. Bacterial medium was then added and the bacteria were incubated for 60 to 90 minutes at 37˚C shaking before being plated on LB-agar plates supplemented with 100ug/mL of Ampicilin. The plates were incubated overnight at 37˚C and then kept at 4˚C.

To identify the clones containing the correct plasmids, a diagnostic digestion was done. For that, four clones were picked from the plates and cultured overnight in LB-Amp medium at 37˚C shaking. The plasmids were extracted using the QIAprep Spin Miniprep Kit (Qiagen) according to manufacturer's instructions. Diagnosis restriction digests allowed the identification of clones containing the correct plasmid.

Plasmid stocks

Clones carrying the correct plasmid construct were cultured overnight to generate a culture stock of transformed bacteria, and to start a midiprep (Macherey-Nigel midiprep kit). Midiprep was performed accordingly to the manufacturer's instructions and a 300µL stock of plasmid in TE buffer was generated.

Plasmid	*Concentration*
pPAC-GFP-LC3	1421 µg/mL
pPAC-GFP-ATG2	1000 µg/mL
pPAC-upd3	390 µg/mL
pPAC-HA	386 µg/mL

Table 2-6: List of plasmids generated and used in this thesis

2.3.2 Cell transfection and infection

$S2R^+$ cells were transiently transfected with either of the plasmid or combination of two plasmids using the effectene transfection reagent from Qiagen. Fully adherent cells were washed and resuspended in starvation medium (M3+1%PS). Cells were detached using a cell scraper and then plated and incubated at 25˚C for 30 minutes prior to transfection. Transfection was optimised and processed according to the manufacturer's instruction and cells were resuspended in transfection medium (transfection mix in cell culture medium).

Experiment	**Plate**	**Cells**	**Plasmid quantity**	**EC buffer**	**Enhancer solution**	**Effectene Reagent**
Imaging, WB	24-well plate	$7.5*10^5$/well	400ng	60	3.2	10
Others	6-well plate	$1.5*10^6$/well	800ng	100	6.4	20

Table 2-7: Settings for transfection

After 22 hours, the transfection medium was removed and cells were washed 3 times with cell culture medium, and were kept in the same medium for 2 hours prior to infection with *M.marinum*. Bacteria were prepared under sterile condition from 5 to 10 days old culture. They were spun down for 5 minutes, the supernatant was removed and cells were resuspended in cell culture medium. Clumps were removed after vortexing thoroughly and after spinning down the culture for 10 minutes at 700g. The supernatant was collected and the OD_{600} was measured. Since at OD_{600}=0.500 there are 100 bacteria/ nL (as previously calculated for whole fly injections), dilutions in cell culture medium were calculated accordingly to infect cells at a multiplicity of infection (MOI) of 10 to 20. The MOI is the ratio of infectious agent to the number of host cells. Cells were infected for 24 hours prior to collection, unless otherwise stated.

2.3.3 Quantitative RT-PCR

After 24 hours of infection, the cell medium was removed and cells were washed once with sterile PBS 1X before addition of TRIzol. TRIzol samples were pipetted up and down several times and then put into a microfuge tube for storage at -20˚C. The samples were then processed for RT-PCR accordingly to the protocol described in the “In vivo” section, with the chloroform and isopropanol quantities recalculated for proportionality to the volume of TRIzol. The primers used are listed in the “In vivo” section.

2.3.4 Cytotoxicity assay

After 24 hours of infection, for each sample, the 2mL supernanant was collected and put directly into a FACs tube. The adherent cells of the same sample were detached using 2mL of cold culture medium and pipetting up and down. The medium was then added to the previously collected supernatant sample. All samples were filtered with a 70µm cell strainer filter (BD Biosciences) and kept on ice prior to FACs analysis. Five minutes prior to analysis, 5µL of propidium iodide was added to 500µL of samples to stain dead cells. Cells were analysed with a FACS Aria II, using a 100µm nozzle and the FACSDiva software. All experiments included the following controls: *M.marinum* only samples with and without PI staining, and non-infected cells with and without PI.

2.3.5 Phagocytosis assay: pHrodo-coated beads

Phagocytosis assay was performed according to the Guermonprez's laboratory protocol. After 48 hours of transfection, supernanant and adherent cells were collected, the former one using cold cell culture medium. 500000 cells were spun down for 3 min at 21˚C, 1400rpm and resuspended in fresh medium. pHrodo-coated beads were added at a concentration of 1/100 v/v and incubated with cells for 30 minutes at 25˚C. Cells were then spun for 3 min at 21˚C, 1400rpm to remove free beads. Fresh medium was added and cells were incubated one more hour prior to analysis by FACs (BD LRS Fortessa). Samples were analysed in the UV chanel (IndoViolet beads) and the Texas red chanel (pHrodo). The experiment included the following controls: cells without beads, and beads-only control (no pHrodo).

2.3.6 Western blotting

After 24 hours of infection in 24-well plates, cells were washed twice with PBS1X and then 75µL of Laemmi buffer was added. Samples were pipetted up and down several times and then kept in microfuge tube at -80˚C. Samples were processed as described in the "In vivo" section. To detect Atg8-PE proteins, PVDF membranes were used and were incubated with Anti-ATG8 antibody (Kohler lab). The secondary antibodies was HRP anti-rabbit IgG (CST #7074) and the HRP signal was detected with Supersignal West Femto (Pierce). The images were processed using the Image Lab™ software from Bio-Rad.

2.3.7 Bacteria number per cell

To count bacteria per cell, a coverslip was added in 24-well plates prior to transfection. 24 hours after infection with dsRed *M.marinum*, samples were washed 2 times with sterile cell culture medium and once with sterile PBS 1X. The cells were then fixed for 20 minutes with 2% PFA, washed 3 times with PBS 1X, once in water and then mounted using Fluoromount-G (Southern Biotech). The slides were left to dry for 24 hours and were then imaged using a confocal microscope (SP5, Leica) with a 63X objective. Cells were observed under the bright field and *M.marinum* was detected in the red chanel, after excitation at 561nm.

To detect the colocalisation of *M.marinum* with Atg2, cells were transfected with *pPAC-GFP-Atg2* and then infected for 24 hours. After fixation, cells were washed 3 times with PBS1X-1%BSA-200mM glycine and then permeabilised for 5 minutes in 0.1% saponin in PBS1X. Cells were then incubated for 2 hours with a rabbit anti-GFP antibody (1:150, Life Technologies) in 0.1% saponin in PBS1X. Cells were then washed 4 times with PBS1X and then incubated for 1 hour at room temperature with an alexa-488 goat anti-rabbit antibody (1:300, Life Technologies) in 0.1% saponin in PBS1X. DAPI (1:1000) was added for the last 20 minutes. Samples were then washed 3 times with PBS1X, once in water, and then mounted using Fluoromount-G (Southern Biotech). The cells were imaged using confocal microscopy (Leica TCS SP5) and the capturing software (Leica LAS-AF). Images were then processed using Imaris (Bitplane).

2.3.8 *M.marinum* Colony Forming Unit (CFUs)

For this experiment (chapter 4), several transfections of $S2R^+$ cells were performed:

(1) *pPAC-HA*, as control;

(2) *pPAC-upd3*, to overexpress *upd3*;

(3) *pPAC HA* + *pPAC-GFP-Atg2*, to overexpress *Atg2*;

(4) *pPAC upd3* + *pPAC-GFP-Atg2*, for epistasis analysis.

After 24 hours of transfection, $S2R^+$ cells were infected with *M.marinum* at MOI 20 for 3 hours. After 3 hours, I removed extracellular bacteria by performing several washes and then added amikacin (200µM) to the cell medium, a bacteriostatic antibiotic efficient against *M.marinum* (Aubry et al. 2000; Oh et al. 2012). The antibiotic was left in the medium until samples were collected to prevent bacteria from growing in the extracellular medium. After 24 hours of infection, cells were washed several times to remove bacteria released from dead cells. Intact cells were then collected, counted with a hemocytometer and lysed with 0.1% triton-X in OBS1X to release intracellular mycobacteria. Serial dilutions were made from the initial sample and plated into Middlebrook 7H9 agar plates (Middlebrook 7H9 broth, 10% OADC, 0.2% glycerol, 0.2% tween-20, 1% agar, 100 µg/mL ampicilin, 10 µg/mL nalidixic acid). The plates were sealed with parafilm, and after 2 weeks of growth at 29˚C, the colony forming units were counted.

2.3.9 Measuring autophagy

To quantify autophagy per cell, a coverslip was added in 24-well plates prior to transfection. 24 hours after infection with *M.marinum*, samples were washed 2 times with sterile cell culture medium and once with sterile PBS1X. The cells were then fixed for 20 minutes with 2% PFA and washed 3 times with PBS1X-1%BSA-200mM glycine. Cells were permeabilised for 5 minutes in 0.1% saponin in PBS1X and then incubated for two hours at room temperature with either a rabbit anti-GFP antibody (1:150, Life technologies, for GFP-LC3 transfected cells) or a rabbit anti-Atg8 antibody (1:75, Cherry lab) in 0.1% saponin in PBS1X. Cells were then washed 4 times with PBS1X and then incubated for 1 hour at room temperature with an alexa-488 goat anti-rabbit antibody (1:300, Life Technologies) in 0.1% saponin in PBS1X or a donkey anti-rabbit Cy3 antibody (1:500, Jackson Immunoresearch, only for samples treated with anti-Atg8 antibody). DAPI (1:1000) was added for the last 20 minutes. Samples were then washed 3 times with PBS1X, once in water, and then mounted using Fluoromount-G (Southern Biotech).

Transfection	*M.marinum*	Primary Ab	Secondary Ab
pPAC-GFP-LC3 with pPAC-HA or pPAC-upd3	*dsRed M.marinum*	Anti-GFP (1:150)	Alexa-488 goat anti-rabbit antibody (1:300)
pPAC-HA or pPAC-upd3 or pPAC-GFP-Atg2	*wt M.marinum*	Anti-Atg8 (1:75)	Alexa-488 goat anti-rabbit (1:300) or Cy3 (1:500)

Table 2-8: Experimental features for the quantification of autophagy punctae

The slides were left to dry for 24 hours and were then imaged using a confocal microscope (SP5, Leica) with a 63X objective. Bright field, the 488nm laser (GFP), the 561nm laser (dsRed) and the UV light (DAPI) were used depending on the experiment. The cells were imaged using confocal microscopy (Leica TCS SP5), and the images were then processed using Imaris (Bitplane).

2.3.10 Measuring lipid droplet formation and morphology

To quantify the lipid droplets per cell, a coverslip was added in 24-well plates prior to transfection. 24 hours after infection with *M.marinum*, samples were washed 2 times with sterile cell culture medium and once with sterile PBS1X. The cells were then fixed for 20 minutes with 2% PFA and washed 3 times with PBS1X-1%BSA-200mM glycine. Cells were permeabilised for 5 minutes in 0.1% saponin in PBS1X and then incubated for two hours at room temperature with a rabbit primary antibody (FITC-conjugated anti-*M.tuberculosis:* 1:50, Thermo scientific*;* or anti-GFP, 1:250, Life Technologies), washed 4 times with PBS1X and then incubated for 1 hour with a secondary antibody (1:500, Alexa-488 goat anti-rabbit, Life Tchnologies)). Cells were then washed 4 times with PBS1X, and incubated for 45 minutes with OilRedO (ORO), a lysochrome dye staining neutral lipids. DAPI (1:1000) was added for the last 20 minutes. Cells were then washed 3 times with PBS1X, stained with DAPI (1:1000) for 20 minutes and rewashed 3 times with PBS1X. Just prior to mounting, cells were washed once in water, and then mounted using Fluoromount-G (Southern Biotech).

Transfection	M.marinum	Primary Ab	Secondary Ab
pPAC-HA or pPAC-upd3 or pPAC- GFP-Atg2	wt M.marinum	Anti-GFP (1:150)	Alexa-488 goat anti-rabbit antibody (1:500)
pPAC-HA or pPAC-upd3	wt M.marinum	FITC-conjugated Anti-M.tuberculosis (1:50)	No secondary

Table 2-9: Experimental features for the quantification of lipid droplets

The slides were left to dry for 24 hours and were then imaged using a confocal microscope (SP5, Leica) with a 63X objective. Bright field, the 488nm laser (GFP), the 561nm laser (ORO) and the UV light (DAPI) were used. The cells were imaged using confocal microscopy (Leica TCS SP5), and the images were then processed using Imaris (Bitplane).

2.4 Statistical analysis

All statistics were done with Graph Pad Prism using descriptive statistics, linear regression, Kaplan-Meyer survival curves, Mann Whitney test and two-way ANOVA analysis.

2.4.1 Descriptive statistics

Descriptive statistics were used to determine the mean, the standard deviation, the standard error of the mean, the minimum and maximum values, the median and the 25% and 75% percentiles of the population of data.

Value	Formula
Mean	$\mu = \Sigma(x_1+x_2+...+x_n)/n$
Variance	$Var[x] = [\ \Sigma(x_1-\mu)^2+(x_2-\mu)^2+...+(x_n-\mu)^2\ ]/n$
Standard deviation	$Stdev= \sqrt{}\ var[x]$
Standard error of the mean	$SEM= stdev/\sqrt{}\ (n)$
Median	If n is even, the median=$(x_{n/2}+x_{(n/2)+1})/2$ If n is odd, the median is the value of rank (n+1)/2

Table 2-10: Formula for the descriptive values used in this thesis

Boxplots are a convenient way of displaying the dispersion of values. In chapter 5 and 6, boxplots were represented with the first, second and third quartile. In chapter 5, the whiskers delimitate the 10 and 90 percentiles, and in chapter 6, they delimitate the minimum and maximal values.

2.4.2 Linear regression

A linear regression was estimated between hemocyte death and bacterial number per fly using the simple formula Y=ax+b (Chapter 3, Figure 3). The model assumed that the values calculated are exact, the samples are independent and all the samples represent the studied phenomenon. The calculation was based on three couple of values (bacteria per fly: hemocyte

death per fly) and was estimated to be: %hemocyte death = $7x10^{-6}$ * bacteria + 3.886. The linear regression is considered to fit due to an r^2 of 0.9995, and the scatter of the data points around the best fit line was computed via Syx =1.152.

2.4.3 Kaplan-Meyer survival curves

The survival curves plot the time until death for each individual fly. The raw data were plotted using the product limit method (Kaplan-Meier) showing the fraction of flies that are still alive after a certain time. The curves from different genotypes were compared using both the log-rank test and the Gehan-Wilcoxon test. The log-rank test (mantel-Cox) is the more powerful of the two tests if the proportional hazards is true, i.e the death rate is the same at all timepoints. It is not the case upon infection with *M.marinum* in *Drosophila*. However, this test gives equal weight to all timepoints while the Gehan-Breslow-Wilcoxon method gives more weight to early timepoints. As a consequence, and because the log-rank test is more standard, it was the test used in this thesis. This test gives back a p value, which tests the hypothesis that the curves are identical between the two genotypes compared (null hypothesis). The curves are considered different if the null hypothesis is refuted, or in other words if $p<0.05$. $p<0.05$ means that there is only 5% chance for the null hypothesis to be true, in consequence the difference is considered statistically significant. If $0.01<p<0.05$ (*), the difference is considered significant; if $0.001<p<0.01$ (**), the difference is considered very significant; if $p<0.001$ (***), the difference is considered extremely significant.

2.4.4 Quantitative RT-PCR analysis

The real-time RT-PCR uses double stranded DNA dyes that fluoresce when bound to DNA. In this thesis, SYBR Green was used. It is an asymmetric cyanine dye that, when bound to DNA, absorbs the light at 488nm and emits green light at 522nm. The PCR process consists of 40 to 45 cycles of amplification where the double stranded cDNA is alternatively separated (95˚C), bound by sequence matching primers (57˚C), and used as template for polymerisation of a new strand by DNA polymerase (72˚C). As a result after each cycle the quantity of the desired double stranded DNA is, in theory, doubled. The application software plots the

fluorescence of the samples after each cycle, allowing the calculation of a linear regression between the cycle number at the threshold fluorescence and the logarythm of the concentration of DNA. The fluorescence threshold is automatically computed to give the best linear regression, as assessed by an r^2>0.99 and an efficiency close to 1.

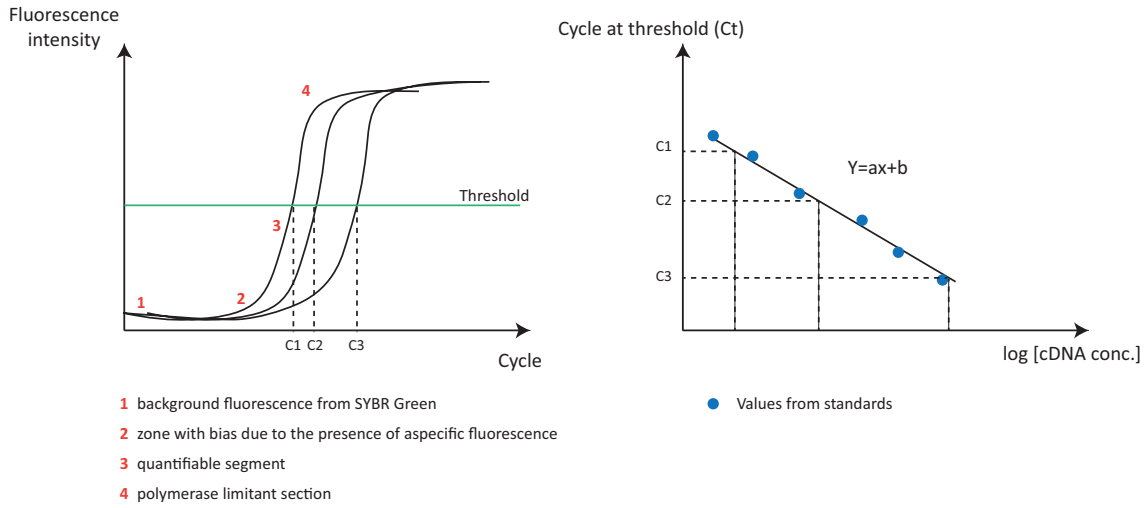

Figure 2-7: Principle of qPCR analysis

The total fluorescence intensity is plotted at each cycle for each of the sample in the experiment. A set of standards was used to determine the DNA concentration per PCR cycle at the threshold of fluorescence, and the threshold of fluorescence was automatically determined to give the best linear regression based on the standard values.

After obtaining the cDNA concentration within each sample, the data were analysed using the Mann-Whitney U test or the two-way analysis of Variance that are presented below.

2.4.5 Mann-Whitney U test

The Mann-Whitney test is a non-parametric test that was used to compare the distribution of values between two genotypes or two conditions (PBS or infected). This test is also called the rank sum test. It first implies to rank all values (mixed samples) from low to high. The smallest value gets the rank of 1 and the latest, N. The sum of the rank of each group are calculated and compared. Similarly to the survival curves, if 0.01<p<0.05 (*), the difference is considered significant; if 0.001<p<0.01 (**), the difference is considered very significant; if p<0.001 (***), the difference is considered extremely significant.

2.4.6 Two-Way analysis of Variance

To measure the effect of the genotype and the time on values, I used the two-way ANOVA analysis. The two-way ANOVA determines how a response is affected by two factors (here time and genotype) and whether these two factors are interconnected. However, one has to be careful when using two-way ANOVA with one quantitative parameter (here the time). For example ANOVA pays no attention to the order of the timepoints, and give a identical weight to early timepoints, where the genotype may have no effect. Therefore, it may affect the p value and the interpretation of the data. In our case, the two-way ANOVA was performed from timepoints late in infection, and was used to integrate all the changes in values during the timecourse of infection. For simplicity, only the p value for the genotype effect was reported.

Chapter 3 Unpaired-3, a Jak-Stat activating cytokine, is detrimental for the host upon mycobacterial infection

3.1 Introduction

Dionne et al. established that *Drosophla melanogaster* is a genetically tractable model host for *M.marinum* that recapitulates some of the key features of *M.tuberculosis* in humans (Dionne et al. 2003). Upon infection, *M.marinum* is phagocytosed and proliferate inside hemocytes, as demonstrated by GFP expression in flies carrying the *mag-24* promoter driving GFP_ Mag-24 being a mycobacterial gene upregulated upon phagocytosis (Ramakrishnan et al. 2000). If phagocytosis is blocked by bead injection, the pathogen is still able to proliferate, a trait that is common to facultative intracellular bacteria. Inside phagocytes, similar to *M.tuberculosis* infected macrophages, phagosomal maturation is arrested, and *M.marinum* does not colocalise with dead *E.coli* conjugated with pHrodo or lysotracker, indicators of vacuolar acidification. The fate of infected immune cells is unknown, but later in the course of infection, bacteria are observed in the extracellular space. In the hemocoel, the bacteria may target other cells for infection, may release virulence factors that damage surrounding host cells or even trigger a systemic response to severe bacteraemia, as suggested by the extensive tissue damage. In consequence, there are many bacterium-filled abscesses in the fat body, and adipocytes appear abnormal with an increasing number of large vacuoles. Possibly as a result of tissue destruction, of exotoxin release, and/or of wasting disease, the fly ultimately dies_usually after 8 to 9 days of infection. Strikingly, AMP expression, a major immune response of insects to $Gram^+$ and $Gram^-$ bacteria, is not induced upon mycobacterial infection indicating that other immune pathways may be activated to control the infection.

Agaisse et al. demonstrated that *upd3* is upregulated in hemocytes by bacterial infection, and it induces the transcription of the JAK-STAT target *TotA* in the fat body (Agaisse et al. 2003). This result strongly suggests a role for Upd3 and JAK-STAT in immune responses to infection in adult flies. This pathway has been broadly studied for the past two decades in mammals and more recently in the fly. It is relevant in innate immunity for its role in

hematopoieisis, tissue homeostasis and regeneration, and secretion of acute phase proteins (Agaisse & Perrimon 2004; Buchon, Broderick, Poidevin, et al. 2009b; O'Shea & Plenge 2012). However, despite its importance in innate immune responses, little is known about its precise function, probably due to the complex compensatory mechanisms of the different JAK and STAT proteins in mammals (Stark & Darnell 2012; Dostert et al. 2005). Recently, however, a first hint towards its control of intra-macrophage bactericidal mechanisms was inferred through the action of one of its ligands, IFN-γ (Harris et al. 2007; MacMicking et al. 1997).

In the fly, three cytokines have been described as putative ligand for the pathway: Upd, Upd2 and Upd3, three Upd-family members that exert different functions and that are activated upon different stimuli (Osman et al. 2012; Harrison et al. 1998; Hombría et al. 2005; Agaisse et al. 2005). Their related genes are located in the same locus, called outstretched (os) due to the wing phenotype observed in os mutants. Os mutants have also a “small eye” phenotype, that is known to come from Upd/Upd2/Upd3 related functions (Bach et al. 2003).

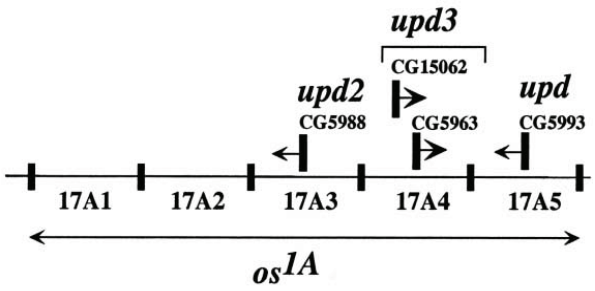

Figure 3-1: *os* locus

Schematic representation of the *os* locus that contain coding regions for three *upd*-family members: *upd*, *upd2* and *upd3.* The genes are designated by their protein coding gene number (CG number) (Agaisse et al. 2003).

Upd3 is the only Upd-family member that was shown to be responsive to bacterial infection in adult flies (Agaisse et al. 2003). It is described as an ancestor of the four-helix bundle cytokines including Interleukin 6 (IL-6) (Oldefest et al. 2013). Upd3 analogy to IL-6 is further implied by its binding to Domeless, a type I cytokine receptor homolog of the mammalian IL-6 receptor, gp130. Upd3 is a monomeric-alpha-helical protein containing a predicted 65

amino acids signal peptide, and its mature form is secreted with a size around 55kDa. It can activate JAK-STAT signalling in an autocrine and/or paracrine fashion (Wright et al. 2011).

This chapter first explores in more details the features of *M.marinum* injection in the fly, including the pattern of infection, the expression of known immune effectors, the mycobacterial replication rate and the fate of the immune cells. Then, it aims at describing the effects of Upd3 and its potential role in immune resistance and tolerance.

3.2 Results

3.2.1 *M.marinum* infection spreads mainly in two areas, induces cytotoxicity and ultimately kills the fly

Flies injected with 500 CFUs of *M.marinum* die after 8 to 9 days of infection (Dionne et al. 2003). As observed by Dionne et al., one of the main *M.marinum* infection sites is the dorsal vessel that contains a vast amount of phagocytic cells. More precisely, confocal imaging of a 400µm section in the back of the fly, revealed the first chamber of the dorsal vessel as one of the major sites of infection and proliferation (**Figure 3-2**). The second major infected area is the head that contains, the brain, fat body tissues, and hemocytes. Since mycobacteria are mainly found in hemocytes, which are distributed throughout the fly, this finding implies a specificity of the head region. At low density (early infection), it is hard to detect dsRed *M.marinum* by intravital imaging, however at higher density (from day 5 onwards), the main sites of bacterial replication appear, showing the specific pattern of infection.

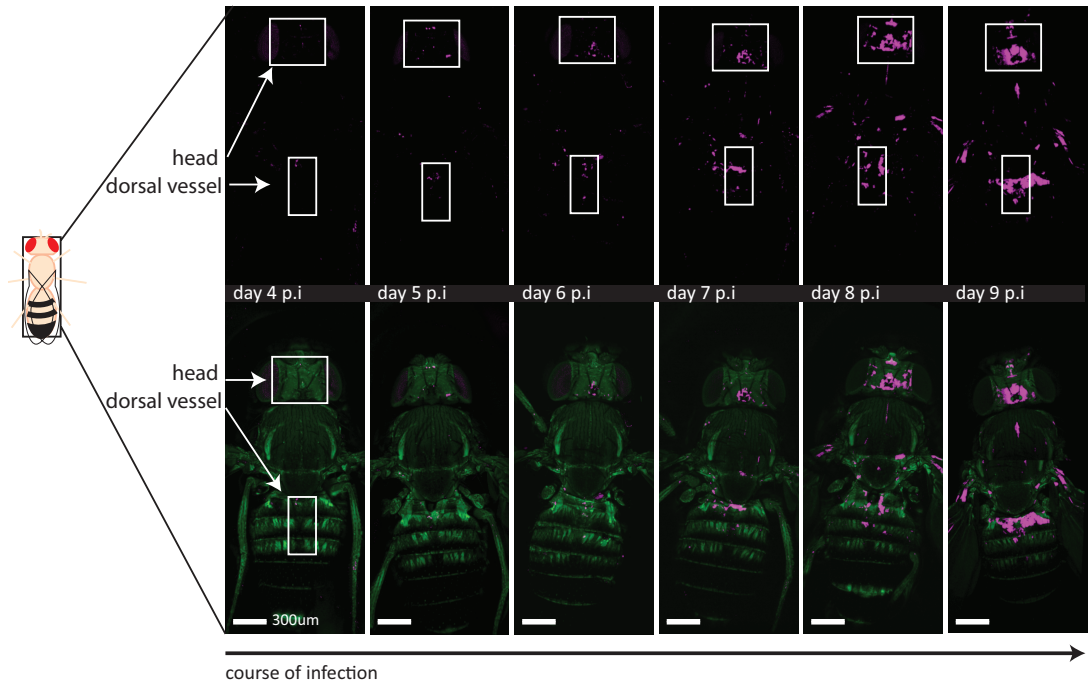

Figure 3-2: Pattern of infection with dsRed *M.marinum*

Flies were imaged each day following infection with dsRed *M.marinum*, 500 CFUs. Images of a 400µm section in the back of wild-type flies (+;+;+, Drosdel) were taken from anesthetised flies. In order to see the flies and the specific localisation of the bacteria, the 10Xstat-GFP construct was used (bottom); bacteria were observed in the red chanel (top). A representative picture for each day is depicted. n=3 per day.

To quantify bacterial replication, I performed quantitative PCR from whole fly samples using specific primers for *M.marinum* (see Material & Methods; **Figure 3-3**). Detection is difficult below 10 000 bacteria, in consequence accuracy of measurement is obtained only from day 4 onwards. The growth seems exponential from day 4 post-infection. However, when log-transformed, the curve is not straight, as would be the case for true exponential growth. Indeed, from day 6 of infection, the replication rate decreases strongly and mycobacteria divide every 12-24 hours instead of every 6-8 hours. Shortly before death, the host harbours more than 12 million bacteria, indicating, in average, a division every 13 hours.

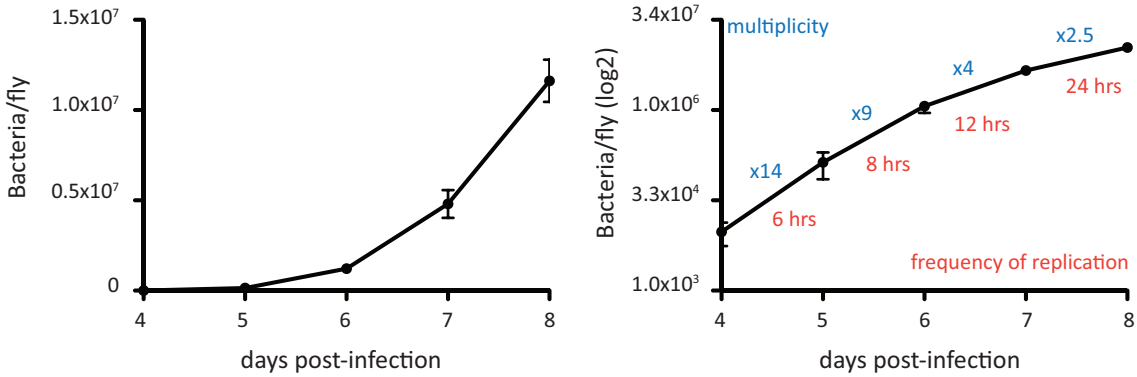

Figure 3-3: *M.marinum* growth and replication rate

The left panel represents the number of bacteria per fly assessed by qPCR relatively to an absolute standard of bacteria. *M.marinum* growth is likely to be exponential from day 4 post-infection and the fly die with more than 12 million bacteria. The binary log graph (right) does not show linearity, and the multiplicity of infectious agents decreases alongside the course of infection (numbers on top of the graph). To calculate the replication frequency I applied the following formula: frequency= 24 (hours) / (multiplicity), and multiplicity= number bacteria at day N/ number of bacteria at day N-1) (numbers below graph). These graphs combine results from 2 independent experiments, with a total of 6 repeats for each timepoint. Intervals between each timepoint are exactly 24hours.

Decreases in replication rate may indicate a host attempt to control bacterial expansion, probably by changing the bacterial environment to render it more toxic. Dionne et al. showed that bacteria initially grow within hemocytes, but are also able to proliferate in the extracellular space when phagocytosis is inhibited by beads injection (Dionne et al. 2003). As induction of necrosis is a strategy adopted by *M.tuberculosis* to escape from macrophages and proliferate, it was interesting to assess the fate of macrophage-like cells in the fly. Indeed, changes in bacterial multiplicity may result from a transition from an intracellular niche to the extracellular space. To answer this question, I looked at hemocyte number by confocal imaging using two hemocyte-specific markers, hemolectin (Hml), a clotting factor, and croquemort (Crq), a scavenger receptor (Goto et al. 2001; Franc et al. 1999). Wild-type flies carrying an *HmlΔ-gal4* or *crq-gal4* construct driving the expression of *UAS-GFP* were imaged each day following injection with *M.marinum* or PBS as control. In addition, *Hml* expression was quantified in the whole fly. The results indicate a decrease in hemocyte number and of *Hml* expression in late infection (**Figure 3-4** A & B). To confirm that *M.marinum* infection does induce cell death and not just a decrease in hemolectin expression, $S2R^{+}$ cells were either infected with *M.marinum* at a MOI of 20 or not infected, and cell death was recorded. After 24hours of incubation with the pathogen, cells were collected and stained with propidium iodide (PI), a DNA intercalating agent that only enters dead or dying host cells. As expected, the infection triggered cell death among

hemocyte-like cells, therefore suggesting that *M.marinum* induces death of immune cells in vivo (**Figure 3-4** C).

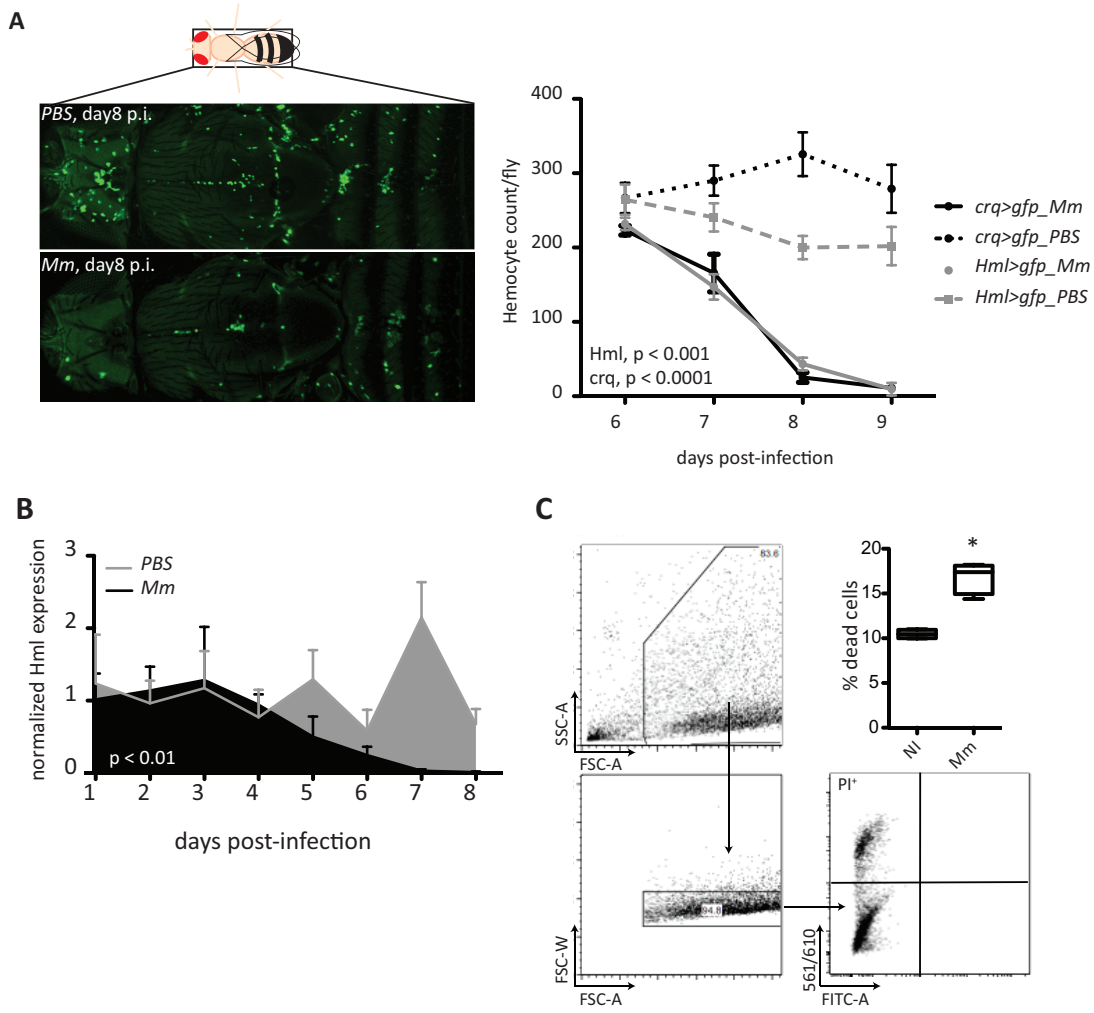

Figure 3-4: Hemocyte death in late infection

(A) The number of hemolectin (Hml) and croquemort (Crq) positive cells decreases overtime in infected samples compared to PBS controls. GFP^+ cells were quantified from a 350µm section on the back of the flies and a representative image taken at day 8 post-injection is presented. 5 to 6 flies were used per timepoint for each genotype. (B) Hemolectin levels decrease from day 5 p.i. until reaching undetectable levels from day 7 onwards (n=3 per timepoint). *Hemolectin* expression was assessed by qPCR and normalised over *RpL1*. (C) *M.marinum* infection induces cells death in $S2R^+$ cells. $S2R^+$ cells were infected with *M.marinum* at MOI 20 and compared to non-infected control. The flow cytometry strategy to exclude doublets (middle) and to select PI^+ cells is presented (right). For panel A and B, p values were calculated using two-way ANOVA. For panel C, the p value was calculated using Mann Whitney test (*p < 0.05).

Hemocyte decline starts between day 6 and 7, when the number of bacteria exceeds 2 million per fly (**Figure 3-5**). Of interest, at this stage, a strong correlation exists between bacterial numbers and hemocyte death that allows making predictions.

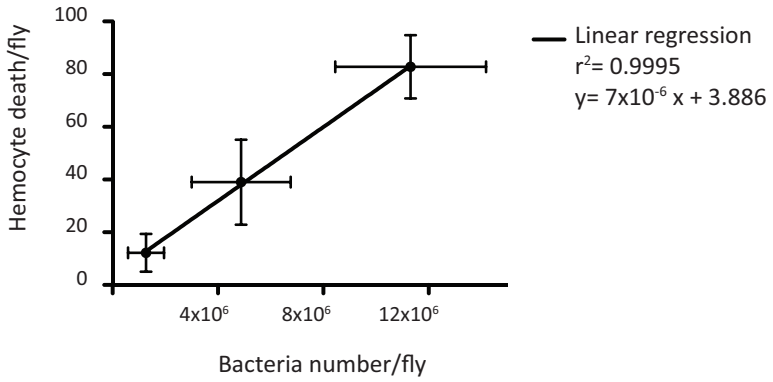

Figure 3-5: Correlation between hemocyte death and bacterial number in late infection

Hemocyte death was measured as percentage of Hml^+ cells in infected control compared to PBS controls. The mean value is the result of 5 to 6 measures. The bacterial number per fly was assessed by qPCR of the whole organism and the mean value is the result of 6 measures. Because different flies were used for hemocyte death measurement and bacterial number, only the mean values are plotted. The linear regression has an r^2 of 0.9995 indicating strong linearity and the deduced equation is as followed: % hemocyte death = $7x10^{-6}$ * bacteria + 3.886.

As previously mentioned, the bacterial replication rate decreases from day 6 post-infection at the time when hemocytes start to decrease in number. Since bacteria were observed in the extracellular space in late infection, it is then possible that hemocyte death allows the release of bacteria into the hemocoel. The hemocoel may then be more hostile to the bacteria than the intra-phagocyte environment. Indeed, the hemolymph contains various toxic peptides that aim at targeting invaders to neutralise and kill them. Among them are the antimicrobial peptides, and the complement-like peptide TEP2. Dionne et al. did not see any upregulation of antimicrobial peptides up to 3 days post-infection (Dionne et al. 2003). However, the data presented in **Figure 3-4** suggest that the bacteria may reach the cytosol in high number after hemocyte death from day 6 p.i, and since Dionne et al. observed damages in fat body tissues from day 5 p.i., all together these data point towards a late regulation of hemolymph effector molecules. To verify that, transcription of several AMPs, and *Tep2* was assessed by qPCR at each day post-infection. As predicted, AMP and *Tep2* expression is increased from day 6 p.i. (**Figure 3-6**).

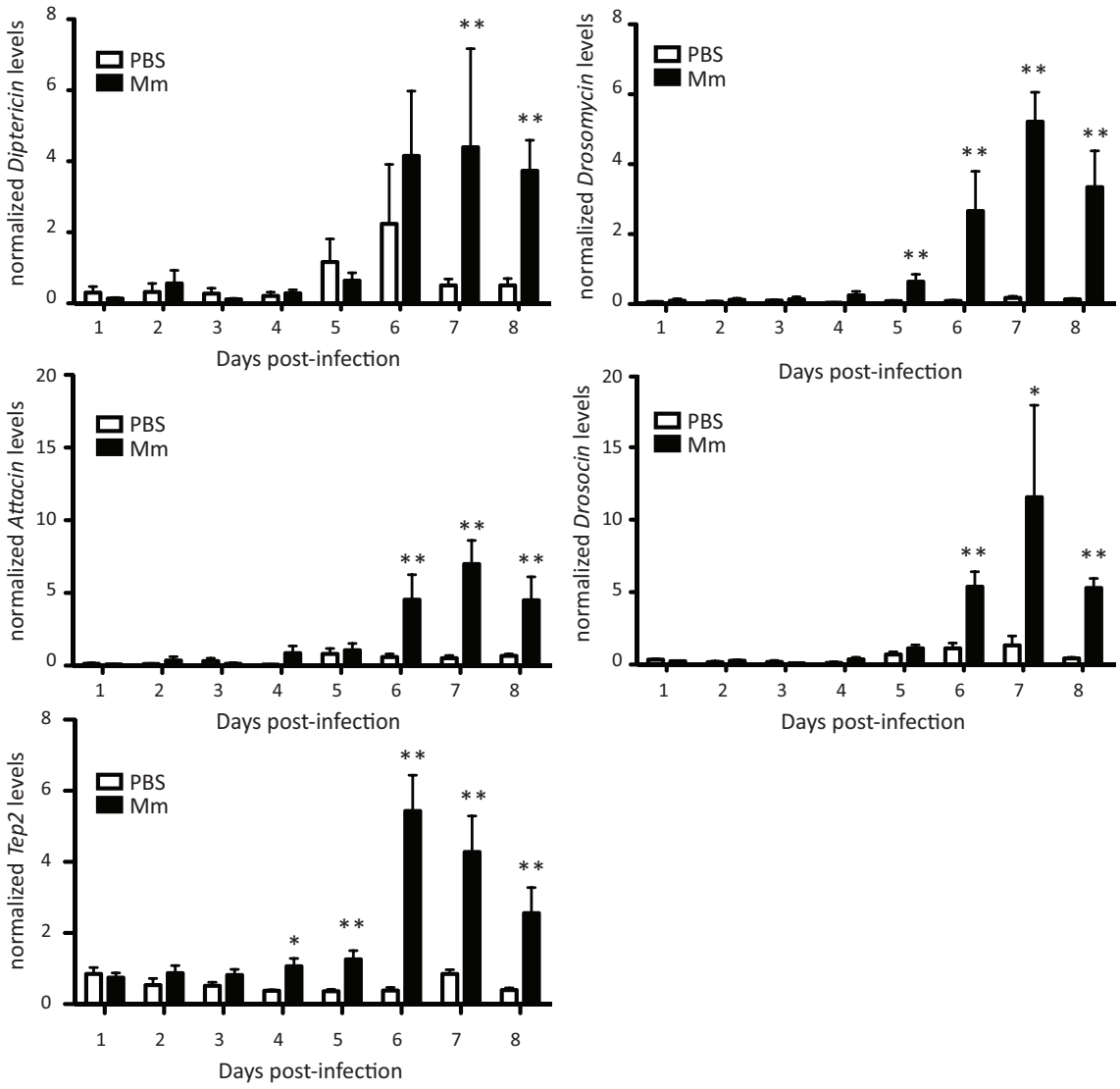

Figure 3-6: Expression of humoral factors during *M.marinum* infection

Expression levels of the different genes were normalised to *RpL1*. Most of AMPs, such as *Diptericin, Drosomycin, Drosocin* and *Attacin*, are upregulated from day 6 p.i. Tep2, a complement-like protein, is upregulated from 4 p.i onwards. p values were calculated using Mann Whitney test (*$p < 0.05$,**$p < 0.01$).

From these results, we can hypothesize that, shortly after hemocyte death, bacteria are released into the extracellular medium, where they proliferate, damage tissues and ultimately cause host death.

From *M.tuberculosis* research it is clear that pathogenicity in humans arise from the inability of the host to control the early proliferation of the bacteria. Therefore, understanding why innate immune pathway fail at controlling the initial phase of the infection is of major importance. In flies, *M.marinum* is highly pathogenic and since the Toll and Imd pathways are

only activated in late infection, our first idea was to look into the JAK-STAT pathway, whose cytokine has been implicated in the early hemocyte response to septic injury.

3.2.2 *upd3* is upregulated in phagocytes upon *M.marinum* infection

A first hint towards the role of the JAK-STAT pathway in the response to *M.marinum* infection came from the analysis of *upd3* expression, its activating cytokine. In the whole organism, no induction was detectable upon infection (**Figure 3-7** A). However, by looking at *upd3* levels in hemocytes by intravital imaging, I found that *M.marinum* triggers a strong *upd3* response in Hml^{+} cells (**Figure 3-7** B). This response was observed as early as 24 hours post-infection with high dose of bacteria (5000 CFUs; data not shown).

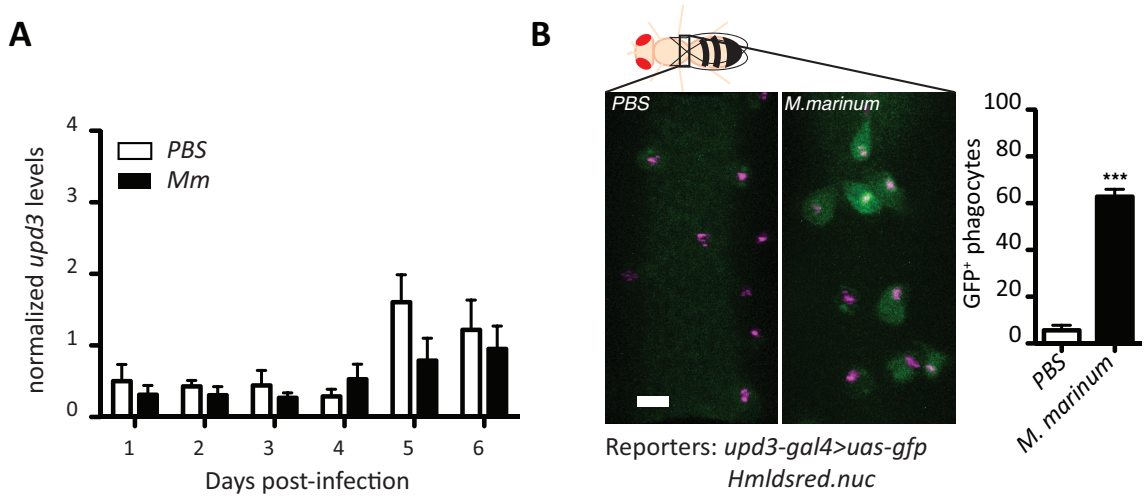

Figure 3-7: *upd3* is upregulated in hemocytes upon infection

(A) *upd3* expression in the whole fly is not changed compared to PBS injected flies. 5 to 7 days old males were injected with 500 CFUs of *M.marinum* or PBS-tween 80 as control. Samples were collected from day 1 to 6 p.i. and *upd3* levels were measured by qPCR and normalized to *RpL1*. (B) *upd3* expression is upregulated in hemocytes in vivo. Images were taken 48 hours after injection of *M.marinum* at 5000 CFUs. Hemocytes were labelled with nuclear marker *hmldsRed* and *upd3* expression was assessed by looking at GFP^{+} cells by confocal imaging, using the *upd3-gal4* reporter driving *UAS-GFP* expression. p values were calculated using Mann-Whitney test (***$p < 0.001$).

3.2.3 Upd3 blockade increases resistance to infection

To understand the role of Upd3 signalling during infection, I used *upd3* mutants and RNAi lines to look at several indicators of resistance: host survival, bacterial growth, hemocyte maintenance and immune effectors.

First, I used an uncharacterised and spontaneous mutation in the *os* locus called *os^{s}*. *os^{s}* is a mutation that upon Gram^{+} and Gram^{-} infections prevents infection-induced JAK-STAT activation (Agaisse et al. 2003). As the locus contains three Upd-family members—namely Upd, Upd2 and Upd3—the authors first verified the contribution of Upd and Upd2 to the phenotype. They generated transheterozygous flies carrying *os^{s}* and a null mutation for *upd (updYM55)* to check the contribution of Upd. They found no change in JAK-STAT activation upon infection, therefore suggesting two potential causes: first, *os^{s}* mutation does not affect the *upd* gene, or *upd* expression is altered but is not induced upon infection, thereby leading to an absence of phenotype. Authors further excluded *upd2* by showing that it is not upregulated by infection then inferring that *os^{s}* mutants affect only infection-induced *upd3* expression, and infection-induced JAK-STAT activation. So far, we do not know if *upd2* and/or *upd* expression at steady state are altered in these flies.

To check whether *os^{s}* affects *upd* or *upd2* expression upon *M.marinum* infection, I looked at their expression levels after injection of 500 CFUs (**Figure 3-8** A). No differences were noted thereby confirming that *os^{s}* may only alter upd3 expression upon infection. To understand better the nature of the mutation, I designed primers to amplify the exon 1, exon 2-3 and exon 4 region of the *upd3* locus. The results indicate that there is a potential deletion or mutation in the exon1 region (**Figure 3-8** B) (Oldefest et al. 2013). To further characterise this mutation, I performed a 5'RACE PCR to sequence the 5' region of the transcript and compare it with the wild-type sequence. The strategy was successful for wild-type flies but did not give coherent results for *os^{s}* (data not shown).

Surprisingly, when looking at *upd3* expression upon *M.marinum* infection in vivo, we noticed a strong upregulation of the altered form of *upd3* in *os^{s}* mutants, probably due to a feedback loop (**Figure 3-8** C). As a conclusion, we confirmed that *os^{s}* is a hypomorphic mutation of *upd3* that alters its expression upon infection in vivo, without affecting *upd* or *upd2* levels.

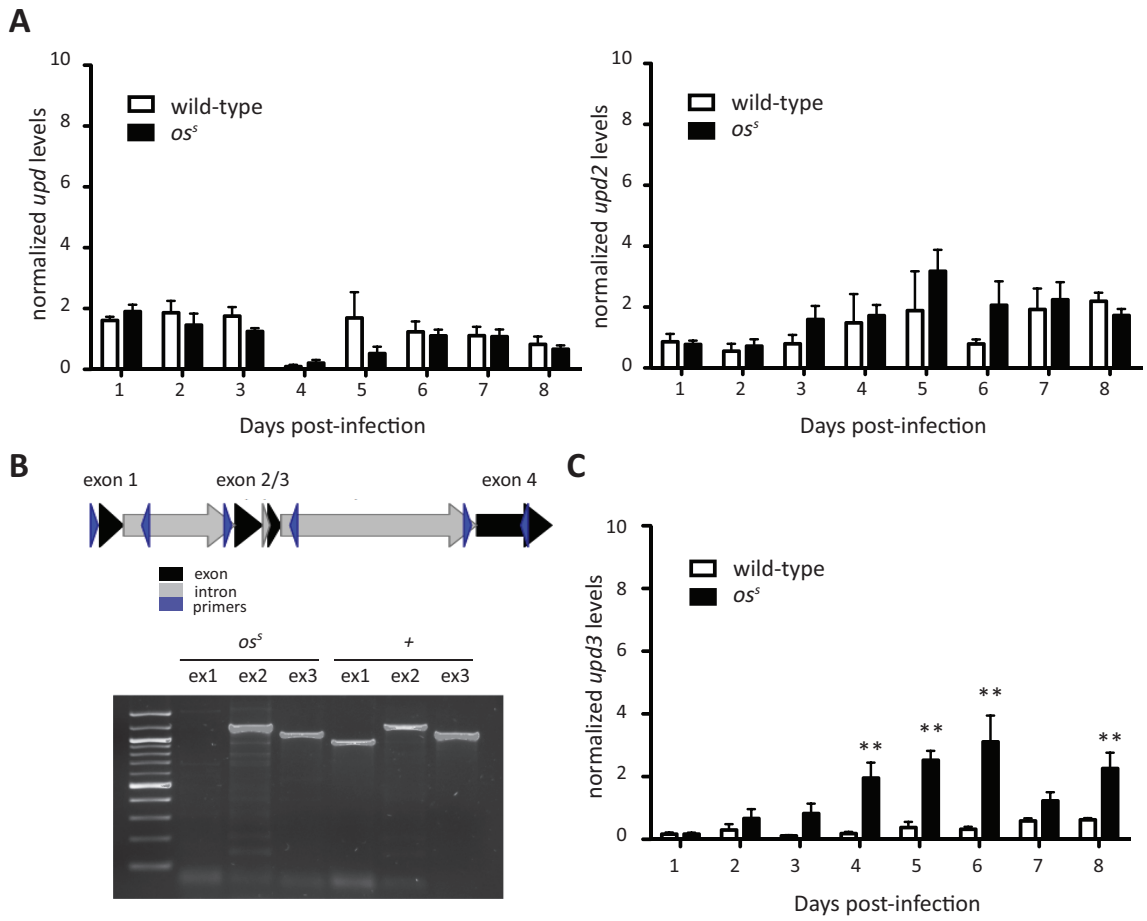

Figure 3-8: *os*^{s}, affects *upd3* expression upon *M.marinum* infection

(A) *upd* and *upd2* levels are unchanged compared to wild-type flies upon infection. Flies were taken from day 1 to 8 after injection with 500CFUs of PBS-tween 80 or *M.marinum. upd* and *upd2* levels were normalized to *RpL1*. For this experiment, n=6 per genotype and per timepoint.(B) *os*^{s} mutants have an alteration in the exon1 region. Genomic DNA fron os^{s} and wild-type flies were amplified with exon1,2-3 and 4 specific-primers. No band was observed for os^{s} flies when using the exon1 primer. For this experiment n=3.(C) *upd3* expression levels are increased in *os*^{s} mutants. This experiment was performed similarly as in A, and n=6 per genotype and per timepoint. p values were calculated using Mann-Whitney test (**p < 0.01).

Strikingly, the hypomorphic mutation of *upd3* or the hemocyte-specific knock down of *upd3* increases host survival to *M.marinum* infection (**Figure 3-9** A & B). In addition, *os*^{s} mutants have a lower bacterial growth suggesting that Upd3 signalling diminishes resistance to infection (**Figure 3-9** A). To exclude any developmental effect, I then looked at survival and bacterial growth in flies carrying a temperature inducible hemocyte-specific knock down for *upd3* (**Figure 3-9** D). At 29 degrees, *upd3* RNAi is activated and *os*^{s} flies die from *M.marinum* infection one day later than control flies. Similarly to the results obtained with *os*^{s}, knocking down *upd3* in adult hemocytes reduced bacterial proliferation and promoted host survival (**Figure 3-9** D).

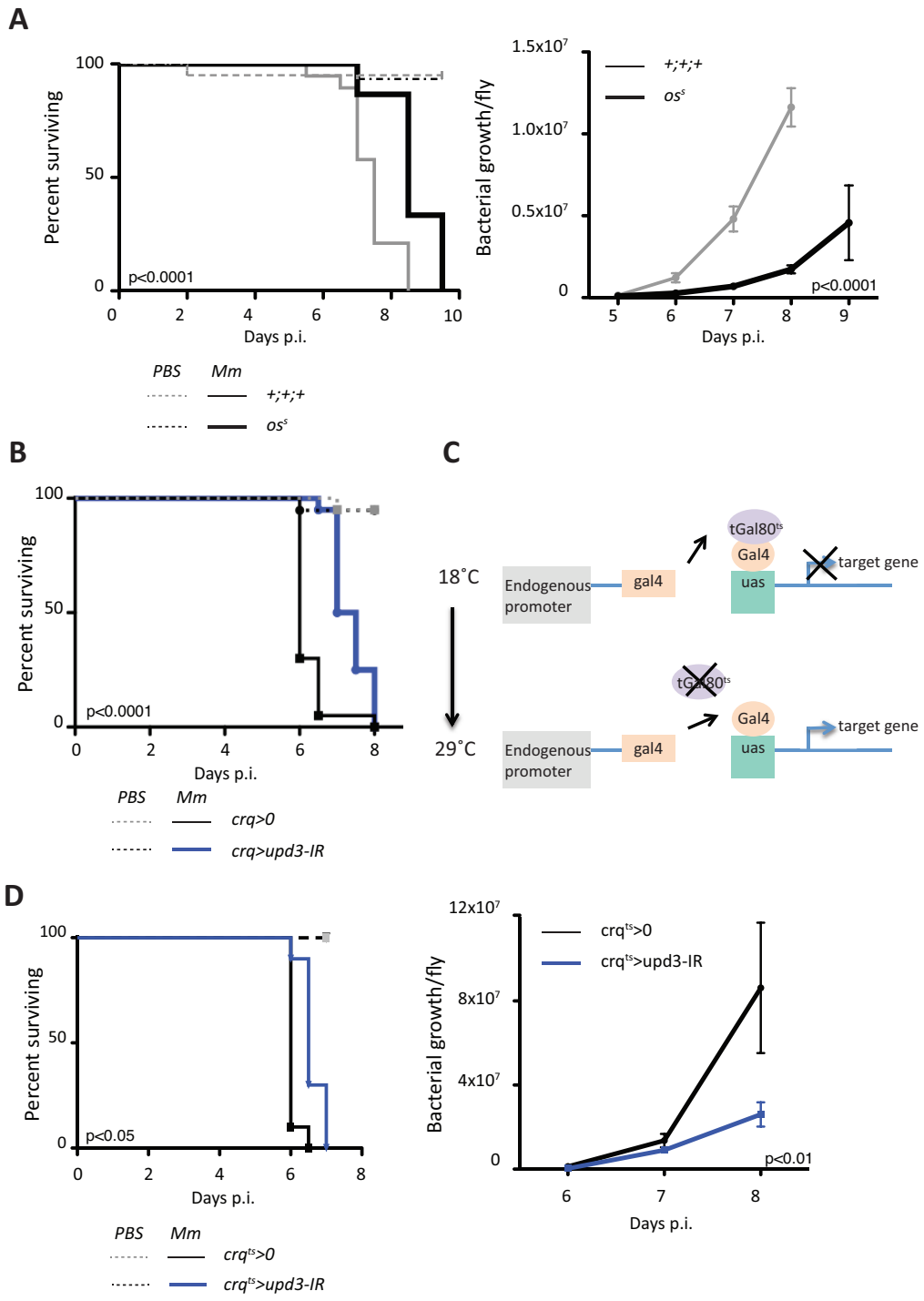

Figure 3-9: upd3 signalling decreases resistance to infection

(A) When infected with *M.marinum*, *os*^{s} mutants survive longer (left) with a lower bacterial number (right). 5 to 7 days old flies were injected with *M.marinum* at 500CFUs or with PBS-tween 80 as control. n=20 per genotype. For bacterial growth per fly, samples were taken from day 5 to 9 p.i. and were run for qPCR using the *M.marinum PyrG* primers. (B) Hemocyte-specific knock down of *upd3* prolonged host survival upon *M.marinum* infection. 5 to 7 days old flies were injected with *M.marinum* at 500CFUs or with PBS-tween 80 as control, Crq was used as driver for *upd3* inverted repeats. (C) Schematic representation of the *gal4/UAS* system in combination with *tubulin-gal80*^{ts} *(tgal80*^{ts}*)*. (D) Flies with reduced *upd3* expression in adult hemocytes have an increased survival time (left) and a lower bacterial replication (right). For this experiment, the TARGET system was used with crq as driver for *upd3* inverted repeats. Flies were kept for 4 to 5 days at 29˚C prior to injection and were then injected with Mm (500CFUs) or PBS-tween80. For bacterial count, samples were taken at day 6, 7 and 8 p.i. For survival experiments, p values were calculated using log-rank test. For bacterial count, p values were calculated using two-way ANOVA.

3.2.4 Hemocyte-specific knock down of *upd3* reduces bacterial proliferation in hemocytes

I established that Upd3 is detrimental for host survival and led to higher accumulation of bacteria in the whole organism. However, we do not know if Upd3 signalling affects bactericidal mechanisms, nutrient sources used by the bacteria or more generally host fitness, neither do we know at which stage of infection is Upd3 signalling detrimental. To assess whether Upd3 acts on immune cell bactericidal mechanisms or immune cell metabolism, I first injected flies with or without beads prior to *M.marinum* infection to block phagocytosis. Surprisingly, when phagocytosis is blocked, *upd3* knock down flies do not have an increased survival time compared to wild-type flies, indicating that Upd3 effect is dependent on phagocytosis of mycobacteria (**Figure 3-10 A**). To assess whether Upd3 signalling is important for bacterial growth inside hemocytes, I infected $S2R^+$ cells with dsRed *M.marinum* and measured the sum of bacterial fluorescence per cell after 24 hours. dsRed is constitutively expressed by the bacteria and is relatively stable for several days allowing the precise measure of bacteria. From this experiment, I found that $S2R^+$ cells overexpressing *upd3* had a higher bacterial load than control cells (+36%), suggesting that upd3 signalling enhances bacterial growth within phagocytes (**Figure 3-10** B).

One could argue that upd3 could act on bacterial uptake and not necessarily on bacterial replication. To verify that, I infected os^s and wild-type flies with a pH-sensitive probe pHrodo-labelled *E.coli* bioparticle that is brightly red in acidic phagosomes. No differences were observed between the two genotypes, suggesting that phagocytosis is not prevented in os^s flies (**Figure 3-10** C & D). Moreover, if the survival phenotype in os^s mutants was the result of partial (or total) inhibition of phagocytosis, then beads injection in wild-type flies would lead to an increased survival time. However, wild-type flies injected with beads prior to *Mm* infection die at the same time as controls that were not pre-treated with beads. It suggests that if os^s have any change in phagocytosis, it would only be to increase it. If this were the case, $S2R^+$ cells overexpressing upd3 would logically have reduced phagocytosis, so fewer bacteria per cell if entry is the only mechanism altered. Instead, these cells have a higher bacterial load after a short infection time (24 hours), indicating that Upd3 signalling has at least a partial effect on bactericidal mechanisms or induce metabolic changes in immune cells.

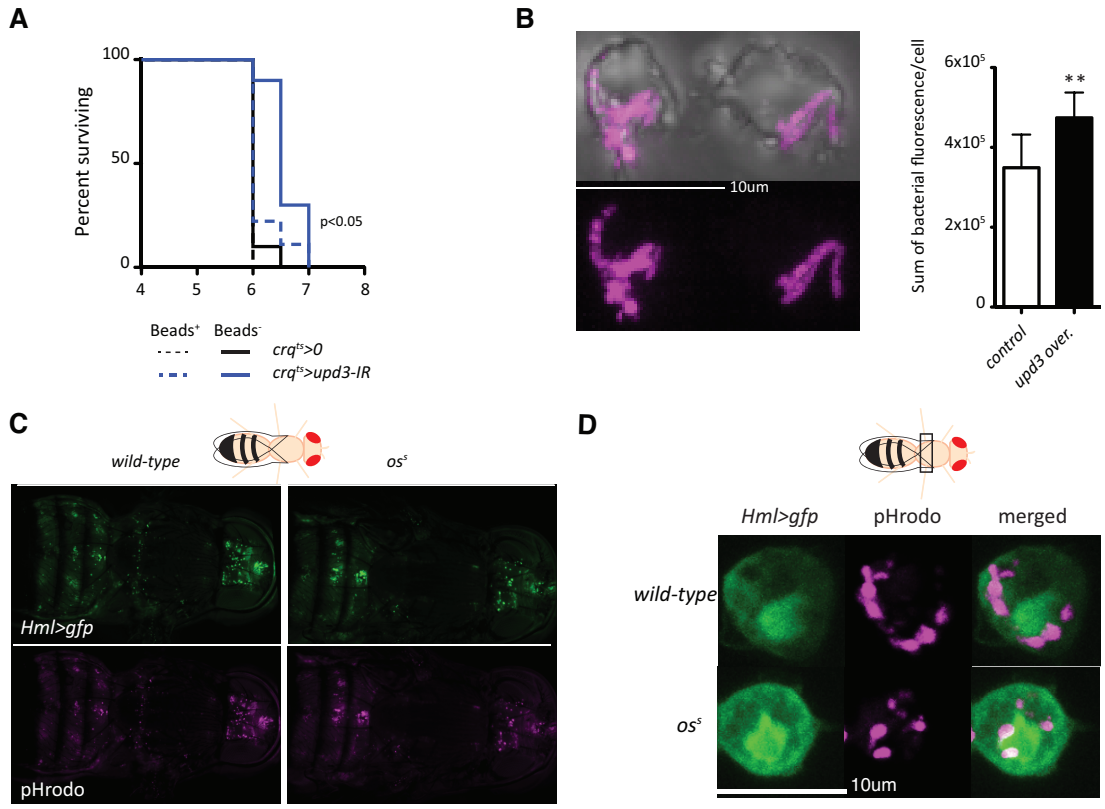

Figure 3-10: upd3 reduces bacterial proliferation in phagocytes

(A) *upd3* knock down flies have an increased survival time upon *M.marinum* infection that is dependent on phagocytosis of *M.marinum*. If beads are injected prior to infection, os^s mutants have similar survival time as wild-type flies. 5 to 7 days old flies were injected with beads (or PBS). 24 hours later, they were infected with *M.marinum* (500CFUs) or PBS-tween80. For this experiment, n=20 per condition and per genotype, and this experiment was repeated 3 times. (B) $S2R^+$ cells that overexpress *upd3* harbor more bacteria than control cells. Cells were transfected with *pPAC-HA* as control or *pPAC-upd3* to overexpress *upd3*. 24 hours later, cells were infected with *dsRed M.marinum* at MOI20. After 24 hours, cells were fixed and imaged by confocal imaging. (C and D) No differences were observed in phagocytosis of pHrodo by wild-type flies and os^s flies. In C, flies were imaged using a flucorescent microscope, and in D, using a confocal microscope. For panel A, p values were calculated using log rank test for os^s compared to wild-type without beads injection. For panel B, the p value was calculated using Mann Whitney (**p<0.01).

Despite the justification that Upd3 does not have an effect on phagocytosis in vivo, cells overexpressing *upd3* may have differences in bacterial uptake due to the stress induced by the transfection. Indeed, using the newly engineered pHrodo-conjugated beads, a method developed by the Guermonprez laboratory (manuscript in progress), we could determine the percentage of cells associated with beads, the percentage of cells that have internalised 1, 2 or more than 2 beads, and the differences in pHrodo intensity per cell. The results indicate that there is a 22% increase in bacterial uptake in cells overexpressing *upd3* compared to cells transfected with a control plasmid (**Figure 3-11** A). To assess whether, this result also reflects an increase in the number of beads per cell, we quantified the number of live cells that had one, two or more than two beads (**Figure 3-11** B & C). The data indicate that cells overexpressing *upd3* have phagocytosed more beads compared to controls. Finally, to assess whether there is a difference in phagosomal acidification between the two genotypes, we quantified the mean fluorescence intensity (MFI) of the $pHrodo^{+}$ cells that have uptaken one, two or more than two beads, and found no differences, indicating that phago-lysosomal processes are not altered when *upd3* is overexpressed (**Figure 3-11** D).

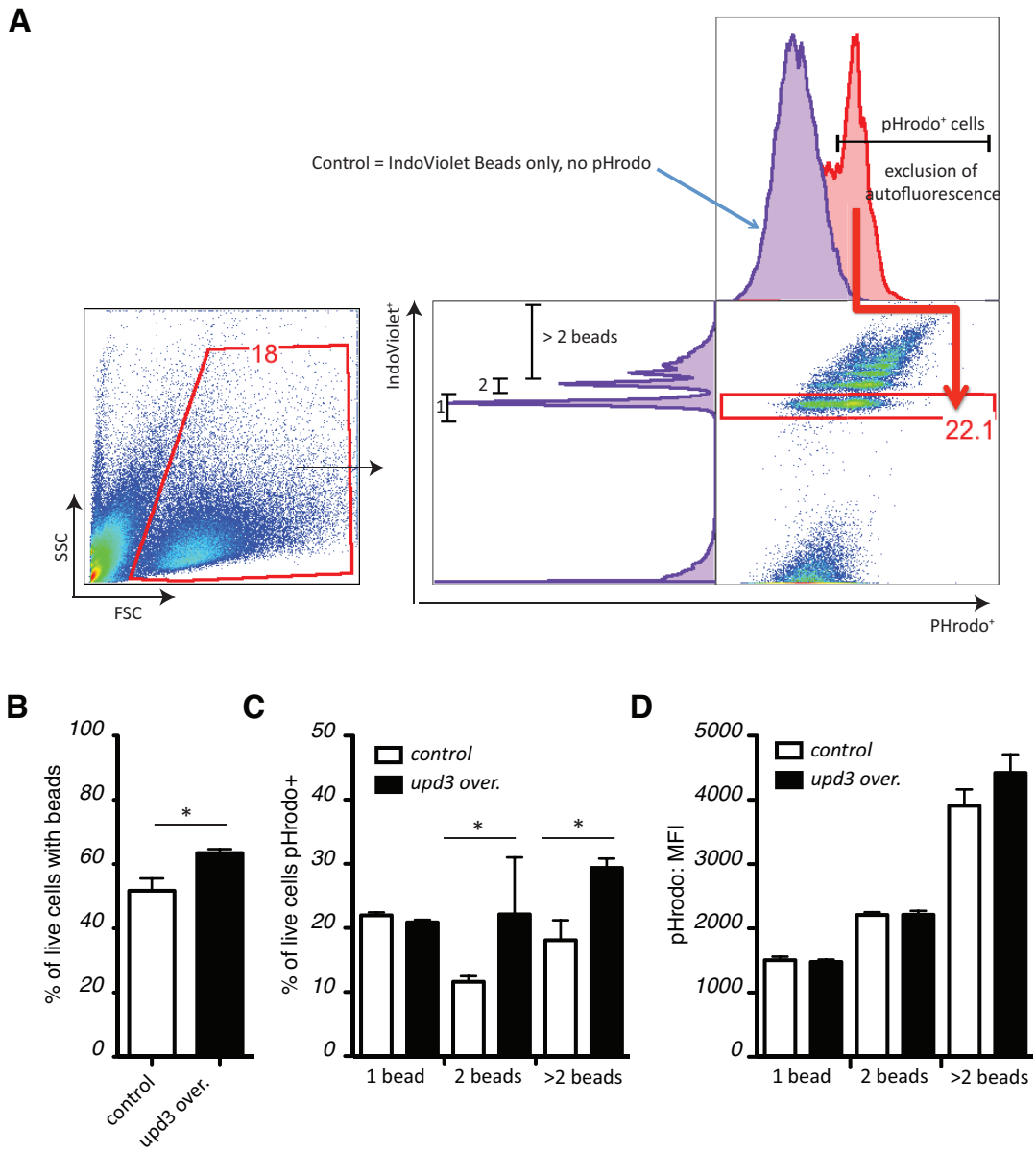

Figure 3-11: Phagocytosis is increased in S2R$^+$ cells overexpressing *upd3*

(A) Gating strategy for S2R$^+$ cells IndoViolet$^+$ and pHrodo$^+$. Live cells were analysed in the Texas Red chanel (pHrodo$^+$) and UV chanel (Indoviolet$^+$ beads). Cells having uptaken 1, 2 or more than 2 beads can be analysed separately due to the differences in Indioviolet intensity. PhRodo$^+$ cells were determined after exclusion of autofluorescence of the beads in the Texas Red chanel. (B) The percentage of live cells with beads is increased by 22% in cells overexpressing *upd3* compared to controls. (C) Cells overexpressing *upd3* contain more beads than controls. (D) The mean fluorescence intensity (MFI) of pHrodo$^+$ cells that have 1, 2 or more than 2 beads is similar in cells overexpressing *upd3* compared to controls. p values were calculated using Mann Whitney test (*p<0.05). The experiment was performed by Chloe Colas from the Guermonprez's laboratory.

Since there is a 22% increase in phagocytosis in cells overexpressing *upd3*, and since the same cells have a 36% increase in bacterial load *upon M.marinum* infection, we can estimate that the actual increase in bacterial growth is more likely to be around 14% and probably not significant.

3.2.5 Loss of Upd3 reduces immune cell death

Finally, and probably as a consequence of less bacterial growth, hemocytes seem to persist longer in os^s mutants compared to wild-type flies. At steady state, os^s mutants, with hemolectin or croquemort as hemocyte-specific drivers for *GFP* expression, do have the same number of hemocytes as controls (**Figure 3-12** A & C). However, upon infection, wild-type flies harbor less Hml^+ or Crq^+ cells than os^s mutants (**Figure 3-12** B & D). This change is most likely due to necrosis or apoptosis of hemocytes, as FACS analysis of PI^+ $S2R^+$ cells overexpressing *upd3* showed enhanced cell death compared to control (**Figure 3-12** E).

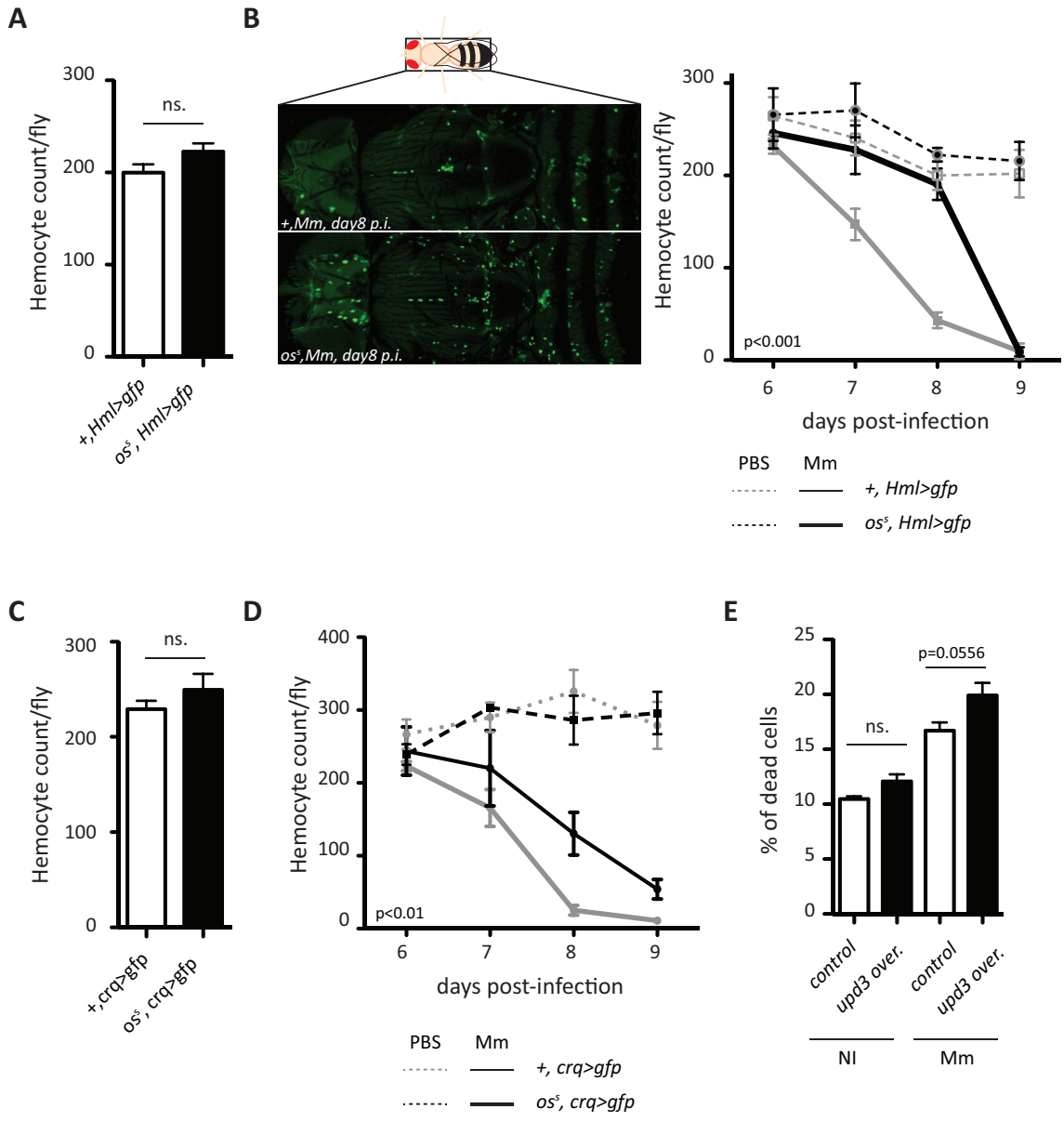

Figure 3-12: *os*^{s} mutants have reduced immune cell death upon infection

(A and C) At steady state, *os*^{s} have the same number of hemocytes as control flies. Hemocytes were counted by confocal imaging of anesthetized flies carrying either *HmlΔ-gal4* driving *UAS-2xeGFP*, or *crq-gal4* driving UAS-2xeGFP. n=10 per genotype. (B and D) Upon infection with *M.marinum* at 500 CFUs, hemocyte death is registered for both genotypes but *os*^{s} hemocytes persist longer than the controls. For this experiment, n=5 per genotype and per condition from day 6 to 8 p.i; n=2 or 3 per genotype and condition for day 9 p.i. (E) S2R^{+} cells overexpressing *upd3* have a higher percentage of dead cells (n=3). Dead cells for each genotype were quantified by FACS analysis of PI^{+} cells. For panel B and D, p values were calculated using two-way ANOVA comparing os^{s} and wild-type infected flies. For panel E, the p value was calculated using Mann Whitney test.

One could hypothesize that the delay in hemocyte death in os^{s} mutants imply that bacteria reach the cytosol later during infection. In that case, the increase in humoral responses should be delayed. However, by looking at gene expression, *os*^{s} mutants seem to have similar profiles as wild-type controls with exception at some timepoints (**Figure 3-13**).

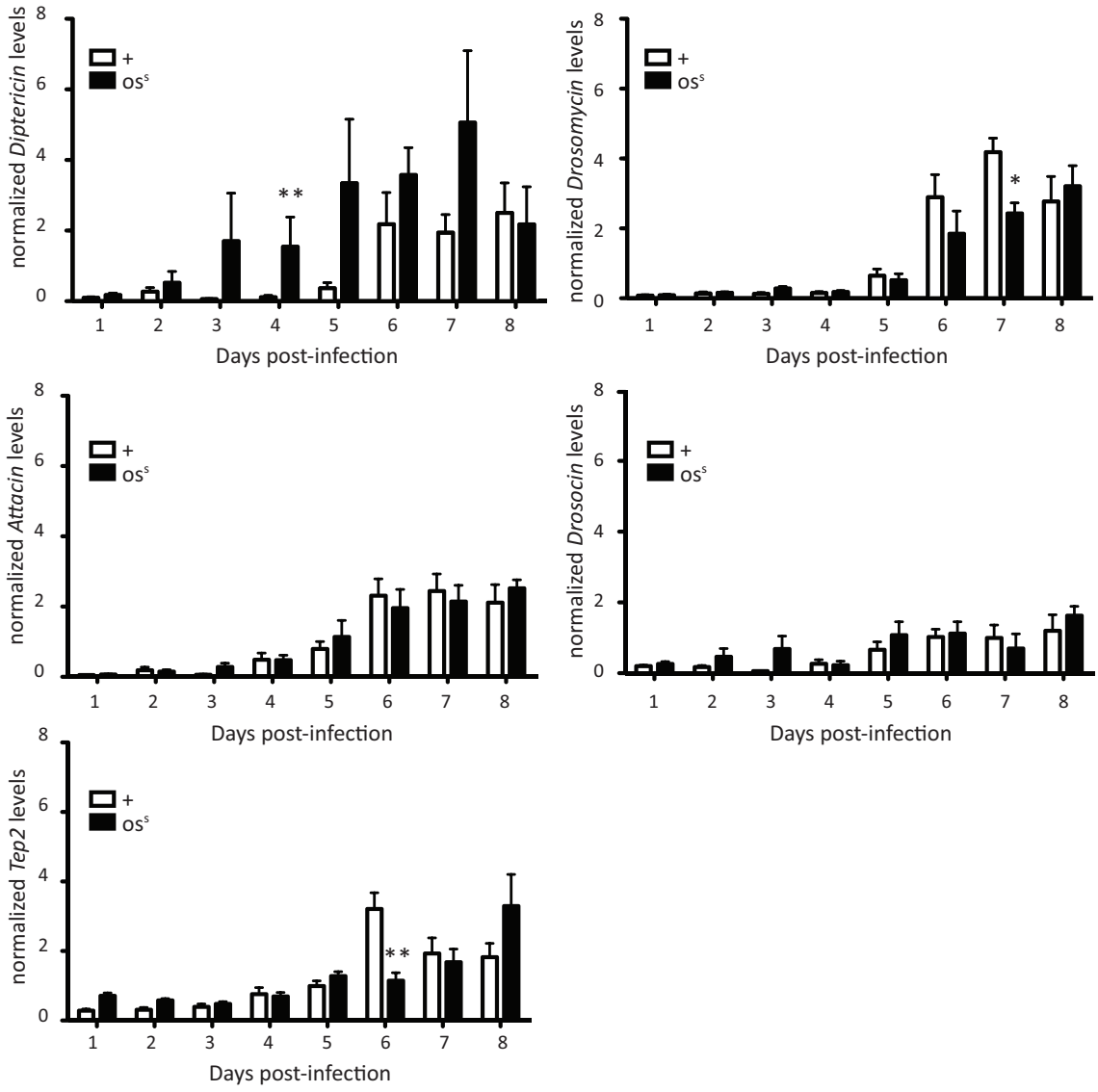

Figure 3-13: *os*^{s} have similar profile as controls for AMP and *Tep2* expression

The levels of expression of the different factors were normalised to *RpL1*. AMPs, such as Diptericin, Drosomycin, Drosocin and Attacin, and *Tep2*, are unchanged from *os*^{s} to wild-type controls infected with *M.marinum* at 500 CFUs. p values were calculated using Mann-Whitney test (*p < 0.05,**p < 0.01).

3.3 Discussion

M.marinum proliferates the fastest in two main areas in the fly host: the head and the dorsal vessel. Both areas contain many hemocytes, which represent the primary target of infection. In the early phase of infection, when bacteria are most likely to be inside hemocytes, the replication rate of *M.marinum* is high. Later, from day 6 onwards, hemocytes strongly decrease in number and the bacterial proliferation slows down, probably due to the onset of the humoral response or to overcrowding in the extracellular space. The increase in humoral responses possibly comes from bacteria-induced damage of fat body tissue or from detection of bacteria in the cytosol. However, this last idea is challenged by the fact that, when phagocytosis is blocked, wild-type flies die at the same time as their beads-injected counterparts. This last result also points towards the inefficiency of the cellular immune response in controlling bacterial growth and killing the invader. Strikingly, such inefficiency is partly due to cytokine signaling through Upd3, an IL-6 analogue that appears to be detrimental. Indeed, while most humoral effectors are unchanged between *upd3* mutants and control flies, hemocyte death and bacterial growth are delayed thereby warranting longer survival of the host. By further analysing hemocyte specific RNAi of *upd3* and survival upon blocked phagocytosis, I demonstrated first that the effect of Upd3 is dependent on its secretion by hemocytes that have undergone phagocytosis and second, that Upd3 signalling has an effect on hemocyte intracellular mechanisms that promote bacterial growth and hemocyte death. These mechanisms could regulate bactericidal immune responses such as decreased phagosomal toxicity or autophagy, metabolism of available resources that are necessary for bacterial growth, or even necrosis and apoptosis therefore increasing or delaying tissue damage. Indeed, *os*^{s} mutants also have delayed hemocyte death resulting from a lower number of bacteria per cell. In addition, since Upd3 has an effect on hematopoiesis, I used an inducible hemocyte-specific RNAi of *upd3* and recapitulated these results, thereby confirming that the improved resistance in os^{s} mutants is not due to developmental changes in hemocytes. The reduced bacterial proliferation in *os*^{s} mutants was shown to be dependent at least partly to a change in bactericidal or metabolic mechanisms inside macrophage-like cells but we cannot exclude a local effect on bacterial entry to hemocytes.

IL-6 was shown to have multiple roles in *M.tuberculosis* infection: inflammation, hematopoiesis and cell differentiation (Flynn & Chan 2001). . However it is only recently that its role in cellular bactericidal events has been demonstrated (Dutta et al. 2012). Dutta et al. showed that, upon infection with *M.tuberculosis*, THP1 macrophages secrete IL-6 in a time-dependent manner to inhibit autophagosome biogenesis (Dutta et al. 2012). This process is thought to be driven by mycobacteria as a protection against intracellular attacks. This recent paper confirms our observation that an IL-6-like signals can be used by bacteria to survive inside hemocytes. However, in the fly, there are major differences in the intra-macrophage environment that may result in a different function of Upd3: first, there is no IFN-γ analogue and second, *M.marinum* is able to escape the phagosome and to acquire an actin-tail for its motility (Stamm et al. 2003).

Interestingly, from their results and the ones presented above, macrophage-like cell lines express IL-6-like cytokine and are responsive to it, suggesting that Upd3 could signal from and to hemocytes in a paracrine or autocrine manner. This has been already demonstrated in vitro, but, in vivo, Upd3 was only shown to activate JAK-STAT signaling only in the fat body in vivo so far (Agaisse et al. 2003; Wright et al. 2011). The identification of the responsive tissue in vivo and the function of Upd3 signalling are analysed in the next chapters.

Chapter 4 Jak/Stat signalling in macrophage-like cells decreases resistance to mycobacteria partly by controlling Atg2-dependent mechanisms

4.1 Introduction

The JAK-STAT pathway is one of the best characterised immune pathways in mammals. It is composed of four JAK and seven STAT family members, whose differential combination activates specific targets in different cells types (Murray 2007). Surprisingly, we are still ignorant about tissue-specific functions, especially in the context of infection and immune diseases. We know that cytokines can signal to immune cells to increase their bactericidal functions, but also to adipose tissues to modulate lipid metabolism, or to neurons to regulate physiological homeostasis (O'Shea & Plenge 2012; Rajan & Perrimon 2012). In my thesis, I started by studying the effect of Upd3 in response to mycobacterial infection. As I found an effect of Upd3 in resistance to infection, I then investigated which tissues were responsive to such signal. In adult flies, the fat body is the only tissue that had previously been shown to respond to Upd3 upon infection (Agaisse et al. 2003). In addition, Wright et al. showed that Upd-family members can signal in an autocrine or paracrine fashion, suggesting that hemocytes can signal to themselves (Wright et al. 2011). All together these observations led us to investigate several potentially responsive tissues such as hemocytes and the fat body using tissue-specific drivers. My results pointed towards autocrine/paracrine signalling to hemocytes in vivo.

Another question to answer is the role of the JAK-STAT pathway in *M.marinum* infected hemocytes. Little information is available on JAK-STAT targets and their function in innate immunity, whether in mammals or in invertebrates. Most of the screens performed in flies aimed at identifying components and regulators of the pathway but not target genes (Müller et al. 2005; Baeg et al. 2005). However, in 2010, Bina et al. looked at transcriptional targets of JAK-STAT in Kc_{167} cell lines upon activation by Upd. They found many genes up and down regulated

in response to Upd at different timepoints (2h, 4h and 10h). Interestingly, among the genes downregulated by JAK-STAT activation were several autophagy genes (**Figure 4-1**).

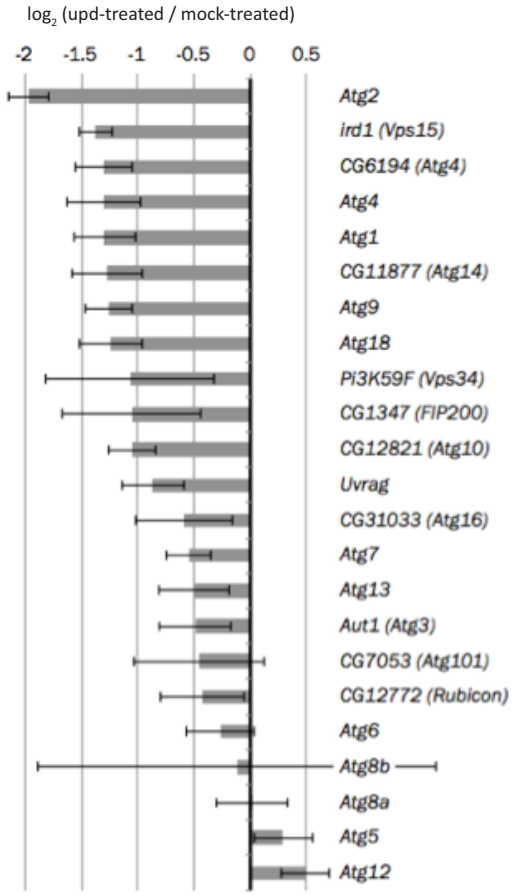

Figure 4-1: JAK-STAT activation by Upd dowregulates several autophagy genes in Kc_{167} cells

Binary logarithm of the normalised expression of several autophagy genes upon Upd stimulation in Kc_{167} cell lines. Gene expression in Upd-stimulated cells was normalised to the corresponding gene expression in mock-treated cells. Figure adapted from (Bina et al. 2010) and provided by Marc Dionne.

As described in Chapter 1, autophagy is an important defence mechanism in *M.tuberculosis* infection in mammals (Gutierrez et al. 2004; Vergne et al. 2006). Components of the core machinery have been broadly described in mammals and in flies, but little is known about their regulation upon infection (Levine et al. 2011; Zirin & Perrimon 2010). Autophagy is highly conserved between *Drosophila melanogaster* and mammals and the characteristic features are presented below (**Figure 4-2**).

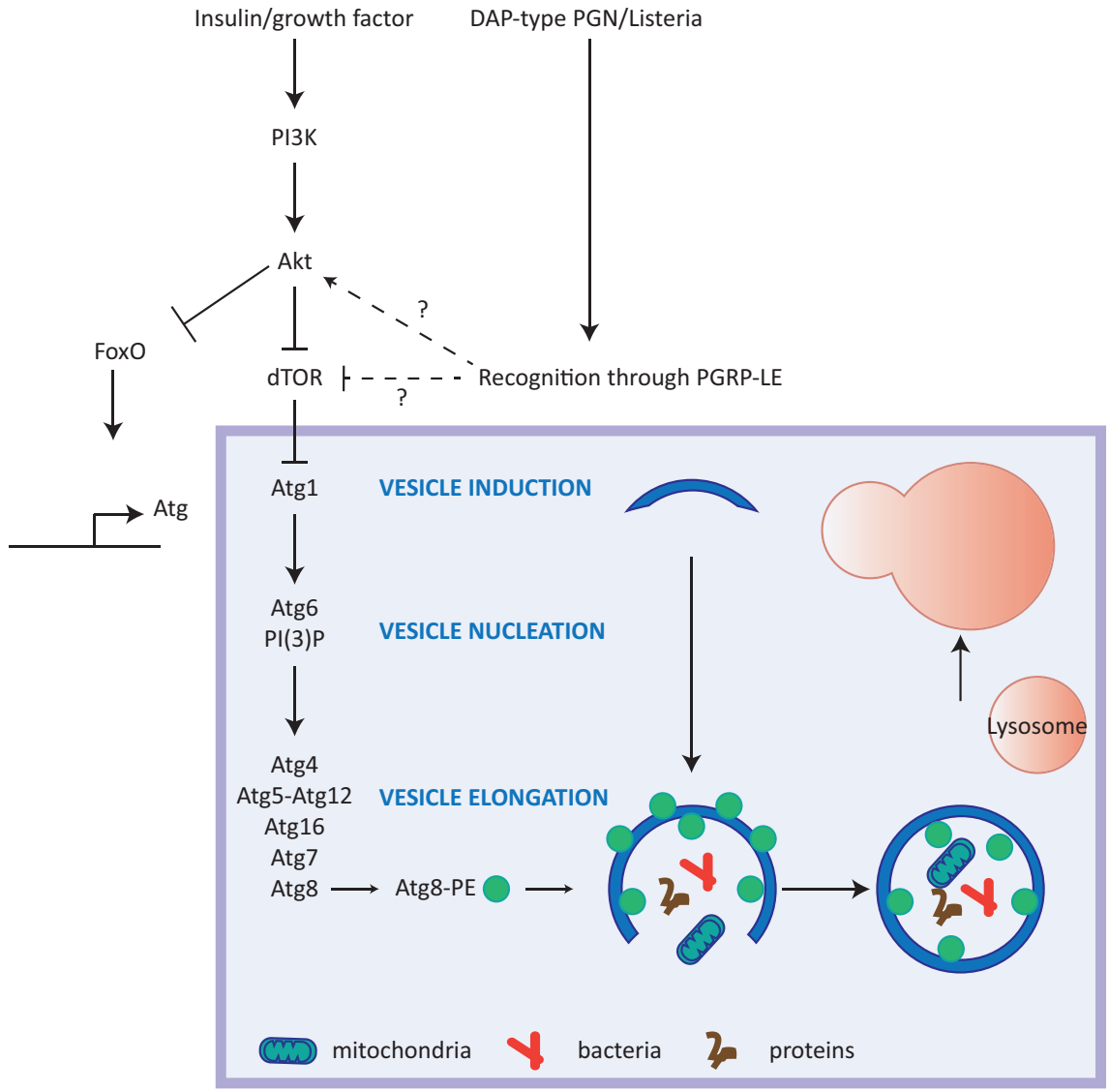

Figure 4-2: *Drosophila* autophagy pathway and its regulation

The autophagy machinery is activated by insulin signalling, but also after starvation, or upon recognition of DAP-type peptidoglycans by the cytosolic receptor PGRP-LE. It is followed by sequential activation of PI3K, Akt and inhibition of *Drosophila* TOR. When preparing for puparial transition, the larval fat body undergoes a massive burst of autophagy that is partly controlled by FoxO-mediated activation of autophagy gene expression. The precise mechanism of FoxO activation/inhibition is unknown. After dTOR inhibition, autophagy is induced. The formation of the autophagosome is a process that requires multiple steps involving a cascade of activation of autophagy proteins. First, after initiation, the autophagosome nucleates to form the phagophore. Progressively the vesicle elongates and enwraps proteins, aggregates, and organelles such as mitochondria or pathogens. Upon closure, several autophagy proteins associated to the external membrane are deconjugated to be recycled. An example is the lipidated form of Atg8, Atg8-PE (phosphatidyl ethanolamine), which goes back to its inactivated form Atg8 after Atg4-mediated cleavage. The autophagosome ultimately fuse with lysosomes to degrade its cargo. Akt/PKB (Protein Kinase B), dTOR (*Drosophila* Target Of Rapamycin), FoxO (Forkhead box O), PI3K (Phosphatidylinositide 3-kinases), DAP-type PGN (Diaminopimelic Acid-type Peptidoglycan), PGRP-LE (Peptidoglycan Receptor Protein-LE), Atg (Autophagy).

Recently, research in mammals showed that IFN-γ induces autophagy by inhibiting mammalian target of Rapamycin (mTOR) and by activating p38 and JNK pathways, while IL-6 counteracts these effects, thereby inhibiting autophagosome formation (Matsuzawa et al. 2012; Deretic & Levine 2009; Dutta et al. 2012). Their results suggest that, upon *M.tuberculosis* infection, IL-6 cytokines can regulate autophagy in macrophages. The precise mechanisms of regulation by IL-6 are unknown, but a common thought is that modulation of autophagy upon infection is mediated at a post-translational level. Based on these data and on the data from Bina et al., we supposed that autophagy can be regulated by the JAK-STAT pathway at a transcriptional level upon infection. For that, I looked at autophagy gene expression (Chapter 4) and at autophagy markers (Chapter 5).

To conclude, this chapter will try to answer the following questions:

(1) What are the tissues responding to upd3 secretion, especially upon M.marinum infection?
(2) Upon mycobacterial infection, what are the targets of JAK-STAT that contribute to the resistance phenotype?

4.2 Results

4.2.1 Inhibition of JAK-STAT signalling in hemocytes increases resistance to infection

The first question to answer is: what are the tissues responding to Upd3? This simple question was rather difficult to answer due to the efficiency of the available genetic tools. Based on the literature and on the results obtained in chapter 3 (**Figure 10, Panel B)**, upon infection, Upd3 can signal to adipose tissues in vivo, and immune cells in vitro (Agaisse et al. 2003; Wright et al. 2011). To verify these results in the context of *M.marinum* infection in vivo, the strategy was to look at resistance phenotypes in flies with reduced JAK-STAT signalling in hemocytes or in the fat body.

To reduce STAT92E activation in hemocytes, I used the Gal4/UAS system with *croquemort* or *Hemolectin* promoters as hemocyte-specific *gal4*-drivers, and *Stat92E* inverted repeats as responder gene. For the fat body, I use the *c564* driver instead. In hemocyte-specific knock downs, I could not observe a defect in *Stat92E* expression levels by analysing whole fly samples. This is probably due its strong expression in several tissues thereby preventing the detection of changes in *Stat92E* expression from whole fly samples when Stat is knocked down solely in hemocytes (data not shown). Then, to verify the efficiency of *Stat92E* knock down, I used the ubiquitous driver *tubulin* together with the *tubulin-gal80^{ts}* construct described in chapter 3. These flies only have a reduction in *Stat92E* expression when switched at 29˚C for 4 to 5 days after emergence. The results indicate that *Stat* knock down is 35% efficient when using one copy of *Stat92E-IR* (**Figure 4-3**). When using two copies of *UAS-Stat92E-IR* on the first and second chromosome, the effect was even stronger with a reduction in *Stat92E* expression close to 90%. Due to its efficiency, for the rest of the presentation, I will use the two copies of *Stat92E-IR*, and for the sake of simplicity it will be mentioned as *Stat-IR*.

Finally, to assess the efficiency of *Stat* knock down in the context of *M.marinum* infection, I measured the expression of the JAK-STAT target *TotA*, an acute phase protein strongly upregulated upon *M.marinum* infection. The results indicate that *TotA* expression is not induced when *Stat* is knocked down in adult hemocytes, confirming the efficiency of *Stat-IR* (**Figure 4-3** B). However, they also indicate that the *UAS-Stat-IR* construct is leaky since a reduction of *TotA* induction is also observed in the absence of driver (**Figure 4-3**B). Even if this

effect is lower than with the driver, I had to be careful when interpreting the results from the next experiments.

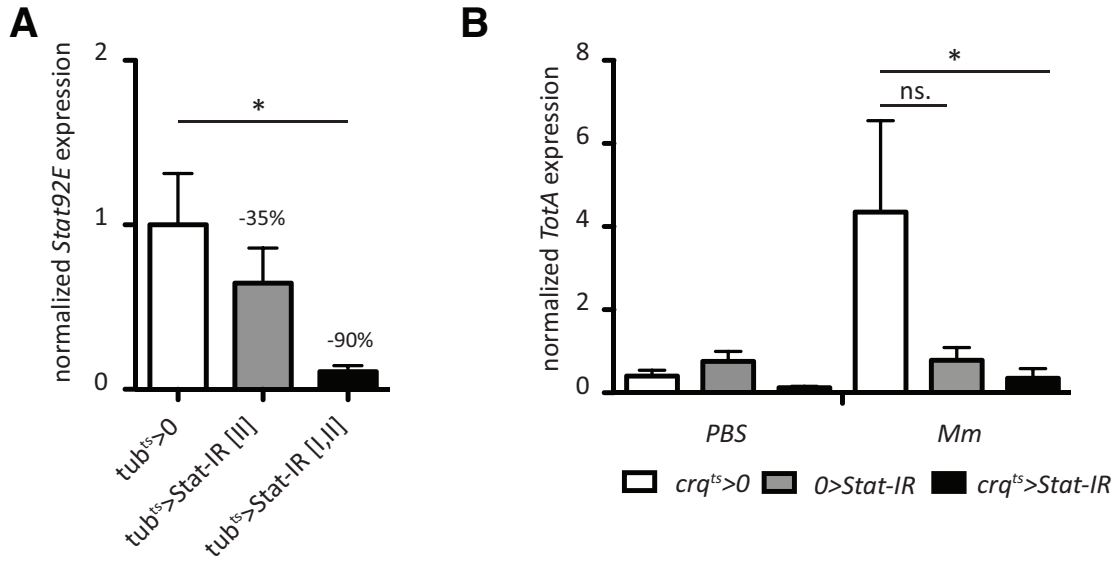

Figure 4-3: Silencing of STAT expression

(A) Efficiency of *Stat-IR* constructs, using a temperature inducible *tubulin-gal4* driving one or two copies of *Stat* inverted repeats *(Stat-IR)* after a four-day switch at 29˚C following emergence of adult flies. Flies carrying two inverted repeats insertions on the first and second chromosome have a reduction of 90% of *Stat* transcripts, while one copy only reduces *Stat* expression by 35%. For this experiment n= 7 for the control and n=5 for each of the knock downs. (B) Knocking down *Stat* in adult hemocytes, using *croquemort-gal4* and *tub-gal80^{ts}*, strongly reduces *TotA* induction upon infection. However, the responder gene only control, 0>Stat-IR, also has a strong decrease in *TotA* expression, despite being non significant. For this experiment, n=6 and samples were taken at day 5 post-infection. The p values were calculated using Mann Whitney test (*p<0.05).

I next looked at host survival upon *M.marinum* infection in hemocyte-specific and fat body-specific knock down of *Stat*. The survival curves indicate that reduced expression of *Stat* in the fat body has no effect on survival compared to controls (**Figure 4-4** A). However, lower levels of *Stat* in hemocytes increases survival, therefore suggesting that Upd3 can signal at least partly to hemocytes (**Figure 4-4** B). In addition, reducing *Stat* in the whole organism did not increase survival implying that knocking down *Stat* in some tissues may have negative outcomes upon infection that counterbalance the positive effect of *Stat* knock down in hemocytes (**Figure 4-4** C).

To further analyse STAT activation in hemocytes in vivo, I used flies carrying a Stat-GFP fusion construct and imaged the flies 48 hours post-infection at 5000 CFUs, but the results were not conclusive (data not shown) (Karsten et al. 2006). Another construct is available to detect JAK/STAT activation in vivo: the *10xStat-GFP* reporter, in which 10 *Stat*-binding sites from the STAT target *Socs36E* were placed upstream of an *hsp* minimal promoter and driving *GFP* expression (Bach et al. 2007). These flies have a strong GFP signal at steady state that renders quantification between the infected and non-infected state difficult (data not shown). Nevertheless, a *2xStat92E-GFP* construct is also available and with a lower signal. I am currently testing this construct. It is possible that upon infection STAT92E does not strongly induce *Socs36E* transcription in hemocytes. In consequence, this construct may not be relevant for this study.

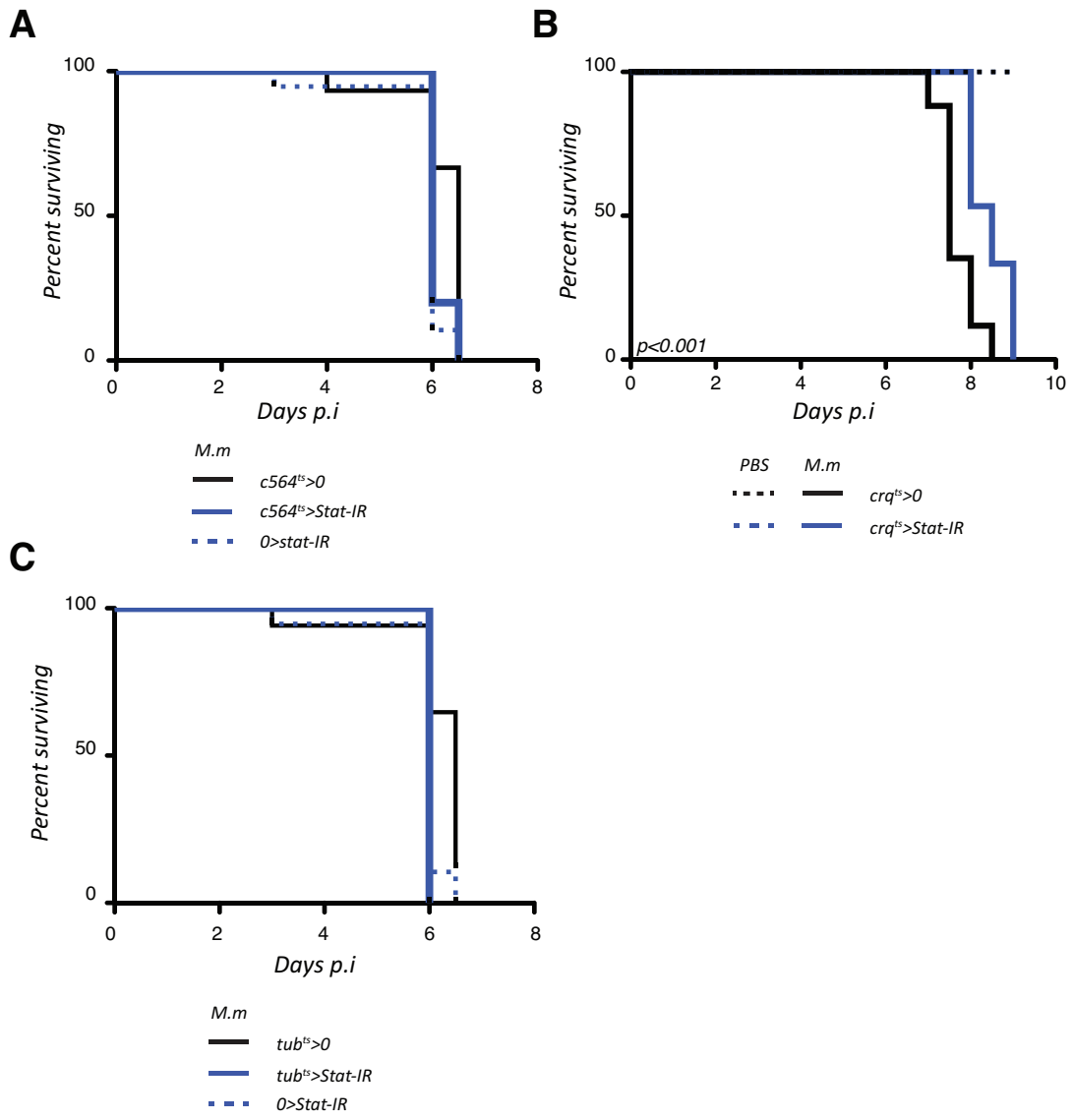

Figure 4-4: Knocking down *Stat* in hemocytes increases survival upon *M.marinum* infection

(A) No difference is observed in fly survival when *Stat92E* is knocked down in the fat body upon *M.marinum* infection. *c564-gal4* was used as fat body driver in combination with *tubulin-gal80^{ts}* that inhibits Gal4 binding at low temperatures. Controls include driver only (*c564^{ts}*>0) and responder gene only control (0>*Stat-IR*). PBS injected controls did not die from the infection (data not shown) (B) Temperature inducible hemocyte-specific knock down of *Stat92E* delays fly death upon *M.marinum* infection. *croquemort-gal4* was used as hemocyte driver in combination with *tubulin-gal80^{ts}*. (C) No difference in fly survival is observed when *Stat92E* is knocked down ubiquitously in adult flies. For this experiment, *tubulin-gal4* was used as a driver for ubiquitous expression with *tubulin-gal80^{ts}*. For all survival curves 20 flies were used per genotypes and per condition (injected, non injected). Panel A: n=2; panel B: n=3 and panel C: n=1. The p value was calculated using the log rank test.

To further analyse the phenotype in hemocyte-specific knock down of *Stat*, I measured bacterial growth at day 5 and 6 post-infection, where the differences in phenotypes are usually stronger. I observed a strong decrease in bacterial replication compared to controls and at a similar level as hemocyte-specific knock downs of *upd3* (**Figure 4-5** A & B).

I then assessed the persistence of hemocytes in these flies. For that, I imaged *Stat* knock down flies compared to controls at steady state to verify that the number of hemocytes was equivalent before infection (**Figure 4-5** C). Hemocyte distribution was similar in stat knock downs and controls (data not shown). I then infected age-matched flies with *M.marinum* or PBS and imaged them at late stages of infection, i.e day 5 and 6 post-infection. PBS injected flies were similar in stat knock downs and controls (see **Figure 3-4** A). For infected flies, the results indicate that hemocyte death is delayed when *Stat* expression is reduced in adult hemocytes (**Figure 4-5** D). Indeed, the quantification of Hml^{+} cells reveals that while a 70% decrease is observed in wild-type flies at day 6 p.i. compared to PBS-injected controls, this reduction is only 14% when Stat is knocked down in adult hemocytes.

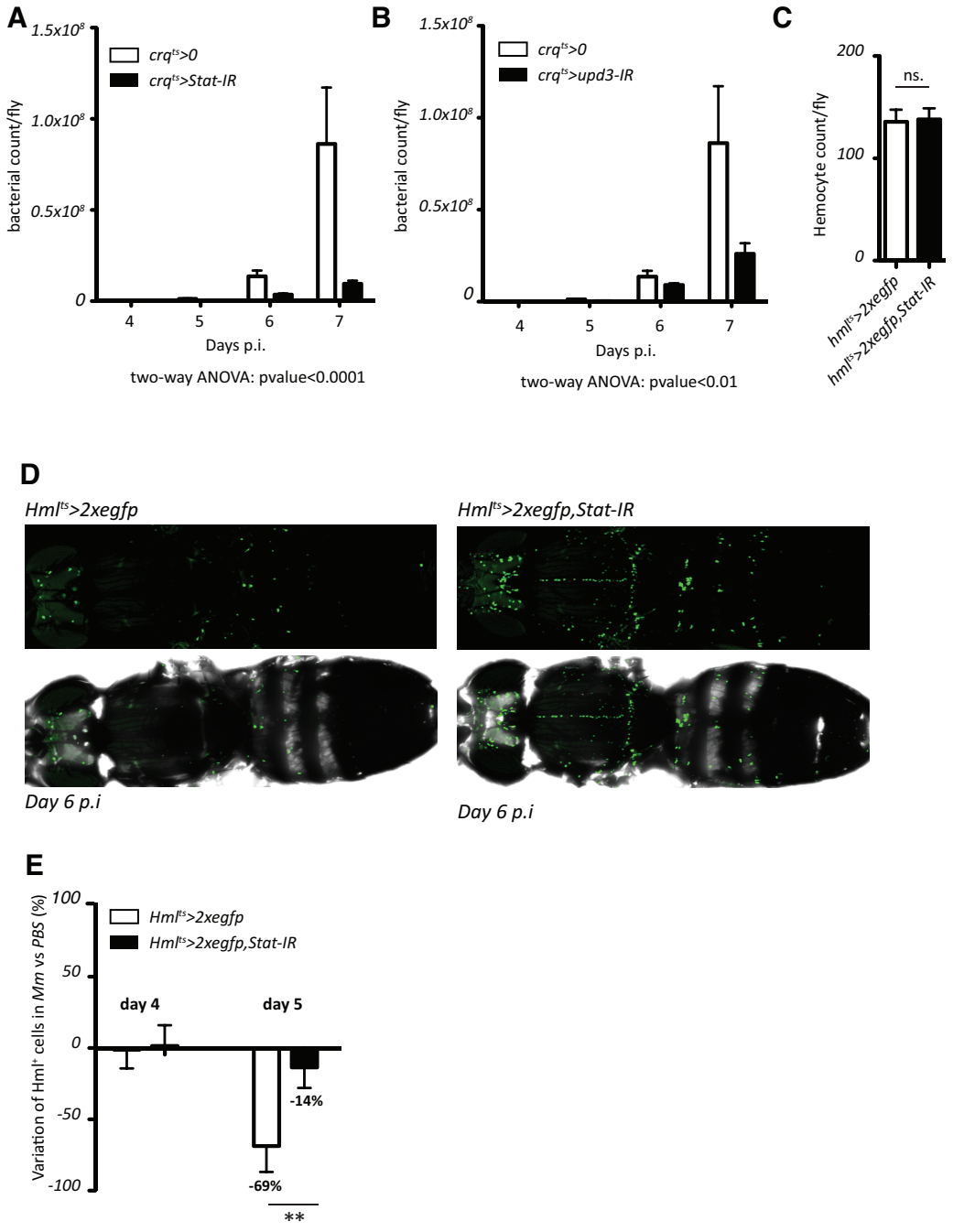

Figure 4-5: *Stat* knock down in adult hemocytes increases resistance to *M.marinum* infection

Knocking down *Stat* in adult hemocytes reduces bacterial growth. Flies carrying croquemort as a driver and *UAS-Stat-IR* in combination with *tubulin-gal80^{ts}* were infected with 500 CFUs of *M.marinum* and samples were collected from day 4 to 7 post-infection. n= 5 per timepoint and per genotype. (A & B) By comparison to *upd3* knock down in adult hemocytes, *Stat* knock downs have similar reduction in bacterial growth. n= 5 per timepoint and per genotype. (C) At steady state, *Stat* knock downs and controls have the same number of hemocytes. For this experiment, control flies carried *HmlΔgal4* driving *UAS-2xeGFP* in combination with *tub-gal80^{ts}*, and in addition *Stat* knock downs carried *UAS-Stat-IR*. Hemocyte number was assessed by imaging counting *Hml^{+}* cells; n=8 per genotype. (D & E) Upon infection with *M.marinum*, hemocytes are maintained for longer in *Stat* knock downs (14% decrease at day 6 p.i.) compared to controls (69% decrease at day 6 p.i.). A representative image of *Stat* knock downs and controls is presented (left) at day 6 p.i., n= 4 to 7 per timepoint and per genotype. For panels A & B, p values were calculated using two-way ANOVA. For panel C & D, p values were calculated using Mann Whitney test (**p<0.01).

4.2.2 JAK/STAT signalling downregulates *Atg2* expression

As stated in the introduction of this chapter, a recent screen on STAT targets identified several core protein of the autophagy machinery (Bina et al. 2010). These proteins participate in distinct stages of the autophagosome formation (**Table 4-1**), therefore their inhibition by JAK-STAT may alter autophagy, an important bactericidal mechanism.

Name	*Mammalian homolog*	*General properties*	*Protein complex*	*Function*
Vesicle induction				
Atg1	ATG1	Serine/Threonine kinase	ATG1 complex	ATG1 and ATG13 form a stable complex independent of TOR. Overexpression of *Atg1* induces autophagy in *Drosophila* but not in mammals.
Atg13	ATG13	Regulation by phosphorylation	ATG1 complex	
Vesicle nucleation				
Atg13	ATG13	Regulation by phosphorylation	ULK complex	
CG1347	FIP200		ULK complex	This complex translocates to early autophagic structures. In Drosphila the contribution of CG7053 has not been yet tested.
CG7053	ATG101	Interacts with ATG13	ULK complex	
PI3K59F	VPS34	PI(3) kinase	Class III PI(3)K complex	
CG11877	ATG14		Class III PI(3)K complex	This complex produces PtdIns(3)P, probably on the ER possibly to recruit additional factors. Rubicon negatively regulated autophagosome-lysosome fusion through interaction with the UVRAG complex in mammals. In *Drosophila* the function of UVRAG, Atg14 and Rubicon is unclear. Atg6 controls blood cell homeostasis.
CG6116	UVRAG		Class III PI(3)K complex	
Atg6	Beclin1		Class III PI(3)K complex	
Ird1	VPS15	Myristoylated	Class III PI(3)K complex	
CG12772	Rubicon		Class III PI(3)K complex	
Atg2	ATG2	Interacts with ATG18 in yeast		ATG2 is also associated with lipid droplets
Atg9	ATG9	Transmembrane protein		ATG9 also exists in other compartments such as endosomes and the Golgi aparatus
Atg18	WIPI-2			Recruited by the PI(3)K complex and involved in autophagy in mammals
Vesicle elongation				
Atg12	ATG12	Ubiquitin-like, conjugates covalently to Atg5	ATG12 conjugation system	
Atg7	ATG7	E1-like enzyme	ATG12 conjugation system	The ATG12-ATG5-ATG16L1 association is important for LC3-PE conjugation. This complex is present on the outer side of the isolation membrane and essential for its elongation.
Atg5	ATG5	Conjugates to Atg12	ATG12 conjugation system	
CG12821	ATG10	E2-like enzyme	ATG12 conjugation system	
CG31033	ATG16L1	Linked non-covalently to AGT12-ATG5	ATG12 conjugation system	
Atg8 a,b	LC3	Ubiquitin-like, conjugates to PE	LC3 conjugation system	The formation of LC3-PE conjugates and their deconjugation by ATG4 is important for elongation and complete/closure. LC3 is present on both the inner and outer membrane of the autophagosomes, and also serves as an adaptor for selective substrate such as p62, NBR1, NDP52 and the yeast mitophagy protein Atg32
Atg4	ATG4 A-D	LC3 carboxy-terminal hydrolase, deconjugating enzyme	LC3 conjugation system	
Atg7	ATG7	E1-like enzyme	LC3 conjugation system	
Aut1	ATG3	E2-like enzyme	LC3 conjugation system	

Table 4-1: Autophagy genes regulated by Upd signalling in Kc_{167} cells

With the exception of Atg8, Atg5 and Atg12, all the listed autophagy genes are downregulated upon JAK-STAT activation in Kc_{167} cells.

To determine if autophagy genes are regulated by the JAK-STAT pathway in *Drosophila* and especially in vivo, I infected flies having a reduction in STAT activation with *M.marinum* and collected whole fly RNA at several timepoints post-infection. I then assessed autophagy gene expression by quantitative RT-PCR.

For this experiment, several genotypes were tested:

(1) An ubiquitous knock down of *upd3*, using actin as driver;

(2) A hemocyte-specific knock down of *upd3* and of Stat*92E*, using *croquemort* as driver;

(3) And a hemocyte-specific induction of a dominant-negative form of the receptor Domeless (Dome), using *croquemort* as driver that I compared to control flies.

I tested the expression of several autophagy genes identified in the Kc_{167} cells screen: *Atg1, Atg2, Atg4, Atg6, Atg9, Atg18* and *ird1*. Their related proteins participate in protein complexes crucial at different stages of autophagosome formation (**Table 4-1**).

First, ubiquitous knock down of upd3 was associated with increased levels of *Atg2* and *Atg18* early in the course of infection indicating that upd3 signalling may regulate the transcription of autophagy genes (**Figure 4-6** A). By knocking down *upd3* in hemocytes, I obtained similar results for *Atg2* at day3 post-infection, before hemocyte death occurs (**Figure 4-6** B). To exclude developmental effects, I used a temperature-inducible hemocyte-specific knock down of *upd3* and corroborated these results at steady state, and at day 5 and 6 post-infection (**Figure 4-6** C & D). In addition, enhanced *Atg18* expression was observed at day 6 post-infection (**Figure 4-6** D). These data suggest that Upd3 regulates *Atg2* expression either strongly in hemocytes or possibly in other tissues. The Upd3-mediated regulation of other autophagy genes is less clear but cannot be excluded (data not shown). Finally, these results are not always significant because of high variability between samples, so they would require more samples, but they are observed in all genotypes tested.

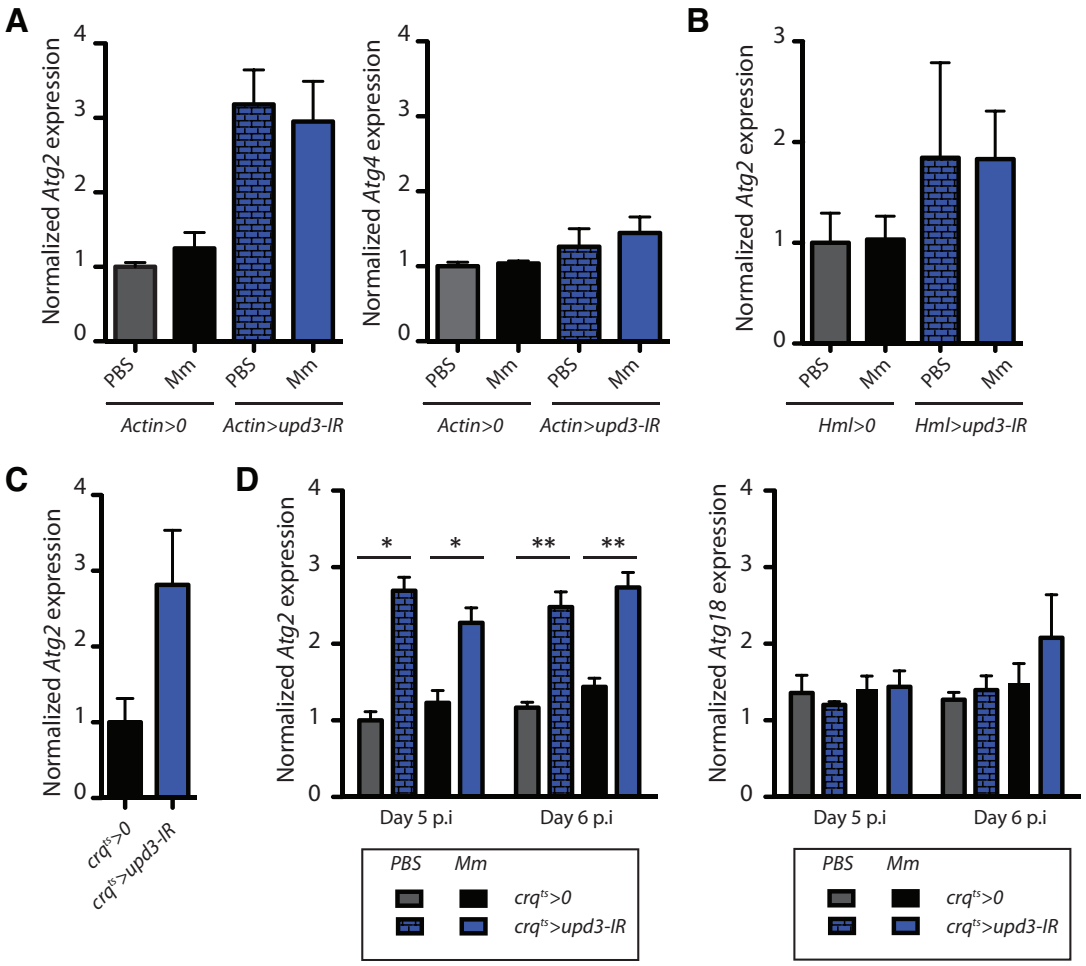

Figure 4-6: Inhibition of upd3 signalling enhances *Atg2* expression

(A) *Atg2* and to a lower extend *Atg4* are upregulated upon ubiquitous knock down of *upd3* using *actin-gal4* as driver. Whole fly samples were collected at day 3 post-infection and analysed by qPCR. n=3. (B) *Atg2* is also upregulated when using a hemocyte-specific knock down of *upd3*, using *HmlΔgal4* as a driver for *UAS-upd3-IR*. Samples were also collected at day 3 p.i. and n=3. (C) To exclude developmental effect, a *croquemort-gal4* construct was used in combination with *tub-gal80^{ts}*. Similarly to the results in panel A and B, *Atg2* expression is upregulated at steady state and upon infection at day 5 and 6 p.i. when *upd3* is knocked down in adult hemocytes. In addition, an effect on *Atg18* expression is observed at day 6 p.i. but is not significant. For this experiment, n=5; p value were calculated using Mann Whitney test on experiments for which n>3 (*p<.05, **p<0.01).

To test whether autophagy gene expression is controlled by JAK-STAT signalling in hemocytes, I collected samples at day 5 and 6 post-infection from hemocyte-specific knock down of *Stat* and from flies carrying a dominant-negative form of the receptor, Domeless, in hemocytes. In infected and PBS-injected samples, hemocyte-specific knock down of *Stat* led to increased *Atg2* and *Atg4* expression before immune cell death at day 5 post-infection (**Figure 4-7** A). Interestingly, this effect was not seen in the *Stat-IR* only control that I previously described as leaky (**Figure 4-3**), therefore suggesting that this effect is specific to hemocytes. In addition, I used a truncated version of the receptor Dome, DomeΔcyt, that had been generated by deletion in the intracellular region involved in signal transduction (Brown et al. 2001). When *UAS-domeΔcyt* is driven by *croquemort-gal4,* flies have a reduced JAK-STAT signalling (**Figure 4-7** B). Upon *M.marinum* infection, these flies have a lower bacterial growth and an increased expression of several autophagy genes, such as *Atg2*, *Atg4* and *Atg18* (**Figure 4-7** C & D). No effect was observed for *Atg1*, *Atg6*, *Atg9* and *ird1* (data not shown). All together, these results indicate that several autophagy genes are upregulated when JAK-STAT signalling is prevented in hemocytes. Finally, despite a high number of STAT knock down samples, the differences are not statistically significant, due to high variability between samples. It may be a consequence of variability between individual flies, and it is also due to the fact that we are here looking in whole fly samples at an effect happening in Crq^{+} cells.

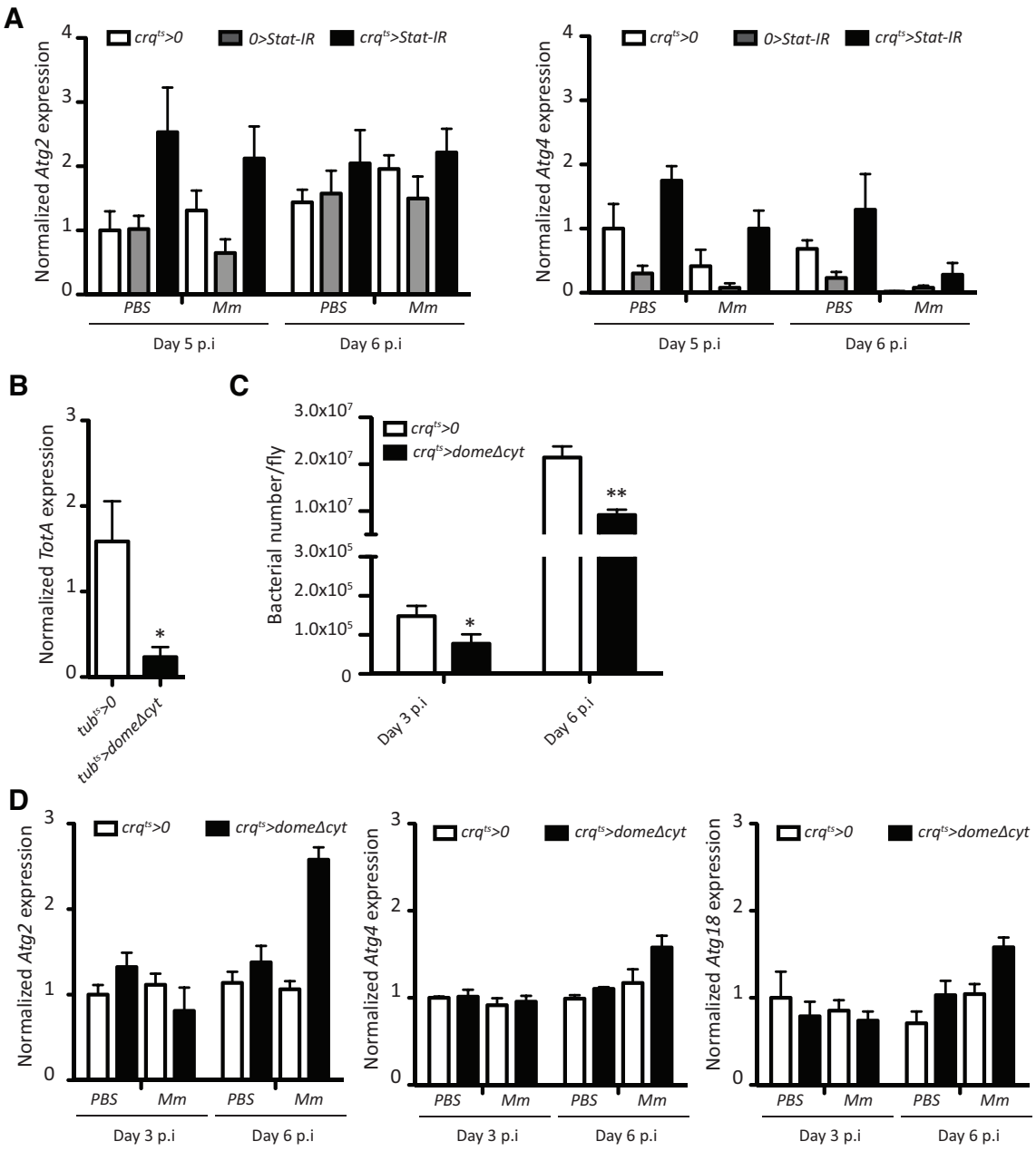

Figure 4-7: Inhibition of JAK-STAT signalling in hemocytes enhances autophagy gene expression

(A) *Atg2* and *Atg4* expression are increased in *M.marinum*-infected and PBS-injected flies for which *Stat92E* is knocked down in adult hemocytes. *croquemort* was used as a driver for *UAS-Stat92E-IR* together with a *tub-gal80^{ts}* construct. Whole fly samples were mashed at day 5 and 6 post-infection and n=6. (B) Flies carrying a ubiquitously active/expressed dominant-negative form of Domeless, DomeΔcyt, have a reduced *TotA* expression when whole fly samples were collected. Samples were taken at steady state following 5 days at 29˚C, n=3. (C) Hemocyte-specific expression of *domeΔcyt* reduces bacterial replication in the whole fly. Whole fly samples were collected at day 3 and 6 post-infection and n=6. (D) *Atg2*, *Atg4* and *Atg18* expression are increased at day 6 post-infection and in infected in flies carrying a *croquemort-gal4* construct driving *UAS-domeΔcyt* together with a *tgal80ts* construct. Whole fly samples were collected at day 3 and 6 post-infection. n=3. p values were calculated using Mann Whitney test for experiments with n>3 (*p<0.05, **p<0.01).

Blocking Upd3 secretion by hemocytes, or inhibiting JAK-STAT signalling in hemocytes, resulted in an increase in autophagy gene expression in vivo. To verify that autophagy genes can be directly regulated by Upd3 signalling in hemocytes, I analysed gene expression in $S2R^+$ cells overexpressing *upd3* compared to controls.

First, I validated the cell culture infection model. Similarly to what was observed in vivo (see Chapter 3), *M.marinum* infection increases *upd3* expression in hemocytes. It resulted in a strong increase in *TotA* expression, indicating that the JAK-STAT pathway is activated in these cells (**Figure 4-8** A & B). Interestingly, *Socs36E*, another STAT target, is only slightly upregulated upon infection with *M.marinum* indicating that *Socs36E* may not be strongly upregulated in hemocytes in vivo (**Figure 4-8**C). Indeed, this may explain why the 10xStat92E-GFP construct did not show a clear phenotype in infected hemocytes by intravital imaging.

I then confirmed that cells overexpressing *upd3* have an enhanced JAK-STAT signalling in hemocytes. For that, I transfected cells with *pPAC-upd3*, to overexpress *upd3*. These cells had a 6000 fold increase in *upd3* expression compared to cells transfected with a control plasmid (**Figure 4-8** A). As a consequence, the JAK-STAT target *TotA* is strongly upregulated and increased 15 times compared to the infected controls (**Figure 4-8** B). Strikingly, *TotA* expression is further increased in *upd3*-overexpressing cells that are infected compared to their non-infected counterparts. It suggests that an additional level of regulation exists, possibly through Relish as suggested by Agaisse et al. upon septic injury (Agaisse et al. 2003).

Finally, I found that cells overexpressing *upd3* have lower *Atg2* and *Atg4* expression, therefore confirming the in vivo data (**Figure 4-8** D). Interestingly, the difference in *Atg2* expression is reduced when cells are infected, indicating that signals from the infected cells or from the bacteria themselves can trigger changes in *Atg2* expression or by modulating transmission of signal in the JAK-STAT pathway or through other pathways. This would require further investigation.

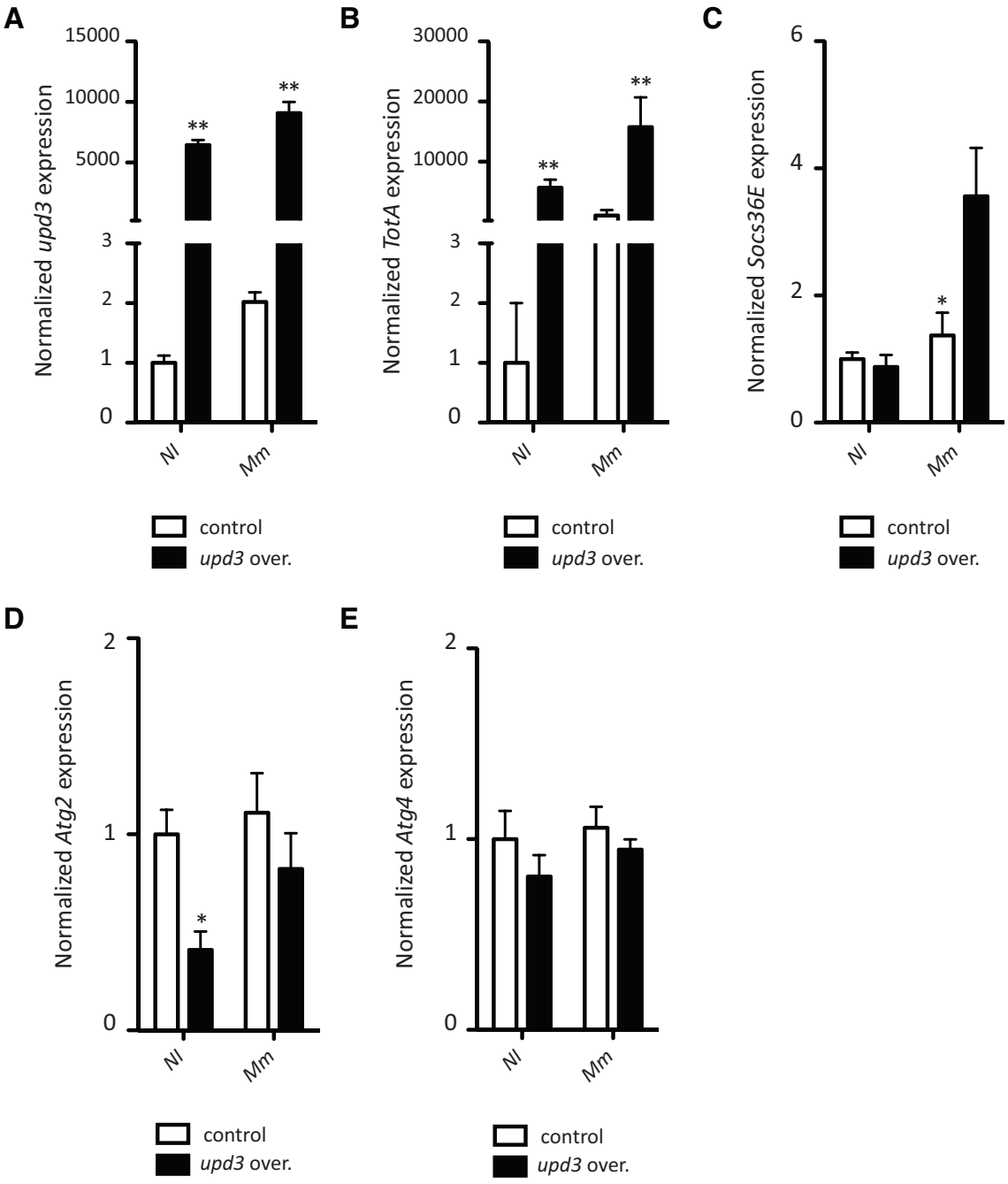

Figure 4-8: *upd3* overexpression in S2R$^+$ cells reduces *Atg2* and *Atg4* transcription

(A) S2R$^+$ cells transfected with *pPAC-upd3* have more than 6000 times increase in *upd3* expression compared to cells transfected with the control plasmid, *pPAC-HA*. Samples were collected 24 hours after infection with *M.marinum*, medium alone was used as control (NI) (B) Cell overexpressing *upd3* have a strong increase in *TotA* transcription, a JAK-STAT target. (C) However, another JAK-STAT target, *Socs36E* was only slightly upregulated. (D) S2R$^+$ cells overexpressing *upd3* have lower levels of *Atg2* and *Atg4* transcripts. For all experiments, n=6 and p values were calculated using Mann Whitney test (*p<0.05, **p<0.01).

4.2.3 *Atg2* levels inversely correlate with bacterial numbers per cell

I have demonstrated that JAK-STAT signalling correlates with changes in transcription of several autophagy genes. Upon JAK-STAT inhibition, the most consistently upregulated gene, and also the strongest effect, is seen for *Atg2*, a gene encoding an autophagy protein participating in the nucleation step of the autophagosome (**Table 4-1**). Since blocking JAK-STAT signalling increases resistance to infection by lowering bacterial replication and increasing host survival, I then looked at the contribution of *Atg2* to the resistance phenotype. For that, I infected $S2R^+$ cells transiently transfected with pPAC-GFP-Atg2 to overexpress *Atg2* and compared them to cells transfected with the control plasmid. The samples were collected after 24 hours of infection with dsRed *M.marinum*, fixed, and analysed by imaging. I quantified the number of bacteria per cell by measuring the sum of dsRed fluorescence per cell, an intensity that is proportional to the number of bacteria. The results indicate that overexpressing *Atg2* reduces the number of bacteria per cell (**Figure 4-9** A).

I previously showed that overexpressing *upd3* resulted in a slight increase in bacterial growth per cell (see Chapter 3), and since our hypothesis is that Atg2 is downstream of JAK-STAT, overexpressing *Atg2* should counteract the *upd3* phenotype and then lower bacterial replication. Indeed, $S2R^+$ cells overexpressing *Atg2* and *upd3* have a reduced number of bacteria per cell compared to $S2R^+$ cells overexpressing *upd3* alone (**Figure 4-9** B). For this experiment, all cells were analysed randomly and since the transfection is not efficient at 100% some cells did not overexpress *Atg2*. As a consequence, the phenotype is likely underestimated.

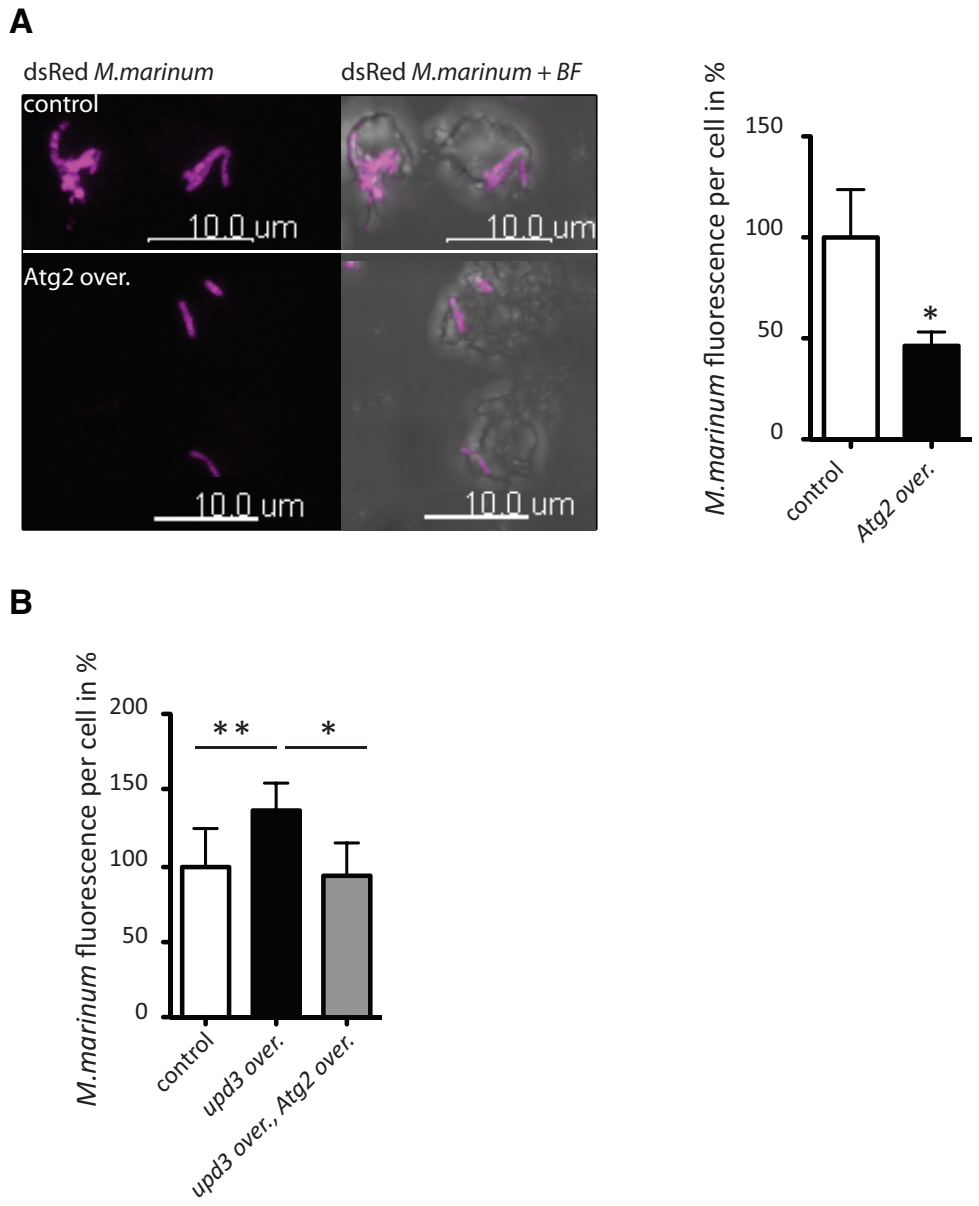

Figure 4-9: *Atg2* overexpression in S2R$^+$ cells reduces bacteria per cell

(A) S2R$^+$ cells overexpressing *Atg2* have a reduced number of bacteria per cell. S2R$^+$ cells were transfected with *pPAC-GFP-Atg2* or *pPAC-HA* as control. After 24 hours of infection, cells were fixed and imaged by confocal imaging. n=46 for controls and n=38 for cells overexpressing *GFP-Atg2*. (B) Overexpressing *Atg2* reverses the *upd3* overexpression phenotype, whereby cells have increased numbers of bacteria. n=46 for controls, n=42 for cells overexpressing *upd3* and n=30 for cells overexpressing *Atg2* and *upd3*. p values were calculated using Mann Whitney test (*p<0.05, **p<0.01).

The method I used for quantification does not distinguish live from dead bacteria. To solve this issue, I counted the colony forming units by plating intracellular mycobacteria on Middlebrook 7H9-Agar plates.

For this experiment, I performed several transfections of $S2R^+$ cells:

(3) *pPAC-HA*, as control;

(4) *pPAC-upd3*, to overexpress *upd3*;

(5) *pPAC HA* + *pPAC-GFP-Atg2*, to overexpress *Atg2*;

(6) *pPAC upd3* + *pPAC-GFP-Atg2*, for epistasis analysis.

I infected these cells with *M.marinum* at MOI 20 for 3 hours, removed all extracellular bacteria, and then collected the samples after 24 hours. Cells were then counted and lysed to release intracellular mycobacteria. Serial dilutions were made from the initial sample and plated into Middlebrook 7H9 agar plates. After 2 weeks of growth, I counted the colony forming units.

The results revealed a 50% decrease of bacteria within cells transfected with *pPAC-GFP-Atg2* (**Figure 4-10**). This amplitude is similar to the one determined by imaging, suggesting that most of bacteria were alive. On the contrary, cells overexpressing *upd3* had similar CFU count as control cells, while imaging data showed an increase, therefore suggesting that there were some dead mycobacteria in the overall fluorescence per cell or that the differences resulted for variability between samples.

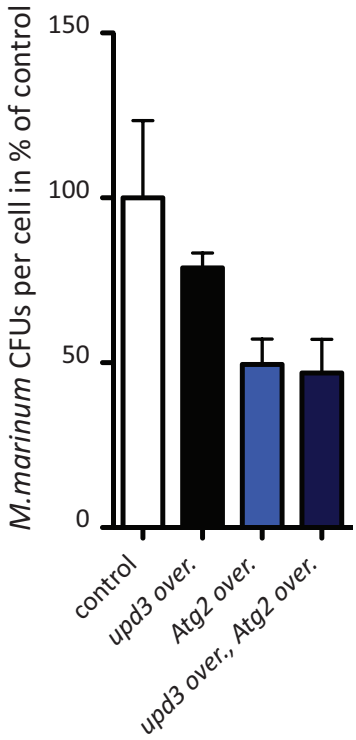

Figure 4-10: *Atg2* overexpression in S2R$^+$ cells reduces live bacteria per cell

S2R$^+$ cells were infected with *M.marinum* at MOI 20 for 3 hours. After 3 hours, cells were washed intensively to remove extracellular bacteria and amikacin was added to inhibit extracellular growth. After 24 hours of infection, cells were washed to remove all bacteria released by dead cells. Cells were collected, counted and lysed. Several dilutions were plated on Middlebrook 7h9-Agar plate and bacteria were counted after 2-3 weeks. Bacterial count was normalised to the number of cells collected. Cells overexpressing Atg2 harbour less CFUs than controls, and cells overexpressing *upd3* and *Atg2* have less bacteria than cells overexpressing *upd3* only. This experiment is preliminary and n=3.

Finally, I looked at hemocyte death in S2R$^+$ cells overexpressing *Atg2* and found that it was reduced in infected cells compared to controls (**Figure 4-11**). In this experiment, I transfected S2R$^+$ cells_ with *pPAC-GFP-Atg2* or *pPAC-HA and then infected them_* with *M.marinum.* The samples were analysed by flow cytometry 24 hours after infection after staining cells with propidium iodide (PI$^+$).

All together, these results indicate that Atg2 has a role in immune cell resistance to *M.marinum* infection.

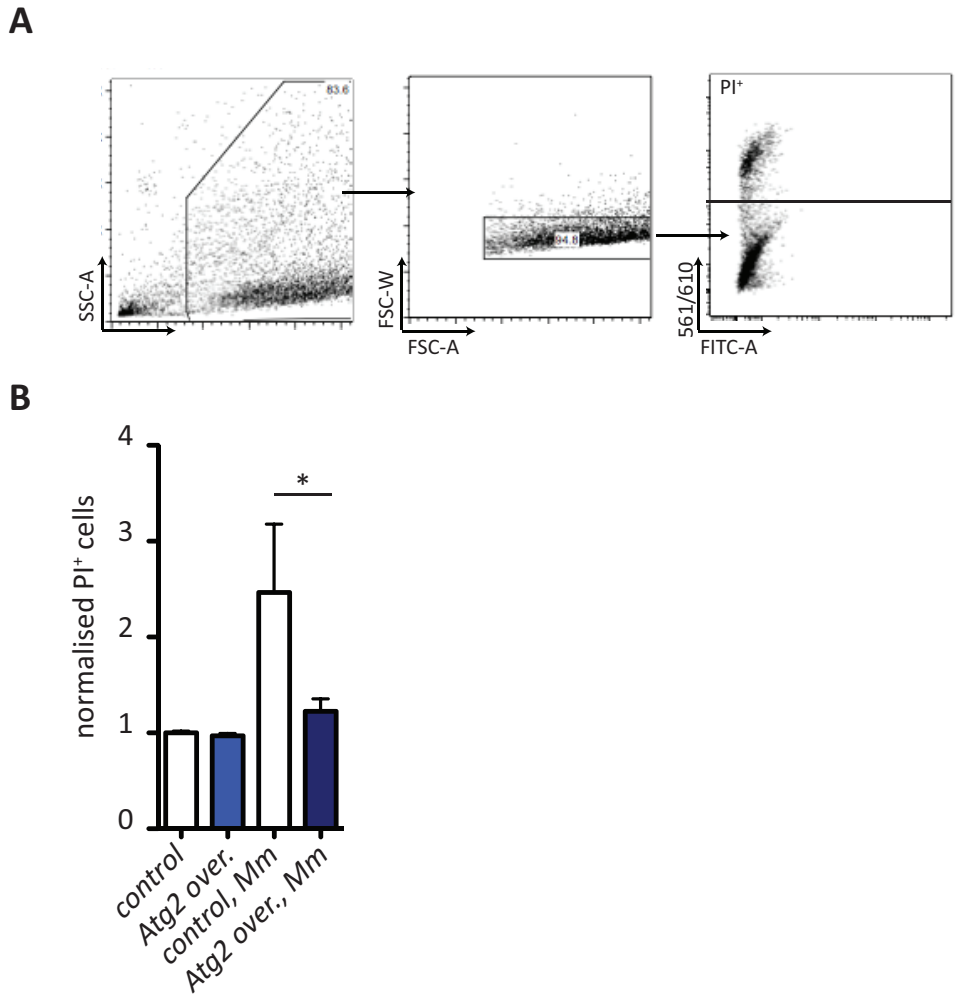

Figure 4-11: *Atg2* overexpression in S2R$^+$ cells reduces hemocyte death

(A) Flow cytometry gating strategy. In all samples, doublets were excluded (middle panel) and PI$^+$ cells determined by intensity in the 561/610 channel (right panel). (B) The percentage of PI$^+$ cells was determined in samples where doublets were excluded, and then normalised for each experiment. Cells were transfected either with *pPAC-HA* as control, or *pPAC-GFP-Atg2* to overexpress *Atg2*. At steady state, no difference was observed in cell death. However, upon *M.marinum* infection at MOI 20, an increase in cell death was observed in control samples, but not in cells overexpressing *Atg2*. For this experiment, n=3 per genotype and per condition. p value was calculated using Mann Whitney (*p<0.05).

4.2.4 A newly identified JAK-STAT target, called *net*, downregulates *Atg2* expression

Now that we have discovered that, by blocking JAK-STAT signalling, flies have an increased resistance to *M.marinum* infection dependent on Atg2 mechanisms, the next step is to understand how is *Atg2* expression regulated, and what is the precise function of Atg2 in controlling bacterial growth within hemocytes. The later question will be assessed in the following chapter. For now, I will concentrate on Atg2 regulation. The pertinence of this question arose from the fact that STAT by definition is a signal transducer and activator of transcription. Then, how is *Atg2* downregulated by JAK-STAT?

By looking at the region upstream of the coding sequence, I tried to identify the consensus binding site for STAT, known as TT[CN_{2-4}G]AA, but without success. Therefore, I then searched for a potential transcriptional repressor target of JAK-STAT that would downregulate *Atg2*. From Bina et al., autophagy genes were observed to be downregulated after 10 hours of stimulation, allowing time for initial transcriptional events to occur. From their study, we identified a transcriptional repressor called *net* that is strongly upregulated after 2 hours of STAT activation. The putative human homolog for *net* is called *Atoh8* and is poorly characterised. It is required for vertebrate development (Inoue et al. 2001; Lynn et al. 2008; Yao et al. 2010). Interestingly, it is associated with iron metabolism and is induced by the BMP/Smad signalling pathway in mammals (Kautz et al. 2008). In *Drosophila melanogaster*, Net has been only associated with the development of the wing imaginal disc (Zhou et al. 2005).

To test the hypothesis that Net might regulate *Atg2* expression, I looked at *Atg2* expression levels in *net* mutants (net^1) at steady state and upon infection. Analysis by quantitative PCR revealed a 260-fold increase of *Atg2* levels in net^1 mutants compared to control flies, and this high expression levels were maintained upon infection with *M.marinum* (**Figure 4-12** A & B). net^1 mutants did not have an effect on other autophagy genes, such as *Atg4*, *Atg6* or *Atg18* suggesting that it may be specific to *Atg2* and potentially to other autophagy genes not yet analysed (**Figure 4-12** C).

To verify that this effect was not due to another random mutation in net^1 mutants, I looked at *Atg2* expression in an uncharacterised mutation of *net*, called net^x, and corroborated the results obtained for net^1 (**Figure 4-12** D).

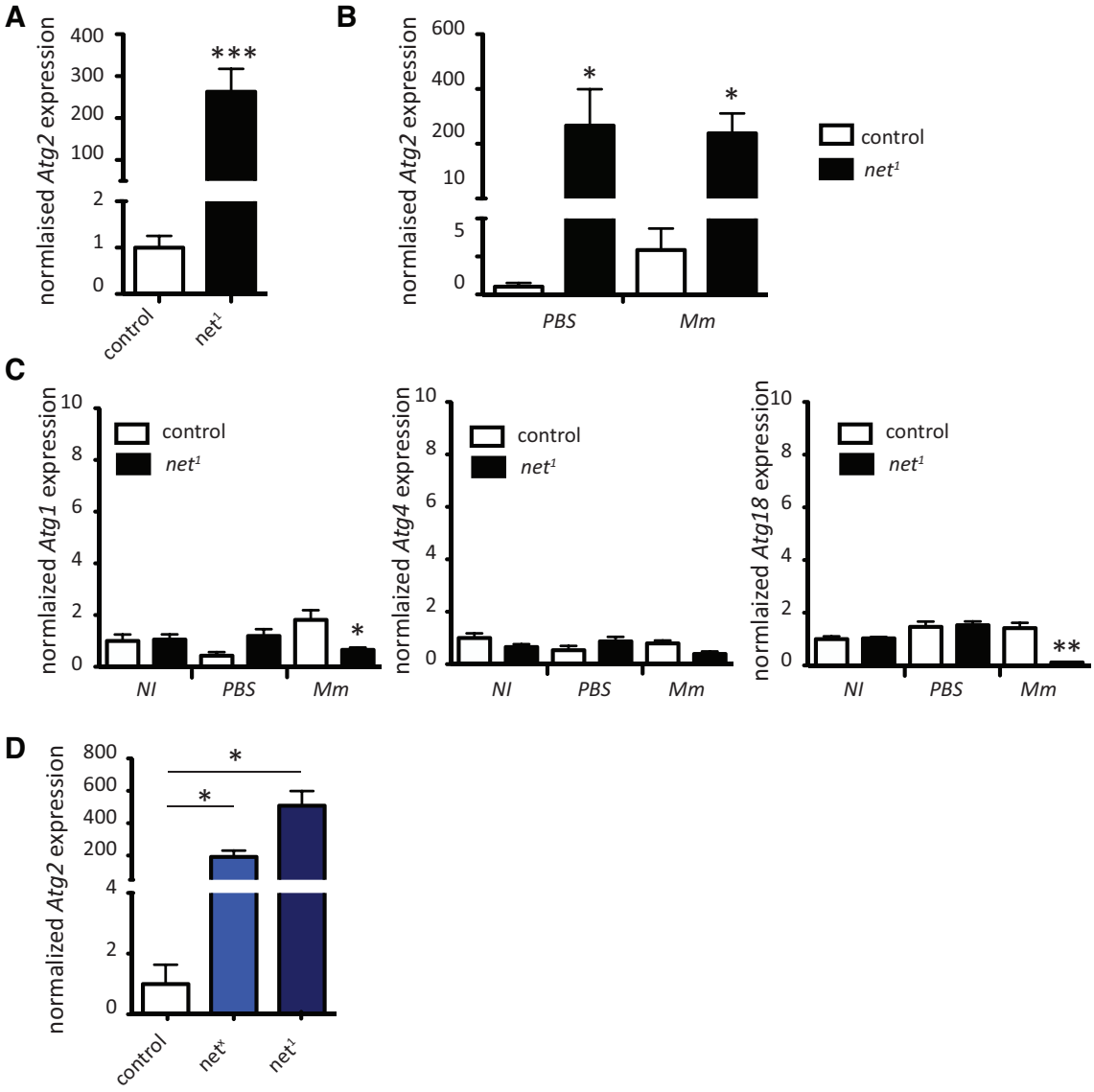

Figure 4-12: *net* mutants have a strong increase in *Atg2* expression in vivo, but not of other autophagy genes

(A) *net*^{1} mutants have a 260-fold increase in *Atg2* expression at steady state. Whole fly samples were taken from 5 days old adult males and n=16. (B) Upon infection, *Atg2* expression remains high in *net*^{1} mutants compared to control flies. For this experiment, n=4 and *M.marinum* samples were taken 24 hours post-infection. (C) A slight decrease in *Atg1* and *Atg18* expression was observed in infected *net* mutants but no changes were observed at steady state or after PBS injection. *Atg4* levels were similar to controls. Whole fly samples were taken at steady state from 5-day old males and 24 hours after injection of bacteria or PBS. (D) The other *net* mutant, *net*^{x}, has a strong increase in *Atg2* expression. p values were calculated using Mann Whitney test (*p<0.05, ***p<0.001).

To assess whether *net* expression levels are controlled in vivo by JAK-STAT signalling, I analysed *net* expression levels in flies carrying *croquemort-gal4* as a driver together with *UAS-domeΔcyt*, or *UAS-upd3-IR*, but did not detect any change in *net* expression levels during infection (A). As whole fly samples were taken, the effect on hemocytes may be hidden by *net* expression in other tissues. It would then be useful to check this expression using a ubiquitous driver such as *tubulin-gal4*. To directly assess whether hemocyte-like cells had a change in *net* expression, I analysed *net* levels at different timepoints (1, 3, and 24 hours) and did not observed an increase in transcription when *upd3* is overexpressed (**Figure 4-13** B). Therefore suggesting that the JAK-STAT pathway may control *net* expression in other tissues than immune cells. Indeed, by looking at the gene expression profile from Flybase and the FlyAtlas website, the highest expression of net in adult flies is detected in the salivary glands. However, we cannot conclude that JAK-STAT has no effect on *net* expression in hemocytes in adult flies as the embryonic cell lines used in vitro are most likely different from hemocytes in vivo.

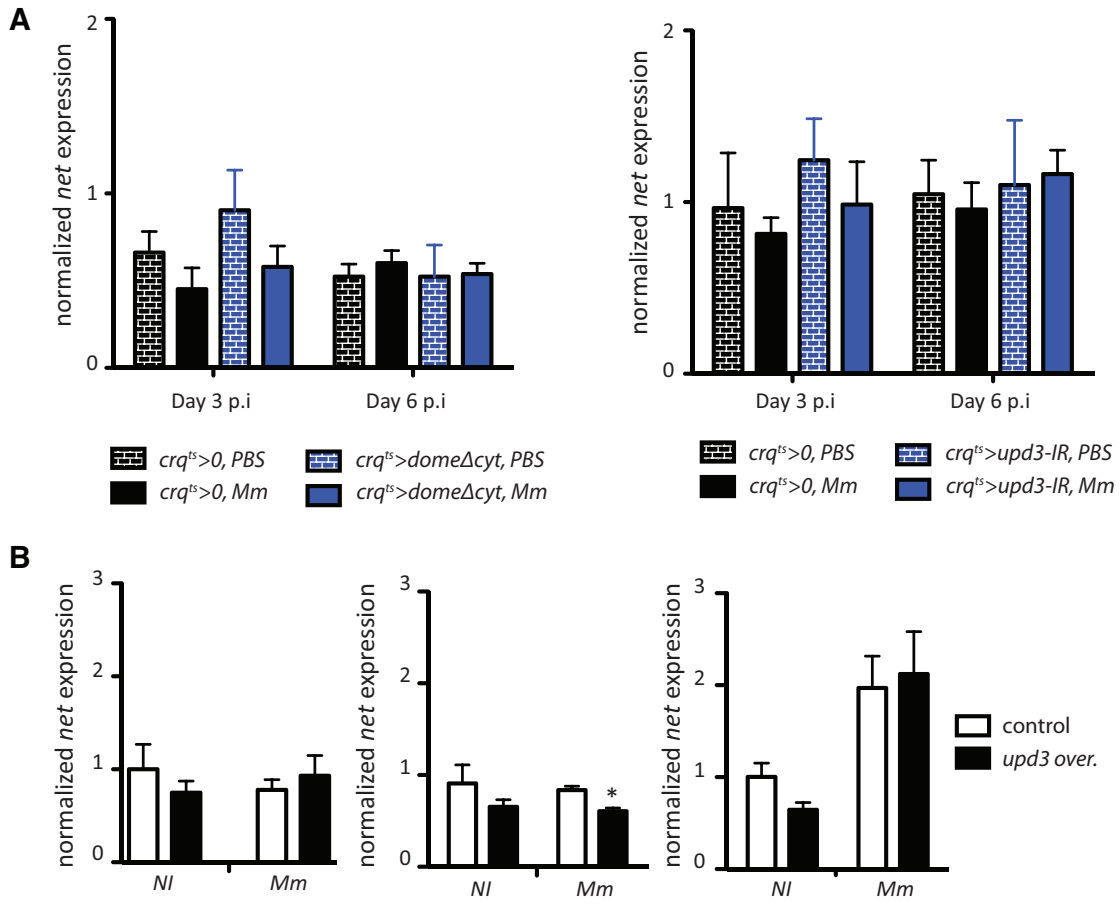

Figure 4-13: Changes in *net* expression are not observed in vivo, nor in vitro

(A) By using a dominant-negative form of Domeless or a knock down of *upd3* in adult hemocytes, no obvious changes in *net* expression were observed. Whole fly samples were taken at day 3 and 6 post-infection. (B) In S2R^{+} cells infected by *M.marinum* at MOI 20 or not infected, no changes in *net* expression were observed after 1 hour (left), 3 hours (middle) or 24 hours of infection (right). p values were calculated using Mann Whitney test (*p<0.05).

4.2.5 *net* mutants have an increased resistance to infection with intracellular pathogens

As I previously showed, bacterial replication is altered when *Atg2* is overexpressed, therefore I wanted to assess whether *net* mutants have an enhanced resistance to infection in vivo. For that I infected the two *net* mutant lines, net^{1} and net^{x}, for survival analysis and bacterial count. The results indicate that *net* mutants have a mild increase in survival to infection (**Figure 4-14** A) and that bacterial replication was reduced (**Figure 4-14** B). These results strongly suggests that *net* has a detrimental role in immune responses to mycobacterial infection, possibly through the downregulation of *Atg2*.

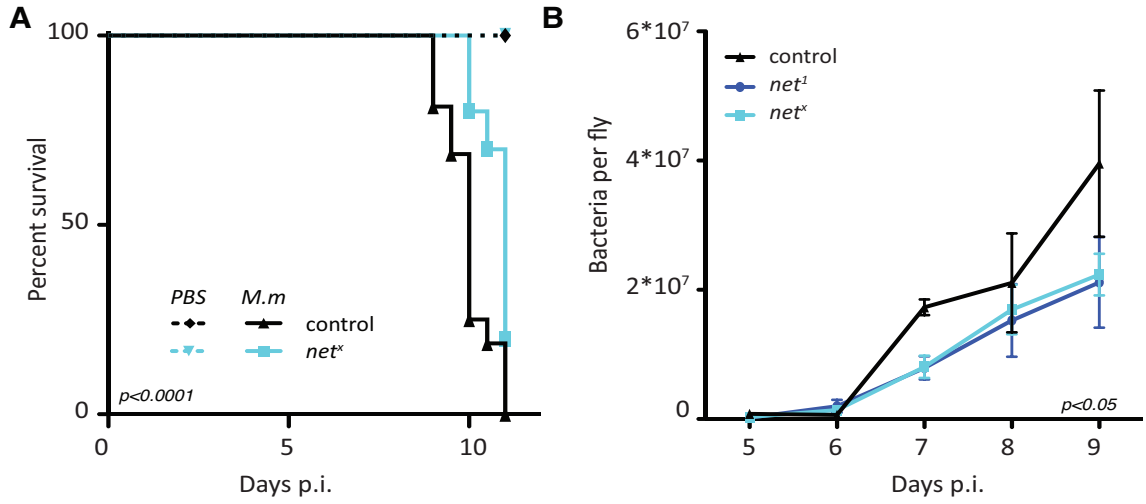

Figure 4-14: *net* mutants are more resistant to *M.marinum* infection

(A) *net* mutants have a slight increase in survival time compared to control flies. Flies were injected with *M.marinum* at 500CFUs. n=2 (20 flies per curve); p values were calculated using log-rank test (*p<0.0001). (B) *net* mutants have less bacteria per fly compared to controls. Whole fly samples were mashed from day 5 to day 6 p.i. n=4 to 5 samples per day and per genotype. For panel A, p values were calculated using log-rank test. For panel B, p values were calculated using two-way ANOVA.

To veriify if *net* mutants are also more resistant to other intracellular pathogens, flies were infected with *Francisella novicida* and the number of bacteria at several timepoints post-infection was counted by plating serial dilutions of infected fly extracts (**Figure 4-15** A). The results indicate a decreased number of clones in *net* mutants compared to controls, thereby confirming a resistance phenotype to at least two intracellular pathogens.

Since *F.novicida* induces *Diptericin* and *Drosomycin* expression, I wanted to assess whether *net* mutants had a change in humoral responses that would explain this resistance phenotype, in addition to the increased *Atg2* expression. No differences were detected in *Diptericin* and *Drosomycin* expression between net^1, net^x and control flies at day 2 and 3 post-injection (**Figure 4-15** B).

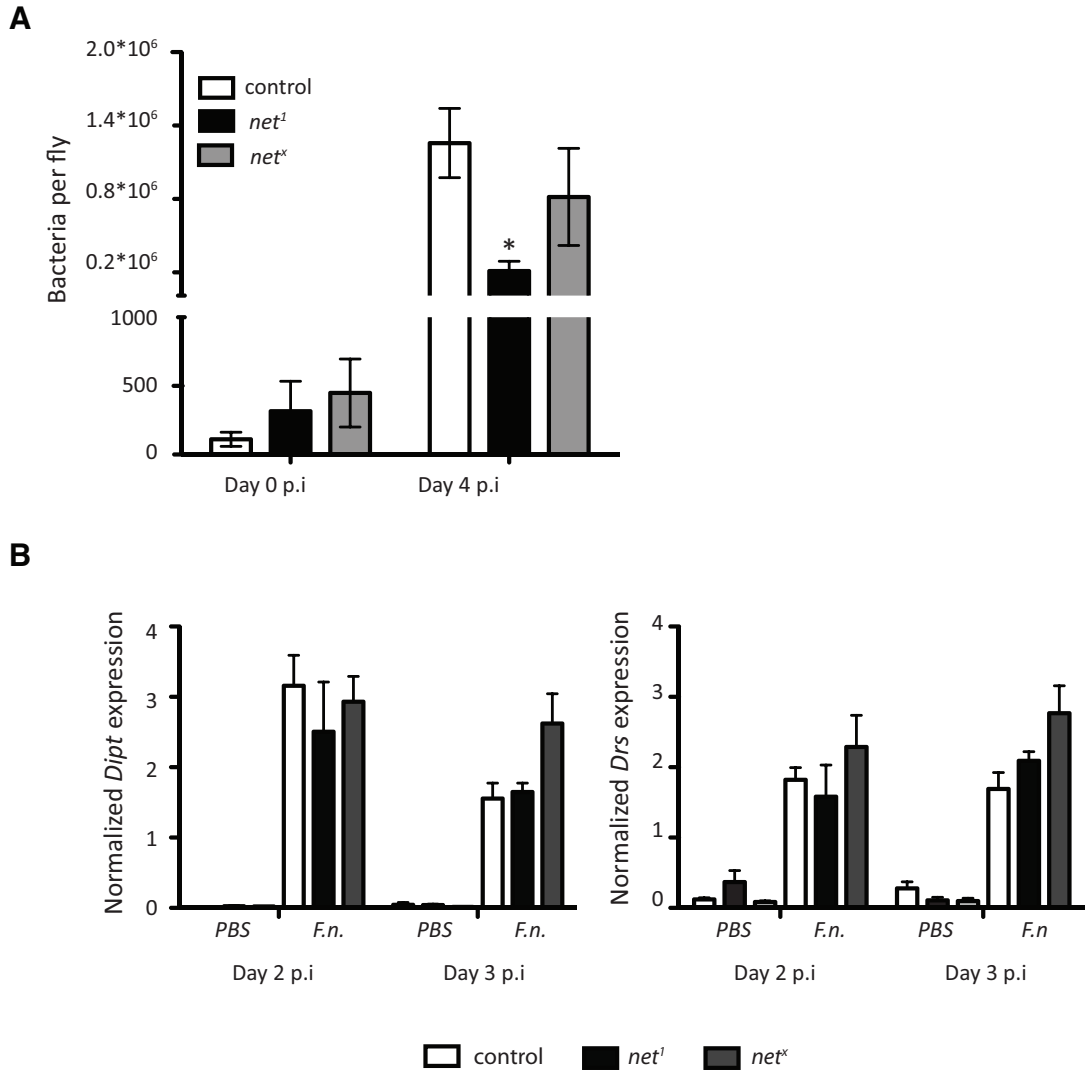

Figure 4-15: *net* mutants are more resistant to *F.novicida* infection

(A) net^1 and net^x mutants have a lower number of *Francisella novicida* after four days of infection compared to controls. Bacteria were counted by plating serial dilutions per fly. n=5 to 7. (B) The increased resistance in *net* mutant flies is not due to a change in transcription of antimicrobial peptides. Whole fly samples were taken 2 and 3 days post-infection with *Francisella novicida* and processed for qPCR. *Diptericin* and *Drosomycin* levels are increased upon infection but no difference was observed in *net* mutant flies (net^1 and net^x). p values were calculated using Mann Whitney test (*p<0.05). Data were generated with the help of Freddie Peakman.

The next step will be to assess whether JAK-STAT signalling controls *net* expression in hemocytes in vivo and/or other tissues, and whether Net directly downregulates *Atg2*. Indeed, it would be interesting to determine which tissue is responsible for the resistance phenotype observed in *net* mutant flies.

4.3 Discussion

I this chapter, I demonstrated that inhibition of JAK-STAT signalling by knocking down *Stat92E* or using a dominant negative form of *Domeless* in hemocytes resulted in increased resistance to infection. Indeed, inhibition of JAK-STAT in hemocytes extended host survival in infection, lowered bacterial replication and decreased hemocyte death.

The point that was clarified was which tissue is responsible for this phenotype. The two obvious tissues to look at were the fat body, which was already demonstrated to respond to Upd3 in vivo, and hemocytes, in which bacteria are found in the early phases of infection. To address this question, I used flies carrying a *UAS-Stat-IR* construct to knock down *Stat* in various tissues. Unfortunately, our results indicate that the construct is leaky, leading to a reduction in expression of the STAT target, *TotA*, upon infection despite the absence of driver. Therefore, It is difficult to link the resistance phenotype to the inhibition of STAT in a specific tissue. However, our results indicate that knocking down *Stat* in the fat body did not induce a resistance phenotype therefore suggesting that another tissue than the fat body is responsible.

Hemocyte-like cell lines that overexpress *upd3* strongly activate *TotA* suggesting that hemocytes respond strongly to Upd3 signalling by secreting acute phase proteins such as *TotA*. In vivo, our data indicate that *TotA* is strongly upregulated during infection and that hemocyte-specific knock down of *Stat* reduces strongly *TotA* expression even further than the *UAS-Stat-IR* construct alone. These results imply that the JAK-STAT pathway is at least partly activated in hemocytes upon infection and lead to the production of acute phase proteins such as *TotA*. In addition, several autophagy genes were upregulated when the JAK-STAT pathway was inhibited. In particular, the effect on *Atg2* expression was the most consistent and the strongest among all genotypes tested. Of particular interest, the *Atg2* phenotype was only seen in the hemocyte-specific knock down of *Stat* compared to the driver and responder gene only controls, and since overexpressing *Atg2* in hemocyte-like cell lines decreased intracellular growth of *M.marinum*, these results strongly suggest that the resistance phenotype in *upd3* and *Stat* knock down flies is partly due to inhibition of JAK-STAT activation in hemocytes and of the subsequent production *Atg2*.

The results presented in this chapter show that by increasing *Atg2*, via inhibition of JAK-STAT signalling, the fly resists *M.marinum* infection better, while a reduction in *Atg2* levels, via overexpression of *upd3*, leads to a phenotype close to controls or to a slight decrease in resistance. All together, these data point towards a threshold of activation for *Atg2*. Below this limit, no or small effects are observed, and over the threshold, a strong response is triggered. In addition, a strong activation of JAK-STAT reduces *Atg2* expression without inhibiting it, therefore suggesting that another pathway may regulate its expression levels, most probably through constant activation. In this view, the JAK-STAT pathway would only have an inhibitory role when activated in the context of infection for example. Obviously, the next question coming to one's mind is: why?

Finally, we identified *net* as a strong repressor of *Atg2* possibly in hemocytes and other tissues. *net* mutants have a strong upregulation of *Atg2* and increased resistance to intracellular pathogens such as *M.marinum* or *F.novicida.* While Bina et al. found it as a JAK-STAT target in Kc_{167} cell lines, we failed to confirm this result in $S2R^+$ cells. It is possible that $S2R^+$ cells do not mimic exactly molecular events taking place in vivo, therefore we cannot exclude that JAK-STAT activation in hemocytes in vivo regulate *net* expression. So far, we have not been able to prove it in vivo, as whole fly samples for qPCR may hide such effect, and because our newly developed cell sorting strategy triggered stress responses in hemocytes, it rendered conclusions difficult (data not shown).

The exact function of *Atg2* remains now to be discovered. Recently, mammalian *Atg2* proteins were shown to be essential not only for autophagosome formation, buy also for the regulation of size and distribution of lipid droplets (Velikkakath et al. 2012). Perhaps, Atg2 could be a regulator of lipid metabolism in immune cells, therefore limiting nutrients access to the bacteria, or it could engage specific bactericidal mechanisms such as autophagy. The next chapter will attempt to decipher the role of Atg2 at steady state and upon infection.

Chapter 5 Atg2 alters bacterial survival and disrupts lipid storage

5.1 Introduction

Atg2 is part of the Atg18-Atg2 complex recruited to autophagic membranes in yeast (Obara et al. 2008). Since our results suggested that JAK-STAT signalling could transcriptionally repress *Atg2*, we assessed the role of Atg2 protein in intracellular mycobacterial infection. Recently, Velikkakath et al. demonstrated the importance of Atg2 in autophagosome closure (Velikkakath et al. 2012). Atg2 is present in two isoforms in mammals, Atg2A and Atg2B. Silencing both forms blocked autophagic flux. In addition to its role in autophagy, Atg2A was shown to localize to the surface of lipid droplets through a conserved region between amino acids 1723 to 1829. Silencing both Atg2 proteins resulted in clustering of lipid droplets in an autophagy-independent manner. Since the autophagy and lipid droplet localization region is conserved in *Drosophila Atg2*, I analysed both mechanisms in vitro in $S2R^+$ cells.

Autophagy and lipid metabolism are two processes known to be altered by mycobacterial infection (See Chapter 1). Autophagy can mediate killing of mycobacteria that escaped phago-lysosomal fusion by re-engaging fusion of the lysosome with the double-membrane autophagy vesicles. Since the autophagosome contains distinct molecular complexes from the phagosome, it then constitutes an alternative intra-vesicular killing mechanism.

Upon *M.tuberculosis* infection, IFN-γ activates autophagy, which results in bacterial colocalization to acidified vacuoles and killing (Gutierrez et al. 2004; Harris et al. 2007). Autophagy activation is inhibited by cytokine signalling through the Th2 cytokines IL4 and IL-13, and also by IL-6 (Dutta et al. 2012; Harris et al. 2007). Although autophagic regulation is thought to be mediated at a post-translational level, I demonstrated in the previous chapter that IL-6-like signals in *Drosophila* can regulate transcription of autophagy genes, especially of *Atg2*. Interestingly, overexpression of *Atg2* resulted in a decrease in bacterial growth, suggesting that

IL-6 signalling could regulate autophagy through modulation of *Atg2* expression. To study autophagy upon *M.marinum* infection, I engineered a human *pPAC-GFP-LC3* plasmid—LC3 being the human analog to *Drosophila* Atg8—for transient transfection in $S2R^+$ cells that overexpress or not *upd3*. LC3 is a commonly used autophagy marker that associates to the autophagosomal membranes after processing (Kabeya et al. 2000). In *GFP-LC3* expressing cells, autophagosomes are observed as punctae due to the accumulation of GFP-LC3 at the autophagosomal membrane. In addition, thanks to the generosity of the Cherry lab and the Kohler lab that generated Atg8 antibodies in *Drosophila*, I also studied the endogenous accumulation of autophagosomes (Shelly et al. 2009; Barth et al. 2011).

Besides bactericidal mechanisms, bacterial growth can also be limited by the shortage of nutrient sources. Since *M.tuberculosis* uses lipid droplets as a nutrient source for persistence in macrophages, the association of Atg2 to lipid droplets is very interesting (Peyron et al. 2008). It has been demonstrated that mycobacterium triggers lipid droplet formation in a TLR2-dependent mechanism through bacterial oxygenated mycolic acids, but the precise mechanisms are unknown (D'Avila et al. 2006; Peyron et al. 2008). Our hypothesis is that cytokine signalling in macrophage-like cells could modulate lipid droplet formation or morphology in an Atg2-dependent mechanism. To understand the role of Atg2, I used the *pPAC-GFP-Atg2* plasmid described in Chapter 3 for overexpression of *Atg2* and to localise Atg2 proteins within $S2R^+$ cells; to determine the amount and morphology of lipid droplets, I used Oil-RedO, a neutral lipid stain. Since human macrophages within the granulomas develop a foamy phenotype through accumulation of lipid droplets, I first verified this phenotype in *Drosophila* cells lines; I then studied the association of bacteria with lipid droplets; and I finally assessed the function of Atg2 in this context.

This chapter presents two potential functions of Atg2 that may contribute to the resistance phenotype observed in flies lacking JAK-STAT signalling in hemocytes. These two functions, autophagy and lipid metabolism, may be independent or tightly associated to regulate bacterial replication within immune cells. In the first part, I will study autophagy in the context of *M.marinum* infection in $S2R^+$ cells and in cells overexpressing *upd3* or *Atg2* compared to controls; in the second part, I will present the mycobacteria-induced effect on lipid droplets and its regulation by Atg2.

5.2 Results

5.2.1 *M.marinum* infection does not induce autophagy in macrophage-like cells

Autophagy is induced upon *M. tuberculosis* infection *in vivo* to overcome the phagosomal maturation arrest imposed by the bacteria, and ultimately to control bacterial replication. (Singh et al. 2006; MacMicking et al. 2003; Gutierrez et al. 2004). We do not know if this is happening in *Drosophila* hemocytes upon *M.marinum* infection. To answer this question, I generated a GFP-LC3 plasmid in which GFP is fused to the amino-terminus of LC3, a human analog to the fly Atg8 protein. In cells transfected with this plasmid, GFP-LC3 proteins bind the autophagosomal membrane and appear in the form of autophagic punctae (**Figure 5-1** A).

To assess whether *M.marinum* infection induces autophagy in $S2R^{+}$ cells, I infected cells previously transfected with the *pPAC-GFP-LC3* plasmid and compared the results to non-infected controls (**Figure 5-1** A). Quantification of GFP-LC3 punctae did not reveal any change in autophagy between *M.marinum* infected and non-infected cells (**Figure 5-1** B). Interestingly, more than 40% of cells have at least one bacterium colocalising with GFP-LC3 punctae suggesting that autophagy can have a role in *M.marinum* infection.

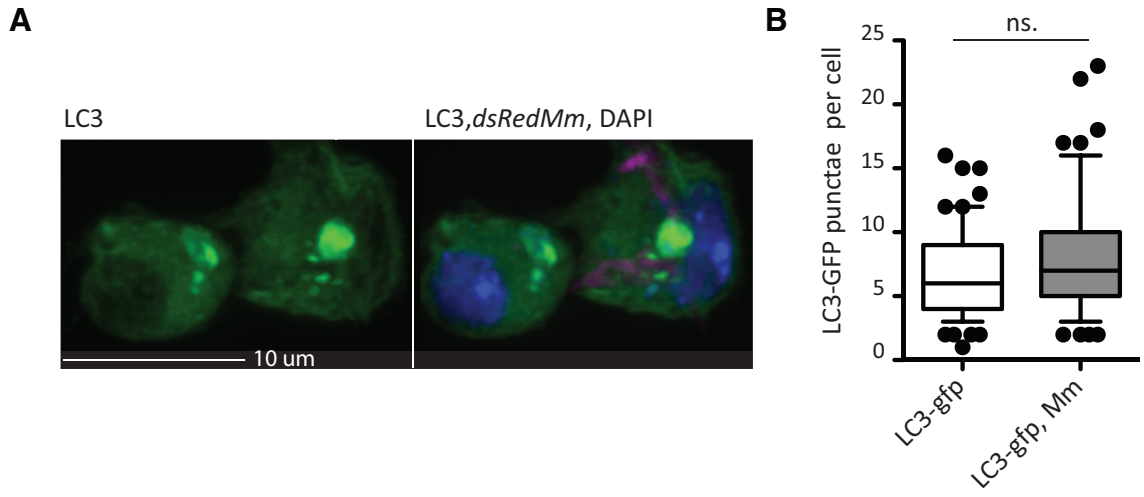

Figure 5-1: Autophagy is not induced by infection when looking at GFP-LC3 punctae by imaging

(A) S2R^{+} cells transfected with *pPAC-GFP-LC3* harbor GFP punctae, markers of autophagosomes. 24 hours after transfection, cells were infected with *dsRed Mm* at MOI 20. After 24 hours of infection, they were fixed and stained with anti-GFP (primary: rabbit anti-GFP; secondary: Alexa 488 goat anti-rabbit) and with DAPI. (B) No differences in GFP-LC3 punctae was observed between infected cells (Mm) and non-infected controls (NI). GFP-LC3 punctae were quantified by imaging. For this experiment, n=60 for non-infected cells and n=89 for infected cells. The p value was calculated using Mann Whitney test, and results were not statistically significant.

Overexpression of *GFP-LC3* was widely used in early studies on autophagy. However, the method can generate several artefacts: first, GFP-LC3 can aggregate in non-autophagic structures; second, the counting of autophagic punctae in imaged cells can be subjective; and finally, GFP fluorescence is quenched at low pH, when the autophagosome fuses with the lysosome, therefore inhibiting detection of late autophagosomes (Barth et al. 2010). For these reasons, I looked at endogenous Atg8 proteins thanks to the *Drosophila* Atg8 antibody generated in the Cherry lab (Shelly et al. 2009). Antibody staining revealed that endogenous Atg8 punctae increase slightly upon infection but without being significant, therefore proving that autophagy is not induced by *M.marinum* infection in *Drosophila* hemocyte-like cells (**Figure 5-2**)

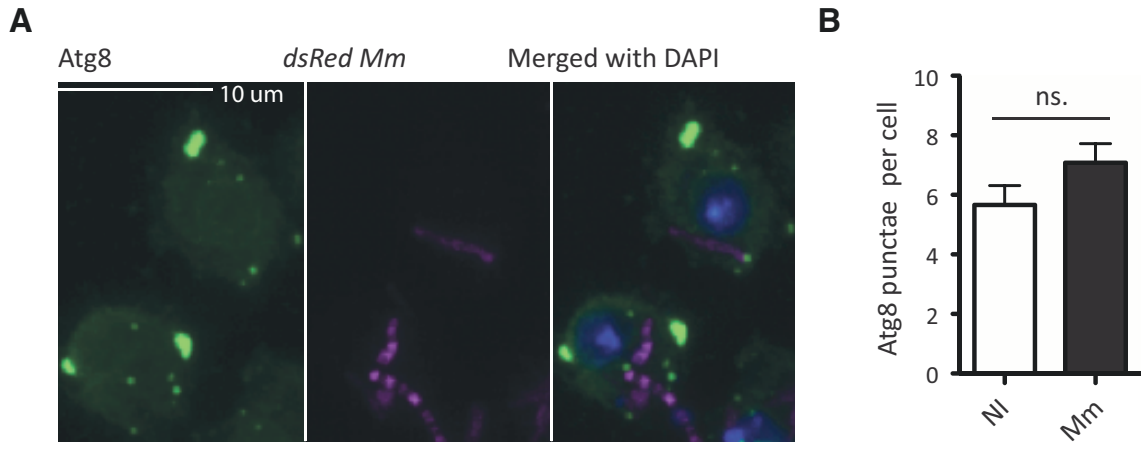

Figure 5-2: Autophagy is not induced by infection when looking at endogenous Atg8 punctae

(A) Representative image of endogenous Atg8 punctae in $S2R^{+}$ cells infected with *dsRed M.marinum*. Cells were infected with *dsRed Mm* at MOI 20 and, after 24 hours, were fixed and stained with rabbit anti-Atg8 (Cherry lab) as primary antibody and Alexa 488 goat anti-rabbit secondary antibody.(B) The number of Atg8 punctae per cell increases slightly upon *M.marinum* infection, but without being significant. Samples were analysed from 2 independent experiments where cells were stained with Atg8 antibodies (Cherry lab), in combination with Alexa-488 goat anti-rabbit secondary antibody or Anti-Rabit Cy5 antibody. For non-infected samples, n= 41 and for infected samples, n= 65. The p value was calculated using the Mann Whitney test.

To further confirm these results, I analysed by western blot the processed form of Atg8, Atg8-II, also known as Atg8-PE, which associates with autophagosomes. Upon stimulation of autophagy, unprocessed Atg8 is lipidated with phosphatidylethanolamine (PE) and becomes associated with the autophagosomal membrane. Therefore, detection of Atg8-II by western blot with endogenous Atg8 antibody allows quantification of autophagy. In the literature, interpretation of LC3 (Atg8) western blots is controversial. Usually, researchers analyse the signal ratio between LC3-I and LC3-II; however, due to differential antibody affinity to LC3-I and LC3-II, and to the rate of LC3-II degradation within autophagolysosomes, researchers have now agreed to quantify LC3-II levels by normalizing them to a loading control (Barth et al. 2010). Accordingly, I analysed Atg8 blots by normalizing Atg8-II levels to tubulin. There is no change in Atg8-II levels in infected samples compared to non-infected controls (**Figure 5-3**).

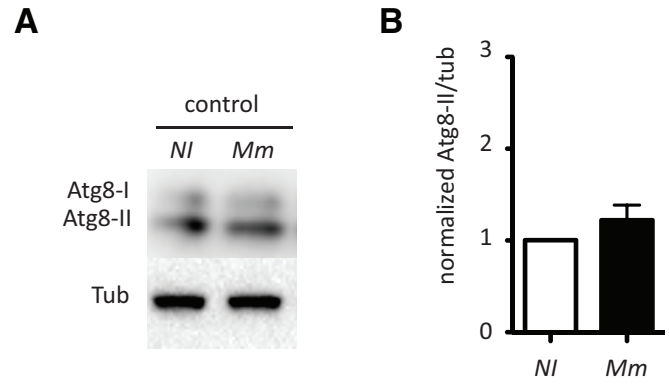

Figure 5-3: Autophagy is unchanged upon infection when looking at endogenous Atg8 punctae

(A) Representative Western Blot showing no difference in Atg8 levels in infected cells compared to non-infected controls. Cells were transfected with *pPAC-HA* and were then infected with *M.marinum* at MOI 20. After 24 hours of infection samples were collected and processes for Western Blot. Atg8 levels (top) and tubulin levels (bottom) were analysed. The quantification is showed in (B). For this experiment, the anti-Atg8 antibody from the Kohler lab was used. n=2. These experiments were performed with the help of Kevin Bronda.

5.2.2 Atg2 accumulates and is found close to *M.marinum*

Atg2 participates in the vesicle nucleation of the autophagosome potentially in a complex with Atg18 (see Chapter 3, Table 1). Since Atg2 binds the autophagic membrane, we should observe Atg2 punctae by imaging. To investigate this, I transfected $S2R^+$ cells with *pPAC-GFP-Atg2* and imaged them 24 hours after infection with dsred *M.marinum* at MOI 20 (**Figure 5-4** A). At steady state, I observed several fluorescent punctae randomly distributed within the cell. Upon infection, these punctae are found close to bacteria, indicating that they may relocalise. Interestingly, the number of punctae per cell increases upon *M.marinum* infection (**Figure 5-4** B). By making the assumption that levels of expression of Atg2 are identical in infected samples compared to controls, these results suggest that Atg2 proteins reorganised to associate with vacuoles. However, a more accurate analysis would require additional samples and a quantification of endogenous Atg2 punctae.

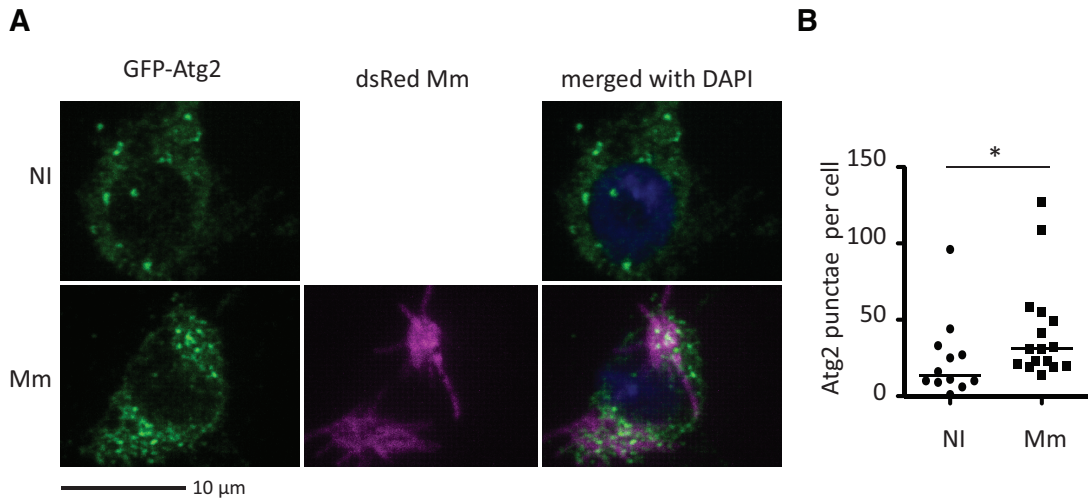

Figure 5-4 In infected S2R$^+$ cells, Atg2 is found close to *M.marinum*

(A) At steady state (top), *GFP-Atg2* is dispersed in S2R$^+$ cells and is also observed in punctae similar to autophagy punctae. Upon infection, GFP-Atg2 punctae are found in close proximity to the bacteria (bottom). (B) The number of Atg2 punctae after infection with *M.marinum*. For this experiment, S2R$^+$ cells were transfected with *pPAC-GFP-Atg2* and were infected 1 day later. After 24 hours of infection, cells were fixed and stained using rabbit anti-GFP as primary antibody, and Alexa-488 goat anti-rabbit as secondary antibody. Cells were imaged using a confocal microscope, and to distinguish punctae from background fluorescence, only the punctae of diameter >0.5µm were quantified. For non-infected samples (NI), n=12, and for infected samples, n=16. The p value was calculated using Mann Whitney test (*p<0.05).

5.2.3 Increasing *Atg2* levels do not affect autophagic flux

I previously demonstrated that bacterial replication is reduced in cells overexpressing *Atg2* and since Atg2 participates in the nucleation phase of the autophagosome, I wanted to assess whether increased levels of *Atg2* correlate with increased autophagy. To investigate this, I infected cells overexpressing *Atg2* and counted the number of Atg8 punctae per cell compared to controls. At steady state or upon infection, I could not observe any significant change in the number of Atg8 punctae between cells overexpressing *Atg2* and controls, indicating that there is no apparent change in autophagic flux, ie increase in autophagosome synthesis or degradation (**Figure 5-5** A & B).

Interestingly, upon infection, Atg8 punctae become larger, possibly to encapsulate mycobacteria (**Figure 5-5** B). In addition, cells overexpressing *Atg2* do have slightly larger punctae per cell at steady state compared to control but no difference is observed upon infection.

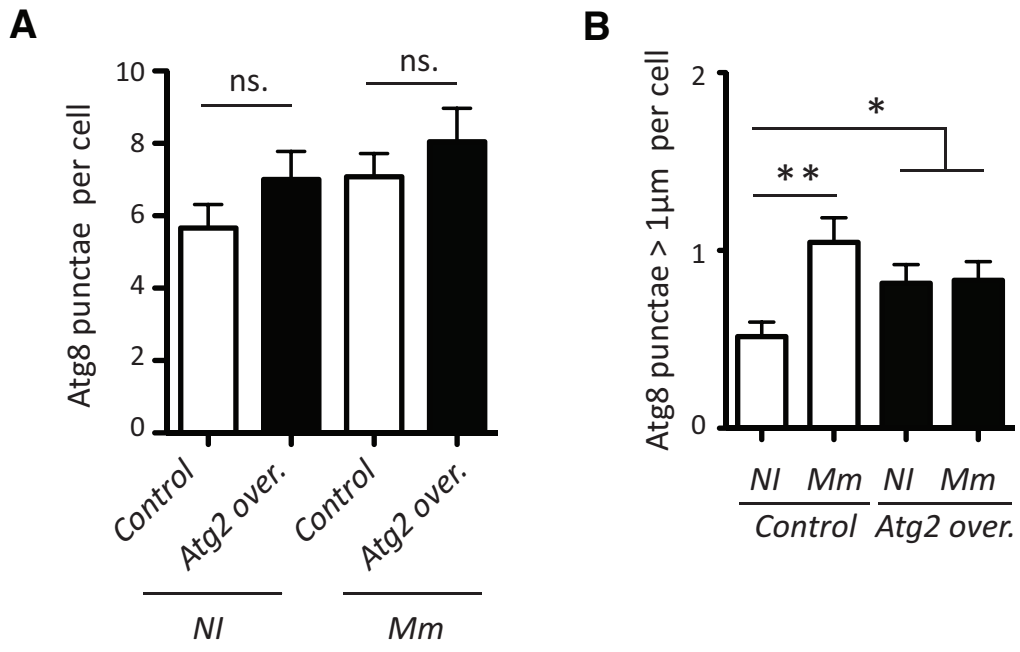

Figure 5-5: *Atg2* overexpression in S2R$^+$ cells does not induce autophagy

(A) At steady state, cells overexpressing *Atg2* have a slight increase in Atg8 punctae per cell but it is not significant. S2R$^+$ cells were transfected with *pPAC-GFP-Atg2* to overexpress *Atg2* or *pPAC-HA* as control. After 48 hours, cells were fixed and stained with rabbit anti-Atg8 (Cherry lab) as primary antibody and Cy5 Anti-Rabbit secondary antibody. For control cells, n= 60 and for *Atg2*-overexpressing cells, n=65. Upon infection with *M.marinum* (MOI20), no difference in Atg8 punctae was observed in cells overexpressing *Atg2* compared to control. For control cells, n=65, and for cells overexpressing *Atg2*, n=48 (B) Upon infection, Atg8 punctae enlarge compared to non-infected controls. At steady stat, when cells overexpress *Atg2,* they have a higher number of large punctae (diameter>1 µm) than controls. Upon infection, there is no difference compared to infected controls. Cells were transfected and infected similarly as in (A) For non-infected controls (NI), n=60,for infected controls, n=65, for non-infected *Atg2* overexpressing cells, n=65, and for infected *Atg2* overexpressing cells, n=48. p values were calculated using Mann Whitney test (*p<0.05, **p<0.01).

Overexpressing *Atg2* did not have a clear effect on autophagy induction, however reduction of *Atg2* levels may have a more dramatic effect. As previously showed, *Atg2* levels are downregulated in response to Upd3 signalling in S2R$^+$ cells, and, as a consequence, bacterial growth is enhanced. This change in bacterial proliferation could be explained by a decrease in autophagy. To verify this hypothesis, I infected cells overexpressing *upd3* with *M.marinum* at MOI 20 and analysed Atg8 punctae after 24 hours of infection. Cells overexpressing *upd3* have an increased number of Atg8 punctae at steady state, which is further enhanced upon infection (**Figure 5-6** A). Interestingly, cells overexpressing *upd3* have also a higher number of large punctae, but the results are not significant due to low number of samples (**Figure 5-6** B).

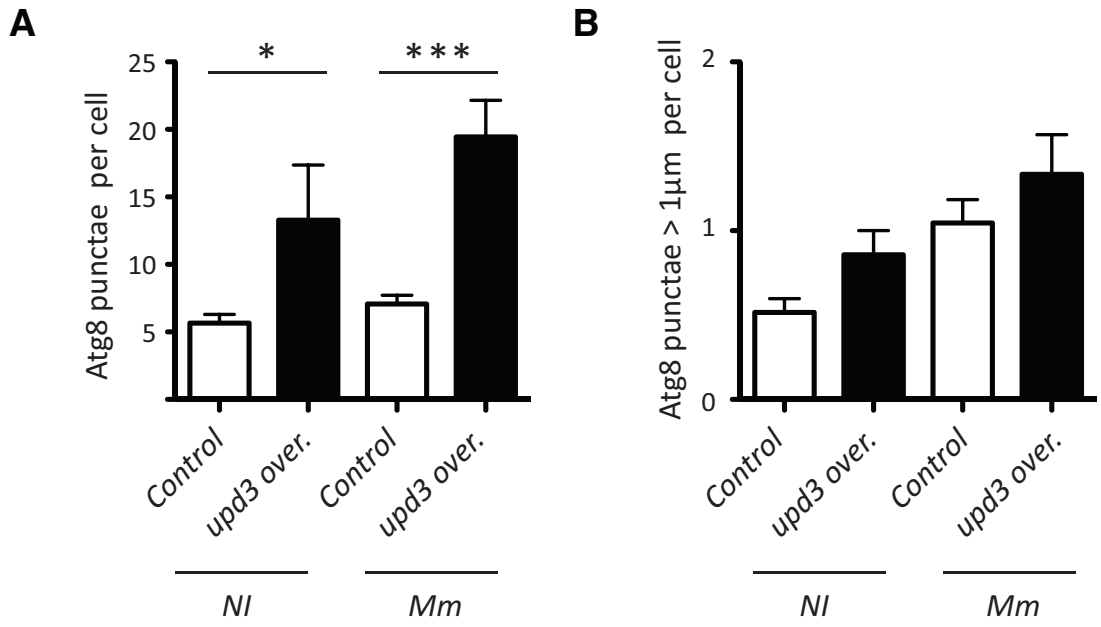

Figure 5-6: *upd3* overexpression in S2R^{+} cells induces changes in autophagy

(A) At steady state and upon infection, the number of Atg8 punctae in enhanced when *upd3* is overexpressed. Cells were transfected with *pPAC-upd3* or *pPAC-HA,* and one day later were infected with *M.marinum* at MOI 20. After 24 hours of infection cells were fixed and stained with rabbit anti-Atg8 (Cherry lab) as primary antibody and with Alexa-488 goat anti-Rabbit secondary antibody. (B) At steady state or upon infection, *upd3* overexpressing cells have, in average, an increase number of large punctae compared to controls. For uninfected controls, n=60, for infected controls, n=65, for uninfected *upd3*-overexpressing cells, n=7, and for infected *upd3*-overexpressing cells, n=9. p values were calculated using Mann Whitney test (*p<0.05, ***p<0.001).

One hypothesis is that *upd3* activates autophagy in a mechanism independent from Atg2, another hypothesis is that autophagosome closure is impaired in cells overexpressing *upd3*, which may result in accumulation of non-functional autophagosomes with altered morphology.

5.2.4 *M.marinum* induces a foamy phenotype in *Drosophila* phagocytes

Since there is not a clear autophagy phenotype, I decided to look at lipid droplets. Upon *M.tuberculosis* infection mammalian macrophages accumulate lipid droplets and become foamy. To assess whether this phenomenon happens in *Drosophila* hemocytes, I stained infected and non-infected cells with OilRedO, a lysochrome diazo dye that stains neutral lipids, including triglycerides. Since lipid droplets contain a neutral lipid core, OilRedO staining allows the detection of lipid droplets. At steady state, lipid droplets have a dot-like shape and can be counted by automated detection with the 3D imaging software Imaris. Several detection methods were used:

(1) Total volume occupied by neutral lipids, to assess the overall change in neutral lipid content;
(2) Number of individual droplets, to assess the number of classical dot-shaped lipid droplets (large structures are counted as 1 single droplet). This method does not take into account the volume of lipid droplets;
(3) And the number of large size droplets (diameter>1µm), to assess the number of abnormal structures.

For the analysis, I combined data from at least three independent experiments. The results suggest that neutral lipid formation is slightly stimulated upon *M.marinum* infection (1.23 fold increase in total OilRedO volume) (**Figure 5-7** A & B).

Interestingly, lipid droplet morphology is altered upon infection: the overall number of droplets is reduced (1.22 fold) while the number of large structures dramatically increases (6 fold) (**Figure 5-7** C & D). All together, these results suggest that *M.marinum* infection triggers changes in lipid droplet formation and morphology favouring the apparition of large structures.

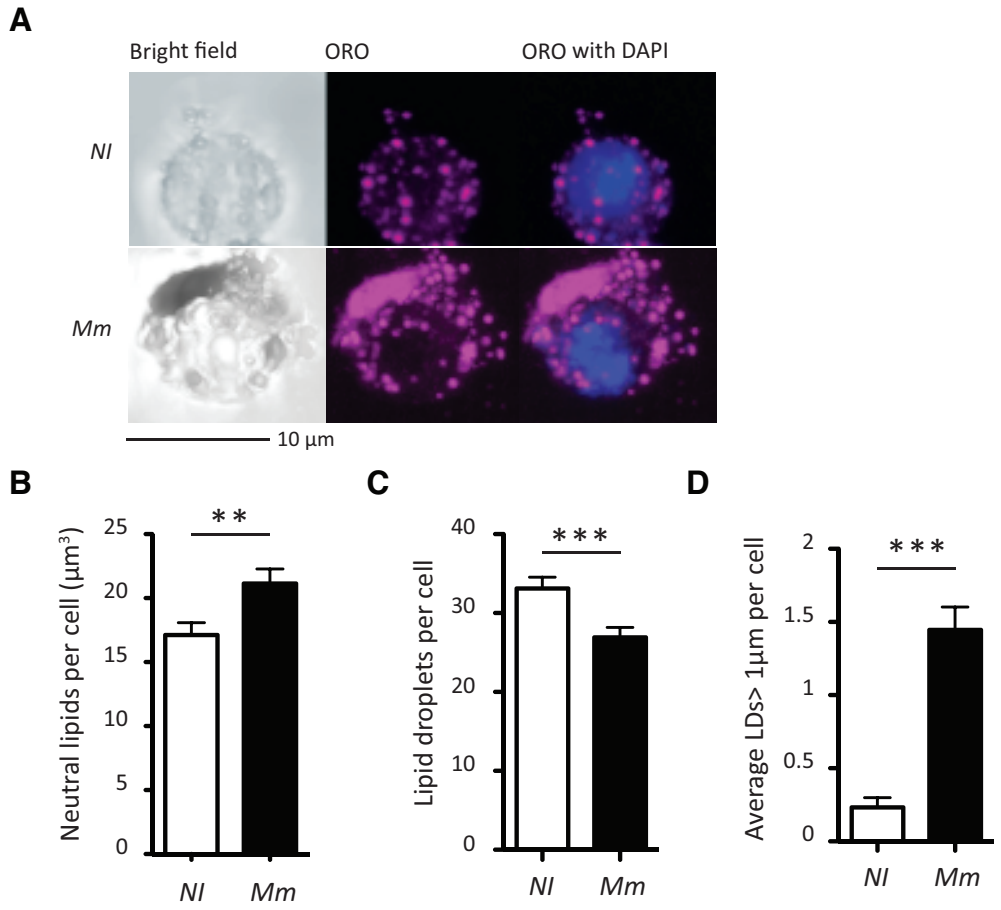

Figure 5-7: *M.marinum* infection stimulates lipid droplet formation and aggregation

(A) Confocal images of S2R^{+} cells infected with *M.marinum* reveals changes in lipid droplets with apparition of large structures. For all panels, cells were transfected with *pPAC-HA* and infected with *M.marinum* at MOI20 for 24 hours before fixation and staining with OilRedO (ORO). (B) The total volume occupied by neutral lipids is increased by 1.23 fold in infected cells compared to control. (C) The number of round-shape lipid droplets is reduced upon infection (1.22 fold reduction). Large structures were counted as a single droplet. (D) The number of large lipid droplets, with a diameter superior to 1 µm, is dramatically increased upon *M.marinum* infection (6 folds increase). For this figure, data were combined from 3 independent experiments and in total n=130 for non-infected cells and n=110 for infected cells. p values were calculated using Mann Whitney (**p<0.01, ***p<0.001).

5.2.5 Heat-killed *M.marinum* induces strong changes in lipid droplet formation and morphology

In the literature, there is evidence for bacterial cell components triggering the formation of foamy macrophages (Peyron et al. 2008). To test whether bacterial components alone can trigger lipid droplet formation in *Drosophila* hemocytes, I infected $S2R^{+}$ cells with heat-killed *M.marinum* and analysed lipid droplets formation and morphology after 24 hours. The heat treatment was performed at 80˚C for 25 minutes and killed the bacteria, as they were no longer able to grow in liquid culture (data not shown).

Heat-killed *M.marinum* induce a strong accumulation of neutral lipids compared to controls (2.1 fold increase) (**Figure 5-8** A & B). Interestingly, heat-killed *M.marinum* also induces a stronger accumulation of neutral lipids compared to infection with live bacteria (1.7 fold increase).

Heat-killed *M.marinum* also induces strong changes in lipid droplet morphology: the number of dot-shape lipid droplets and large structures is enhanced compared to controls and compared to infection with active mycobacteria (**Figure 5-8** C & D). The number of lipid droplets is increased by 1.4 fold compared to controls, and the number of large punctae dramatically increased by 11 fold compared to control and by 1.7 fold compared to infection with active *M.marinum*.

All together, these results show that *M.marinum* components alter host-cell lipid metabolism. Since active *M.marinum* infection reduces these changes, it suggests that the bacteria can consume lipid droplets probably to form intracellular inclusions. This hypothesis would fit with the data from the literature stipulating that lipid droplets are a nutrient source for mycobacteria (Peyron et al. 2008). Accordingly, when examining *M.marinum* localisation using a specific FITC conjugated antibody for *M.tuberculosis*, I found bacteria colocalising with and surrounding lipid droplets, indicating that they are tightly associated (**Figure 5-8** A).

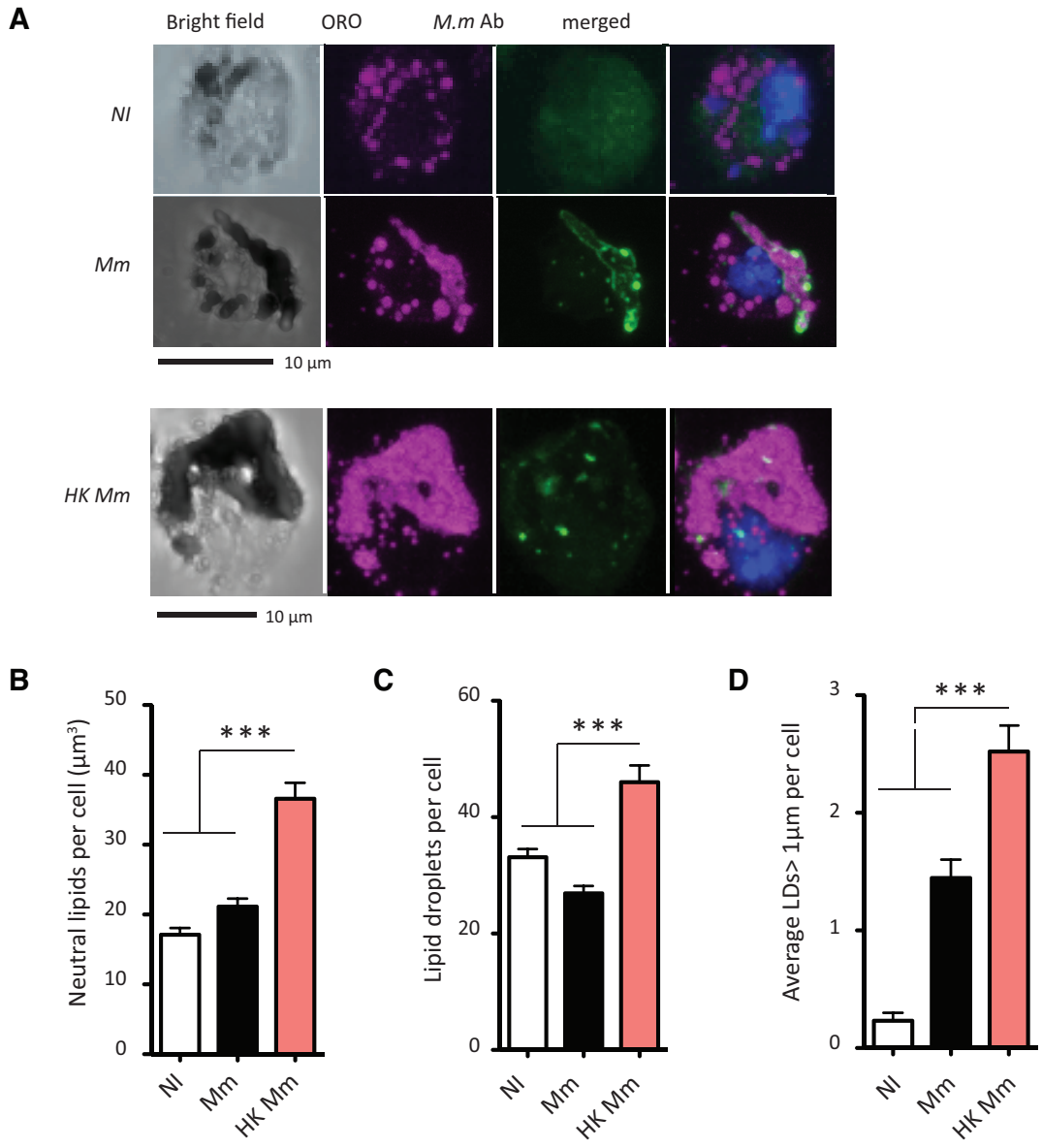

Figure 5-8: *M.marinum* components induce strong changes in lipid droplet formation and morphology

(A) Representative images of lipid droplets in *pPAC-HA* transfected cells infected with active *M.marinum* or heat-killed *M.marinum* compared to non-infected controls. Cells were infected with live *M.marinum* and heat-killed *M.marinum* at MOI20 for 24 hours and then fixed, stained with FITC conjugated anti-*M.tuberculosis* antibody and then with OilRedO. (B) Infection with heat-killed *M.marinum* increases the total OilRedO volume per cell by 2.1 fold compared to control and by 1.7 fold compared to infection with active *M.marinum*. (C) Heat-killed *M.marinum* enhanced the number of lipid droplets by 1.4 compared to controls. (D) Heat-killed *M.marinum* increases the number of large lipid droplets, with a diameter superior to 1 µm, compared to controls (11 fold) and active bacteria (1.7 fold). For this figure, data were combined from 3 independent experiments for non-infected and *M.marinum* infected samples, and from 2 independent experiments for heat-killed *M.marinum* samples. In total n=130 for non-infected cells, n=110 for *M.marinum* and n=96 for heat-killed *M.marinum*. p values were calculated using Mann Whitney (***p<0.001).

Upon infection of mammalian macrophages, *M.tuberculosis* is able to uptake lipids from the host cell for persistence (Garton et al. 2002; Daniel et al. 2004). To verify whether, *M.marinum* has intracellular lipid inclusions, I infected S2R$^+$ cells with *M.marinum* at MOI 20 and after 24 hours samples were fixed and processed for transmission electron microscopy (TEM) (**Figure 5-9**). The images suggest that lipid-like structures are present in the bacteria. To further confirm that lipid droplets are taken up from host lipids, and to check whether OilRedO is able to stain intrabacterial lipid inclusion, further experimentation is ongoing. Such experiments imply the observation of OilRedO staining of fixed bacteria and the quantification of the levels expression of genes involved in lipid metabolism.

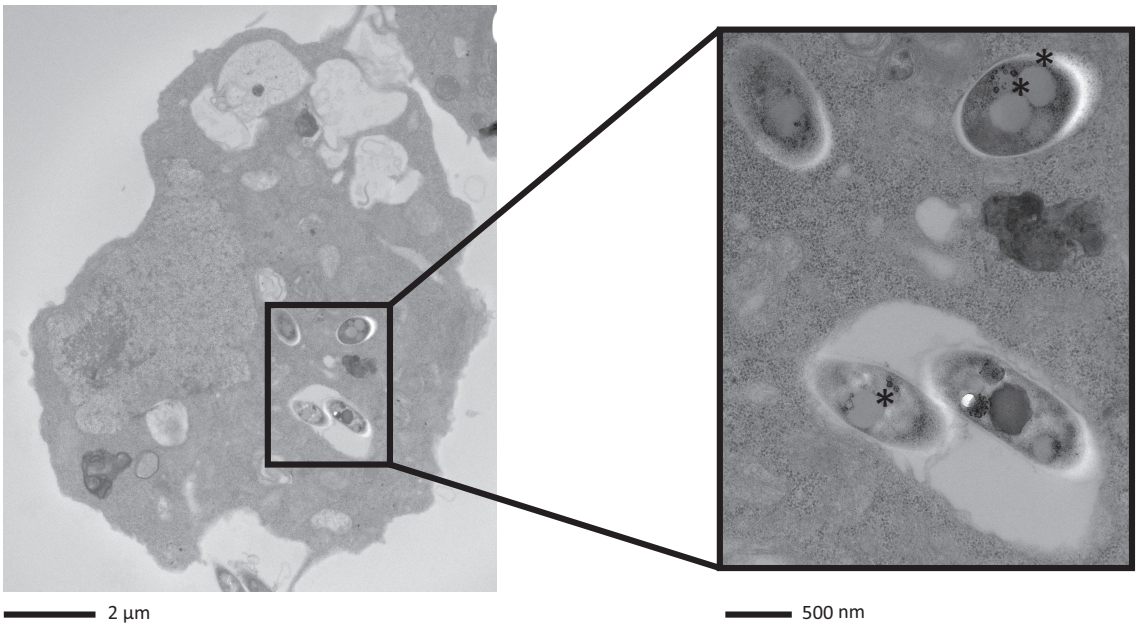

Figure 5-9: *M.marinum* have intracellular lipid inclusions within infected S2R$^+$ cells

Cells transfected with *pPAC-HA* were infected with *M.marinum* at MOI 20. After 24 hours, samples were collected, fixed and processed for TEM. A representative image of infected S2R$^+$ cells is shown here (left). A high magnification image (right) indicates bacterial intracellular lipid inclusions (*).

5.2.6 Other bacteria, such as *E.coli*, do not induce a foamy phenotype

To test whether other bacteria could induce a foamy phenotype in S2R^{+} cells, I infected them with *E.coli,* and analysed the amount and morphology of lipid droplets. The data indicate that, while *M.marinum* infection triggers changes in lipid droplet formation and morphology (**Figure 5-10**), *E.coli* infection does not induce any change. Indeed, the overall volume of neutral lipid per cell, the number of lipid droplets and the number of large structures in *E.coli* infected cells are similar to the non-infected controls.

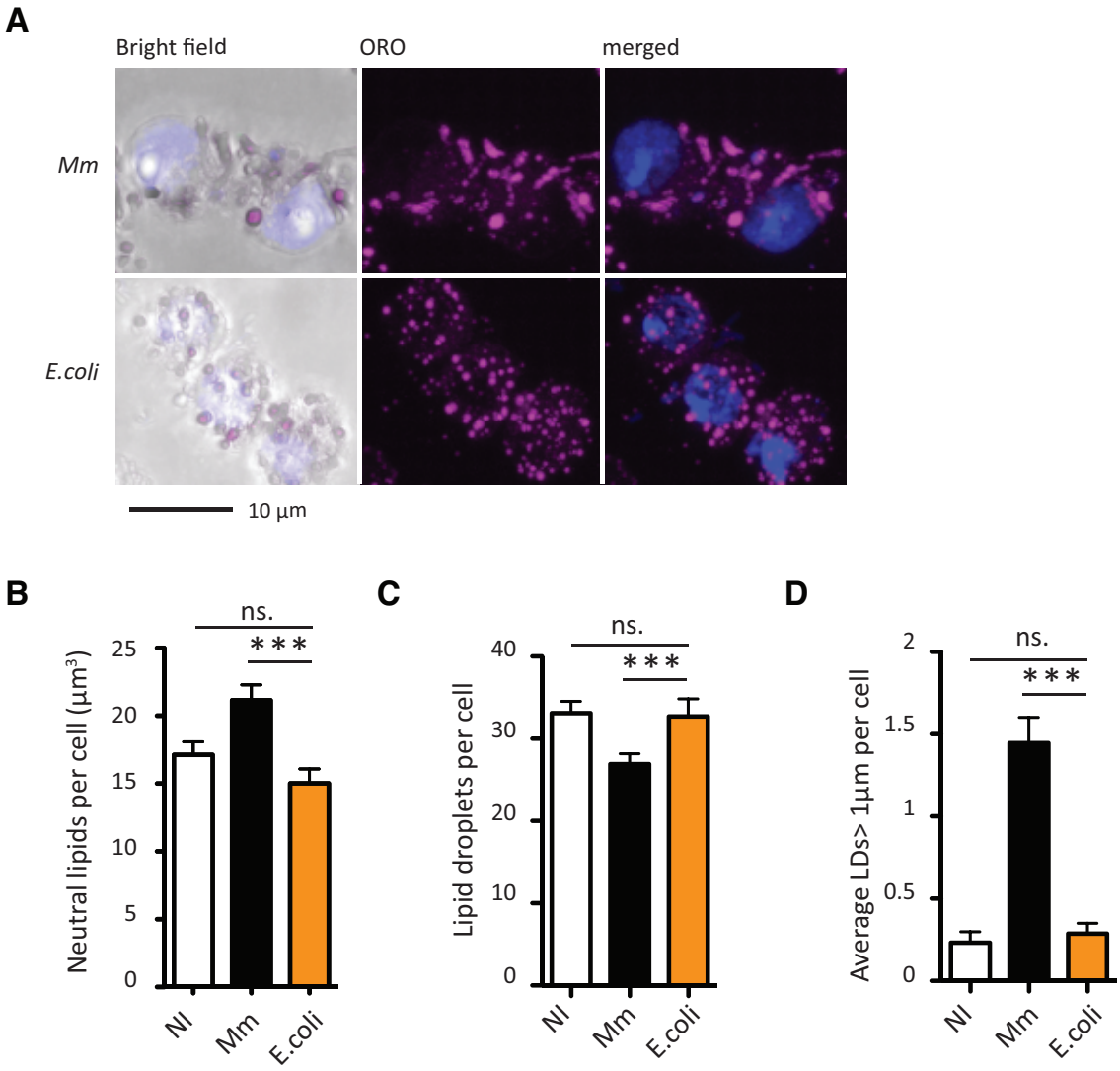

Figure 5-10: Infection with *E.coli* does not change lipid droplet formation and morphology

(A) Representative image of cells infected with *M.marinum* and *E.coli* that show no formation of large lipid droplets in *E.coli*-infected cells. Cells were transfected with *pPAC-HA* and then infected with either *M.marinum* at MOI20 or *E.coli* at MOI20. After 24 hours of infection, cells were fixed and stained with OilRedO. (B) Unlike *M.marinum* infection, *E.coli* infection does not induce lipid droplets formation. (C) The number of lipid droplets is unchanged in cells infected with *E.coli* compared to controls. (D) While *M.marinum* infection strongly induces the formation

of large lipid droplets, *E.coli* infection does not have the same effect and the number of large structures is similar to that of control cells. For non-infected controls and for *M.marinum* infected cells, data were combined from 3 independent experiments, and for *E.coli* infected cells, data were combined from 2 independent experiments. In total, n=130 for non-infected cells, n=110 for *M.marinum*-infected cells, and n=94 for *E.coli* infected cells. p values were calculated using Mann Whitney (***p<0.001).

5.2.7 Atg2 associates with lipid droplets

Bacteria associate with lipid droplets in *Drosophila* hemocyte-like cells, likely to use them as a source of nutrients. Since Atg2 proteins organise into punctae-like structures and relocalise close to bacterial cells, I wondered whether Atg2 could affect lipid droplets instead of directly targeting the bacteria. First, I looked at Atg2 colocalisation with neutral lipids. For that, I transfected cells with *pPAC-GFP-Atg2* and infected them with *M.marinum* one day later. After 24 hours of infection, cells were fixed and stained with a primary rabbit anti-GFP antibody and a secondary Alexa-488 goat anti-rabbit antibody, and then with OilRedO. Cells were then analysed by confocal imaging, and the images revealed that Atg2 colocalises and surrounds lipid droplets (**Figure 5-11**).

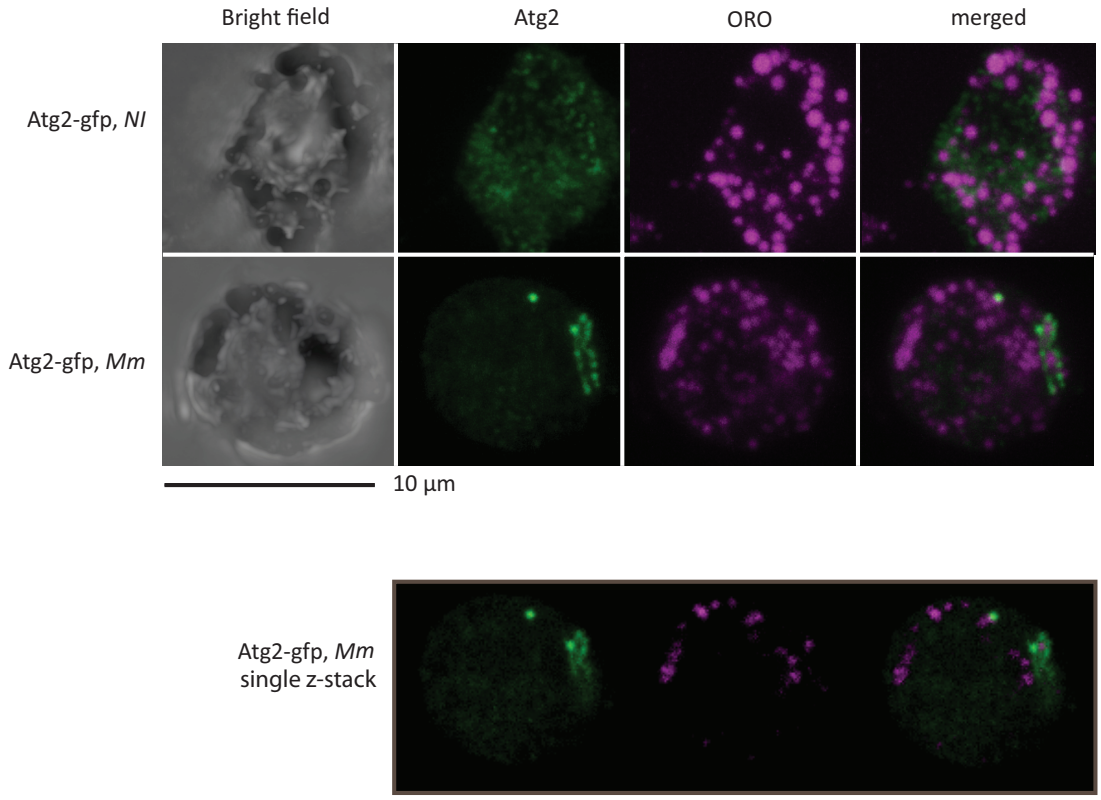

Figure 5-11: Atg2 associates with lipid droplets

Confocal images of cells overexpressing Atg2 revealed that upon infection, Atg2 proteins reorganise into larger punctae that surround or colocalise with lipid droplets (top) as showed in single slice images (bottom).

5.2.8 *Atg2* overexpression induces morphological changes in lipid droplets

Since *Atg2* colocalises with lipid droplets, the next step was to assess the effect of *Atg2* overexpression on lipid droplets formation at steady state and upon infection. A steady state and upon infection, a slight increase in lipid droplet formation is observed in *Atg2* overexpressing cells compared to controls (1.1 fold increase (**Figure 5-12** A & B).

Interestingly, upon infection, changes in lipid droplet morphology were strongly reduced in *Atg2* overexpressing cells (**Figure 5-12** A & C & D). Indeed, in control cells, the number of punctae is reduced upon infection while it stays constant in *Atg2* overexpressing cells. In addition, upon infection, the accumulation of large lipid droplets is reduced by 1.6 fold compared to controls indicating that cells overexpressing *Atg2* have less fused lipid droplets (**Figure 5-12** D). It is important to mention that in cells transfected with *pPAC-GFP-Atg2*, GFP fluorescence was barely detectable after fixation and ORO staining, therefore selection of successfully

transfected cells was not possible. As a consequence, the phenotype observed may be underestimated.

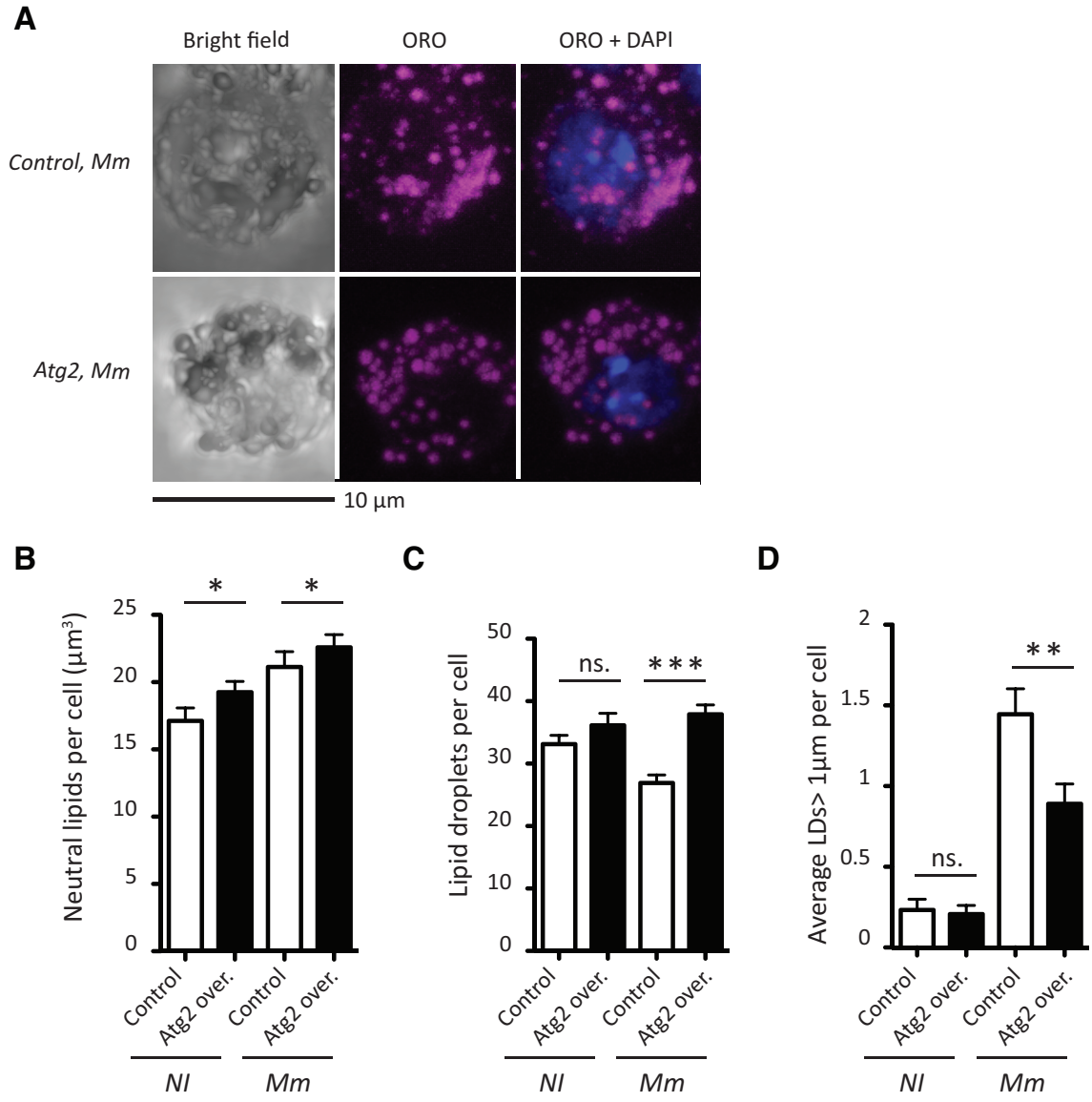

Figure 5-12: *Atg2* overexpression reduces morphological changes in lipid droplets upon infection

(A) Representative image of *M.marinum*-infected S2R$^+$ cells showing a lack of large lipid droplets in *Atg2* overexpressing cells. Cells were transfected either with *pPAC-HA* as control or with *pPAC-GFP-Atg2* to overexpress *Atg2* and then infected with *M.marinum* at MOI20. After 24 hours, cells were fixed, stained with FITC-conjugated *M.tuberculosis* antibody and then with OilRedO. (B) Cells overexpressing *Atg2* have only a very slight increase in lipid droplet formation compared to controls. (C) The number of lipid droplets per cell stays constant in cells overexpressing Atg2, while control cells have a decrease in lipid droplets upon infection. (D) Upon infection, control cells harbor large lipid droplets. This number is strongly reduced in *Atg2* overexpressing cells (1.6 fold decrease). For this figure, data were combined from 3 independent experiments. In total, for control cells: n=130 for non-infected cells and n=110 for *M.marinum*-infected cells. For *Atg2* overexpresssing cells: n= 107 for non-infected cells and n=100 for infected cells. p values were calculated using Mann Whitney (*p<0.05, **p<.01, ***p<0.001).

5.2.9 *upd3* overexpression does not induce changes in lipid droplet formation and morphology

To return to the role of *upd3* signalling, I analysed lipid droplets at steady state and upon infection in cells overexpressing *upd3* and compared them to control cells. As previously shown, cells overexpressing *upd3* have decreased *Atg2* expression levels, then the results were expected to be opposite to those obtained for cells overexpressing *Atg2* or similar to controls. Despite a slight increase in the number of lipid droplets upon infection (1.1 fold increase), cells overexpressing *upd3* had no change in lipid droplet formation and morphology (**Figure 5-13**).

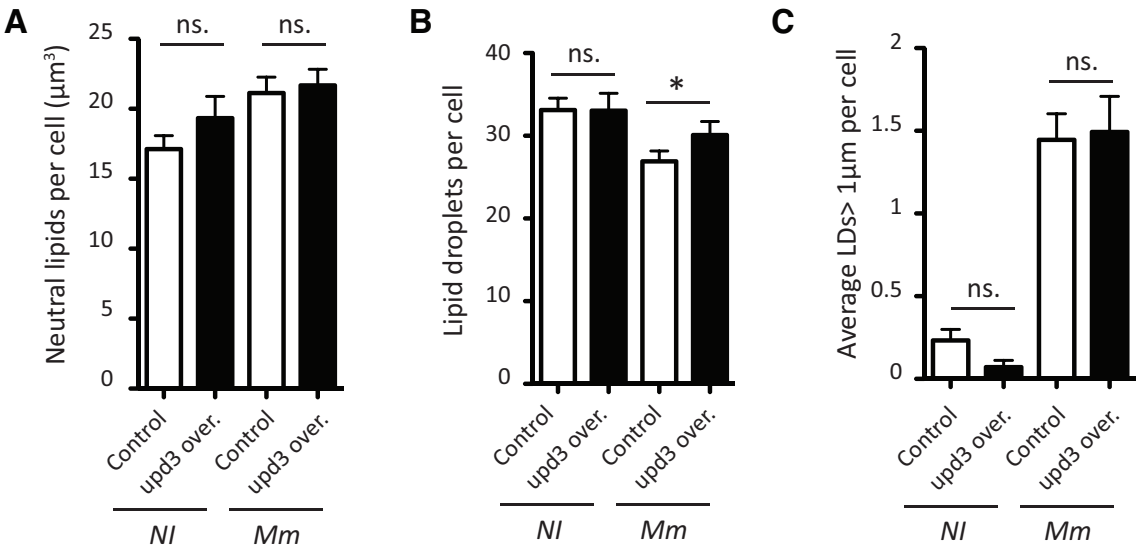

Figure 5-13: *upd3* overexpression does not change lipid droplet formation and morphology

(A) Cells overexpressing *upd3* do not have changes in lipid droplet formation compared to controls. Cells were transfected either with *pPAC-HA* as control or with *pPAC-upd3* to overexpress *upd3.* They were then infected with *M.marinum* at MOI20, and after 24 hours, cells were fixed and stained with ORO. (C) The number of lipid droplets per cell is unchanged in cells overexpressing *upd3* compared to controls. However, upon infection, a slight increase in the number of lipid droplets is observed in cells overexpressing *upd3* (1.1 fold increase). For *pPAC-HA* transfected cells, data were combined from 3 independent experiments and for *pPAC-upd3* transfected cells, data were combined from 2 independent experiments. In total, for control cells: n=130 for non-infected cells and n=110 for *M.marinum*-infected cells. For *upd3* overexpresssing cells: n=42 for non-infected cells and n=81 for infected cells. p values were calculated using Mann Whitney (*p<0.05).

5.3 Discussion

In this chapter I studied two potential Atg2-dependent mechanisms that can affect bacterial proliferation: autophagy and lipid metabolism. In mammals, IFNγ induces the formation of autophagosomes and the subsequent killing of *M.tuberculosis* (Harris et al. 2007). Besides, Th2 cytokines IL-4 and IL-13, or IL-6, could inhibit such mechanisms (Harris et al. 2007; Dutta et al. 2012). In *Drosophila*, there is no known analog to IFNγ, and only innate immune responses. Therefore, it is not surprising that autophagy levels stay constant at steady state and upon infection. I then verified the role of Atg2 in formation of autophagosome and did not observe changes in autophagic flux compared to controls and neither in the morphology of the autophagic punctae. In the contrary, overexpressing *upd3* did increase Atg8 punctae at steady state and upon infection compared to control. The number of large punctae also increased slightly therefore indicating a slight change in morphology. The results presented in Chapter 4, showed that *Atg2* overexpression reduces bacterial growth per cell while *upd3* increases it slightly. Since autophagy is unchanged when overexpressing *Atg2* and increased when overexpressing *upd3*, it cannot explain the observed changes in bacterial replication. These results suggest that other mechanisms are responsible for controlling bacterial growth.

I showed that *M.marinum* colocalises with and surrounds lipid droplets. Since I observed that Atg2 punctae relocalise towards the bacteria upon infection and since mammalian Atg2 induce changes in lipid droplets formation and morphology, I wondered whether Atg2 could control such mechanisms in the fly and whether it could affect bacterial replication (Velikkakath et al. 2012).

First, I demonstrated that similarly to *M.tuberculosis* infection in mammals, *M.marinum* infection induces a foamy phenotype in hemocyte-like cells ($S2R^{+}$) where cells accumulate neutral lipids (Peyron et al. 2008). Interestingly, the infection also induced morphologic changes in lipid droplets with a decrease in round-shape lipid droplets and a strong increase in large neutral lipid structures that may result from fusion events. I then showed that heat-killed *M.marinum*, trigger a huge increase in lipid droplet formation and morphology therefore demonstrating that, similarly to mammals, mycobacterial components induce changes in host lipid metabolism. Since infection with active *M.marinum* reduces such phenotype, it suggests

that bacteria are able to degrade host lipids probably to use them as source of nutrients and as energy storage. In mammals, *M.tuberculosis* entering the persistent phase accumulate intracellular lipid inclusions from host origin (Peyron et al. 2008; Daniel et al. 2004; Garton et al. 2002). Transmission Electron Microscopy (TEM) of *Drosophila* hemocyte-like cells revealed that *M.marinum* contains intracellular lipid inclusions. However, it remains to be determined if they are from host origins of if they were uptaken from the culture medium. Since *M.marinum* has the ability to accumulate lipids intracellularly, one could argue that changes in lipid droplet formation and morphology could also be a result of the bacteria's own intracellular lipids.. However, we do observe bacteria, which are free of lipid droplets suggesting that *M.marinum* did not contain intracellular lipid inclusions prior to entry into $S2R^+$ cells. Concerning morphological changes, infection with heat-killed bacteria strongly increased the number of large neutral lipid structures, therefore confirming that they result from fusion of host-lipids. Nevertheless, it would be useful to check whether OilRedO staining could enter and stain live bacteria. This analysis is ongoing. Finally, changes in neutral lipids are specific to some bacteria such as *M.marinum* as infection with *E.coli* did not induce any change in lipid droplets formation and morphology compared to the non-infected control.

Second, I assessed the role of Atg2 in lipid droplet formation and morphology and found that Atg2-dependent mechanisms may induce changes mainly in lipid droplet morphology, probably by reducing fusion events between lipid droplets. On the contrary, overexpressing *upd3* did not induce changes in neutral lipid content therefore suggesting that Atg2 functions may depend on a threshold of activation. Understanding the precise mechanisms that allow Atg2 to reduce fusion events would require further investigation.

Finally, a recent paper suggested that lipid droplets might also constitute a reservoir for histones, potent bactericidal molecules. Upon infection, histones are released from lipid droplets and contribute to bacterial killing in *Drosophila* embryos (Kolter 2012; Anand et al. 2012). In our model, both the nutrient deprivation theory and the lipid-droplet mediated killing can explain the lower bacterial replication in *Atg2* overexpressing cells. To distinguish between the two mechanisms, I will compare the expression levels of key genes involved in bacterial lipid metabolism in cells overexpressing *Atg2* compared to controls, and *in vivo* in flies with impaired JAK-STAT signalling compared to control. In addition, lipid droplets can be isolated and put into contact with bacteria to assess their role in bacterial growth. These studies are ongoing.

Chapter 6 Upd3 signalling regulates glucose homeostasis

6.1 Introduction

The previous chapters gave insights into bactericidal mechanisms that, when activated, could restore killing of mycobacteria. While increasing our knowledge in innate immunity, they do not address one key question: how do mycobacterial infections cause pathology?

Recent studies have identified several causes for fly death upon infection: anorexia, strong metabolic changes, excessive inflammation and tissue damage (Ayres & Schneider 2009; Dionne et al. 2006; Brandt et al. 2004; Chambers et al. 2012). Each pathogen drives distinct metabolic and immune responses in the host and as a consequence distinct pathologies. Dionne et al. were the first to examine the metabolic consequences of infection in *Drosophila* (Dionne et al. 2006). They used microarray analysis to identify metabolic factors involved in response to *M.marinum* infections. They show that *M.marinum* infection induces a progressive loss of metabolic stores such as glycogen and triglycerides, in association with hyperglycaemia. This effect likely results from a decrease in systemic Akt activation, which activates FOXO and Gsk-3, two transcription factors causing loss of energy stores. Dionne et al. excluded insulin resistance in this model and hypothesized that the systemic loss of Akt resulted either in low levels of circulating insulin, or from inactivation of Akt itself.

Interestingly, mutation of *FoxO* increased survival of flies infected with *M.marinum* without altering bacterial growth. FoxO mutants exhibit less wasting than control flies when infected with *M. marinum* suggesting that the insulin pathway is a key mediator of the metabolic changes induced upon *M.marinum* infection, and that, in wild-type flies, death is likely due to inadequate immune and metabolic host responses.

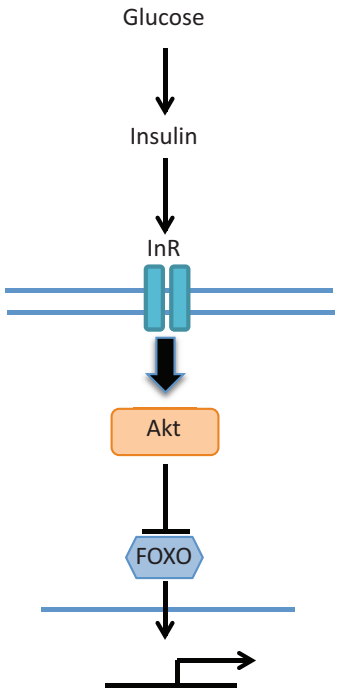

Figure 6-1: Metabolic Akt signalling in *Drosophila*

Elevated glucose levels activate the insulin pathway through binding of Insulin-like peptides to the Insulin-like Receptor (InR). This induces Akt phosphorylation. p-Akt then prevents FOXO from going to the nucleus to activate transcription of metabolic genes. As a consequence, activation of the insulin pathway prevents degradation of energy stores.

In mammals, cytokines have long been associated with changes in glucose and fat metabolism during critical illness (Souba 1994). However the precise contribution and mechanism of action of the different cytokines is unknown.

Recently, Rajan et al. demonstrated that the *Drosophila* cytokine Upd2, which shares similarities with type I cytokines, regulates physiological homeostasis by remotely controlling insulin secretion (Rajan & Perrimon 2012). They showed that Upd2 is expressed in response to fat and sugar sensing to control systemic growth and triglyceride levels. In the fed state, *upd2* is secreted by adipocytes and activates JAK-STAT signalling in a population of GABAergic neurons and as a consequence, insulin-producing cells release insulin-like peptides to activate insulin signalling in target cells. Interestingly, *upd2* was identified as an analogue of Leptin since human Leptin can rescue the *upd2* mutant phenotype.

Another study, identified a hemocyte-dependent insulin-signalling repression after localised DNA damage, suggesting that hemocytes and their associated secreted factors can modulate insulin signalling upon DNA-damage (Karpac et al. 2011).

All together, these studies point towards a systemic regulation of insulin signalling by cytokines secreted from the fat body or from hemocytes, and led us to investigate the role of cytokine signalling in the wasting disease induced by *M.marinum* infection. This study is preliminary and focuses on the role of *upd3* in the control of metabolism upon *M.marinum* infection.

The results show that *os*^{s} mutants, hypomorphic *upd3* mutants, have a strong accumulation of glucose and glycogen at steady state while fat levels are unchanged. As a consequence, upon infection these levels stay high and, before death, *os*^{s} mutant have similar glycogen levels as non-infected controls. Interestingly, upon infection, Akt activation is maintained in this flies while decreased in controls, possibly due to the high glucose content or to the lower bacterial growth observed in *upd3* mutants. Finally, while mutation of *upd3* is beneficial to limit bacterial growth and to increase host survival upon infection, *os*^{s} flies have a reduced lifespan probably as a result of osmotic and metabolic changes.

6.2 Results

6.2.1 Upd3 blockade strongly upregulates glucose and glycogen but not triglyceride levels

To assess whether upd3 has an effect on metabolic stores, I quantified glucose, glycogen and triglyceride levels. Glucose levels were measured directly with a glucose oxidase reagent, while glycogen content was measured after amyloglucosidase treatment to liberate glucose units. As a consequence, glycogen levels were measured as µg of glucose per fly. Triglyceride content was measured indirectly as µg of glycerol per fly using the McGowan method (McGowan et al. 1983).

I observed that *os*^{s} flies have a strong increase in glucose and glycogen levels at steady state compared to controls (**Figure 6-2** A & B). However, the levels of triglycerides are unchanged (**Figure 6-2** C).

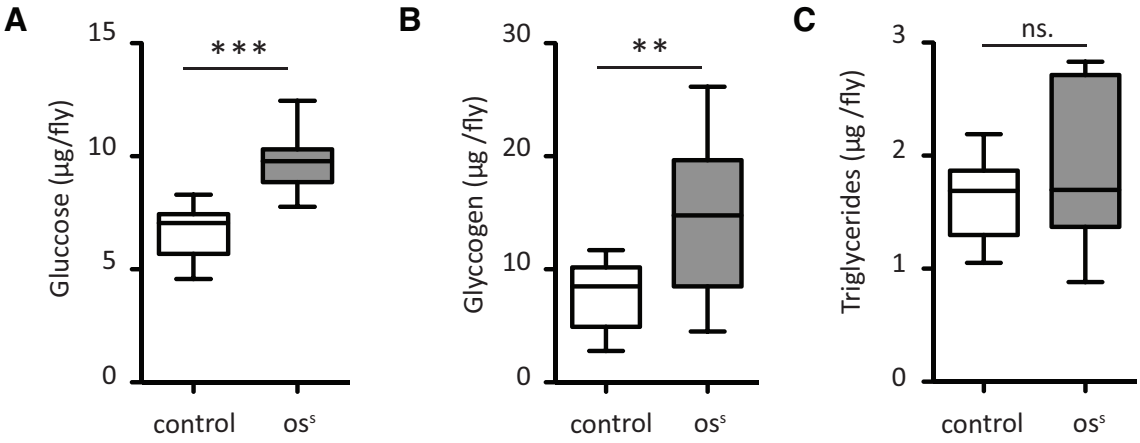

Figure 6-2: os^{s} flies have higher glucose and glycogen levels

(A) os^{s} flies have higher glucose levels. The glucose content of five to seven day old flies was measured by spectrophotometry with a liquid glucose oxidase reagent. (B) To measure glycogen content, the glucose reagent was supplemented with amyloglucosidase. The amount of glycogen is extrapolated from the total amount of glucose minus free glucose, and is expressed in µg of glucose per fly. The results indicate that *os*^{s} flies have higher glycogen content compared to controls. (C) *os*^{s} and control flies have similar triglyceride levels at steady state. Triglyceride content was measured using the McGowan method (McGowan et al. 1983). For panels A, B and C, n=13 for wild-type flies and n=16 for os^{s} flies. p values were calculated using Mann Whitney (**p<0.01, ***p<0.001).

Upon infection with *M.marinum*, flies progressively lose their glycogen and triglyceride levels and are hyperglycaemic (Dionne et al. 2006). In os^s flies glucose levels stay high and further increase in late infection (**Figure 6-3** A). Their glycogen levels decrease but remain high compared to controls, and os^s flies die with the same glycogen content as uninfected control (**Figure 6-3** B).

These experiments are preliminary and for a more relevant quantification, it would be necessary to normalise glucose, glycogen and fat levels to the total protein content. Indeed, by measuring fly weight, I observed that os^s flies are slightly heavier than controls, however, due to the low number of samples, it is not significant (**Figure 6-3**C).

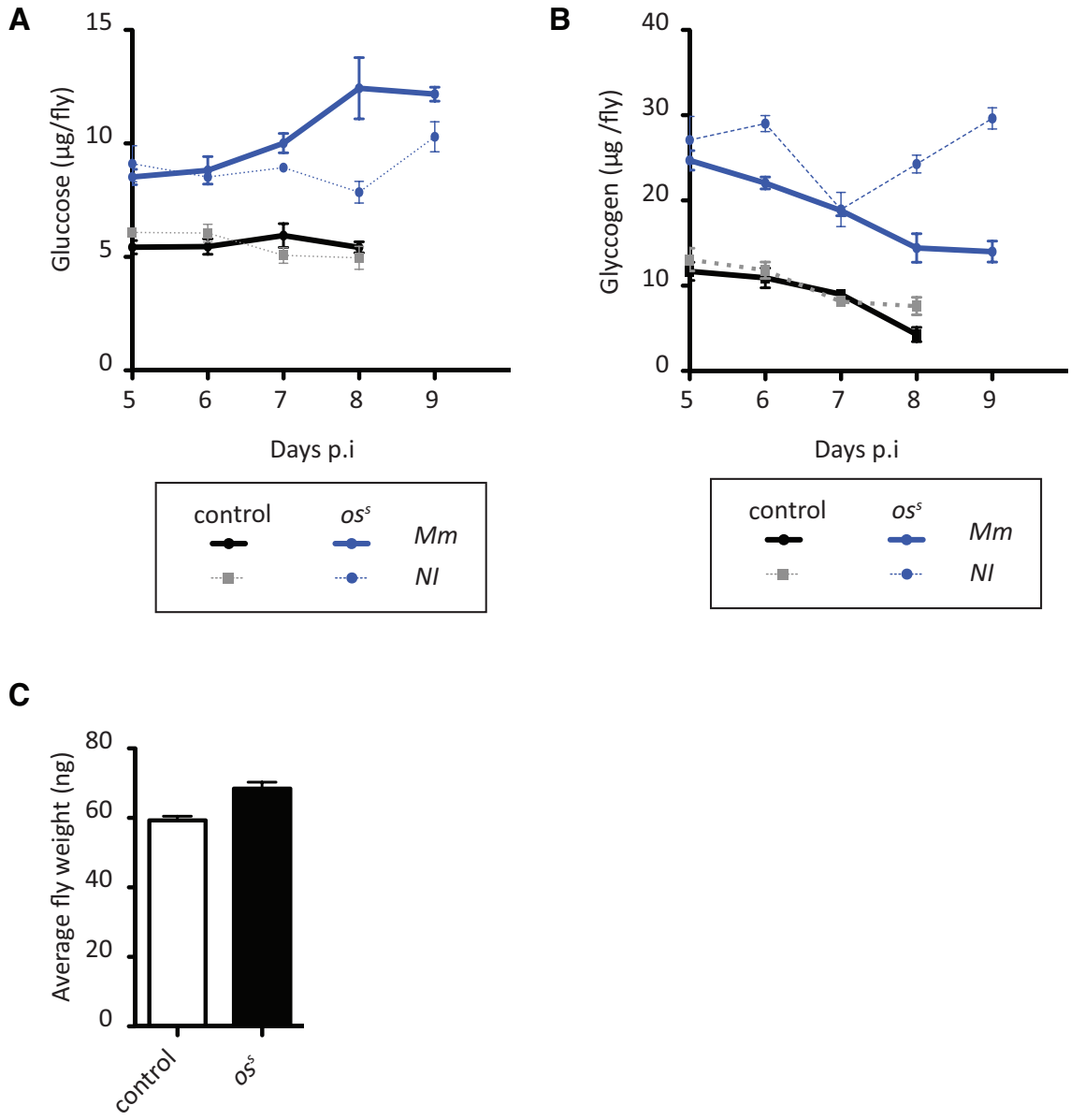

Figure 6-3: Glucose and Glycogen levels stay high upon infection in os^s flies

(A) Upon infection with *M.marinum*, glucose levels stay high in *os*^{s} flies compared to controls. A strong increase in glucose content is observed in *os*^{s} flies from day 7 post-infection, while control flies have only a slight increase. For (A) and (B), 5 to 7 days old flieswere injected with either PBS-tween80 or *M.marinum* (500CFUs). Samples were collected from day 5 o.i. for quantification of glucose and glycogen levels. n=6 per genotype, condition and timepoint. (B) Similarly to control flies, glycogen content progressively decreases upon *M.marinum* infection. However, just before death, *os*^{s} flies have similar levels of glycogen as PBS-injected controls. (C) *os*^{s} flies have a slight increase in weight compared to controls. For this experiment, 100 age-matched flies were used per measurement: n=3 for controls and n=4 for os^s flies. For panel A and B, two-way ANOVA between *os*^{s} curves (infected or not-infected) and related controls, indicate that the differences between the two genotypes are significant ($p < 0.0001$).

Interestingly, when wild-type flies are fed sugar-free food, they maintain their glucose content by degrading their glycogen stores, while *os*^{s} flies seem unaffected (**Figure 6-4** A & B). It suggests that changes in food intake are not the cause for the excess of glucose and glycogen observed in *os*^{s} flies. In addition, feeding assays using the blue dye method did not indicate any change in feeding (data not shown). However, this method to evaluate feeding has been proven to be inexact (Ja et al. 2009; Wong et al. 2009). As consequence, the capillary method is preferred and experiments are ongoing.

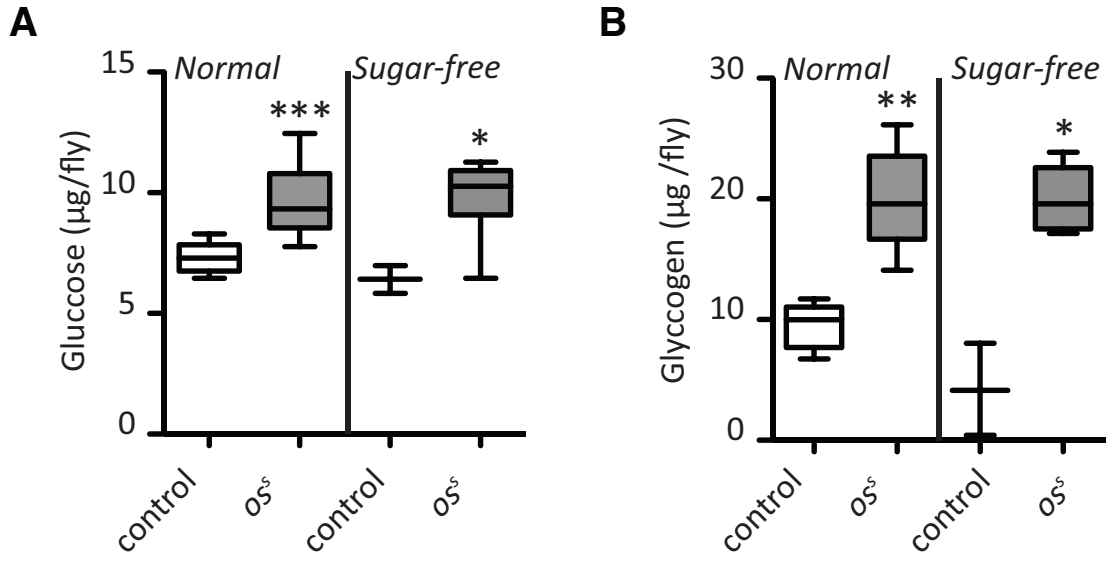

Figure 6-4: *os*^{s} flies conserve high glucose and glycogen content when fed a sugar-free food

(A) *os*^{s} and control flies maintain constant glucose levels when fed sugar-free food for a week. (B) On the contrary, glycogen levels are strongly decreased in wild-type flies fed a sugar-free food, while they are maintained for *os*^{s} flies. For panel A and B, after emergence, adult flies were put for 7 days in the different foods. For control flies, n=5 for normal food and n=3 for sugar-free food. For *os*^{s} flies, n=8 for normal food, and n=7 for sugar-free food. p values were calculated using Mann-Whitney test (*p<0.05, **p<0.01, ***p<0.001).

6.2.2 Upd3 blockade maintains insulin signalling upon *M.marinum* infection

It was previously shown that insulin signalling is altered in infected flies (Dionne et al. 2006). Upon infection, Akt activation is progressively reduced and likely contributes to the wasting disease (**Figure 6-5**).

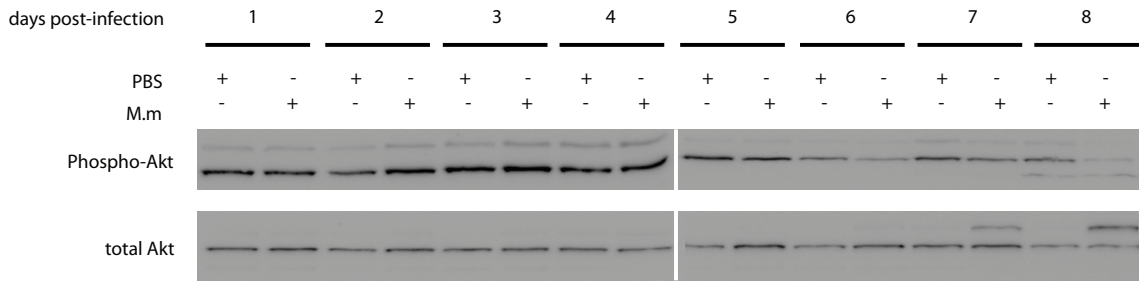

Figure 6-5: Akt activation is progressively reduced upon infection with *M.marinum*

From day 5 post-injection and onwards, phospho-Akt levels are reduced in infected flies compared to controls. Also, a new isoform of total Akt appears from day 7 post-infection, indicating changes in the insulin pathway. For this experiment, 5 to 7 days old males were either injected with PBS-tween80 or *M.marinum* (500CFUs) and samples were collected every day post-injection. This western blot is a representative image from 3 independent experiments.

Interestingly, in os^s mutants, Akt activation is maintained possibly as a result of less bacterial growth or enhanced glucose levels (**Figure 6-6** A & B & C). When Akt is phosphorylated, it prevents FOXO from going to the nucleus, but when Akt levels are reduced, FOXO can activate transcription of its target genes, which results in loss of energy stores. To verify that FOXO activity was reduced in os^s flies, I quantified the expression of the insulin-like receptor gene (*InR*), a FOXO target, and found that its transcription was reduced (**Figure 6-6** D). .

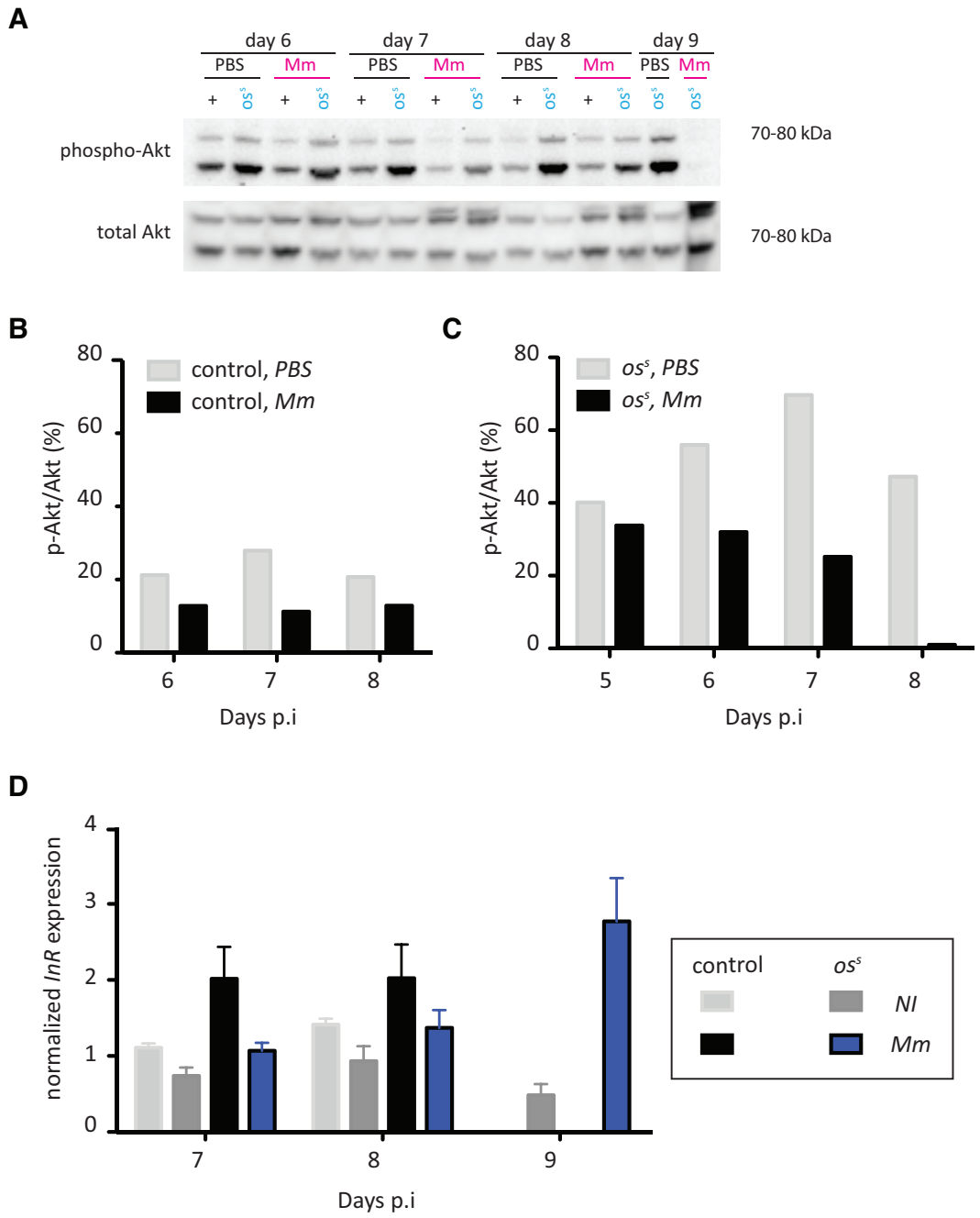

Figure 6-6: Upon infection, activation of the insulin pathway is reduced in control flies, while maintained in *os*^{s} flies

(A) Phospho-Akt levels are decreased in *M.marinum*-infected flies compared to PBS-injected controls. Despite a similar decrease in phospho-Akt, *os*^{s} flies have higher basal phospho-Akt levels indicating higher insulin pathway activation. The quantification of this western blot is shown in B and C, where phospho-Akt levels are represented as a percentage of total Akt levels (D) Whether infected or PBS-injected, *os*^{s} have lower expression of the *Insulin-like Receptor (InR)*, a target of FOXO, compared to controls. For this experiment, 5 to 7 days old males were injected with M.marinum (500CFUs) and samples were collected from day 7 to 9 post-infection. Wild-type flies were already dead at day 9 p.i. n=3 per timepoint and per genotype.

Since Upd2 indirectly regulates Ilp2 levels, I wondered whether it was also the case for Upd3. I found that, upon infection, Ilp2 expression levels were higher in os^s flies compared to controls, which could explain the changes in insulin pathway activation (**Figure 6-7**).

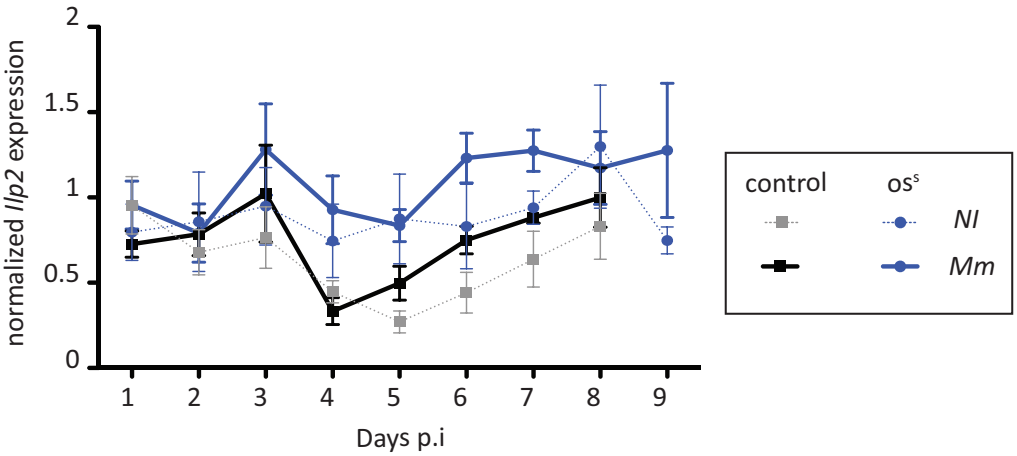

Figure 6-7: Ilp2 levels are increased in *os*^{s} flies compared to controls

At steady state, *Ilp2* levels are increased in *os*^{s} flies compared to controls (two-way ANOVA, $p<0.01$). Upon infection, Ilp2 levels are increased from day5 onwards in control flies (two-way ANOVA from day 5, $p<0.05$). In *os*^{s} flies levels of *Ilp2* upon infection are similar to steady state, and higher than infected controls (two-way ANOVA, $p<0.001$). For this experiment, 5 to 7 days old flies were injected with 500 CFUs of *M.marinum* and collected for qPCR analysis from day 1 to 9 post-injection. This graph is a combination of two independent experiments. n=6 per timepoint and per genotype.

6.2.3 *upd3* mutant flies have a reduced lifespan

In Chapter 3, I showed that *os*^{s} mutant survive longer upon *M.marinum* infection and have less bacteria. One hypothesis is that flies die later due to less tissue damage as they contain less bacteria. However, since *os*^{s} flies have an altered glucose and glycogen homeostasis, and since glucose levels are further increased after infection, it suggests that metabolic changes or even osmotic shock in these flies could cause their death. To verify whether prolonged glucose and glycogen levels are sustainable for flies, I did a lifespan assay of *os*^{s} flies compared to controls (**Figure 6-8**). The results indicate that *os*^{s} flies die earlier in the absence of induced infection.

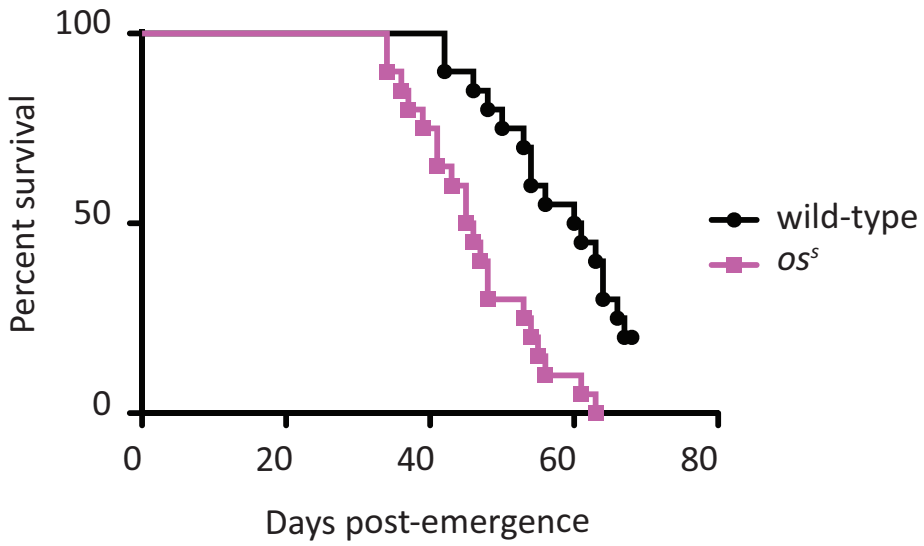

Figure 6-8: *os*^{s} flies have a reduced lifespan

Representative survival curve out of 3 independent experiments showing a reduced lifespan in *os*^{s} mutants compared to controls. For this experiment 20 flies were used per genotype and vials were changed every 3 to 4 days. The survival curves are statistically significant: Log-rank test (Mantel-Cox), $p<0.0001$.

6.3 Discussion

In this chapter, I showed that *os*^{s} mutants, hypomorphic mutants for *upd3*, have a strong accumulation of glucose and glycogen at steady state but not of triglycerides, suggesting that the phenotype cannot simply be a consequence of more feeding. To verify these results, I tested the feeding rate and the amount of food eaten by *os*^{s} flies compared to controls without detecting any difference. However, the blue food assay is highly criticised and it would be useful to verify these results using the capillary assay in which the precise volume of liquid food consumed over a period of time can be measured.

M.marinum infection induces a wasting disease with loss of fat and glycogen associated with hyperglycemia, which is likely to be the consequence of a decrease in insulin signalling. Interestingly, *os*^{s} flies have a reduction in glycogen content upon infection but these levels stay high, when the levels in controls diminish. On the contrary, glucose levels highly increase in late infection compared to controls. Consequently, the cause of death in wild-type flies or in *os*^{s} flies may well be different. While, in late infection, wild-type flies display intense tissue damage and a wasting disease that can result in death, os^{s} flies have less bacterial growth_and therefore probably less tissue damage, in addition they exhibit less wasting but a strongly enhanced hyperglycemia which may result in osmotic shock.

Possibly as a consequence of excessive glucose content, insulin signalling is maintained upon infection in *os*^{s} flies while being decreased in controls. Indeed, *Ilp2* , and Akt activation are all enhanced in *os*^{s} flies. However, constant insulin activation and high glucose content may explain why *os*^{s} flies have a reduced lifespan. Thus, what may be beneficial upon infection may be detrimental in the long term.

The results presented in this chapter give rise to more question than answers. Why are glucose and glycogen levels enhanced in *os*^{s} flies? Is there an enhanced gluconeogenesis? Glycogenesis or glycogenolysis? Glycolysis? In *os*^{s} flies, glycogen is elevated and degraded upon infection, likely excluding effects on glycogenesis or glycogenolysis. Therefore, why would gluconeogenesis or glycolysis be altered? In their paper, Rajan and Perrimon demonstrated that another Upd-family cytokine, Upd2, responds to the fed state and stimulate insulin signalling. While in their paper, Upd2 regulates mainly fat content and subsequently fly growth; it suggests

that another mechanisms could control glucose and glycogen levels. For this reason, one can hypothesize that Upd3 control glucose levels by regulating gluconeogenesis, glycolysis and insulin signalling accordingly. This would require further investigation.

Chapter 7 General conclusion

In this thesis, I present complex host and bacterial mechanisms that ultimately promote bacterial replication and pathology. The combination of in vivo and in vitro analysis, allowed us to answer, at least partly, the following question: why is cytokine signalling detrimental upon mycobacterial infection? Since the results have been discussed at the end of each result chapter, I present here things from a different perspective, enunciating the succession of events that leads to bacterial growth and pathology, and making general hypotheses on host defence and bacterial virulence mechanisms.

7.1 What are the characteristics of *M.marinum* infection in *Drosophila*?

M.marinum is a facultative intracellular bacterium, that primarily infects hemocytes when injected into the fly hemocoele (Dionne et al. 2003). Hemocytes have functional similarities with mammalian leukocytes, and as such, likely constitute a major proliferation site for mycobacteria (Tirouvanziam et al. 2004). When entering macrophages, *M.marinum* encounters host defense mechanisms in the form of phagocyte-associated toxicity. Similarly to *M.tuberculosis* in mammals, *M.marinum* inhibits phago-lysosomal fusion therefore preventing acidification and activation of bactericidal mechanisms (Dionne et al. 2003). Then *M.marinum* has two choices: to adapt to the phagosomal environment that may still be toxic, or to escape the phagosome and access the cytosol. Recent studies demonstrated that *M.marinum* uses the second strategy in mammals and in *Drosophila* S2 cells through an ESX-1-dependent mechanism (Koo et al. 2008; Stamm et al. 2003). After reaching the cytosol, bacteria acquire actin-tail motility probably to spread to adjacent cells (Koo et al. 2008).

To escape selective autophagy in the cytosol, *M.marinum* sheds its ubiquitinated cell wall and then polymerises actin to acquire motility and escape lysosomal degradation in macrophages (Collins et al. 2009). Losing cell wall components may force *M.marinum* to search

for host polysaccharides and lipid stores for its regeneration. Indeed, literature on *M.tuberculosis* infection in mammals has demonstrated that mycobacteria are able to use host triacylglycerol and specifically host fatty acids as source of carbon and lipids (Garton et al. 2002; Daniel et al. 2004; McKinney et al. 2000). In *M.marinum*-infected Drosophila cells, we do not know if this happens.

In the hemocyte environment *M.marinum* proliferates and spreads to adjacent cells. Around six days after infection, however, hemocytes die, possibly as a consequence of bacterial overload or bacterial toxins (Chapter 3). From this time onwards, bacteria are seen proliferating in the extracellular space and damaging tissues such as the fat body (Dionne et al. 2003). Probably as an answer to the extracellular presence of *M.marinum*, fat body cells and also probably other tissues secrete antimicrobial peptides and complement-like proteins into the hemolymph in a desperate attempt to control the bacterial load (Chapter 3). However, possibly as a consequence to tissue damage, excessive inflammation and wasting disease with loss of fat and glycogen, the fly dies after 8 to 9 days of infection (Dionne et al. 2006).

The specific features of *M.marinum* infection are summarised in **Figure 7-1**.

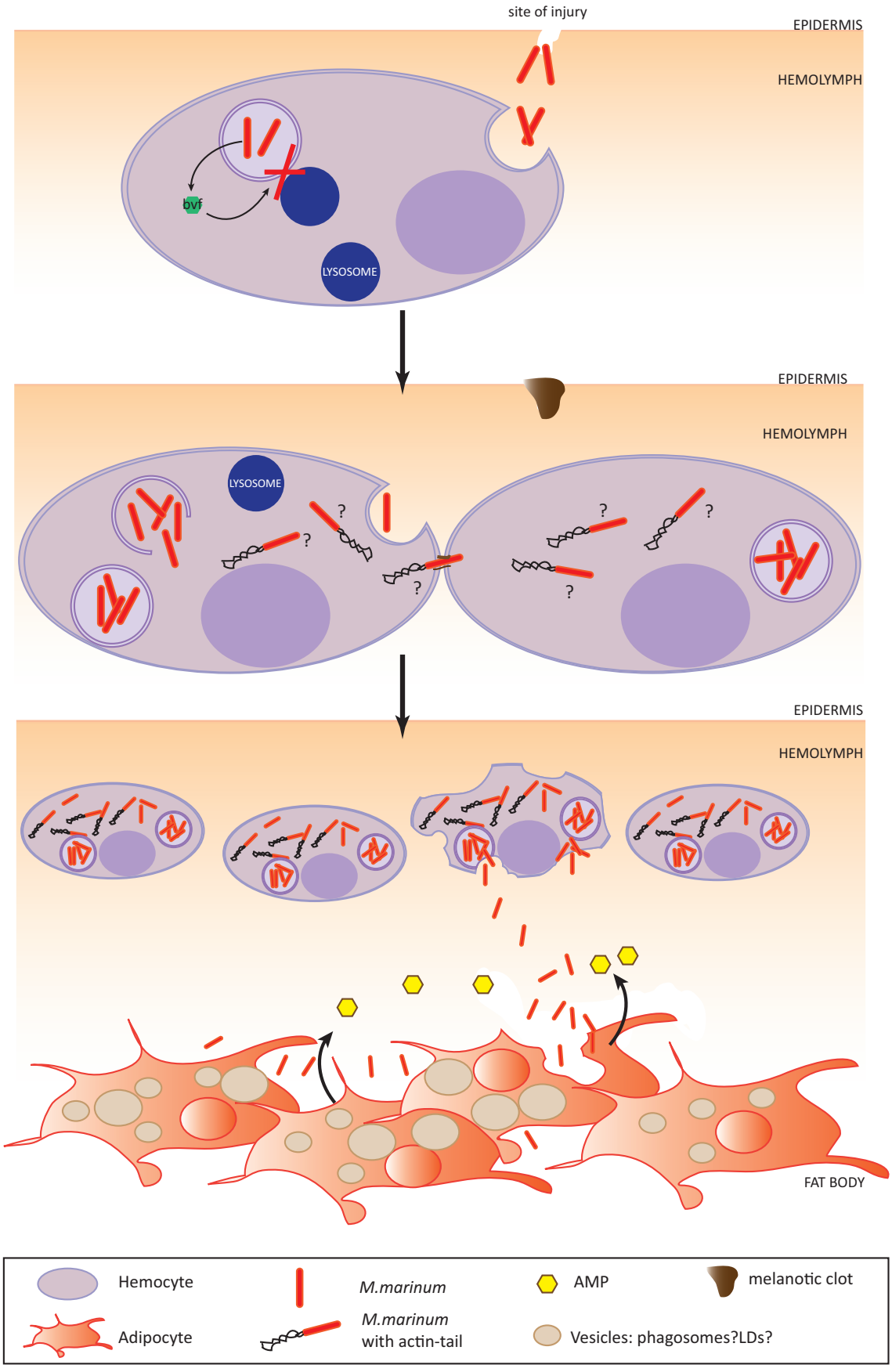
site of injury
EPIDERMIS
HEMOLYMPH
bvf
LYSOSOME
EPIDERMIS
HEMOLYMPH
LYSOSOME
?
?
?
?
?
?
EPIDERMIS
HEMOLYMPH
FAT BODY
Hemocyte
Adipocyte
M.marinum
M.marinum
with actin-tail
AMP
Vesicles: phagosomes?LDs?
melanotic clot

Figure 7-1: The course of *M.marinum* infection in *Drosophila*

Upon injection of *M.marinum* in the *Drosophila* hemolymph, bacteria are phagocytosed by the sessile and tissue-linked hemocytes. Similarly to *M.tuberculosis* infection in mammals, vacuolar acidification is inhibited through the action of an unknown bacterial virulence factor. While the clot is forming at the injury site, the bacteria proliferate inside phagosome and in the cytosol after phagosomal escape. Cytosolic bacteria acquire an actin-tail that render them motile and allow cell-to-cell spreading. As a consequence to bacterial overload and/or bacterial toxins, hemocytes start to die, probably by necrosis. Bacteria are then released into the hemolymph where they can infect other hemocytes or other cell types. In late infection, around day 5 post-injection, tissue damage is observed, especially in the fat body that contains many abcesses filled with *M.marinum*. At this stage, fat body cells appear abnormal with an accumulation of large vacuoles.

7.2 A complex interplay between bacterial evasion mechanisms and host defence

M.marinum infection triggers several immune responses in and from hemocytes. The focus of this thesis is on the function of induced cytokine expression, specifically of Upd3, an IL-6 analog, which in returns activates JAK-STAT signalling in hemocytes (Chapter 4). While this signalling pathway should be beneficial for the host, JAK-STAT signalling appears detrimental for it in the context of *M.marinum* infection in *Drosophila* (Chapter 3 & 4 and (Dostert et al. 2005). Indeed, when Upd3 secretion from hemocytes is prevented or when JAK-STAT signalling is inhibited in hemocytes, bacterial growth is slower in these cells and in the whole organism, hemocytes death is reduced, and the host survive longer (Chapter 3 & 4).

The main question is then: why would a host immune response be detrimental?

Several scenarios may explain this phenotype:

(1) *M.marinum* inhibits JAK-STAT signalling downstream of Upd3;

(2) *M.marinum* virulence factors inhibit the processes activated by JAK-STAT signalling;

(3) *M.marinum* subverts the mechanisms or signals activated by JAK-STAT signalling at its own advantage.

Since I showed that JAK-STAT signalling downregulates indirectly *Atg2* expression in macrophage-like cells, I decided to focus on the mechanisms requiring this molecule for their full function (Chapter 4 & 5). Following that path, I found in the literature that mammalian Atg2

proteins are required for autophagosome formation and for the regulation of the size and morphology of lipid droplets (Velikkakath et al. 2012). Indeed, silencing of *Atg2* causes appearance of unsealed autophagosomes and aggregation of enlarged lipid droplets.

Based on this, the first questions to answer were: Is autophagy reduced upon Upd3 signalling? If yes, is this effect maintained upon infection? Why would a cell inhibit a bactericidal mechanism when infected?

Surprisingly, autophagy is not induced by infection in $S2R^{+}$ cells and since *upd3* is upregulated upon infection, it indicates that either Upd3 signalling does not have an effect on autophagy, either the bacteria or other host mechanisms inhibit this effect (Chapter 4 & 5). Interestingly, while autophagy is not induced, Atg8 punctae are enlarged upon infection and colocalise with bacteria suggesting that it may contribute to bacterial killing (Chapter 5). When Upd3 signalling is activated, it downregulates *Atg2* and potentially inhibits autophagy. If this hypothesis is correct, overexpressing *upd3* should reduce autophagy, and, on the contrary, overexpressing *Atg2* should increase autophagy. However, overexpressing *Atg2* does not have an effect on Atg8 punctae, and overexpressing *upd3* increases Atg8 punctae (Chapter 5). This former result, while surprising, may result from accumulation of unclosed and non-functional autophagosomes. Further investigation would be required to verify the functionality of autophagosomes in cells overexpressing *upd3* and *atg2*.

Based on the in vivo and in vitro data, when Upd3 signalling is prevented, *Atg2* is upregulated bacterial proliferation is reduced and flies survive longer (Chapter 3 & 4). Since overexpressing Atg2 reduced bacterial load per cell but did not induce autophagy, it suggests that Atg2 controls bacterial replication in a mechanism independent from autophagy.

Now, based on these results and on the role of mammalian Atg2 proteins the following questions arose: Do lipid droplets have an important role in the infection with *M.marinum*? Does Atg2 control lipid droplet formation and morphology in *Drosophila* cells? Can Atg2 control bacterial replication through modulation of lipid droplets?

Similarly to *M.tuberculosis* infection in mammals, *M.marinum* induces a foamy phenotype in hemocytes with accumulation of neutral lipids (Chapter 5). A specific feature of this phenotype is the apparition of fused lipid droplets that form large irregular structures. Bacterial components alone from heat-killed *M.marinum* are able to trigger a massive change in

lipid droplet formation and morphology that is significantly higher than the effect triggered by live bacteria (Chapter 5). These results suggest that accumulation of lipid droplets in *Drosophila* hemocytes is *M.marinum*-specific, especially since we show that it does not occur upon infection with other bacteria such as *E.coli* (Chapter 5). Since the foamy phenotype upon infection with live *M.marinum* is reduced compared to infection with heat-killed bacteria, it also suggests that *M.marinum*, similarly to *M.tuberculosis*, consume lipid droplets and use them as source of nutrients (Chapter 5, (Peyron et al. 2008)).

What is the role of Atg2 in this phenotype? Our results indicate that Atg2 controls the fusion of lipid droplets and the apparition and accumulation of enlarged irregular lipid structures. As a consequence, when Upd3 signalling is activated, *Atg2* expression is reduced and enlarged structures are allowed to form, to the benefit of the bacteria which can accumulate intracytoplasmic lipid inclusions. On the contrary, when *Atg2* is overexpressed, lipid droplets fusion is prevented, which may limit bacterial access to nutrients and concomitantly its growth.

The specific features of host defence and bacterial virulence are summarised in **Figure 7-2**.

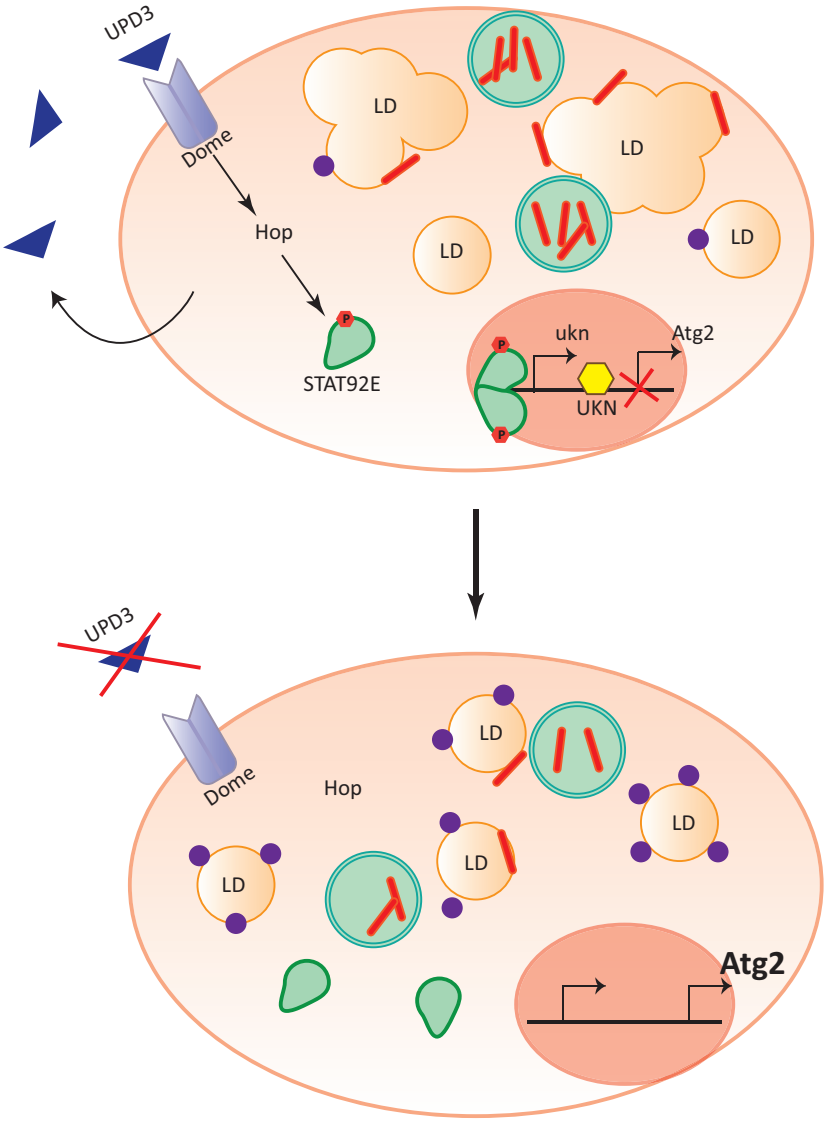

Figure 7-2: Model for the role of Upd3 signalling upon infection with *M.marinum*

Infection with *M.marinum* induces a foamy phenotype in hemocytes, in which an accumulation and a change in lipid droplet morphology is observed (top). The rational for the bacteria-induced fusion of lipid droplets is unknown, however, Upd3 signalling has been associated with the control of this phenotype. When Upd3 signalling is activated, STAT92E proteins are phosphorylated and form dimers to activate the transcription of several target genes. Among them, an unknown (ukn) transcription factor is likely responsible for the downregulation of *Atg2*. In infected cells with activated JAK-STAT signalling, some lipid droplets fusion and form enlarged neutral lipid structures. When Upd3 signalling is inhibited in hemocytes by RNAi of *upd3* or *Stat92E*, *Atg2* expression is increased and correlates with a decrease in the fusion of lipid droplets and with a lower bacterial load per cell. Since Atg2 associate and surround lipid droplets, (purple discs) it suggests that Atg2-dependent mechanisms control the morphology of lipid droplets upon infection.

7.3 Why is Upd3 signalling detrimental for the host?

Our data suggest that Upd3 signalling maintains *Atg2* levels below some threshold level. When Upd3 signalling is prevented, *Atg2* levels strongly increase and when *upd3* is overexpressed, *Atg2* expression is reduced, therefore suggesting that another pathway activates *Atg2* and that Upd3 signalling represses it. As a consequence, upon infection, Upd3 signalling maintains the quantity of lipid droplets and allows their fusion. Why maintain lipid stores upon infection?

The recent literature gives some insight into the function of lipid droplets in immunity and host-pathogen interactions. Upon infection, maintaining lipid droplet content may be beneficial to the host defence mechanisms for several reasons (**Figure 7-3**):

(1) Lipid droplets are a platform for protein-binding, especially of immune-related proteins such as the Immunity-Related GTPases (IRGs), whose binding to LD is mediated by IFN-γ in mice (Bougnères et al. 2009; Saka & Valdivia 2012);
(2) Lipid droplets naturally contain histones that can be released upon bacterial challenge to directly kill pathogens (Anand et al. 2012; Kolter 2012);
(3) Lipid droplets are a centre for eicosanoid metabolism that regulates plasma membrane integrity and inflammation (Chen et al. 2008; Divangahi et al. 2010);
(4) Lipid droplets maintain lipid homeostasis and protect from lipotoxicity through storage of fatty acids in the form of neutral TAG, DAG, ceramids and Acetyl-CoA (Saka & Valdivia 2012; Listenberger et al. 2003);
(5) Lipid droplets limit oxidative stress through the action of the LD-bound metalloprotease, Invadolysin, on mitochondrial integrity (Di Cara et al. 2013);

According to these publications, it is in the host interest to maintain lipid droplets upon infection to limit oxidative stress and lipotoxicity, to promote inflammation, and to induce immune responses (**Figure 7-3**). However, this process is subverted by *M.marinum*, which stimulates abnormal fusion of lipid droplets. Enlarged lipid droplets can be the result of a host response to stimulate bactericidal mechanism that is then subverted by the bacteria, or can be stimulated by bacterial factors to inactivate the immune functions of lipid droplets, to perturb immune cell homeostasis, or to use lipid droplets as nutrient sources (**Figure 7-3**). As a

consequence, Upd3 signalling is detrimental upon infection because of a specific interaction of host and pathogen biology. Indeed, Upd3 stimulates processes that are subverted by the bacteria for their growth. When Upd3 signalling is prevented, lipid droplets maintain a round morphology and bacterial replication is reduced (Chapter 5).

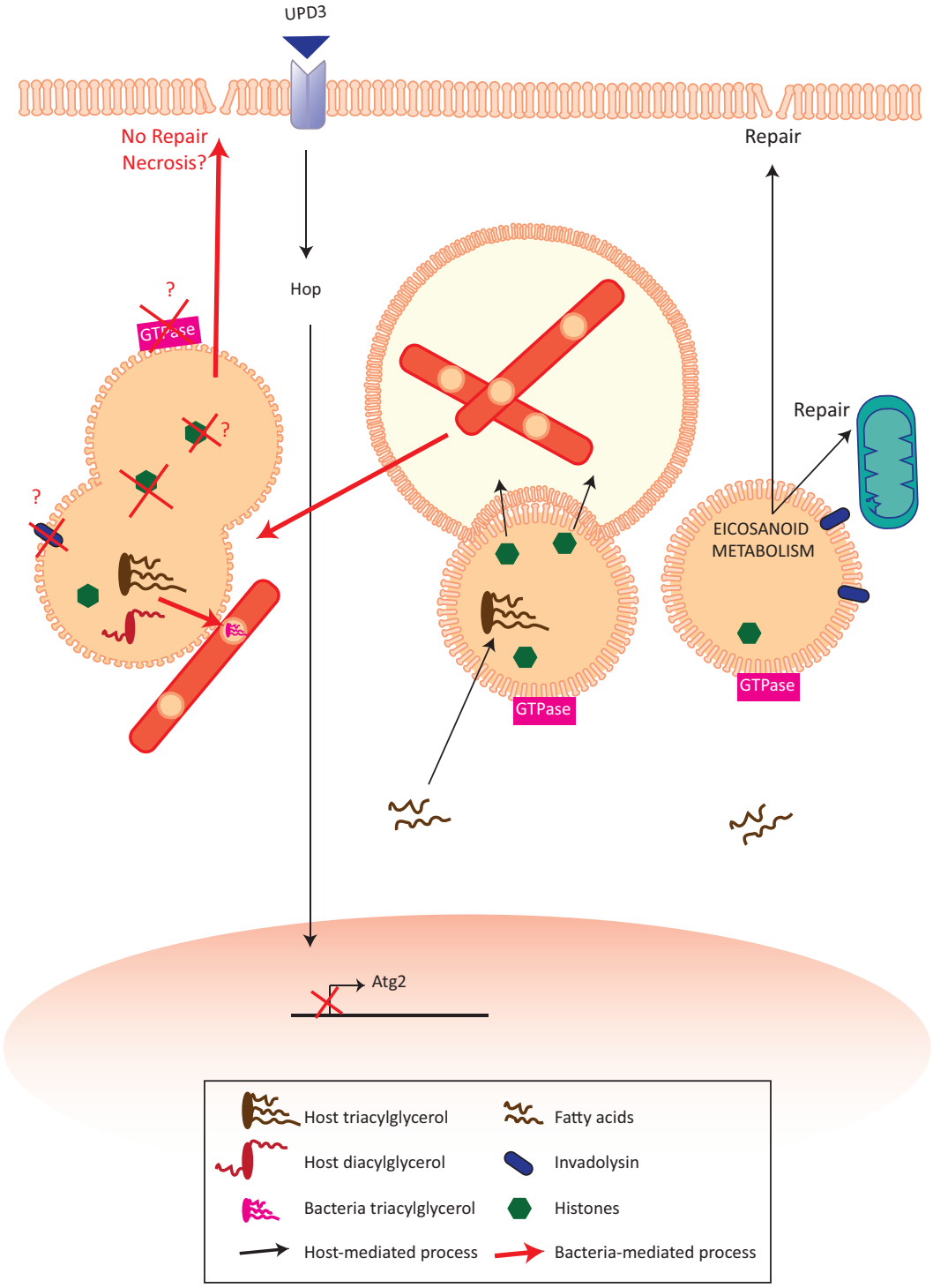

Figure 7-3: Upd3 signalling maintains lipid droplet homeostasis

Upd3 signalling maintains lipid droplets homeostasis and allows fusion events. Lipid droplets homeostasis is important for several processes that can mediate host fitness upon infection. Lipid droplets constitute a centre for eicosanoid metabolism, which maintain plasma membrane and mitochondrial integrity. Lipid droplets contain various proteins that have immune functions (GTPases and histones) or that reduce cell toxicity (Invadolysin, protein involved in the formation of triacylaglycerol and diacylglycerols). Histone are potent antimicrobial molecules that can be released upon bacterial challenge in *Drosophila* larvae; they could also constitute an immune defence against *M.marinum.* Invadolysin is a protein that participates in the control of mitochondrial integrity and prevent excessive ROS production. To prevent cell toxicity, lipid droplets also diminish lipotoxicity by integrating free fatty acid into triacylglycerols and diacylglycerols. *M.marinum* affect all these processes by mediating changes in lipid droplet formation and morphology, which may result in alteration of their functions.

7.4 How can Atg2 regulate the size and morphology of LDs?

Most of the studies on lipid droplets have looked at changes in total neutral lipid content, and not at the size and morphology of lipid droplets. However, recent functional genomic screenings, proteomics analysis, and candidate approaches have identified host factors involved in the control of LD size and morphology (Atg2 was not found in these screens) (Fei et al. 2008; Guo et al. 2008; Beller et al. 2006; Szymanski et al. 2007). The first characterised protein was the lipodystrophy protein seipin that is found at the junction between the endoplasmic reticulum and the lipid droplets, and that regulates lipid droplet morphology (Fei et al. 2008; Szymanski et al. 2007). Seipin mutants in yeast and humans have irregular lipid droplets alongside the ER and have some giant lipid structures. Out of their screen, authors also identified 58 other candidate genes that, when mutated, cause aberrant lipid droplets. They include genes coding for proteins involved in phago-lysosomal trafficking. Interestingly, within the same cell, lipid droplets may have different shape and different protein composition, thus presumably different functions (Beller et al. 2006; Saka & Valdivia 2012). Finally, a genome wide RNAi screen in *Drosophila* identified genes encoding enzymes of phospholipid biosynthesis as determinants for lipid droplet formation and size. It suggests that alteration in the composition of the phospholipid monolayer of lipid droplets affects lipid droplet morphology and function. In addition, authors found that a subset of the Arf1-COPI vesicular transport protein resulted in a similar phenotype.

In conclusion, little is known about the cellular processes regulating lipid droplet morphology, especially in the context of bacterial infection. Our study is the first to show a cytokine-dependent modulation of lipid morphology through regulation of the autophagy protein Atg2. However, the Atg2-dependent mechanisms regulating lipid droplet size and shape are unknown. Based on previous publications, Atg2 may regulate trafficking processes, lipid biogenesis or even the lipid composition of lipid droplets. To understand the Atg2–related processes controlling lipid droplet morphology, it would be interesting to perform an RNAi screen on infected cells overexpressing or not *Atg2*. Also, it would be interesting to identify the lipid composition of lipid droplets in cells overexpressing *Atg2* or *upd3*, and to assess whether it could affect their functions.

7.5 A localised and systemic cytokine-mediated regulation of metabolic stores

From our results, Upd3 signalling controls lipid droplet homeostasis within innate immune cells (Chapter 5). In the same time, Upd3 signalling seems to control systemic levels of glucose and glycogen, which in return decrease *Ilp2* expression and reduce activation of the insulin pathway upon infection (Chapter 6). The results from Rajan et al. suggest that cytokines, are expressed in response to the fed state and signal to a population of GABAergic neurons that project onto the Insulin Producing Cells (IPCs) (Rajan & Perrimon 2012). The activation of JAK-STAT in these neurons provoked the release and secretion of insulin-like peptides to regulate metabolic stores. By looking more closely at their data, mutation of *upd2* affected only triacylglycerol levels and not glucose levels in the whole organism. Since mutation of *upd3* did not affect the overall triacylglycerol content, and since, from my results, *upd3* mutants had a strong increase in glucose levels and glycogen stores, it suggests that Upd3 controls glucose homeostasis. In this hypothesis, Upd2 and Upd3 may have complementary role in regulating metabolic stores, Upd2 in response to triglyceride sensing and Upd3 in response to glucose and/or glycogen sensing. By analogy to their study, Upd3 may signal to the brain but to distinct population of neurons, probably to regulate glucogenesis and glycolysis.

Rajan et al. demonstrated that Upd2 is produced and secreted by the fat body. Upd3, so far, has been shown to be secreted by hemocytes, especially upon infection (Agaisse et al. 2003). Interestingly, upon local epidermal DNA damage, insulin signalling is reduced in an hemocyte-dependent fashion, suggesting a link between hemocyte function and regulation of metabolic stores (Karpac et al. 2011). Therefore, one can hypothesize that hemocytes can sense glucose levels through glucose transporters, insulin receptors or other mechanisms, and in response produce Upd3. Upd3 may then signal to relevant tissues to inhibit glucogenesis and glycolysis. In the context of infection, Upd3 may signal to infected hemocyte to maintain lipid droplet homeostasis, but also to other tissues to prevent a systemic rise in glucose likely provoked by the bacteria. Further investigation is required to confirm this hypothesis.

7.6 In the context of *M.tuberculosis* infection

A necessary and sometimes rather confusing exercise is to interpret our research in the context of human immunobiology.

Our results demonstrate for the first time that an IL-6-like cytokine signals to macrophage–like cells to control, in an Atg2-dependent mechanism, the homeostasis and morphology of lipid droplets. This is the first time that JAK-STAT signalling is shown to regulate the transcription of autophagy genes upon infection and specifically of *Atg2*. It is also the first time that the role of Atg2 in controlling lipid droplet morphology is put into the context of infection, and is correlated with a decrease in bacterial replication. The originality of this work also resides in the fact that most of key features of *M.tuberculosis* infections—cytokine signalling, intra-macrophage mycobacterial replication and the foamy phenotype—are recapitulated in *M.marinum* infection in *Drosophila*, and are shown to be intimately linked by a specific signalling pathway. Finally, most of this study is performed *in vivo* and demonstrates that by inhibiting IL-6 signalling, we could diminish bacterial replication and improve the fitness of the host. Now, it would be beneficial to corroborate these findings by studying the role of IL-6 in the formation and morphology of lipid droplets within artificial granulomas and within the granuloma of infected patients.

Our data also showed a clear change in lipid droplets morphology within macrophage-like cells upon infection with heat-killed *M.marinum*, a phenotype that, so far, has not been seen or studied in *M.tuberculosis* infection. Therefore, it would be interesting to verify if this happens in human macrophages infected with heat-killed *M.tuberculosis* or mycobacterial components, and to understand the mechanisms that trigger this phenotype.

7.7 Unanswered questions and future plans

Several questions remain unanswered, including:

(A) Is *M.marinum* strictly intracellular in the early phase of infection?

(B) How is JAK-STAT signalling decreasing *Atg2* expression in hemocytes? Is it dependent on the JAK-STAT target, *net*, in vivo?

(C) What triggers the changes in lipid droplet formation and morphology upon infection with heat-killed or active mycobacteria?

(D) What are the signals inducing lipid droplet formation? Is there a role for the *Toll* pathway, the *ERK* pathway?

(E) What are the different functions of Atg2?

(F) How can Atg2 regulate the size of lipid droplets?

(G) How is Upd3 controlling glucose and glycogen levels during infection?

(H) What are the tissues responsive to Upd3 at steady state and upon infection?

One major aspect presented in this thesis is the under-appreciated role of lipid droplets in the control of infection. Several researchers are now investigating the function of lipid droplets in immunity and infectious diseases, and an important question is whether lipid droplets could interact with phagosomes for the exchange of bactericidal molecules or nutrients. Indeed, one major difference between *Drosophila* and humans when studying macrophage biology, is the cellular localisation of mycobacteria. While *M.marinum* escapes the phagosome, to access the cytosol and acquire actin-based motility; *M.tuberculosis* remains in phagosomes and only escape towards the cytosol upon necrosis (Stamm et al. 2003; Simeone et al. 2012; van der Wel et al. 2007; Welin & Lerm 2012). Therefore, understanding how bacteria interact with lipid droplets would give information about how they exchange molecules. In addition, since lipid droplets may control mitochondrial integrity, it would be interesting to look at the production of ROS and nitrogen intermediates to assess whether JAK-STAT signalling could alter these processes.

References

Abramovitch, R.B. et al., 2011. aprABC: a Mycobacterium tuberculosis complex-specific locus that modulates pH-driven adaptation to the macrophage phagosome. *Molecular microbiology*, 80(3), pp.678–694.

Adams, M.D. et al., 2000. The genome sequence of Drosophila melanogaster. *Science (New York, N.Y.)*, 287(5461), pp.2185–2195.

Aderem, A. & Underhill, D.M., 1999. Mechanisms of phagocytosis in macrophages. *Annual review of immunology*, 17, pp.593–623.

Agaisse, H. & Perrimon, N., 2004. The roles of JAK/STAT signaling in Drosophila immune responses. *Immunological reviews*, 198, pp.72–82.

Agaisse, H. et al., 2005. Genome-wide RNAi screen for host factors required for intracellular bacterial infection. *Science (New York, N.Y.)*, 309(5738), pp.1248–1251.

Agaisse, H. et al., 2003. Signaling role of hemocytes in Drosophila JAK/STAT-dependent response to septic injury. *Developmental cell*, 5(3), pp.441–450.

Alatas, F. et al., 2004. Vascular endothelial growth factor levels in active pulmonary tuberculosis. *Chest*, 125(6), pp.2156–2159.

Alonso, S. et al., 2007. Lysosomal killing of Mycobacterium mediated by ubiquitin-derived peptides is enhanced by autophagy. *Proceedings of the National Academy of Sciences of the United States of America*, 104(14), pp.6031–6036.

Anand, P. et al., 2012. A novel role for lipid droplets in the organismal antibacterial response. *eLife*, 1, p.e00003.

Andries, K. et al., 2005. A diarylquinoline drug active on the ATP synthase of Mycobacterium tuberculosis. *Science (New York, N.Y.)*, 307(5707), pp.223–227.

Appelberg, R., 2006. Macrophage nutriprive antimicrobial mechanisms. *Journal of leukocyte biology*, 79(6), pp.1117–1128.

Aubry, A. et al., 2000. Antibiotic susceptibility pattern of Mycobacterium marinum. *Antimicrobial agents and chemotherapy*, 44(11), pp.3133–3136.

Ayres, J.S. & Schneider, D.S., 2009. The role of anorexia in resistance and tolerance to infections in Drosophila. *PLoS biology*, 7(7), p.e1000150.

Ayres, J.S., Freitag, N. & Schneider, D.S., 2008. Identification of Drosophila mutants altering defense of and endurance to Listeria monocytogenes infection. *Genetics*, 178(3), pp.1807–1815.

Bach, E.A. et al., 2003. A sensitized genetic screen to identify novel regulators and components of the Drosophila janus kinase/signal transducer and activator of transcription pathway. *Genetics*, 165(3), pp.1149–1166.

Bach, E.A. et al., 2007. GFP reporters detect the activation of the Drosophila JAK/STAT pathway in vivo. *Gene expression patterns : GEP*, 7(3), pp.323–331.

Baeg, G.-H., Zhou, R. & Perrimon, N., 2005. Genome-wide RNAi analysis of JAK/STAT signaling components in Drosophila. *Genes & development*, 19(16), pp.1861–1870.

Barth, J.M.I. et al., 2011. Autophagy in Drosophila ovaries is induced by starvation and is required for oogenesis. *Cell death and differentiation*, 18(6), pp.915–924.

Barth, S., Glick, D. & Macleod, K.F., 2010. Autophagy: assays and artifacts. *The Journal of pathology*, 221(2), pp.117–124.

Beebe, K., Lee, W.-C. & Micchelli, C.A., 2010. JAK/STAT signaling coordinates stem cell proliferation and multilineage differentiation in the Drosophila intestinal stem cell lineage. *Developmental biology*, 338(1), pp.28–37.

Behar, S.M. et al., 2011. Apoptosis is an innate defense function of macrophages against Mycobacterium tuberculosis. *Mucosal immunology*, 4(3), pp.279–287.

Beller, M. et al., 2006. Characterization of the Drosophila lipid droplet subproteome. *Molecular & cellular proteomics : MCP*, 5(6), pp.1082–1094.

Bidla, G., Dushay, M.S. & Theopold, U., 2007. Crystal cell rupture after injury in Drosophila requires the JNK pathway, small GTPases and the TNF homolog Eiger. *Journal of cell science*, 120(Pt 7), pp.1209–1215.

Bina, S. et al., 2010. Transcriptional targets of Drosophila JAK/STAT pathway signalling as effectors of haematopoietic tumour formation. *EMBO reports*, 11(3), pp.201–207.

Bishai, W., 2000. Lipid lunch for persistent pathogen. *Nature*, 406(6797), pp.683–685.

Blander, J.M. & Medzhitov, R., 2006. Toll-dependent selection of microbial antigens for presentation by dendritic cells. *Nature*, 440(7085), pp.808–812.

Bonah, C., 2005. The “experimental stable” of the BCG vaccine: safety, efficacy, proof, and standards, 1921–1933. *Studies in History and Philosophy of Science Part C: Studies in History and Philosophy of Biological and Biomedical Sciences*, 36(4), pp.696–721.

Boshoff, H.I.M. et al., 2003. DnaE2 Polymerase Contributes to In Vivo Survival and the Emergence of Drug Resistance in Mycobacterium tuberculosis. *Cell*, 113(2), pp.183–193.

Bougnères, L. et al., 2009. A role for lipid bodies in the cross-presentation of phagocytosed antigens by MHC class I in dendritic cells. *Immunity*, 31(2), pp.232–244.

Boutros, M., Agaisse, H. & Perrimon, N., 2002. Sequential activation of signaling pathways during innate immune responses in Drosophila. *Developmental cell*, 3(5), pp.711–722.

Brand, A.H. & Perrimon, N., 1993. Targeted gene expression as a means of altering cell fates and generating dominant phenotypes. *Development (Cambridge, England)*, 118(2), pp.401–415.

Brandt, S.M. et al., 2004. Secreted Bacterial Effectors and Host-Produced Eiger/TNF Drive Death in aSalmonella-Infected Fruit Fly. *PLoS biology*, 2(12), p.e418.

Brennan, P.J. & Nikaido, H., 1995. The envelope of mycobacteria. *Annual review of biochemistry*, 64, pp.29–63.

Brown, S., Hu, N. & Hombría, J.C., 2001. Identification of the first invertebrate interleukin JAK/STAT receptor, the Drosophila gene domeless. *Current biology : CB*, 11(21), pp.1700–1705.

Buchon, N., Broderick, N.A., Chakrabarti, S., et al., 2009a. Invasive and indigenous microbiota impact intestinal stem cell activity through multiple pathways in Drosophila. *Genes & development*, 23(19), pp.2333–2344.

Buchon, N., Broderick, N.A., Poidevin, M., et al., 2009b. Drosophila intestinal response to bacterial infection: activation of host defense and stem cell proliferation. *Cell host & microbe*, 5(2), pp.200–211.

Cáceres, N. et al., 2009. Evolution of foamy macrophages in the pulmonary granulomas of experimental tuberculosis models. *Tuberculosis (Edinburgh, Scotland)*, 89(2), pp.175–182.

Chambers, M.C., Song, K.H. & Schneider, D.S., 2012. Listeria monocytogenes Infection Causes Metabolic Shifts in Drosophila melanogaster. *PloS one*, 7(12), p.e50679.

Chan, J. et al., 1992. Killing of virulent Mycobacterium tuberculosis by reactive nitrogen intermediates produced by activated murine macrophages. *The Journal of experimental medicine*, 175(4), pp.1111–1122.

Chan, K. et al., 2002. Complex pattern of Mycobacterium marinum gene expression during long-term granulomatous infection. *Proceedings of the National Academy of Sciences of the United States of America*, 99(6), pp.3920–3925.

Chen, M. et al., 2008. Lipid mediators in innate immunity against tuberculosis: opposing roles of PGE2 and LXA4 in the induction of macrophage death. *The Journal of experimental medicine*, 205(12), pp.2791–2801.

Clark, R.I. et al., 2011. Multiple TGF-β Superfamily Signals Modulate the Adult Drosophila Immune Response. *Current biology : CB*.

Clay, H. et al., 2007. Dichotomous Role of the Macrophage in Early Mycobacterium marinum Infection of the Zebrafish. *Cell host & …*.

Colangeli, R. et al., 2007. Transcriptional Regulation of Multi-Drug Tolerance and Antibiotic-Induced Responses by the Histone-Like Protein Lsr2 in M. tuberculosis. *PLoS pathogens*, 3(6), p.e87.

Cole, S.T. et al., 1998. Deciphering the biology of Mycobacterium tuberculosis from the complete genome sequence. *Nature*, 393(6685), pp.537–544.

Collins, C.A. et al., 2009. Atg5-independent sequestration of ubiquitinated mycobacteria. *PLoS pathogens*, 5(5), p.e1000430.

Cooper, A.M., 2009. Cell-mediated immune responses in tuberculosis. *Annual review of immunology*, 27, pp.393–422.

Corbo, J.C. & Levine, M., 1996. Characterization of an immunodeficiency mutant in Drosophila. *Mechanisms of development*, 55(2), pp.211–220.

Cosma, C.L., Humbert, O. & Ramakrishnan, L., 2004. Superinfecting mycobacteria home to established tuberculous granulomas. *Nature immunology*, 5(8), pp.828–835.

Cossart, P. & Kocks, C., 1994. The actin-based motility of the facultative intracellular pathogen Listeria monocytogenes. *Molecular microbiology*, 13(3), pp.395–402.

Crozatier, M. & Meister, M., 2007. Drosophila haematopoiesis. *Cellular microbiology*, 9(5), pp.1117–1126.

Crozatier, M. et al., 2004. Cellular immune response to parasitization in Drosophila requires the EBF orthologue collier. *PLoS biology*, 2(8), p.E196.

D'Avila, H. et al., 2006. Mycobacterium bovis bacillus Calmette-Guérin induces TLR2-mediated formation of lipid bodies: intracellular domains for eicosanoid synthesis in vivo. *Journal of immunology (Baltimore, Md. : 1950)*, 176(5), pp.3087–3097.

D'Avila, H., Maya-Monteiro, C.M. & Bozza, P.T., 2008. Lipid bodies in innate immune response to bacterial and parasite infections. *International immunopharmacology*, 8(10), pp.1308–1315.

Daniel, J. et al., 2004. Induction of a novel class of diacylglycerol acyltransferases and triacylglycerol accumulation in Mycobacterium tuberculosis as it goes into a dormancy-like state in culture. *Journal of bacteriology*, 186(15), pp.5017–5030.

Daniel, J. et al., 2011. Mycobacterium tuberculosis uses host triacylglycerol to accumulate lipid

droplets and acquires a dormancy-like phenotype in lipid-loaded macrophages. *PLoS pathogens*, 7(6), p.e1002093.

Darwin, K.H., 2003. The Proteasome of Mycobacterium tuberculosis Is Required for Resistance to Nitric Oxide. *Science (New York, N.Y.)*, 302(5652), pp.1963–1966.

Davis, A.S. et al., 2007. Mechanism of inducible nitric oxide synthase exclusion from mycobacterial phagosomes. *PLoS pathogens*, 3(12), p.e186.

Davis, J. et al., 2002. Immunity - Real-Time Visualization of Mycobacterium-Macrophage Interactions Leading to Initiation of Granuloma Formation in Zebrafish Embryos. *Immunity*.

Davis, J.M. & Ramakrishnan, L., 2009. The role of the granuloma in expansion and dissemination of early tuberculous infection. *Cell*, 136(1), pp.37–49.

De Gregorio, E. et al., 2001. Genome-wide analysis of the Drosophila immune response by using oligonucleotide microarrays. *Proceedings of the National Academy of Sciences of the United States of America*, 98(22), pp.12590–12595.

De Gregorio, E. et al., 2002. The Toll and Imd pathways are the major regulators of the immune response in Drosophila. *The EMBO journal*, 21(11), pp.2568–2579.

Decker, T. et al., 2002. IFNs and STATs in innate immunity to microorganisms. *The Journal of clinical investigation*, 109(10), pp.1271–1277.

Delaney, J.R. et al., 2006. Cooperative control of Drosophila immune responses by the JNK and NF-kappaB signaling pathways. *The EMBO journal*, 25(13), pp.3068–3077.

Deretic, V. & Levine, B., 2009. Autophagy, immunity, and microbial adaptations. *Cell host & microbe*, 5(6), pp.527–549.

Dheda, K. et al., 2005. Lung remodeling in pulmonary tuberculosis. *The Journal of infectious diseases*, 192(7), pp.1201–1209.

Di Cara, F. et al., 2013. Invadolysin, a conserved lipid droplet-associated metalloprotease, is required for mitochondrial function in Drosophila. *Journal of cell science*.

Dionne, M.S. & Schneider, D.S., 2008. Models of infectious diseases in the fruit fly Drosophila melanogaster. *Disease models & mechanisms*, 1(1), pp.43–49.

Dionne, M.S. et al., 2006. Akt and FOXO dysregulation contribute to infection-induced wasting in Drosophila. *Current biology : CB*, 16(20), pp.1977–1985.

Dionne, M.S., Ghori, N. & Schneider, D.S., 2003. Drosophila melanogaster is a genetically tractable model host for Mycobacterium marinum. *Infection and immunity*, 71(6), pp.3540–3550.

Divangahi, M. et al., 2010. Eicosanoid pathways regulate adaptive immunity to Mycobacterium tuberculosis. *Nature immunology*, 11(8), pp.751–758.

Dostert, C. et al., 2005. The Jak-STAT signaling pathway is required but not sufficient for the antiviral response of drosophila. *Nature immunology*, 6(9), pp.946–953.

Dutta, R.K. et al., 2012. IL-6 inhibits IFN-γ induced autophagy in Mycobacterium tuberculosis H37Rv infected macrophages. *The international journal of biochemistry & cell biology*, 44(6), pp.942–954.

Ehrt, S. & Schnappinger, D., 2009. Mycobacterial survival strategies in the phagosome: defence against host stresses. *Cellular microbiology*, 11(8), pp.1170–1178.

Ehrt, S. et al., 2001. Reprogramming of the macrophage transcriptome in response to interferon-gamma and Mycobacterium tuberculosis: signaling roles of nitric oxide synthase-

2 and phagocyte oxidase. *The Journal of experimental medicine*, 194(8), pp.1123–1140.

Ekas, L.A. et al., 2006. JAK/STAT signaling promotes regional specification by negatively regulating wingless expression in Drosophila. *Development (Cambridge, England)*, 133(23), pp.4721–4729.

Elrod-Erickson, M., Mishra, S. & Schneider, D., 2000. Interactions between the cellular and humoral immune responses in Drosophila. *Current biology : CB*, 10(13), pp.781–784.

Fabri, M. et al., 2011. Vitamin D Is Required for IFN-{gamma}-Mediated Antimicrobial Activity of Human Macrophages. *Science translational medicine*, 3(104), p.104ra102.

Fairn, G.D. & Grinstein, S., 2012. How nascent phagosomes mature to become phagolysosomes. *Trends in immunology*, 33(8), pp.397–405.

Falschlehner, C. & Boutros, M., 2012. Innate immunity: regulation of caspases by IAP-dependent ubiquitylation. *The EMBO journal*, 31(12), pp.2750–2752.

Fei, W. et al., 2008. Fld1p, a functional homologue of human seipin, regulates the size of lipid droplets in yeast. *The Journal of cell biology*, 180(3), pp.473–482.

Ferrandon, D., 2009. Host tolerance versus resistance and microbial virulence in the host-pathogen equation. *Cell host & microbe*, 6(3), pp.203–205.

Ferrari, G. et al., 1999. A coat protein on phagosomes involved in the intracellular survival of mycobacteria. *Cell*, 97(4), pp.435–447.

Fessler, L.I., Nelson, R.E. & Fessler, J.H., 1994. Drosophila extracellular matrix. *Methods in enzymology*, 245, pp.271–294.

Flynn, J.L. & Chan, J., 2001. Immunology of tuberculosis. *Annual review of immunology*, 19, pp.93–129.

Ford, C.B. et al., 2011. Use of whole genome sequencing to estimate the mutation rate of Mycobacterium tuberculosis during latent infection. *Nature genetics*, 43(5), pp.482–486.

Franc, N.C. et al., 1999. Requirement for croquemort in phagocytosis of apoptotic cells in Drosophila. *Science (New York, N.Y.)*, 284(5422), pp.1991–1994.

Gan, H. et al., 2008. Mycobacterium tuberculosis blocks crosslinking of annexin-1 and apoptotic envelope formation on infected macrophages to maintain virulence. *Nature immunology*, 9(10), pp.1189–1197.

Gao, L.Y. et al., 2004. A mycobacterial virulence gene cluster extending RD1 is required for cytolysis, bacterial spreading and ESAT-6 secretion - Gao - 2004 - Molecular Microbiology - Wiley Online Library. *Molecular …*.

Garton, N.J. et al., 2002. Intracellular lipophilic inclusions of mycobacteria in vitro and in sputum. *Microbiology (Reading, England)*, 148(Pt 10), pp.2951–2958.

Gengenbacher, M. & Kaufmann, S.H.E., 2012. Mycobacterium tuberculosis: success through dormancy. *FEMS microbiology reviews*, 36(3), pp.514–532.

Georgel, P. et al., 2001. Drosophila immune deficiency (IMD) is a death domain protein that activates antibacterial defense and can promote apoptosis. *Developmental cell*, 1(4), pp.503–514.

Gill, W.P. et al., 2009. A replication clock for Mycobacterium tuberculosis. *Nature medicine*, 15(2), pp.211–214.

Goto, A. et al., 2001. A Drosophila haemocyte-specific protein, hemolectin, similar to human von Willebrand factor. *The Biochemical journal*, 359(Pt 1), pp.99–108.

Gradmann, C., 2001. Robert Koch and the pressures of scientific research: tuberculosis and tuberculin. *Medical history*.

Greenspan, R.J., 2004. *Fly Pushing*, CSHL Press.

Guo, Y. et al., 2008. Functional genomic screen reveals genes involved in lipid-droplet formation and utilization. *Nature*, 453(7195), pp.657–661.

Gutierrez, M.G. et al., 2004. Autophagy is a defense mechanism inhibiting BCG and Mycobacterium tuberculosis survival in infected macrophages. *Cell*, 119(6), pp.753–766.

Ha, E.-M. et al., 2005. A direct role for dual oxidase in Drosophila gut immunity. *Science (New York, N.Y.)*, 310(5749), pp.847–850.

Hagedorn, M. et al., 2009. Infection by tubercular mycobacteria is spread by nonlytic ejection from their amoeba hosts. *Science (New York, N.Y.)*, 323(5922), pp.1729–1733.

Harris, J. et al., 2007. T helper 2 cytokines inhibit autophagic control of intracellular Mycobacterium tuberculosis. *Immunity*, 27(3), pp.505–517.

Harrison, D.A. et al., 1998. Drosophila unpaired encodes a secreted protein that activates the JAK signaling pathway. *Genes & development*, 12(20), pp.3252–3263.

Herb, F. et al., 2008. ALOX5 variants associated with susceptibility to human pulmonary tuberculosis. *Human molecular genetics*, 17(7), pp.1052–1060.

Hewinson, R.G., Vordermeier, H.M. & Buddle, B.M., 2003. Use of the bovine model of tuberculosis for the development of improved vaccines and diagnostics. *Tuberculosis (Edinburgh, Scotland)*, 83(1-3), pp.119–130.

Hinchey, J. et al., 2007. Enhanced priming of adaptive immunity by a proapoptotic mutant of Mycobacterium tuberculosis. *The Journal of clinical investigation*, 117(8), pp.2279–2288.

Holz, A. et al., 2003. The two origins of hemocytes in Drosophila. *Development (Cambridge, England)*, 130(20), pp.4955–4962.

Hombría, J.C.-G. et al., 2005. Characterisation of Upd2, a Drosophila JAK/STAT pathway ligand. *Developmental biology*, 288(2), pp.420–433.

Igaki, T. et al., 2002. Eiger, a TNF superfamily ligand that triggers the Drosophila JNK pathway. *The EMBO journal*, 21(12), pp.3009–3018.

Inoue, C. et al., 2001. Math6, a bHLH gene expressed in the developing nervous system, regulates neuronal versus glial differentiation. *Genes to cells : devoted to molecular & cellular mechanisms*, 6(11), pp.977–986.

Irving, P. et al., 2001. A genome-wide analysis of immune responses in Drosophila. *Proceedings of the National Academy of Sciences of the United States of America*, 98(26), pp.15119–15124.

Irving, P. et al., 2005. New insights into Drosophila larval haemocyte functions through genome-wide analysis. *Cellular microbiology*, 7(3), pp.335–350.

Ja, W.W. et al., 2009. Water- and nutrient-dependent effects of dietary restriction on Drosophila lifespan. *Proceedings of the National Academy of Sciences of the United States of America*, 106(44), pp.18633–18637.

Jang, I.-H. et al., 2006. A Spätzle-processing enzyme required for toll signaling activation in Drosophila innate immunity. *Developmental cell*, 10(1), pp.45–55.

Jayachandran, R. et al., 2007. Survival of Mycobacteria in Macrophages Is Mediated by Coronin 1-Dependent Activation of Calcineurin. *Cell*, 130(1), pp.37–50.

Jinks, T.M. et al., 2000. The JAK/STAT signaling pathway is required for the initial choice of sexual identity in Drosophila melanogaster. *Molecular cell*, 5(3), pp.581–587.

Juárez, E. et al., 2012. NOD2 enhances the innate response of alveolar macrophages to Mycobacterium tuberculosis in humans. *European journal of immunology*, 42(4), pp.880–889.

Jung, S.-H. et al., 2005. The Drosophila lymph gland as a developmental model of hematopoiesis. *Development (Cambridge, England)*, 132(11), pp.2521–2533.

Kabeya, Y. et al., 2000. LC3, a mammalian homologue of yeast Apg8p, is localized in autophagosome membranes after processing. *The EMBO journal*, 19(21), pp.5720–5728.

Kallio, J. et al., 2005. Functional analysis of immune response genes in Drosophila identifies JNK pathway as a regulator of antimicrobial peptide gene expression in S2 cells. *Microbes and infection / Institut Pasteur*, 7(5-6), pp.811–819.

Karpac, J., Younger, A. & Jasper, H., 2011. Dynamic coordination of innate immune signaling and insulin signaling regulates systemic responses to localized DNA damage. *Developmental cell*, 20(6), pp.841–854.

Karsten, P. et al., 2006. Mutational analysis reveals separable DNA binding and trans-activation of Drosophila STAT92E. *Cellular signalling*, 18(6), pp.819–829.

Kaufmann, S.H.E., 2003. Immune response to tuberculosis: experimental animal models. *Tuberculosis (Edinburgh, Scotland)*, 83(1-3), pp.107–111.

Kauppila, S. et al., 2003. Eiger and its receptor, Wengen, comprise a TNF-like system in Drosophila. *Oncogene*, 22(31), pp.4860–4867.

Kautz, L. et al., 2008. Iron regulates phosphorylation of Smad1/5/8 and gene expression of Bmp6, Smad7, Id1, and Atoh8 in the mouse liver. *Blood*, 112(4), pp.1503–1509.

Keane, J. et al., 1997. Infection by Mycobacterium tuberculosis promotes human alveolar macrophage apoptosis. *Infection and immunity*, 65(1), pp.298–304.

Kim, M.-J. et al., 2010. Caseation of human tuberculosis granulomas correlates with elevated host lipid metabolism. *EMBO molecular medicine*, 2(7), pp.258–274.

Kimbrell, D.A. & Beutler, B., 2001. The evolution and genetics of innate immunity. *Nature reviews. Genetics*, 2(4), pp.256–267.

Kindler, V. et al., 1989. The inducing role of tumor necrosis factor in the development of bactericidal granulomas during BCG infection. *Cell*, 56(5), pp.731–740.

Koch, R., 1882. *Die Aetiologie der Tuberculose*,

Koch, R., 1982. The Etiology of Tuberculosis. *Clinical Infectious Diseases*, 4(6), pp.1270–1274.

Kolter, R., 2012. Histones join the fight against bacteria inside cells. *eLife*, 1, p.e00302.

Koo, I.C. et al., 2008. Role for lysosomal enzyme beta-hexosaminidase in the control of mycobacteria infection. *Proceedings of the National Academy of Sciences of the United States of America*, 105(2), pp.710–715.

Koul, A. et al., 2011. The challenge of new drug discovery for tuberculosis. *Nature*, 469(7331), pp.483–490.

Krzemień, J. et al., 2007. Control of blood cell homeostasis in Drosophila larvae by the posterior signalling centre. *Nature*, 446(7133), pp.325–328.

Lagueux, M. et al., 2000. Constitutive expression of a complement-like protein in toll and JAK

gain-of-function mutants of Drosophila. *Proceedings of the National Academy of Sciences of the United States of America*, 97(21), pp.11427–11432.

Lanot, R. et al., 2001. Postembryonic Hematopoiesis in Drosophila. *Developmental biology*.

Lawn, S.D. & Zumla, A.I., 2011. Tuberculosis. *Lancet*, 378(9785), pp.57–72.

Lawrence, P.A. & Johnston, P., 1986. Observations on cell lineage of internal organs of Drosophila. *Journal of embryology and experimental morphology*, 91, pp.251–266.

Lebestky, T. et al., 2000. Specification of Drosophila hematopoietic lineage by conserved transcription factors. *Science (New York, N.Y.)*, 288(5463), pp.146–149.

Lee, W.L. et al., 2009. Mycobacterium tuberculosisexpresses methionine sulphoxide reductases A and B that protect from killing by nitrite and hypochlorite. *Molecular microbiology*, 71(3), pp.583–593.

Leemans, J.C. et al., 2001. Depletion of alveolar macrophages exerts protective effects in pulmonary tuberculosis in mice. *Journal of immunology (Baltimore, Md. : 1950)*, 166(7), pp.4604–4611.

Lemaitre, B., 2004. *The road to Toll*,

Lemaitre, B. & Hoffmann, J., 2007. The host defense of Drosophila melanogaster. *Annual review of immunology*, 25, pp.697–743.

Lemaitre, B. et al., 1995. A recessive mutation, immune deficiency (imd), defines two distinct control pathways in the Drosophila host defense. *Proceedings of the National Academy of Sciences of the United States of America*, 92(21), pp.9465–9469.

Lemaitre, B. et al., 1996. The dorsoventral regulatory gene cassette spätzle/Toll/cactus controls the potent antifungal response in Drosophila adults. *Cell*, 86(6), pp.973–983.

Lemaitre, B., Reichhart, J.M. & Hoffmann, J.A., 1997. Drosophila host defense: differential induction of antimicrobial peptide genes after infection by various classes of microorganisms. *Proceedings of the National Academy of Sciences of the United States of America*, 94(26), pp.14614–14619.

Lesley, R. & Ramakrishnan, L., 2008. Insights into early mycobacterial pathogenesis from the zebrafish. *Current opinion in microbiology*, 11(3), pp.277–283.

Levashina, E.A. et al., 1998. Two distinct pathways can control expression of the gene encoding the Drosophila antimicrobial peptide metchnikowin. *Journal of molecular biology*, 278(3), pp.515–527.

Levine, B., Mizushima, N. & Virgin, H.W., 2011. Autophagy in immunity and inflammation. *Nature*, 469(7330), pp.323–335.

Levy, F. et al., 2004. Peptidomic and proteomic analyses of the systemic immune response of Drosophila. *Biochimie*, 86(9-10), pp.607–616.

Lin, Y. et al., 1996. Absence of a prominent Th2 cytokine response in human tuberculosis. *Infection and immunity*, 64(4), pp.1351–1356.

Listenberger, L.L. et al., 2003. Triglyceride accumulation protects against fatty acid-induced lipotoxicity. *Proceedings of the National Academy of Sciences of the United States of America*, 100(6), pp.3077–3082.

Liu, P.T. & Modlin, R.L., 2008. Human macrophage host defense against Mycobacterium tuberculosis. *Current opinion in immunology*, 20(4), pp.371–376.

Lynn, F.C. et al., 2008. Identification of the bHLH factor Math6 as a novel component of the

embryonic pancreas transcriptional network. *PloS one*, 3(6), p.e2430.

Mabery, E.M. & Schneider, D.S., 2010. The Drosophila TNF ortholog eiger is required in the fat body for a robust immune response. *Journal of innate immunity*, 2(4), pp.371–378.

MacMicking, J., Xie, Q.W. & Nathan, C., 1997. Nitric oxide and macrophage function. *Annual review of immunology*, 15, pp.323–350.

MacMicking, J.D., Taylor, G.A. & McKinney, J.D., 2003. Immune control of tuberculosis by IFN-gamma-inducible LRG-47. *Science (New York, N.Y.)*, 302(5645), pp.654–659.

Maglione, P.J. & Chan, J., 2009. How B cells shape the immune response against Mycobacterium tuberculosis. *European journal of immunology*, 39(3), pp.676–686.

Maini, R. et al., 1999. Infliximab (chimeric anti-tumour necrosis factor alpha monoclonal antibody) versus placebo in rheumatoid arthritis patients receiving concomitant methotrexate: a randomised phase III trial. ATTRACT Study Group. *Lancet*, 354(9194), pp.1932–1939.

Makki, R. et al., 2010. A short receptor downregulates JAK/STAT signalling to control the Drosophila cellular immune response. *PLoS biology*, 8(8), p.e1000441.

Maloney, E. et al., 2009. The two-domain LysX protein of Mycobacterium tuberculosis is required for production of lysinylated phosphatidylglycerol and resistance to cationic antimicrobial peptides. *PLoS pathogens*, 5(7), p.e1000534.

Matsuzawa, T. et al., 2012. IFN-γ Elicits Macrophage Autophagy via the p38 MAPK Signaling Pathway. *Journal of immunology (Baltimore, Md. : 1950)*.

McGowan, M.W. et al., 1983. A peroxidase-coupled method for the colorimetric determination of serum triglycerides. *Clinical chemistry*, 29(3), pp.538–542.

McGraw, L.A. et al., 2004. Genes regulated by mating, sperm, or seminal proteins in mated female Drosophila melanogaster. *Current biology : CB*, 14(16), pp.1509–1514.

McGuire, S.E. et al., 2003. Spatiotemporal rescue of memory dysfunction in Drosophila. *Science (New York, N.Y.)*, 302(5651), pp.1765–1768.

McGuire, S.E., Roman, G. & Davis, R.L., 2004. Gene expression systems in Drosophila: a synthesis of time and space. *Trends in genetics : TIG*, 20(8), pp.384–391.

McKinney, J.D. et al., 2000. Persistence of Mycobacterium tuberculosis in macrophages and mice requires the glyoxylate shunt enzyme isocitrate lyase. *Nature*, 406(6797), pp.735–738.

Medzhitov, R., Preston-Hurlburt, P. & Janeway, C.A., 1997. A human homologue of the Drosophila Toll protein signals activation of adaptive immunity. *Nature*, 388(6640), pp.394–397.

Mehta, P.K. et al., 2006. Identification of Mycobacterium marinum macrophage infection mutants. *Microbial Pathogenesis*, 40(4), pp.139–151.

Meister, M., 2004a. Blood cells of Drosophila: cell lineages and role in host defence. *Current opinion in immunology*, 16(1), pp.10–15.

Meister, M., 2004b. Blood cells of Drosophila: cell lineages and role in host defence. *Current opinion in immunology*.

Metchnikoff, E., 1905. Metchnikoff: Immunity in infective diseases - Google Scholar.

Molle, V. et al., 2006. pH-dependent pore-forming activity of OmpATb from Mycobacterium tuberculosis and characterization of the channel by peptidic dissection. *Molecular*

microbiology, 61(3), pp.826–837.

Murray, P.J., 2007. The JAK-STAT signaling pathway: input and output integration. *Journal of immunology (Baltimore, Md. : 1950)*, 178(5), pp.2623–2629.

Müller, P. et al., 2005. Identification of JAK/STAT signalling components by genome-wide RNA interference. *Nature*, 436(7052), pp.871–875.

Nappi, A.J. et al., 2000. Nitric oxide involvement in Drosophila immunity. *Nitric oxide : biology and chemistry / official journal of the Nitric Oxide Society*, 4(4), pp.423–430.

Nappi, A.J. et al., 1995. Superoxide anion generation in Drosophila during melanotic encapsulation of parasites. *European journal of cell biology*, 68(4), pp.450–456.

Nathan, C. & Shiloh, M.U., 2000. Reactive oxygen and nitrogen intermediates in the relationship between mammalian hosts and microbial pathogens. *Proceedings of the National Academy of Sciences of the United States of America*, 97(16), pp.8841–8848.

Newton, G.L., Buchmeier, N. & Fahey, R.C., 2008. Biosynthesis and functions of mycothiol, the unique protective thiol of Actinobacteria. *Microbiology and molecular biology reviews : MMBR*, 72(3), pp.471–494.

Ng, V.H. et al., 2004. Role of KatG catalase-peroxidase in mycobacterial pathogenesis: countering the phagocyte oxidative burst. *Molecular microbiology*, 52(5), pp.1291–1302.

O'Shea, J.J. & Plenge, R., 2012. JAK and STAT Signaling Molecules in Immunoregulation and Immune-Mediated Disease. *Immunity*, 36(4), pp.542–550.

Obara, K. et al., 2008. The Atg18-Atg2 complex is recruited to autophagic membranes via phosphatidylinositol 3-phosphate and exerts an essential function. *The Journal of biological chemistry*, 283(35), pp.23972–23980.

Oh, C.-T. et al., 2012. Mycobacterium marinum infection in Drosophila melanogaster for antimycobacterial activity assessment. *The Journal of antimicrobial chemotherapy*.

Oldefest, M. et al., 2013. Upd3 - An ancestor of the four-helix bundle cytokines. *Biochemical and biophysical research communications*, 436(1), pp.66–72.

Ooi, J.Y. et al., 2002. The Drosophila Toll-9 activates a constitutive antimicrobial defense. *EMBO reports*, 3(1), pp.82–87.

Orme, I.M., 2003. The mouse as a useful model of tuberculosis. *Tuberculosis (Edinburgh, Scotland)*, 83(1-3), pp.112–115.

Osman, D. et al., 2012. Autocrine and paracrine unpaired signaling regulate intestinal stem cell maintenance and division. *Journal of cell science*, 125(Pt 24), pp.5944–5949.

Ottenhoff, T.H.M. & Kaufmann, S.H.E., 2012. Vaccines against tuberculosis: where are we and where do we need to go? *PLoS pathogens*, 8(5), p.e1002607.

Pandey, A.K. & Sassetti, C.M., 2008. Mycobacterial persistence requires the utilization of host cholesterol. *Proceedings of the National Academy of Sciences of the United States of America*, 105(11), pp.4376–4380.

Parent, L.J. et al., 1995. Disseminated Mycobacterium marinum infection and bacteremia in a child with severe combined immunodeficiency. *Clinical infectious diseases : an official publication of the Infectious Diseases Society of America*, 21(5), pp.1325–1327.

Park, H.D. et al., 2003. Rv3133c/dosR is a transcription factor that mediates the hypoxic response of Mycobacterium tuberculosis - Park - 2003 - Molecular Microbiology - Wiley Online Library. *Molecular …*.

Peyron, P. et al., 2008. Foamy macrophages from tuberculous patients' granulomas constitute a nutrient-rich reservoir for M. tuberculosis persistence. *PLoS pathogens*, 4(11), p.e1000204.

Pieters, J., 2008. Mycobacterium tuberculosis and the macrophage: maintaining a balance. *Cell host & microbe*, 3(6), pp.399–407.

Pilátová, M. & Dionne, M.S., 2012. Burkholderia thailandensis is virulent in Drosophila melanogaster. *PloS one*, 7(11), p.e49745.

Pozos, T.C., Ramakrishnan, L. & Ramakrishan, L., 2004. New models for the study of Mycobacterium-host interactions. *Current opinion in immunology*, 16(4), pp.499–505.

Puissegur, M.-P. et al., 2004. An in vitro dual model of mycobacterial granulomas to investigate the molecular interactions between mycobacteria and human host cells. *Cellular microbiology*, 6(5), pp.423–433.

Purwantini, E. & Mukhopadhyay, B., 2009. Conversion of NO2 to NO by reduced coenzyme F420 protects mycobacteria from nitrosative damage. *Proceedings of the National Academy of Sciences of the United States of America*, 106(15), pp.6333–6338.

Qiu, P., Pan, P.C. & Govind, S., 1998. A role for the Drosophila Toll/Cactus pathway in larval hematopoiesis. *Development (Cambridge, England)*, 125(10), pp.1909–1920.

Rajan, A. & Perrimon, N., 2012. Drosophila cytokine unpaired 2 regulates physiological homeostasis by remotely controlling insulin secretion. *Cell*, 151(1), pp.123–137.

Ramakrishnan, L. et al., 1997. Mycobacterium marinum causes both long-term subclinical infection and acute disease in the leopard frog (Rana pipiens). *Infection and immunity*, 65(2), pp.767–773.

Ramakrishnan, L., Federspiel, N.A. & Falkow, S., 2000. Granuloma-specific expression of Mycobacterium virulence proteins from the glycine-rich PE-PGRS family. *Science (New York, N.Y.)*, 288(5470), pp.1436–1439.

Rämet, M., Lanot, R., et al., 2002a. JNK signaling pathway is required for efficient wound healing in Drosophila. *Developmental biology*, 241(1), pp.145–156.

Rämet, M., Manfruelli, P., et al., 2002b. Functional genomic analysis of phagocytosis and identification of a Drosophila receptor for E. coli. *Nature*, 416(6881), pp.644–648.

Rengarajan, J., Bloom, B.R. & Rubin, E.J., 2005. Genome-wide requirements for Mycobacterium tuberculosis adaptation and survival in macrophages. *Proceedings of the National Academy of Sciences of the United States of America*, 102(23), pp.8327–8332.

Rizki, R.M. & Rizki, T.M., 1980. Hemocyte responses to implanted tissues inDrosophila melanogaster larvae. *Wilhelm Roux's Archives of Developmental Biology*, 189(3), pp.207–213.

Rizki, T.M. & Rizki, R.M., 1959. Functional significance of the crystal cells in the larva of Drosophila melanogaster. *The Journal of biophysical and biochemical cytology*, 5(2), pp.235–240.

Roach, D.R. et al., 2002. TNF regulates chemokine induction essential for cell recruitment, granuloma formation, and clearance of mycobacterial infection. *Journal of immunology (Baltimore, Md. : 1950)*, 168(9), pp.4620–4627.

Rohde, K.H., Abramovitch, R.B. & Russell, D.G., 2007. Mycobacterium tuberculosis invasion of macrophages: linking bacterial gene expression to environmental cues. *Cell host & microbe*, 2(5), pp.352–364.

Roy, E. et al., 2008. Beneficial effect of anti-interleukin-4 antibody when administered in a murine model of tuberculosis infection. *Tuberculosis (Edinburgh, Scotland)*, 88(3), pp.197–

202.

Rubin, G.M. et al., 2000. Comparative genomics of the eukaryotes. *Science (New York, N.Y.)*, 287(5461), pp.2204–2215.

Ruley, K.M., Ansede, J.H. & Pritchett, C.L., 2004. Identification of Mycobacterium marinum virulence genes using signature-tagged mutagenesis and the goldfish model of mycobacterial pathogenesis - Ruley - 2006 - FEMS Microbiology Letters - Wiley Online Library. *FEMS microbiology ….*

Russell, D.G., 2007. Who puts the tubercle in tuberculosis? *Nature reviews. Microbiology*, 5(1), pp.39–47.

Russell, D.G. et al., 2009. Foamy macrophages and the progression of the human tuberculosis granuloma. *Nature immunology*, 10(9), pp.943–948.

Russo, J. et al., 1996. Insect immunity: early events in the encapsulation process of parasitoid (Leptopilina boulardi) eggs in resistant and susceptible strains of Drosophila. *Parasitology*, 112 (Pt 1), pp.135–142.

Rutschmann, S., Kilinc, A. & Ferrandon, D., 2002. Cutting Edge: The Toll Pathway Is Required for Resistance to Gram-Positive Bacterial Infections in Drosophila. *The Journal of ….*

Ryder, E. & Russell, S., 2003. Transposable elements as tools for genomics and genetics in Drosophila. *Briefings in functional genomics & proteomics*, 2(1), pp.57–71.

Saita, N. et al., 2000. Trehalose 6,6'-Dimycolate (Cord Factor) of Mycobacterium tuberculosis Induces Corneal Angiogenesis in Rats. *Infection and immunity*, 68(10), pp.5991–5997.

Saka, H.A. & Valdivia, R., 2012. Emerging roles for lipid droplets in immunity and host-pathogen interactions. *Annual review of cell and developmental biology*, 28, pp.411–437.

Samakovlis, C. et al., 1992. In vitro induction of cecropin genes--an immune response in a Drosophila blood cell line. *Biochemical and biophysical research communications*, 188(3), pp.1169–1175.

Sassetti, C.M. & Rubin, E.J., 2003. Genetic requirements for mycobacterial survival during infection. *Proceedings of the National Academy of Sciences of the United States of America*, 100(22), pp.12989–12994.

Schaible, U.E. et al., 1998. Cytokine activation leads to acidification and increases maturation of Mycobacterium avium-containing phagosomes in murine macrophages. *Journal of immunology (Baltimore, Md. : 1950)*, 160(3), pp.1290–1296.

Scherfer, C. et al., 2004. Isolation and characterization of hemolymph clotting factors in Drosophila melanogaster by a pullout method. *Current biology : CB*, 14(7), pp.625–629.

Scherfer, C. et al., 2006. The Toll immune-regulated Drosophila protein Fondue is involved in hemolymph clotting and puparium formation. *Developmental ….*

Schlesinger, L.S., 1993. Macrophage phagocytosis of virulent but not attenuated strains of Mycobacterium tuberculosis is mediated by mannose receptors in addition to complement receptors. *Journal of immunology (Baltimore, Md. : 1950)*, 150(7), pp.2920–2930.

Schmidt, R.L. et al., 2008. Infection-induced proteolysis of PGRP-LC controls the IMD activation and melanization cascades in Drosophila. *FASEB journal : official publication of the Federation of American Societies for Experimental Biology*, 22(3), pp.918–929.

Schnappinger, D. et al., 2003. Transcriptional Adaptation of Mycobacterium tuberculosis within Macrophages: Insights into the Phagosomal Environment. *The Journal of experimental medicine*, 198(5), pp.693–704.

Schneider, D. & Shahabuddin, M., 2000. Malaria parasite development in a Drosophila model. *Science (New York, N.Y.)*, 288(5475), pp.2376–2379.

Schneider, D.S. et al., 2007. Drosophila eiger mutants are sensitive to extracellular pathogens. *PLoS pathogens*, 3(3), p.e41.

Schneider, I., 1972. Cell lines derived from late embryonic stages of Drosophila melanogaster. *Journal of embryology and experimental morphology*, 27(2), pp.353–365.

Shelly, S. et al., 2009. Autophagy is an essential component of Drosophila immunity against vesicular stomatitis virus. *Immunity*, 30(4), pp.588–598.

Sherman, D.R. et al., 2001. Regulation of the Mycobacterium tuberculosis hypoxic response gene encoding alpha -crystallin. *Proceedings of the National Academy of Sciences of the United States of America*, 98(13), pp.7534–7539.

Shinzawa, N. et al., 2009. p38 MAPK-dependent phagocytic encapsulation confers infection tolerance in Drosophila. *Cell host & microbe*, 6(3), pp.244–252.

Simeone, R. et al., 2012. Phagosomal rupture by Mycobacterium tuberculosis results in toxicity and host cell death. *PLoS pathogens*, 8(2), p.e1002507.

Singh, S.B. et al., 2006. Human IRGM induces autophagy to eliminate intracellular mycobacteria. *Science (New York, N.Y.)*, 313(5792), pp.1438–1441.

Smith, C.D. et al., 2007. The Release 5.1 annotation of Drosophila melanogaster heterochromatin. *Science (New York, N.Y.)*, 316(5831), pp.1586–1591.

Soldati, T. & Neyrolles, O., 2012. Mycobacteria and the intraphagosomal environment: take it with a pinch of salt(s)! *Traffic (Copenhagen, Denmark)*, 13(8), pp.1042–1052.

Solomon, J.M., Leung, G.S. & Isberg, R.R., 2003. Intracellular replication of Mycobacterium marinum within Dictyostelium discoideum: efficient replication in the absence of host coronin. *Infection and immunity*, 71(6), pp.3578–3586.

Souba, W.W., 1994. Cytokine control of nutrition and metabolism in critical illness. *Current problems in surgery*, 31(7), pp.577–643.

Sow, F.B. et al., 2007. Expression and localization of hepcidin in macrophages: a role in host defense against tuberculosis. *Journal of leukocyte biology*, 82(4), pp.934–945.

Stamm, L.M. & Brown, E.J., 2004. Mycobacterium marinum: the generalization and specialization of a pathogenic mycobacterium. *Microbes and infection / Institut Pasteur*, 6(15), pp.1418–1428.

Stamm, L.M. et al., 2003. Mycobacterium marinum escapes from phagosomes and is propelled by actin-based motility. *The Journal of experimental medicine*, 198(9), pp.1361–1368.

Stark, G.R. & Darnell, J.E., 2012. The JAK-STAT Pathway at Twenty. *Immunity*, 36(4), pp.503–514.

Stinear, T.P. et al., 2008. Insights from the complete genome sequence of Mycobacterium marinum on the evolution of Mycobacterium tuberculosis. *Genome Research*, 18(5), pp.729–741.

Stone, E.F. et al., 2012. The circadian clock protein timeless regulates phagocytosis of bacteria in Drosophila. *PLoS pathogens*, 8(1), p.e1002445.

Stuart, L.M. et al., 2007. A systems biology analysis of the Drosophila phagosome. *Nature*, 445(7123), pp.95–101.

Sturgill-Koszycki, S. et al., 1994. Lack of acidification in Mycobacterium phagosomes produced

by exclusion of the vesicular proton-ATPase. *Science (New York, N.Y.)*, 263(5147), pp.678–681.

Sullivan, W. et al., 2000. *Drosophila protocols*, Cold Spring Harbor Laboratory Press.

Sweeney, K.A. et al., 2011. A recombinant Mycobacterium smegmatis induces potent bactericidal immunity against Mycobacterium tuberculosis. *Nature medicine*, 17(10), pp.1261–1268.

Szymanski, K.M. et al., 2007. The lipodystrophy protein seipin is found at endoplasmic reticulum lipid droplet junctions and is important for droplet morphology. *Proceedings of the National Academy of Sciences of the United States of America*, 104(52), pp.20890–20895.

Søndergaard, L., 1993. Homology between the mammalian liver and the Drosophila fat body. *Trends in genetics : TIG*, 9(6), p.193.

Tanji, T., Yun, E.-Y. & Ip, Y.T., 2010. Heterodimers of NF-kappaB transcription factors DIF and Relish regulate antimicrobial peptide genes in Drosophila. *Proceedings of the National Academy of Sciences of the United States of America*, 107(33), pp.14715–14720.

Tauchi-Sato, K. et al., 2002. The surface of lipid droplets is a phospholipid monolayer with a unique Fatty Acid composition. *The Journal of biological chemistry*, 277(46), pp.44507–44512.

Tauszig, S. et al., 2000. Toll-related receptors and the control of antimicrobial peptide expression in Drosophila. *Proceedings of the National Academy of Sciences of the United States of America*, 97(19), pp.10520–10525.

Tepass, U. et al., 1994. Embryonic origin of hemocytes and their relationship to cell death in Drosophila. *Development (Cambridge, England)*, 120(7), pp.1829–1837.

Tirouvanziam, R. et al., 2004. Fluorescence-activated cell sorting (FACS) of Drosophila hemocytes reveals important functional similarities to mammalian leukocytes. *Proceedings of the National Academy of Sciences of the United States of America*, 101(9), pp.2912–2917.

Tobin, D.M. & Ramakrishnan, L., 2008. Comparative pathogenesis of Mycobacterium marinum and Mycobacterium tuberculosis. *Cellular microbiology*, 10(5), pp.1027–1039.

Tzou, P. et al., 2000. Tissue-Specific Inducible Expression of Antimicrobial Peptide Genes in Drosophila Surface Epithelia. *Immunity*, 13(5), pp.737–748.

Tønjum, T. et al., 1998. Differentiation of Mycobacterium ulcerans, M. marinum, and M. haemophilum: mapping of their relationships to M. tuberculosis by fatty acid profile analysis, DNA-DNA hybridization, and 16S rRNA gene sequence analysis. *Journal of clinical microbiology*, 36(4), pp.918–925.

Urdahl, K.B., Shafiani, S. & Ernst, J.D., 2011. Initiation and regulation of T-cell responses in tuberculosis. *Mucosal immunology*, 4(3), pp.288–293.

van der Wel, N. et al., 2007. M. tuberculosis and M. leprae translocate from the phagolysosome to the cytosol in myeloid cells. *Cell*, 129(7), pp.1287–1298.

van Manen, H.-J. et al., 2005. Single-cell Raman and fluorescence microscopy reveal the association of lipid bodies with phagosomes in leukocytes. *Proceedings of the National Academy of Sciences of the United States of America*, 102(29), pp.10159–10164.

Vandal, O.H. et al., 2008. A membrane protein preserves intrabacterial pH in intraphagosomal Mycobacterium tuberculosis. *Nature medicine*, 14(8), pp.849–854.

Vandal, O.H. et al., 2009. Acid-Susceptible Mutants of Mycobacterium tuberculosis Share Hypersusceptibility to Cell Wall and Oxidative Stress and to the Host Environment. *Journal*

of ….

Velikkakath, A.K.G. et al., 2012. Mammalian Atg2 proteins are essential for autophagosome formation and important for regulation of size and distribution of lipid droplets. *Molecular biology of the cell*, 23(5), pp.896–909.

Velmurugan, K. et al., 2007. Mycobacterium tuberculosis nuoG is a virulence gene that inhibits apoptosis of infected host cells. *PLoS pathogens*, 3(7), p.e110.

Vergne, I. et al., 2006. Autophagy in immune defense against Mycobacterium tuberculosis. *Autophagy*, 2(3), pp.175–178.

Vergne, I. et al., 2004. Cell biology of mycobacterium tuberculosis phagosome. *Annual review of cell and developmental biology*, 20, pp.367–394.

Vergne, I. et al., 2005. Mechanism of phagolysosome biogenesis block by viable Mycobacterium tuberculosis. *Proceedings of the National Academy of Sciences of the United States of America*, 102(11), pp.4033–4038.

Via, L.E. et al., 1998. Effects of cytokines on mycobacterial phagosome maturation. *Journal of cell science*, 111 (Pt 7), pp.897–905.

Via, L.E. et al., 2008. Tuberculous granulomas are hypoxic in guinea pigs, rabbits, and nonhuman primates. *Infection and immunity*, 76(6), pp.2333–2340.

Vierstraete, E. et al., 2004. A proteomic approach for the analysis of instantly released wound and immune proteins in Drosophila melanogaster hemolymph. *Proceedings of the National Academy of Sciences of the United States of America*, 101(2), pp.470–475.

Vierstraete, E. et al., 2003. Proteomics in Drosophila melanogaster: first 2D database of larval hemolymph proteins. *Biochemical and biophysical research communications*, 304(4), pp.831–838.

Volkman, H.E. et al., 2004. Tuberculous granuloma formation is enhanced by a mycobacterium virulence determinant. *PLoS biology*, 2(11), p.e367.

Wallgren, A., 1948. The time-table of tuberculosis. *Tubercle*, 29(11), pp.245–251.

Wallis, R.S., 2008. Tumour necrosis factor antagonists: structure, function, and tuberculosis risks. *The Lancet infectious diseases*, 8(10), pp.601–611.

Watson, F.L. et al., 2005. Extensive diversity of Ig-superfamily proteins in the immune system of insects. *Science (New York, N.Y.)*, 309(5742), pp.1874–1878.

Weissbach, H. et al., 2002. Peptide Methionine Sulfoxide Reductase: Structure, Mechanism of Action, and Biological Function. *Archives of Biochemistry and Biophysics*, 397(2), pp.172–178.

Welin, A. & Lerm, M., 2012. Inside or outside the phagosome? The controversy of the intracellular localization of Mycobacterium tuberculosis. *Tuberculosis (Edinburgh, Scotland)*, 92(2), pp.113–120.

Wolf, A.J. et al., 2008. Initiation of the adaptive immune response to Mycobacterium tuberculosis depends on antigen production in the local lymph node, not the lungs. *The Journal of experimental medicine*, 205(1), pp.105–115.

Wolf, A.J. et al., 2007. Mycobacterium tuberculosis infects dendritic cells with high frequency and impairs their function in vivo. *Journal of immunology (Baltimore, Md. : 1950)*, 179(4), pp.2509–2519.

Wong, D. et al., 2011. Mycobacterium tuberculosis protein tyrosine phosphatase (PtpA) excludes host vacuolar-H+–ATPase to inhibit phagosome acidification. *Proceedings of the*

….

Wong, R. et al., 2009. Quantification of food intake in Drosophila. *PloS one*, 4(6), p.e6063.

World Health Organization, 2012. *Global Tuberculosis Report 2012*, World Health Organization.

World Health Organization (WHO), 1993. World Health Organization (WHO): WHO declares tuberculosi... - Google Scholar. *WHO/31*.

World Health Organization (WHO), 2011. World Health Organization: Tuberculosis fact sheet... - Google Scholar. *Tuberculosis Fact Sheet*.

Wright, V.M. et al., 2011. Differential activities of the Drosophila JAK/STAT pathway ligands Upd, Upd2 and Upd3. *Cellular signalling*, 23(5), pp.920–927.

Wu, C.H. et al., 1998. Identification and subcellular localization of a novel Cu,Zn superoxide dismutase of Mycobacterium tuberculosis. *FEBS letters*, 439(1-2), pp.192–196.

Yanagawa, S., Lee, J.S. & Ishimoto, A., 1998. Identification and characterization of a novel line of Drosophila Schneider S2 cells that respond to wingless signaling. *The Journal of biological chemistry*, 273(48), pp.32353–32359.

Yao, J. et al., 2010. Atoh8, a bHLH transcription factor, is required for the development of retina and skeletal muscle in zebrafish. *PloS one*, 5(6), p.e10945.

Yuk, J.-M. et al., 2009. Vitamin D3 induces autophagy in human monocytes/macrophages via cathelicidin. *Cell host & microbe*, 6(3), pp.231–243.

Zhou, R. et al., 2005. The role of ubiquitination in Drosophila innate immunity. *The Journal of biological chemistry*, 280(40), pp.34048–34055.

Zirin, J. & Perrimon, N., 2010. Drosophila as a model system to study autophagy. *Seminars in immunopathology*, 32(4), pp.363–372.

Zumla, A., Nahid, P. & Cole, S.T., 2013. Advances in the development of new tuberculosis drugs and treatment regimens. *Nature reviews. Drug discovery*, 12(5), pp.388–404.

Zuñiga, J. et al., 2012. Cellular and humoral mechanisms involved in the control of tuberculosis. *Clinical & developmental immunology*, 2012, p.193923.